ROLE AND PROPERTIES OF [2FE-2S] CENTERS IN FERROCHELATASES

by

ANGELA-NADIA ALBETEL

(Under the Direction of Michael K. Johnson)

ABSTRACT

Ferrochelatase (E.C. 4.99.1.1), the terminal enzyme of the heme biosynthetic pathway, catalyzes the insertion of ferrous iron into protoporphyrin IX. All metazoan, Actinobacterial, and a few Gram negative bacterial ferrochelatases contain a labile $[2Fe\text{-}2S]^{2+}$ center that is crucial for activity, but its specific role has yet to be determined. In this work the role and spectroscopic properties of $[2Fe\text{-}2S]^{2+}$ centers in ferrochelatase have been investigated by using a combination of analytical and spectroscopic studies. Detailed spectroscopic characterization of various $[2Fe\text{-}2S]^{2+,+}$ cluster-containing ferrochelatases reveals major differences in the coordination environment and electronic properties of the $[2Fe\text{-}2S]^{2+,+}$ clusters that are ligated by distinct primary sequence arrangements of conserved cysteine residues. Parallel EPR and UV-visible studies indicate that anaerobic incubation of different recombinant ferrochelatases with the NO-donor, diethylamine NONOate, results in rapid loss of the $[2Fe\text{-}2S]^{2+}$ cluster concomitant with the formation of a dinitrosyl-iron-cysteine complex (DNIC). The rates for the NO-induced $[2Fe\text{-}2S]^{2+}$ cluster degradation/DNIC formation are comparable among all ferrochelatases studied, suggesting that the cluster is unlikely to play a primary role as a NO-sensor in eukaryotes, but rather serves as part of a general oxidative stress response to degrade the cluster, thereby

decreasing heme biosynthesis, in response to cellular conditions in both eukaryotes and prokaryotes. Furthermore, investigations on the role of $[2Fe\text{-}2S]^{2+}$ clusters from *Arabidopsis thaliana* sirohydrochlorin ferrochelatase (AtSirB Fc), the terminal enzyme of siroheme biosynthesis in chloroplast, demonstrate that monothiol glutaredoxins, which play a crucial role in both Fe-S cluster and heme biosynthesis in eukaryotes, play a vital role in regulating siroheme/heme biosynthesis by functioning as the [2Fe-2S] cluster donor for the maturation of AtSirB Fc. Detailed analytical and spectroscopic studies reveal that the $[2Fe\text{-}2S]^{2+}$ center in AtSirB Fc undergoes a conformational change as a function of pH that is associated with a dimer/tetramer interconversion and that the cluster can only be inserted in the tetrameric form. Thus, this work provides direct evidence for an intimate connection between Fe-S clusters biogenesis and heme biosynthesis, by indicating that the [2Fe-2S] cluster-binding site in eukaryotic ferrochelatases functions in sensing the cellular Fe-S cluster status via the extent of cluster loading of the monothiol glutaredoxin [2Fe-2S] cluster donor.

INDEX WORDS: Ferrochelatase, monothiol glutaredoxin, Grx, Fe-S cluster biosynthesis, Heme biosynthesis, Cluster transfer, Cluster carrier, Electron Paramagnetic Resonance, Resonance Raman, Circular Dichroism

ROLE AND SPECTROSCOPIC CHARACTERIZATION OF [2FE-2S] CENTERS IN FERROCHELATASES

by

ANGELA-NADIA ALBETEL

FORB, Babes-Bolyai University, Cluj-Napoca, Romania, 2000

FORM, Babes-Bolyai University, Cluj-Napoca, Romania, 2001

A Dissertation Submitted to the Graduate Faculty of The University of Georgia in Partial Fulfillment of the Requirements for the Degree

DOCTOR OF PHILOSOPHY

ATHENS, GEORGIA

2012

ROLE AND SPECTROSCOPIC CHARACTERIZATION OF [2FE-2S] CENTERS IN FERROCHELATASES

by

ANGELA-NADIA ALBETEL

Major Professor: Michael K. Johnson

Committee: Harry A. Dailey

William N. Lanzilotta

Electronic Version Approved:

Maureen Grasso

Dean of the Graduate School

The University of Georgia

May 2012

ACKNOWLEDGEMENTS

My advisor, Professor Michael K. Johnson is thanked for his generous mentorship and support throughout my graduate studies. I wish to thank Professor Harry A. Dailey and Tamara A. Dailey for their essential contribution in initiating this project, for practical training and scientific discussions that enabled me to understand the microbiology and molecular biology aspects of this research project. Professor William N. Lanzilotta is thanked for help and involvement with crystallographic studies on *M. xathus* ferrochelatase and anaerobic crystallography on *A. thaliana* GrxS14. I wish to thank Professor Donald M. Kurtz Jr. for guidance, strong support and encouragement during the first year of my graduate studies. Past and present members of the Johnson group are thanked for quality, enthusiastic and friendly work environment, from which this research project has benefited greatly.

Words cannot express my gratitude to my husband who has been a tremendous help throughout my graduate school not only by showing continuous support and encouragement, but for helping with the preparation of all Pymol figures presented in this manuscript; without his support, love and understanding this work would not be possible.

Last but not least, I would like to express a special thank you to my parents for always encouraging me and understanding the importance of accomplishing my career goals, in spite of how far it has brought us from each other.

TABLE OF CONTENTS

LIST OF TABLES

Page

LIST OF FIGURES

Page

CHAPTER 1

INTRODUCTION AND LITERATURE REVIEW

Iron is an essential metal for almost all organisms due to its unique versatility as a biological redox catalyst. It is the ability of iron to cycle between two oxidation states, ferrous and ferric, that enable the mitochondrion to catalyze electron transport via heme and iron-sulfur (Fe-S) cluster - containing proteins and use this process in energy transduction. In fact, in higher eukaryotes the mitochondrion is the sole site of heme synthesis and a major generator of iron-sulfur clusters, both of which are present in mitochondria and cytosol (*1*). In plants iron is also used for the biosynthesis of siroheme, a biological cofactor synthesized in plastids and used to catalyze the second step of sulfate and nitrate reduction reactions (*2*). This review will briefly describe the heme and siroheme biosynthetic pathways, with particular emphasis on the enzymes that catalyze the last steps of these two pathways, namely ferrochelatase and sirohydrochlorin ferrochelatase, respectively. In addition, the potential mechanism by which heme/siroheme and iron sulfur cluster biosynthesis are interrelated and regulated will also be discussed.

Heme: Significance and Biosynthesis

Heme, a complex of iron with protoporphyrin IX, is a cofactor found in essentially all aerobic organisms and a majority of anaerobic and facultative anaerobic organisms. While the traditional textbook roles for heme as a cofactor include hemoglobin- and myoglobin (involved in oxygen transport and storage), cytochromes a, a_3 b, c, and c_1 (responsible for providing energy to biological processes through the electron transport chain), and as active sites in a wide range of metalloenzymes, considerable evidence has emerged that demonstrates a central role for

heme in regulation of gene transcription (*3;4*), as a gas sensor (*5*), in the regulation of circadian rhythm (*6*), during development (*7*) and in RNAi processing (*8*). For example, heme is involved in the biosynthesis of nitric oxide (NO), an important signaling molecule in detoxification through mixed oxidation functions by cytochrome P_{450}, and in protection of the body through the regulation of H_2O_2 with peroxidase and catalase (*9;10*). All of these functions underline the adaptability of the heme cofactor to various protein environments, enabling it to catalyze very diverse reactions. In fact, disordered heme metabolism can have profound developmental and health consequences (*11;12*).

The value of heme in cellular metabolism is emphasized by the fact that virtually all heme-containing organisms possess a complete biosynthetic pathway for this compound. Only archaea, some pathogenic prokaryotes, and a limited number of unicellular eukaryotes have been shown to not contain heme (*10*). With the exception of *Caenorhabditis elegans* and related helminthes (*13*), heme acquired via dietary sources is generally degraded to release free iron and is not utilized as a source of cellular heme (*14*). In particular, eukaryotic organisms cannot acquire heme from their diet since the macrocycle is degraded in mucosal cells to liberate iron (*15*), therefore eukaryotes possess all eight heme biosynthetic enzymes necessary for producing this tetrapyrrole compound (*10*). This is true for most prokaryotes as well.

The eight sequential reactions involved in the heme biosynthetic pathway take place in the mitochondrion and cytoplasm (*10*) (Fig. 1.1). The first step of heme synthesis, the condensation of succinyl-CoA and glycine into 5-aminolevulinic acid (ALA), is catalyzed by 5-aminolevulinate synthase (ALAS) in the mitochondrial matrix of erythroid precursor cells. ALA is exported to the cytosol, and the subsequent six steps of heme synthesis take place either in the cytosol or in the intermembrane space of mitochondria. In the last step, ferrochelatase inserts a

ferrous iron into protoporphyrin IX to produce heme (*10*). The enzymes participating in the heme production catalyze a variety of interesting reactions and utilize both common and unique cofactors and metals. Thus, aminolevulinate dehydratase from all organisms and ferrochelatase from higher animals are both metalloenzymes, ALAS uses pyridoxal phosphate as a cofactor, and porphobilinogen deaminase uses a unique dipyrrole cofactor. Uroporphyrinogen III decarboxylase and coproporpyrinogen III oxidase catalyze multiple decarboxylations and yet have no cofactors, whereas one pathway enzyme catalyzes a six-electron oxidation with a single FAD. To add additional scientific interest there exist biochemically and clinically distinct human genetic diseases for every step in the heme biosynthetic pathway (*10*). In mammals, genetic or chemically induced defects in the enzyme that catalyzes the first step of heme biosynthesis, ALAS, result in the disease known as sideroblastic anemia, whereas deletion and/or point mutations in any of last seven enzymes of the pathway result in diseases commonly referred to as porphyrias (*11;16*). These diseases are generally transmitted in an autosomal dominant fashion, with many of them showing incomplete penetrance. It has been popular to group porphyrias into acute porphyrias – characterized by episodic neurovisceral manifestations (i.e. Doss heritable porphyria, acute intermittent porphyria, hereditary coproporphyria, and variegate porphyria caused by deficiencies in 5-aminolevulinate dehydratase, porphobilinogen deaminase, coproporphyrinogen oxidase and protoporphyrinogen oxidase, respectively), and non-acute porphyrias, with cutaneous manifestations (i.e. congenital erythropoietic protoporphyria, porphyria cutanea tarda and hepatoerythropoietic porphyria, as well as erythropoietic protoporphyria caused by deficiencies in uroporphyrinogen III synthase, uroporphyrinogen decarboxylase and ferrochelatase, respectively) (*17*).

Ferrochelatase: Background and Significance

The terminal step of heme biosynthesis is the insertion of ferrous iron into protoporphyrin IX, resulting in the formation of protoheme IX (*18*). Therefore, this step represents the convergence of two cellular pathways: the synthesis of the organic macrocycle protoporphyrin and the supply of ferrous iron (*19*). Both biosynthetic pathways are tightly regulated, since their substrates are both chemically reactive and potentially damaging to the cell (*20;21*).

Although considerable biochemical understanding of the heme biosynthetic pathway began in the 1940s, it wasn't until 1960's that the last enzyme in the pathway was identified. In 1956 Goldberg's group reported the presence of an enzyme in avian erythrocytes that catalyzed the insertion of iron into protoporphyrin IX, resulting in the formation of protoheme IX (*22*). The enzyme was called ferrochelatase (ferrohaemprotolyase, haem synthetase, ferrohaem-protolyase, protoheme ferrolyase, E.C. 4.99.1.1). Following the initial characterization, ferrochelatase activity was reported in a variety of cell types and organisms (*23;24*). Later, Jones' group published some preliminary kinetic characterizations of the enzyme in crude cell extracts from animals, plants, and bacteria (*25-33*), and in spite of low activity levels, the general agreement was that the activity was of enzymatic nature. However, in 1972 and 1973, Tokunaga's and Kassner's groups independently suggested that *in vitro* iron could be inserted non-enzymatically into protoporphyrin under what they called physiological conditions (*34;35*). Although these authors' opinion concerning what "physiological conditions" meant is questionable, their results raised doubts at the time regarding the need for an enzyme to catalyze the biological metallation of protoporphyrin. The enzymatic requirement for iron chelation was finally established in 1974 with the discovery of a ferrochelatase-deficient mutant of the bacterium *Spirillum itersonii* which was unable to synthesize heme (*36*). This mutant lacked any detectable ferrochelatase activity in

crude cell extracts and was completely dependent on heme supplied exogenously. Heme could not be substituted by either aminolevulinate or protoporphyrin, but spontaneous revertants of this mutant were able to recover ferrochelatase activity and exogenous heme supplementation was no longer necessary.

Between 1970s and 1980s, several attempts to purify the enzyme ferrochelatase were reported, but low activity levels and protein instability, as well as the fact that the ferrochelatases studied were membrane-associated and required detergents in order to be kept in solution, hindered progress in characterization. The first successful purification was accomplished in 1981 when Taketani and Tokunaga isolated a detergent-solubilized mitochondrial ferrochelatase from rat liver, with a total protein recovery of less than 1 mg (*37*). Subsequently, ferrochelatase was purified from bovine liver (*38;39*), chicken erythrocytes (*40;40*), and yeast (*41*) with similar yields. An important step forward was made by Labbe-Bois who succeeded in cloning ferrochelatase for *Saccharomyces cerevisiae* by using complementation of an yeast auxotroph *(42)*. Shortly after, cloning of human (*43*) and murine (*44;45*) ferrochelatases were reported. In 1992 the recombinant yeast enzyme was expressed and purified from a baculovirus (*46*), followed by expression of murine normal and protoporphyric ferrochelatases in *Escherichia coli* later that same year (*47*). In 1994, relatively high expression levels of recombinant human and mouse ferrochelatase were obtained (*48*), facilitating the beginning of biophysical characterization of the pure enzyme. Since then, ferrochelatases from *Gallus (49)*, *Xenopus (49),* and *Drosophila (50)*, as well as from the bacteria *Bacillus subtilis,(51) Myxococcus xanthus (52), Mycobacterium tuberculosis (53)* and *Caulobacter crescentus (53)* have also been cloned, expressed and purified.

The gene for ferrochelatase was first sequenced from *S. cerevisiae* in 1990 (*42;54*), followed soon after by the sequencing of the mammalian gene (*44;45*). Currently, there are over 90 ferrochelatase cDNA and DNA sequences present in public databases, ranging from animals to plants to eubacteria and archae. Yet, only a small number of ferrochelatases have actually been expressed and characterized.

Of particular interest to this thesis is information concerning gene regulation of the mammalian enzyme, the genetic disease erythropoietic protoporphyria caused by deficiencies in ferrochelatase, and the potential roles for the enzyme in the regulation of iron metabolism and heme biosynthesis that have been recently proposed.

Erythropoietic Protoporphyria (EPP)

Point mutations and/or deletion in the human gene that encodes for ferrochelatase can result in the heritable disease erythropoietic protoporphyria (EPP), a condition that was first described by Magnus et al (*55*). This disease is inherited in an autosomal dominant manner (*11*), and manifests as accumulation of protoporphyrin IX in blood (erythrocytes, plasma) and tissues (skin, liver). The characteristic clinical manifestation of the disease is painful photosensitivity due to accumulation of protoporphyrin IX in the skin. Protoporphyrin IX is a photosensitive pigment that may form free radicals upon exposure to sunlight, causing blistering in cutaneous tissues starting in early infancy or childhood (*10;56;57*). The protoporphyrin molecule absorbs light radiation in a range of wavelengths from 320 to 595 nm. The absorption of these wavelengths increases the energy content of the protoporphyrin molecule (inducing a triplet state) and enables the excess energy to be transferred to oxygen, resulting in a reactive oxygen species that may interact with many biological molecules, such as proteins, lipids and DNA via photodynamic reactions (*58*). As protoporphyrin is a hydrophobic molecule, it tends to

accumulate in cellular membranes. Upon irradiation with the specific wavelengths mentioned above, a photodynamic reaction takes place in tissues where protoporphyrin is present (skin, red blood cells in skin blood vessels) and cellular membranes are damaged because of membrane lipids peroxidation. Production of oxygen species may also injure tissues by complement activation and mast cell degranulation phenomena that explain the vasodilatation and edema components of the skin photosensitivity reactions in EPP patients.

In less than 5% of EPP patients, porphyrin crystals were found to accumulate in the liver resulting in hepatobiliary blockage and possibly causing liver failure. However, the incomplete penetrance of EPP is not understood. One report of 8 patients that required liver transplants suggested that mutations causing liver damage produced structural alterations in the ferrochelatase protein (*59*), and although this major structural alteration of ferrochelatase is not sufficient to cause liver damage, it appears to be a factor.

One interesting characteristic of EPP is that symptomatic patients characteristically have <50% ferrochelatase activity (*60*), while with most autosomal dominant diseases one would expect only a 50% reduction of activity of the affected enzyme. Several theories have been proposed to explain this decrease in activity, including the presence of a third allele, low expression of the wild-type allele, dimerization problems with mutant proteins, and dietary considerations (*57*). Evidence to support some of the suggestions above exists, but it appears to be more complex than a single explanation (*57;61*).

EPP has also been shown to be naturally occurring in bovine, but in an autosomal recessive fashion. A point mutation that causes the stop codon of bovine ferrochelatase to code for a leucine residue and therefore extend the polypeptide chain 27 extra amino acids has been shown to cause EPP in cattle (*62*). To date, there exist two mice models of EPP, including (*i*) a

chemically induced ferrochelatase mutant mouse (*63*), and (*ii*) a mice engineered to have exon 10 deleted (*60*). The chemically induced mutation is a point mutation causing a M98K substitution (*64*). This animal model, like the bovine model, must be inherited as a recessive allele to show characteristics similar to that seen in human EPP (*63*). Initial analysis of the exon 10 deletion mouse model in the heterozygous state shows that ferrochelatase activity is only decreased 50%, not 15 to 30% as seen in EPP patients (*60*). This suggests that additional genetic or environmental factors contribute to the phenotype seen in EPP.

To date, over 40 mutations that cause EPP have been described (*59;65-67*). Many of the mutations identified cause exon deletions, including exons 2, 3, 4, 7, 8, 9, and 10, or truncations of the protein. Rufenacht and coworkers classified the mutations causing EPP into single nucleotide mutations within the coding region (42%), exon skipping (34%), and small deletions or insertions (21%) (*66*). Some interesting point mutations that cause EPP are located in the carboxy terminus of the protein. Several of these directly involve the ligands of a [2Fe-2S] cluster present in eukaryotic ferrochelatases and understandably these gene products do not have enzymatic activity (*68;69*).

Recently, families have been described in which EPP is inherited in an X-linked dominant pattern (*70*). Patients with this disorder have normal ferrochelatase activities but higher erythrocyte total protoporphyrin concentrations than other types of EPP, of which around 40% is zinc-protoporphyrin. This high proportion of zinc-protoporphyrin suggests that protoporphyrin accumulates because supply of its metal substrate, Fe^{2+}, becomes rate-limiting. Additionally, the increase in erythrocyte zinc-protoporphyrin in combination with a marked increase in free protoporphyrin appears to be a distinguishing feature of this form of EPP (*71;72*).

Ferrochelatase: Structure

Considerable structural diversity exists among ferrochelatases from different kingdoms of life. Studies using bovine and recombinant human ferrochelatases have shown the enzyme to be a homodimer (*73;74*), whereas the recombinant protein from bacterial *B. subtilis* and *M. tuberculosis* were determined to be monomeric (*53;75*). Except for Gram negative bacteria which comprise soluble ferrochelatases, in the majority of the other bacterial organisms and all eukaryotes studied to date, ferrochelatase was found to be bound to cellular membranes (*19;51;53*). In animal cells, the enzyme is associated with the matrix side of the mitochondrial inner membrane (*31;76;77*), while in plants it is located in both the mitochondria and chloroplasts (*78-80*). Actually, plant cells possess two distinct isoenzymes for ferrochelatase, one targeted to mitochondria and the second form specifically targeted to chloroplasts, presenting an interesting alternative to bacterial and animal ferrochelatases (*78-80*).

Encoded in the nucleus, eukaryotic ferrochelatase is synthesized in the cytoplasm with an amino-terminal targeting sequence responsible for targeting the protein to the mitochondrion, where it is facing the matrix of the inner membrane (*77*). The translocation process requires an energy-dependent step and proteolytic processing of the precursor form to the mature enzyme (*76*).

Primary structure. The overall sequence homology of all known ferrochelatases is very low, with less than 15% similarity, and only approximately 20 amino acid residues being invariant (Fig. 1.2.). With few exceptions, most of the conserved residues are located in the active site pocket (*57*). Human and *B. subtilis*, the two best characterized ferrochelatases to date share approximately 7% identity, but these proteins are clearly closely related. A comparison of all currently known ferrochelatase sequences reveals the presence of three distinct domains: the first domain (I) is an amino-terminal organelle-targeting motif and is present in all eukaryotes,

being involved in targeting the enzyme to the mitochondrion and/or chloroplasts (*76*). Bacterial ferrochelatases lack this domain since such translocation does not occur. The second domain (II) represents the core 330 amino acid residues of the enzyme, contains all of the amino acids involved in catalysis, and it is present in all ferrochelatases. Finally, eukaryotes, a small number of recently identified prokaryotes including *C. crescentus, M. tuberculosis, Propionibacter freudenreichii*, *Streptomyces coelicolor* and *Rickettzia prowazekii,* as well as plants contain ferrochelatases that possess a carboxy terminal extension (domain III) that varies in length from 30 to 50 amino acids, with plants having the longest extensions (*53;57*). One interesting observation is that domain III from bacteria exhibits barely any similarity with one another and no similarity to the eukaryotic carboxyl-terminal extension (Fig. 1.2.). The carboxyl 30 amino acid residues of all animal ferrochelatases can be aligned using alignment programs such as ClustalW (*81*), while bacterial sequences cannot be aligned with the eukaryotic animal sequences. However, visual alignment of bacterial ferrochelatases results in pairing *C. crescentus* with *R. prowazekii*, *S. coelicolor* with *P. freudenreichii*, whereas *M. tuberculosis* is placed in a separate group (see Figure 1.2 and Table 1.1) (*57*).

In animal ferrochelatases, the carboxyl-terminal extension is involved in the dimerization motif for these enzymes and contains three of the four coordinating ligands of a [2Fe-2S] cluster, the fourth cluster ligand residue being present in domain II (*48-50;82;83*). Although plant ferrochelatases also contain domain III, they do not contain the cysteinyl residues in this region and do not possess a [2Fe-2S] cluster (*53*). Yeast *Schizosaccharomyces pombe (84), Neurospora crassa, Candida albicans* and *Aspergillus niger* amino acid sequences contain three cysteinyl residues in their C-terminal domain and ligate a [2Fe-2S] cluster. *S. cerevisiae* ferrochelatase appears to be somewhat of an exception among yeast since it lacks the ability to bind a [2Fe-2S]

cluster; in spite of the presence of a carboxyl terminal extension. Aside from its role in the dimerization, the function of the carboxyl-terminal extension is unknown, but its removal from *S. cerevisiae* or animal ferrochelatases result in loss of enzyme activity (*48*).

Secondary, tertiary and quaternary structure: Despite intensive research on ferrochelatases from various sources over the past 50 years, a detailed understanding of the nature of the active site and catalytic mechanism emerged only after crystal structures of ferrochelatases from *B. subtilis* and human became available.

The first crystal structure of a tetrapyrrole metallation enzyme or any ferrochelatase to be solved at 1.9Å resolution was that of the *B. subtilis* ferrochelatase in 1997 (Figure 1.3) (*75*), followed by the determination of the crystal structure of the human (Figure 1.4) (*83*) and *S. cerevisiae (85)* enzymes in 2000 and 2002, respectively. To date, multiple crystal structures are available for *B. subtilis (75;86-89)* and human ferrochelatases (*83;90-93*) along with numerous structure/function studies (*75;94-98*), and taken together these results have provided major molecular-level insights into the reaction mechanism.

The overall structures of human and *B. subtilis* ferrochelatases are very similar. Thus, both structures are folded into two domains, each composed of four-stranded parallel β sheets flanked by α helices, resulting in a β-α-β motif (*75;83*) that resembles the periplasmic-binding protein family (*99*). In terms of the structures and amino acid sequence comparison, most of the conserved residues are found in the active site pocket, and others have structural functions, specifically glycine and proline residues (*83*).

However, comparison of *B. subtilis* (Figure 1.3) and human ferrochelatase (Figure 1.4) crystal structures revealed interesting features in terms of the active site and overall structure-function relationship. The characteristics of the *B. subtilis* enzyme are quite different compared

to the human enzyme. As mentioned above, unlike the human protein, *B. subtilis* ferrochelatase is soluble and monomeric. More importantly, the *B. subtilis* enzyme does not possess the carboxy terminal extension or a [2Fe-2S] cluster (Figure 1.3) (*75*). The dimer interface in the human ferrochelatase structure is in fact of great interest since the majority of the interactions stabilizing this region are hydrophobic, with the remaining interactions coming from 30 hydrogen bonds, 18 of which being associated with the carboxyl terminus regions (Figure 1.4) (*83*).

The differences in the crystal structures of human and *B. subtilis* ferrochelatases include the area surrounding the active site pocket, in particular the "upper" lip (Figure 1.4) which is absent in the *B. subtilis* structure (Figure 1.3). Each subunit of human ferrochelatase contains a deep, but open, active-site pocket as predicted by earlier spectroscopic studies (*100*). In the homodimer, both active-site pockets are located on a single surface of the molecule (Figure 1.4). The opening of each active-site pocket consists of two hydrophobic lips composed of residues 90–130 and 300–311 (Figure 1.4). The external sides of these lips are rich in hydrophobic residues, the result being that the active site-containing surface of the homodimer is the largest non-polar molecular surface. Compared to the lips, the active-site pocket is relatively hydrophilic and contains most of the highly conserved amino acid residues. Consistent with the purification protocols, in the first published crystal structure of human ferrochelatase three detergent molecules were found to be associated with the "upper" lip and therefore this region was identified as the membrane associating region. This region, which is absent in the *B. subtilis* enzyme, has been previously identified as a putative membrane associating segment in the yeast form of ferrochelatase (*101*). This finding is of particular interest since at neutral pH the substrate, protoporphyrin IX, and product, protoheme IX, are both poorly soluble in aqueous environments. By facing the active sites towards the hydrophobic inner membrane, the substrate

and product would be allowed to enter and leave via the membrane, and the need for exposing the substrate and product to the aqueous mitochondrial matrix would be eliminated.

Interestingly, the crystal structure of human ferrochelatase with bound substrate revealed major differences in the active site residues orientation and overall active site pocket shape. Thus, when protoporphyrin is bound, the "mouth" of the active site pocket is closed surrounding the substrate macrocycle in a snug fit. The two porphyrin propionates interact via hydrogen and ionic bonds with active site residues, ensuring a highly specific orientation of the substrate in the active site pocket (*91*). In comparison, the published *B. subtilis* ferrochelatase structures with and without the *N*-methylmesoporphyrin (*N*-MeMP) IX inhibitor do not show any differences in the active site amino acid side chain positions (*89*). Additionally, unlike *B. subtilis* ferrochelatase structure with bound *N*-MeMP in which the macrocycle adopts a distorted conformation of about 36°, in the case of human enzyme, the substrate appears to be significantly less distorted (approximately 11.5°) (*91*).

Of additional interest is the crystallographic observation that besides the porphyrin molecules bound to the active site of human ferrochelatase, "free" porphyrin has also been observed to be associated nearby, but outside the active site pocket. The observation was in accordance with previously published resonance Raman data that reported spectra characteristic to both planar and ruffled macrocycle conformations (*91;95*).

In terms of the crystal structure, the location of various point mutations that lead to the disease erythropoietic protoporphyria (EPP) are also of great interest, especially since these mutations are scattered throughout the protein, except two of them which are located within the active site pocket of the enzyme (*57*).

Ferrochelatase: Structure-Based Mechanism

In contrast to copper metabolism and iron-sulfur cluster assembly about which entire research fields have evolved over the past twenty years (*102-105*), relatively little progress has been made in understanding the molecular mechanism employed by ferrochelatase in order to insert iron into protoporphyrin IX. Interestingly, this is in spite of the fact that almost 50 years ago ferrochelatase was the first enzyme activity identified as being mandatorily involved in iron chelation (*22;106*).

A complete catalytic cycle involves acquisition of substrate, desolvation of ferrous iron, deprotonation of two pyrrole rings, macrocycle distortion to allow metallation, and, finally, planarization and product release (*19;107;108*). The metallation of porphyrin molecules by ferrochelatase has been proposed to occur through an ordered sequential bi-bi reaction mechanism. However, in addition to substrate metal selectivity, ferrochelatases have the challenge of binding and differentiating between two similar molecules: the substrate, protoporphyrin IX, and the product, protoheme IX. Since the only difference between the substrate and product bound by ferrochelatase consists in the absence/presence of an iron atom inserted in their planar macrocycles, respectively, ferrochelatase must either have a mechanism to distinguish between these two macrocycles, or to bind transiently both substrate and product such that the product will not remain bound to the enzyme following catalysis.

Based upon enzymatic studies that demonstrated strong competitive inhibition of ferrochelatase by N-alkyl porphyrins (*38*), Lavalee (*109*) proposed that N-alkyl porphyrins, because of their distorted macrocycle, may represent a transition state analog for the ferrochelatase reaction (*19;110*). Therefore, the initial general consensus regarding the mechanism by which ferrochelatase inserts iron into protoporphyrin IX suggested that the

macrocycle was distorted by ~ 30° upon binding to the protein, a view supported by the fact that this process was thermodynamically favored (*109-111*). Additional support for this model came from a variety of approaches including non-enzymatic solution studies (*112*), kinetic studies of the enzyme, characterization of metallation by catalytic antibodies (*113*), catalytic DNAs (*114*) and RNAs (*115*), and resonance Raman spectroscopic studies of both ferrochelatase and catalytic antibodies (*95;116;117*). These last studies revealed that ferrochelatase binds porphyrin and distorts it into a domed (*117*) or ruffled (*95*) conformation. This mechanistic model has been reviewed, discussed and refined, and was generally accepted. It was, however, the series of crystallographic studies on ferrochelatase from *B. subtilis* with bound *N*-MeMP that seemed to solidify this argument (*89*). A more recently reviewed catalytic model proposes that the enzyme undergoes minor structural motion as the substrate protoporphyrin binds in a distorted (ruffled or saddled) conformation (*107*). Metallation is then facilitated by macrocycle distortion and product release from the active site is due to the strain created by metal insertion (*88*).

Yet, the most recent structural data of human ferrochelatase challenged the view that the enzyme exhibits only minor backbone movement and opens slightly upon porphyrin binding (*89;91*). Specifically, a substrate bound form of human ferrochelatase revealed that the active site mouth closes around the porphyrin substrate with a select group of active site residues becoming reoriented in a way that substantially remodels the shape of the active site pocket (see Figure 1.5). A series of reactions revolving around the conserved His263 residue which is located centrally in the active site pocket and a complex active site hydrogen network appear to be involved in these structural rearrangements. As a result, the porphyrin macrocycle is distorted only about 12°, facilitating the metal iron insertion (*90;91;93*). Furthermore, the crystal structure of the product-bound form of the human ferrochelatase revealed that after iron insertion

additional secondary structure reorganization occurs that may facilitate heme release as highlighted in Figure 1.5 (*93*). These changes involve a previously identified π-helix that is structurally conserved in all ferrochelatases (*118*). In human ferrochelatase the conserved π-helix extends from Asp340 to Cys360. In the product-bound form of the enzyme, this conserved π-helix adopts an extended, unwounded conformation, which is relatively turned compared to the conformation adopted in the resting state of the enzyme (Figure 1.5). These changes are triggered by movement of His263 imidazole side chain and the position 6 of the propionate side chain of heme. The reorientation of the side chains results in an altered electrostatic surface contour in this region. The conserved acid patch is eliminated, the active site mouth opens, and a relatively non-polar "slide" is created for the heme to exit (*93*). Although unexpected, the considerable spatial movement that seems to occur during catalysis explains the kinetic data which previously demonstrated that the enzymatic metallation was irreversible (*119*).

In spite of the abundance of crystallographic data and the general agreement regarding some aspect of the catalytic mechanism, there remain a few unresolved issues including the identification of the ferrous iron donor, the identification of the route for substrate metal entry into the active site, identification of the residue(s) involved in metal insertion, and an explanation for the metal specificity observed in previous steady-state kinetic studies. What is known is that besides the physiologic metal substrate Fe^{2+}, both human and the *B. subtilis* ferrochelatases utilize several other divalent metal ions including Co^{2+}, Ni^{2+}, Cu^{2+} and Zn^{2+}, whereas Pb^{2+}, Hg^{2+}, Cd^{2+}, and Mn^{2+} serve as competitive inhibitors *in vitro* and *in vivo* (*120*). Some other divalent metal ions, including Mg^{2+} and Ca^{2+} are neither substrates nor inhibitors, whereas ferric iron, as well as other monovalent and trivalent metals cannot be used (*110*). Species-dependent specificity has been observed wherein the *B. subtilis* enzyme can incorporate Cu^{2+} but not Co^{2+}

(*19;51;110;110*), while the opposite has been observed for human ferrochelatase (*19*). Also, *Azospirillum brasilense* ferrochelatase was shown to be able to use Ni^{2+} and Cu^{2+} (*121*). Various mechanisms have been proposed to explain the different metal specificities (*96;122;123*). One point in common to the proposed models for metal specificity is that they involve a selection mechanism that occurs prior to the chelation reaction. It has been suggested that metal specificity results from the nature of active-site residues or from variations in macrocycle distortion (*96;108;122;123*), but arguments in favor of the later hypothesis became less attractive after structural studies on human ferrochelatase and theoretical modeling calculations indicated that the macrocycle undergoes only minor distortion upon binding to the active site (*91;124-126*). As stated above, the first hypothesis suggests that differences in the active-site residues may provide the mechanism for metal selectivity (*96;127*). For instance, at the top of the active-site pocket a methionine residue (Met76) is found in the human enzyme, while a tyrosine residue (Tyr13) is found in the *B. subtilis* ferrochelatase. However, both of these hypotheses were built on *in vitro* investigations of the steady-state kinetics in the presence and absence of inhibitor metals, as well as on crystallographic data, which are somewhat ambiguous. One important fact that needs to be considered is that recent investigations into the transient kinetics of human ferrochelatase revealed that the metal and porphyrin substrates bind rapidly, whereas the heme product release occurs slowly (*119*).

Based on *in vitro* structural studies on human ferrochelatase with inhibitor metals, Medlock and coworkers proposed in 2009 that metal specificity for the enzyme is determined by product release rather than a selection mechanism that occurs prior to metal chelation (*92*). These researchers suggest that neither the amount of macrocycle distortion, nor the specific amino acid residues present in the active site play a crucial role in selectivity, although active-site residues

may play some role in pre-chelation interactions, thus influencing the rate and order of competing metal insertion. Surprisingly, these authors discovered that inhibitory metals such as Hg^{2+}, Cd^{2+}, and Mn^{2+} all act as substrates and are inserted into the porphyrin macrocycle (*92*). However, the need for metal selectivity for ferrochelatase is debatable since *in vivo* specific metal chaperones (*128*) are expected to ensure that only ferrous iron is delivered to the enzyme.

The position of the catalytic metal binding site and the pathway involved in ferrous iron insertion is still a controversial debate to date, despite the multitude of crystal structures that have become available over the past decade, probably due to the fact that, except for the 1.7Å resolution structure of *B. subtilis* enzyme (*86*), none of the crystallographic structures of ferrochelatases published contain the ferrous iron substrate. Crystallographic data with surrogate metals such as Hg^{2+} and Co^{2+} suggest that there is an outer metal binding site near the surface facing the matrix of the mitochondrion, involving residues His231 and Asp383, which appear to be part of a channel that leads from the surface of the protein to the active site pocket where the porphyrin binds (*83;85*). Mutational studies of the human and yeast enzymes and the recent structure of *B. subtilis* ferrochelatase favor the argument that this invariant His residue is involved in Fe^{2+} binding and insertion into protoporphyrin IX (*85;86;90*).

The available human ferrochelatase crystal structures show that the conserved His263 residue in the active site pocket is positioned with its side chain facing one side of the porphyrin macrocycle (*86;91;122*). Two hypotheses exist for the role of His263, and there are biochemical, biophysical, and structural evidence to support both hypotheses. One hypothesis considers His263 and Glu343 as terminal ligands for iron, which is then inserted into porphyrin from the same side as His263 (*86*). The second hypothesis holds that the metallation is occurring from Arg164 and Tyr165 residues located along the conserved π-helix on the opposite site of His263,

which abstract two pyrrole protons that are then shuttled away from the active site via Glu343 and other residues in the π-helix (*90*). All site-directed mutants of His263 have no measurable activity (*90*) and this strongly suggests that regardless of whether it is an iron ligand or not, this residue plays a crucial role in catalysis. Yet, while site directed mutagenesis studies and the crystal structures available provide much needed insight, they have not answered the lingering question: how is iron transported to the active site and what structural features are involved? Recent hydrogen/deuterium-exchange mass spectrometry studies demonstrate that in solution iron is transported to the catalytic active site where the porphyrin macrocycle binds through a channel that extends from the surface of the protein. The results provide support for the second hypothesis by indicating that in the active site of ferrochelatase, residues on the side of the pocket opposite to residue His263 are most likely involved in the formation of a terminal iron binding site (*129*).

Another question that remains to be answered with respect to the catalytic mechanism of ferrochelatase concerns the identity of the metal substrate donor. Some researchers believe that frataxin may provide iron to the ferrochelatase-catalyzed last step of heme biosynthesis (*130;131*). However Friedreich ataxia patients who suffer from loss of frataxin activity (*132*) do not demonstrate significant anemia, suggesting that frataxin is not essential for heme synthesis and erythropoiesis, or that frataxin-deficiency is not present in erythropoietic tissues of Friedreich ataxia patients.

The [2Fe-2S] Center in Ferrochelatases

The presence of a [2Fe-2S] center in ferrochelatases was first suggested in 1994 by Dailey et al. in the human form of the enzyme (*48*). Later that year, spectroscopic data provided definitive evidence for the presence of a [2Fe-2S] cluster in both human and mouse

ferrochelatases (*82;133*). The cluster was subsequently found in chicken (*49*), *X. laevis* (*49*), and *D. melanogaster* (*50*) ferrochelatases, as well as in enzymes from yeast *S. pombe (84), N. crassa, C. albicans* and *A. niger*.

In general, [2Fe-2S] clusters are the simplest type of Fe–S clusters found in nature, and are able to undergo redox cycling between +2 and +1 core oxidation states. The vast majority of [2Fe-2S] clusters are bound to proteins via four cysteinyl ligands, with complete tetrahedral coordination at each Fe site. These all cysteinyl-ligated [2Fe-2S] clusters have low redox potentials ranging from +100 to -460 mV. Another large group of [2Fe-2S] clusters denominated Rieske-type [2Fe-2S] centers have two histidyl ligands at one Fe site (*134*). Due to the more electropositive nature of the histidine ligands present at the Fe site, Rieske-type [2Fe-2S] clusters have higher redox potentials, ranging from +380 to -150 mV, and redox-dependent protonation of histidyl imidazole ring facilitates coupling of proton and electron transfer (*134*). However, there exist a few exceptions from these two major categories of [2Fe-2S] centers, including the [2Fe-2S] centers with one non-cysteinyl ligand, such as those found in some succinate dehydrogenases and sulfide dehydrogenases which have one aspartate ligand (*135;136*), or the sacrificial [2Fe-2S] cluster in biotin synthase that has one arginine ligand (*137*). Additionally, the functionally ill-defined [2Fe-2S] cluster in the MitoNEET protein which has one histidine ligand (*138-140*) is another example of such metal center that does not belong to any of the two major classes of [2Fe-2S] clusters. Based on structural and electronic properties, the [2Fe-2S] clusters are considered the building block of almost all types of higher nuclearity Fe–S clusters.

The electronic, magnetic and vibrational properties of $[2Fe\text{-}2S]^{2+,+}$ clusters have been extensively characterized using various spectroscopic techniques such as UV-visible absorption, EPR, resonance Raman, CD, VTMCD, Mössbauer, and ENDOR. All known examples of

oxidized $[2Fe\text{-}2S]^{2+}$ clusters are diamagnetic, with a ground state spin $S = 0$ as a result of antiferromagnetic coupling of two high-spin ($S = 5/2$) Fe^{3+} centers. On the other hand, all known types of reduced $[2Fe\text{-}2S]^{+}$ centers are paramagnetic species with an $S = 1/2$ ground state as a result of antiferromagnetic coupling of valence-localized high-spin ($S = 5/2$) Fe^{3+} and ($S = 2$) Fe^{2+} centers.

As expected, the [2Fe-2S] cluster in human ferrochelatase was found to be EPR silent in the oxidized form indicative of a $S = 0$ $[2Fe\text{-}2S]^{2+}$ cluster. When reduced in the presence of sodium dithionite, the cluster exists in a mixed valence state with a $S = 1/2$ $[2Fe\text{-}2S]^{+}$ core and high-spin (S=5/2) Fe^{3+} centers, which exhibits a nearly rhombic EPR signal with g-values of 2.00, 1.94, and 1.91 (*82*). Although similar to EPR spectra of [2Fe-2S] clusters from *Clostridium pasteurianum* and *Azotobacter vinelandii* ferredoxins, the EPR spectrum of $[2Fe\text{-}2S]^{+}$ cluster from human ferrochelatase is distinct from all spectra of [2Fe-2S] clusters characterized to date (*141*). The midpoint redox potential of the cluster from the human (*74*) and mouse (*142*) enzymes have been reported to be –450 mV and -405 mV, respectively. No midpoint potentials have been reported for any microbial cluster-containing ferrochelatases. The UV-visible absorption spectrum of human ferrochelatase exhibits bands at 330, 460 and 550 nm, indicative of $[2Fe\text{-}2S]^{2+}$ clusters. Some preparations of the enzyme may possess a small amount of bound heme product that contributes to the 410-425 nm peak (*48*).

The spectroscopic properties of human ferrochelatase [2Fe-2S] cluster are consistent with coordination of the cluster via protein cysteine residues (Figure 1.6) (*82*). Site-directed mutagenesis, as well as crystallographic and spectroscopic studies suggested an unusual Cys-X_{206}-Cys-X_2-Cys-X_4-Cys coordinating motif for the [2Fe-2S] cluster in human ferrochelatase (*50;82;141*). The results indicated that three of the four conserved cysteine residues involved in

ligating the [2Fe-2S] cluster are located in the 30-residue C-terminal extension (*141*). Although the overall pattern of coordinating cysteines in ferrochelatase is similar to that found in simple [2Fe-2S]-containing ferredoxins, *e.g.* Cys-X_4-Cys-X_2-Cys-X_{29}-Cys in chloroplast ferredoxins (*143;144*), the remote cysteine is located closest to the NH_2 terminus in ferrochelatase (*50*). The crystal structure of human ferrochelatase provides detailed information on the environment of the [2Fe-2S] cluster and its location in the protein as seen in Figure 1.4 and Figure 1.5. Both [2Fe-2S] clusters are located at the dimer interface, each cluster being solvent accessible and located approximately 15Å away from the center of the active-site pocket (*83*).

The [2Fe-2S] cluster present in the human ferrochelatase exhibits a number of interesting features. Resonance Raman and variable-temperature magnetic circular dichroism measurements on the human enzyme suggested different dihedral angles, spatial orientation, and surrounding environment for the coordinating cysteine residues of the [2Fe-2S] cluster compared to other structurally characterized [2Fe-2S] clusters. Indeed, the initial interpretation of the resonance Raman results was that one of the ligands coordinating the [2Fe-2S] cluster might be oxygenic in nature (*82;141*). However, the crystal structure of human ferrochelatase revealed that two of the coordinating cysteine Fe-S_γ-C_β-C_α dihedral angles were close to 180°, explaining the unusual resonance Raman and VTMCD data (*83*). As a consequence of this unique geometry, the peptide backbone is moved further away from the [2Fe-2S] cluster, resulting in a distinctly more "open" binding site. Crystallographic results also indicate that unlike most [2Fe-2S] cluster-containing proteins, the ligand geometry of the [2Fe-2S] cluster from human ferrochelatase minimizes any potential hydrogen bonding from the backbone imide protons. As a result, each cluster is only bonded by the ligating cysteine residues and has no additional hydrogen bonds. However, despite the limited interactions between the [2Fe-2S] cluster and the C-terminal extension, the presence

of the cluster is required for enzyme activity in all eukaryotic ferrochelatases (*57*). Interestingly, crystallographic results indicate that no significant changes occur in the cluster-binding domain upon binding of substrate protoporphyrin IX, suggesting that the site is somewhat rigid (*83*). This is similar to the open and rigid active site of nitric oxide synthase (*145*); taken together, these observations may be consistent with a role for the cluster as a NO sensor (see below).

Although the initial published bacterial ferrochelatase sequences did not contain the carboxyl-terminal domain and their spectral properties revealed no evidence of an Fe-S cluster, it is now apparent that a small number of bacterial ferrochelatases, including *C. crescentus* and *M. tuberculosis* (*53*), also possess a C-terminal extension of a length similar to that of animal ferrochelatases, and that this region contains three [2Fe-2S] cluster-ligating cysteine residues. However, mutagenesis studies indicate that the spacing between these residues (C-X_6-C-X-C and C-X_8-C-X_4-C for *C. crescentus* and *M. tuberculosis*, respectively) is unlike that found in animal and *S. pombe* ferrochelatases (C-X_2-C-X_4-C) (*48-50;53;57;84*) (see Figure 1.2 and Table 1.1). More significant was the discovery that the amino-proximal cluster-ligating cysteine residue of animal (C196 in human ferrochelatase) and *S. pombe* ferrochelatase (C162) was absent in *C. crescentus (53)*. The identity of the four amino-acid residues ligating the [2Fe-2S] cluster in *C. crescentus* ferrochelatase was revealed by site-directed mutagenesis studies to be C158, C332, C339, and C341, to yield a C-X_{173}-C-X_6-C-X-C binding motif that is unique among all known [2Fe-2S] cluster-containing proteins (see Figure 1.2 and Table 1.1). In *M. tuberculosis* ferrochelatase the putative amino-proximal cysteine ligand is located two or three amino acid residues away from the corresponding cysteine of animal and *S. pombe* ferrochelatases, but this has yet to be confirmed by mutagenesis studies (see Figure 1.2 and Table 1.1) (*53*). As mentioned above, *R. prowazekii* was paired with *C. crescentus* by visual alignment of just

bacterial ferrochelatase primary sequences, whereas *S. coelicolor* was paired with *P. freudenreichii*. Close examination of *C. crescentus* and *R. prowazekii* primary sequences reveals that the two enzymes share a similar three cysteine motif (C-X_6-C-X-C) in the carboxyl-terminal region, possibly indicating that the [2Fe-2S] center in *R. prowazekii* ferrochelatase might be coordinated in a similar fashion to that from *C. crescentus* enzyme. Interestingly, *S. coelicolor* and *P. freudenreichii* ferrochelatases appear to possess yet a different three cysteine arrangement (C-X_3-C-C) in the this region (see Figure 1.2 and Table 1.1) (*53*). However, the implication of these cysteine residues in ligating a [2Fe-2S] centers from *R. prowazekii, S. coelicolor* and *P. freudenreichii* ferrochelatases remains to be determined.

The recent discovery of a [2Fe-2S] center in the bacterial *M. xanthus* ferrochelatase that does not have a C-terminal extension adds further diversity to the [2Fe-2S] centers in ferrochelatases (*52*). Mutagenesis studies indicate that this cluster is ligated by four cysteine residues present in a centrally located cysteines-rich insertion of approximately 20 amino acid residues, with the coordination motif for the [2Fe-2S] cluster being C-X_5-C-C-X_9-C. Sequence alignments indicate that analogous clusters are present in ferrochelatases from several other bacterial organisms, including *A. vinelandii*, *Bdellovibrio bacteriovorus,* and *Pseudomonas syringae* (see Figure 1.2 and Table 1.1) *(52)*.

In contrast to eukaryotic ferrochelatases, [2Fe-2S] cluster-lacking mutants of *C. crescentus* and *M. xanthus* ferrochelatases appear to retain up to 5% catalytic activity *in vitro*, whereas no enzymatic activity was observed when the C-terminal extension was truncated in *C. crescentus* enzyme (*52;53*). However, due to a current lack of crystallographic data available for any of the cluster-containing bacterial ferrochelatases, the significance of this observation is unclear at present.

Interestingly, in addition to the protoporphyrin IX ferrochelatases discussed thus far, iron-sulfur clusters have also been identified in other branches of tetrapyrrole metabolism, such as the [2Fe-2S] center that has recently been shown to be present in sirohydrochlorin ferrochelatase from plant *Arabidopsis thaliana (146).*

***Arabidopsis thaliana* Sirohydrochlorin Ferrochelatase**

*A. thaliana s*irohydrochlorin ferrochelatase, AtSirB Fc*,* catalyzes the last step of siroheme biosynthesis, which in plants is an important cofactor for only two enzymes: sulfite and nitrite reductases. A [4Fe-4S] cluster siroheme active site is present in both of these enzymes and catalyzed the six electron reduction of sulfite and nitrite, respectively (*147;148*). Therefore, assimilation of all inorganic S and the majority of N in the biosphere depends on the availability of siroheme and without siroheme, there would be no reduced S for the synthesis of the amino acids cysteine and methionine, and for the biogenesis of Fe-S centers.

Siroheme is synthesized from the tetrapyrrole primogenitor uroporphyrinogen III in three steps which involve methylation, oxidation and ferrochelation, a process that in higher plants occurs in plastids (Figure 1.7) (*146;149*). Methylation of uroporphyrinogen III intermediate directs the process toward siroheme synthesis, whereas decarboxylation of this precursor would steer the reaction toward heme and chlorophylls synthesis (*150*), thus representing the first branch point in the tetrapyrrole biosynthetic pathway (Fig. 1.7). For siroheme synthesis metallation results in the formation of dihydrosirohydrochlorin (*151*) and is carried out by uroporphyrinogen III methyltransferase, an enzyme localized to the chloroplast in plant *A. thaliana (152).* To complete the biosynthesis of siroheme, dihydrosirohydrochlorin has to be oxidized to sirohydrochlorin, followed by iron chelation. The last step of siroheme biosynthesis, namely the insertion of ferrous iron into sirohydrochlorin to form siroheme, is carried out by

sirohydrochlorin (SirB) ferrochelatase (*153;154*), an enzyme that belongs to class II tetrapyrrole biosynthetic chelatases. Chelatases from this class such as protoporphyrin IX ferrochelatases (*57;75*), the sirohydrochlorin cobaltochelatases associated with cobalamin biosynthesis, CbiK (*155*) and CbiX (*156*), as well as SirB ferrochelatase exist as both monomers and homodimers (*157*). Despite low sequence homology (~10%), protoporphyrin IX ferrochelatases and CbiK have been shown to share a high level of structural similarity as observed from crystallographic data (*75;155*), suggesting that these proteins have probably arisen from a common ancestor by divergent evolution. AtSirB Fc is also expected to be structurally similar to CbiK, although they display low sequence homology (less than 15%) (*146*). One interesting observation is that the sequence comparison of the mature form of AtSirB Fc reveals that the plant enzyme appears to be only about half the size of the bacterial SirB ferrochelatases (Figure 1.8) (*146*).

Spectroscopic characterization of the mature form of AtSirB Fc revealed the presence of a [2Fe-2S] cluster, the first such center reported for higher plant ferrochelatases (*146*). EPR analysis of dithionite-reduced AtSirB Fc revealed a rhombic signal with g-values of 2.04, 1.94, and 1.90, and relaxation behavior characteristic of a $S = 1/2$ $[2Fe\text{-}2S]^{+}$ center. The apparent midpoint potential for cluster reduction was determined to be -370 mV, although the reduced cluster is labile and readily degraded. Based on amino acid sequence comparison, it has been proposed that the [2Fe-2S] cluster is ligated by a set of three cysteine residues located in the C-terminus ($C\text{-}X_2\text{-}C\text{-}X_5\text{-}C$), and a conserved central cysteine, reminiscent of the mammalian protoporphyrin ferrochelatases (Figure 1.8) (*146*).

Hypotheses Regarding the Role of [2Fe-2S] Cluster in Ferrochelatases

Since the discovery of the [2Fe-2S] cluster in human and mouse ferrochelatases in 1994 (*48;133*), there has been considerable interest concerning its function and evolution.

Recent evidence has demonstrated the functional diversity of biological Fe-S clusters (*105*). Although the majority of biological Fe-S clusters are involved in electron transport, it is now evident that numerous redox (e.g., nitrogenases, hydrogenases, radical-SAM enzyme superfamily) and nonredox enzymes (e.g., aconitase and other (de)hydratases) utilize homometallic or heterometallic Fe-S clusters for substrate binding and activation. In addition, Fe–S clusters are also responsible for sensing environmental or intracellular conditions in order to regulate enzyme activity or gene expression at the translational or transcriptional level (*158*). The role of Fe-S clusters as sensors that react to certain stimuli is achieved via proteins which use distinct sensing mechanisms involving cluster assembly or degradation, cluster conversion or cluster redox chemistry. The resulting change in protein structure induces changes in the DNA binding ability, thus triggering gene regulation (e.g., IRP1 which is involved in Fe-sensing (*159-162*); FNR which is involved in O_2 sensing (*158;163-167*), and SoxR which is involved with oxidative stress sensing (*168-171*)). The key role of Fe-S clusters in determining the protein structure makes them important regulatory targets for controlling enzyme activity in response to external stimuli such as superoxide concentrations. In this case, the regulatory control can be accomplished via cluster degradation/reassembly (e.g., the [4Fe-4S] cluster from phosphoribosylpyrophosphate amidotransferase in *B. subtilis* acts as an O_2 sensor (*172;173*)).

Currently the only answers concerning the role of the [2Fe-2S] clusters in ferrochelatases are negative ones. Since organisms such as plants, the yeast *S. cerevisiae*, and many prokaryotes possess a ferrochelatase that lacks the cluster and still has enzymatic activity, it is clear that the $[2Fe\text{-}2S]^{2+}$ cluster does not play a direct role in catalysis (*57;82*). Likewise, there is no direct evidence that it could be involved in ferric iron reduction since ferrochelatase assays always have ferrous iron and removal of the cluster destroys the enzyme activity (*52;53;82;83*). A role in the

dimerization motif alone is not supported by the discovery of *M. tuberculosis* ferrochelatase, which is monomeric as isolated, and contains both a C-terminal domain and a [2Fe-2S] cluster (*57;83*). In vivo experiments demonstrated that a decrease in cellular ferrochelatase activity occurred when cells were exposed to NO (*174*) and *in vitro* studies have demonstrated that NO inactivates mammalian ferrochelatase via destruction of the [2Fe-2S] cluster (*175*). The sensitivity of mammalian [2Fe-2S] cluster to NO led to the suggestion that it may play a role in local immune response preventing bacteria from using heme synthesized by the host organism (*175*). The subsequent finding of a cluster in *Drosophila* (*50*), yeast *S. pombe* (*53*), and bacterial ferrochelatases diminish but do not eliminate support for this hypothesis. An alternative hypothesis that has arisen from the discovery of extensive [2Fe-2S] cluster trafficking in both eukaryotic and prokaryotic cells, is that the [2Fe-2S] cluster-binding site in ferrochelatases serves a sensor for the cellular [2Fe-2S] cluster concentration in order to regulate the use of Fe for heme and Fe-S cluster biosynthesis. As discussed below, monothiol glutaredoxins have been shown to participate in the storage and trafficking of [2Fe-2S] clusters and to play important *in vivo* roles in both heme and Fe-S cluster biosynthesis. Consequently, there is a pressing need to investigate the possibility that monothiol glutaredoxins serve as the cluster donors to ferrochelatases in order to evaluate this hypothesis.

Role of Monothiol Glutaredoxins in Fe-S Cluster Homeostasis

Glutaredoxins (Grxs) are small ubiquitous redox proteins representing a group of thioltransferases that were initially thought to be important solely for the reduction of oxidized glutathione (GSH) and/or for removal of GSH modifications of proteins. Under oxidative stress, the cysteine thiol groups of many proteins are protected by the reversible addition of the tripeptide GSH (γ-Glu-Cys-Gly), in a process known as glutathionylation, and the removal of

GSH requires reduction of the disulfide bond formed between the cysteine of GSH and the cysteine thiol of target proteins (*176-178*). However, over the last decade extensive research on this group of proteins lead to the proposal that Grxs play many additionally functions. Of these, the role attributed to the monothiol Grxs (CGFS active site) in Fe regulation and Fe–S cluster biogenesis in baker's yeast (*179;180*) is most relevant to the role of [2Fe-2S] cluster in ferrochelatases.

Two major classes of Grxs have been recognized, dithiol Grxs which generally contain CXXC active site motifs and monothiol Grxs, which contain a CGFS active-site motif. Dithiol Grxs catalyze the reduction of thiol disulfides involving two cysteinyl groups and also of mixed disulfides between a protein cysteine residue and a GSH group (*181*). In contrast, the monothiol Grx mechanism of action exclusively involves the deglutathionylation of mixed disulfides (*182*). Discovery of several Grx isoforms with diverse active site sequences, as well as fusion proteins comprising a Grx domain resulted in the reorganization of these proteins into six classes based not only on the active site sequence, but also on conserved motifs involved in GSH binding (*183;184*). Classes I and II are the most widespread, being found, with a few exceptions, in most prokaryotic and eukaryotic organisms (*184;185*). Of interest to this study are Grxs belonging to class II shown in Figure 1.9.

The involvement of Grxs in Fe-S biogenesis was first indicated based on gene-disruption studies in yeast *S. cerevisiae* Grx5 (*180;186*). As of today seven Grxs, and at least one Grx-like protein have been identified in *S. cerevisiae*, of which three belong to class II monothiol Grxs with CGFS active sites, namely the cytosolic Grx3 and Grx4, and the mitochondrial Grx5. The phenotypic defects of Grx5 deficiency in *S. cerevisiae* manifest as impaired respiratory growth and increased sensitivity to oxidative stress due to inactivation of the mitochondrial aconitase and succinate dehydrogenase, two Fe–S cluster containing enzymes, as well as iron

accumulation inside the cell (*179*). These phenotypes were suppressed by overexpression of two Fe-S cluster biosynthetic proteins, SSQ1 or ISA2, but not by the addition of the dithiothreitol (DTT), suggesting that defects of the Grx5 mutant were not due to the alteration of intracellular redox potential, but rather to a specific role in biogenesis of Fe-S clusters (*180;186;187*). The ability of other class II monothiol Grx homologs from both prokaryotic and eukaryotic organisms to rescue Fe-S cluster synthesis in Grx5 mutant yeast, suggested that the function of Grx5 has been conserved during evolution (*188;189*). Furthermore, by radiolabelling yeast cells with ^{55}Fe, Mühlenhoff and coworkers demonstrated an increase of iron associated with the primary scaffold protein Isu1p upon deletion of Grx5, thus providing *in vivo* evidence for a role for Grx5 in accepting clusters preassembled on Isu1 (*186*). In addition, the specific interaction of Grx5 with the A-type Fe-S cluster carrier proteins as indicated by two hybrid interaction studies (*190*), as well as the direct physical interaction *in situ* between Grx5 and Isa1 and Isa2 demonstrated via bimolecular fluorescence complementation experiments in yeast *S. pombe (191),* further support the proposal that yeast Grx5 functions in cellular cluster trafficking.

The human genome contains four Grxs, two dithiol Grxs, Glrx1 and Glrx2, a cytosolic multidomain monothiol Grx, Glrx3 (aka PICOT) that appears to be analogous to the yeast Grx3/4 protein (*178*), and the mitochondrial single-domain monothiol, Glrx5, a yeast Grx5 homolog conserved among eukaryotes. In higher plants more than 30 distinct Grx genes are expressed, but little is currently known concerning their functional diversity (*192*).

To date, numerous recombinant mono- and dithiol Grx proteins have been purified with a bound intermolecular [2Fe-2S]$^{+2}$ cluster that is ligated between a Grx dimer by the active-site cysteines of two Grxs and by two GSH peptides *(176;193-197)*. The [2Fe-2S] cluster assembled by monothiol Grxs is labile and decays rapidly on exposure to oxygen, unlike those ligated by

dithiol Grxs which exhibit decreased oxygen lability and have distinct spectroscopic properties, suggesting that they may play different roles (*176;198*). Recently, two plant chloroplastic monothiol Grxs, the plastidial GrxS14 and GrxS16, were shown to incorporate an labile [2Fe-2S] cluster *in vitro* upon reconstitution in the presence of GSH, leading to the suggestion that Grx5-like proteins may function as scaffold or carrier proteins in chloroplastic Fe-S cluster biogenesis (*176*). This is further supported by CD studies which have shown that chloroplastic GrxS14 can rapidly and stoichiometrically transfer its intact [2Fe-2S] cluster to the apoform of plant chloroplast ferredoxin (Fdx) (*176*). The ability of CGFS Grxs to assemble and efficiently transfer [2Fe-2S] clusters to physiologically relevant acceptor proteins points to potential roles for these proteins in the *de novo* assembly, trafficking and storage of Fe−S clusters and as sensors for the cellular Fe−S cluster status.

Mutagenesis studies, as well as structural characterization of both dithiol and monothiol Grxs indicate similar and complete cysteinyl ligation for the [2Fe-2S] cluster, in accordance with the published spectroscopic and analytical data. The cluster is ligated at the center of the Grx homodimer by the active site cysteine residues of each monomer and by the cysteine moiety of two GSH molecules as shown in Figure 1.10 (*193;195;197;199*). Examination of the crystal structures of monothiol *E. coli* Grx4 and dithiol *H. sapiens* Grx2 or plant GrxC1 homodimers reveal tetrahedral environment for each of the iron atoms of the [2Fe-2S] cluster, as well as the fact that a lysine residue, previously shown by site directed mutagenesis to be important for Fe-S cluster assembly (*198*), makes contact with both the GSH and the adjacent Grx. Yet, the relative orientation of the monomers is different in monothiol *E. coli* Grx4 compared to dithiol human Grx2 and plant GrxC1. Compared to the dithiol Grxs, one monomer in the monothiol Grx is rotated 90° relative to the other, in a fashion that allows direct interaction between the monomers

(Figure 1.11). Moreover, structure overlay of *E. coli* Grx4 monomeric apo-, and homodimeric cluster-bound forms indicate important conformational modifications upon cluster binding that involve movement of two of the amino acid residues important for the assembly of the [2Fe-2S] cluster. As a result, the active site Cys30 and Lys22 residues are moved by 7.0Å and 6.4Å, respectively from their position in the cluster bound form, resulting in a conformation in which it would be difficult to establish the necessary interactions for cluster binding (Figure 1.10A). Unlike *E. coli* monothiol Grx4, superimposition of human dithiol Grx2 apo monomer, GSH-bound monomer and cluster-bound homodimer structures revealed only minor conformational differences as shown in Figure 1.10B.

The recently published crystal structure of human monothiol Grx5 revealed a novel tetrameric organization involving two [2Fe-2S] cluster-bridged Grx5 dimers rather than the single [2Fe-2S] cluster-bridged Grx dimer observed in the crystal structure of *E. coli* monothiol Grx4 (*196;199*). However, similar to *E. coli* Grx4 structure, the human Grx5 crystal structure indicates that the [2Fe-2S] clusters are ligated in a head-to-toe fashion via two active site Cys residues and by the cysteine moiety of two GSH molecules, while Lys59 interacts with one GSH molecule and the adjacent monomer. Moreover, the human Grx5 structure also has one monomer rotated by 90° when compared to the dithiol Grx structures. Of interest is the observation that in human Grx5, the [2Fe-2S] cluster is completely buried and solvent inaccessible, with the GSH molecules as well as the position of the Phe69 side-chain apparently further reducing the solvent accessibility of the cluster (*199*).

The structural differences observed for the [2Fe-2S] cluster-bound form of the monothiol and dithiol Grxs are believed to account for the differences observed in the electronic environment, therefore explaining the different spectroscopic properties between monothiol and

dithiol Grxs as reported by Bandyopadhyay and coworkers (*176*). Taken together, these findings indicate that cluster-bound monothiol Grxs need to undergo a major conformational rearrangement in order to release the [2Fe-2S] cluster, with the thermodynamic driving force for cluster release being attaining the stable structure of the apo monomer. The ability of monothiol Grxs to incorporate and release [2Fe-2S] clusters is consistent with roles in storage, transport, and delivery of clusters to apo acceptor proteins.

Role of Fe-S Cluster Assembly Machinery in the Regulation of Heme Biosynthesis

Iron homeostasis in mammals is largely regulated at the posttranscriptional level (*21;200;201*) by the iron regulatory proteins IRP1 and IRP2 (*161;202*). Currently it is not clear what form of iron is sensed by IRP2, but IRP1 senses Fe by assembling a [4Fe-4S] cluster to yield a holoform that functions as a cytosolic aconitase. In the apoform, IRP1 undergoes a substantial conformational change and functions as an iron responsive element (IRE) -binding protein which accommodates the IRE stem-loop structure in mRNAs of several iron-regulated proteins, such as ferritin, ALAS2, ferroportin, and mitochondrial aconitase (*160*). The binding of IRP1 to the IRE located at the 5'-untranslated region (UTR) of the mRNA blocks the passage of the scanning ribosome and thus inhibits translation initiation of those proteins.

The association of the Fe-S cluster with IRP1 critically depends on the function of several components of the Fe-S cluster assembly system, hence, it is expected that Fe-S protein biogenesis will influence iron regulation. This has been directly shown for the human Isu proteins in that the depletion of mitochondrial Isu1 by RNAi resulted in increased iron levels inside the cell (*203*). The Fe-S cluster assembly machinery had a similar impact on the cellular iron status of the zebrafish mutant *shiraz*, which was deficient in the mitochondrial monothiol glutaredoxin Grx5 (*204*). The defect in zebrafish Grx5 knockout mutant resulted in lower heme

levels which were caused by low expression of ALAS2, the mitochondrial-located erythroid-specific δ-aminolevulinate synthase that catalyzes the first committed step of heme biosynthesis. The deletion of Grx5 in zebrafish resulted in severe hypochromic anemia and was embryonically lethal. It was reasoned that by losing its Fe-S cluster due to deficiency of Grx5, the apoform of IRP1 from zebrafish was activated to an IRE-binding protein, thus decreasing the translation of ALAS2, which contains IRE in its 5' - UTR (Figure 1.12). Expression of ALAS2 RNA lacking a functional 5'-IRE restored heme synthesis supporting this interpretation. Likewise, depletion of IRP1 by the morpholino technique resulted in normal heme biosynthesis (*204*). These elegant studies suggested an intimate connection between Fe-S cluster biogenesis and heme biosynthesis in the erythroid system via the regulatory function of IRP1 on ALAS2 translation. It is therefore expected, although not directly shown, that zebrafish Fe-S cluster component Grx5 has a direct impact on iron regulation and heme regulation.

A complementation experiment has demonstrated that human Glrx5 is able to rescue Fe-S cluster synthesis in Grx5 mutant yeast, suggesting that the function of Glrx5 has been conserved during evolution (*188*). In humans, the Glrx5 mutation causes microcytic sideroblastic anemia (SA), as shown by a recently identified male patient from Italy (*205*). Sideroblastic anemias are anemias characterized by the presence of ring sideroblasts, which represent erythroid precursor cells that contain iron-overloaded mitochondria which congregate in a ring around the nucleus and are detected by the Prussian blue stain for iron. However, although Glrx5 knockdown affects both Fe-S cluster biogenesis and heme synthesis pathways and affects almost all tissues, most tissues do not manifest significant pathology, perhaps because other proteins can compensate for the defect of Fe-S cluster biogenesis and cells other than erythroid cells do not need to make large amounts of heme. Despite the association of deficiency of Grx5 in both zebrafish (*204*) and

a human patient (*205*) with anemia, the molecular relationship between the anemia and the status of Fe-S cluster assembly has not been characterized thus far in Glrx5-deficient mammalian cells.

Of significant importance are a set of recent *in vivo* studies which have shown that depletion of the human IscU protein leads to defective Fe-S cluster biogenesis and to mitochondrial iron overload in skeletal muscle. Without sufficient Fe-S cluster biogenesis, protoporphyrin IX ferrochelatase is unstable and is significantly degraded in patient muscle (*206*). IscU is the major scaffold protein upon which the transient Fe-S clusters are initially assembled and from which they are then delivered to recipient proteins (*103-105;207*). Thus, normal Glrx5 activity allows expression of ALAS2 and ferrochelatase to increase during hemoglobinization for erythropoiesis (*208*), and based on the discovery that the ferrochelatase is readily degraded in the absence of its Fe-S cluster (*206*) and that ferrochelatase protein levels are substantially decreased in Glrx5 deficient patient lymphoblasts (*208*), seems reasonable to propose that Glrx5 may deliver the preassembled [2Fe-2S] cluster to ferrochelatase.

Summary of Present Work

The above discussion clearly demonstrates that more studies at both cellular and molecular levels are required to clarify the role and diversity of the [2Fe-2S] clusters in bacterial, plant and mammalian ferrochelatases. Hence, this thesis reports on the preparation, characterization and comparison of the properties and NO sensitivity of the [2Fe-2S] clusters in ferrochelatases from a variety of different organisms. In addition, the role of monothiol Grxs in the maturation of the functional [2Fe-2S] cluster-bound forms of ferrochelatases has been assessed by *in vitro* cluster transfer studies, in order to address the possibility that the [2Fe-2S] cluster binding site serves as a sensor of the cellular iron-sulfur cluster status.

Chapter 2 reports the spectroscopic characterization and comparison of $[2Fe\text{-}2S]^{2+,+}$ centers from recombinant ferrochelatases isolated from a variety of both prokaryotic and eukaryotic organisms, including the microbial *M. tuberculosis*, *M. xathus, C. crescentus, S. coelicolor*, *P. freudenreichii,* the yeast *S. pombe* and the mammalian *H. sapiens*. The combination of UV-visible, room temperature CD, and resonance Raman spectroscopic techniques indicate different electronic and vibrational properties for the $[2Fe\text{-}2S]^{2+,+}$ clusters present in each of the ferrochelatases investigated. EPR studies of the dithionite-reduced enzymes show the presence of paramagnetic S=1/2 species with nearly rhombic EPR signals, and g values ranging from 1.89 to 2.054. The reduced [2Fe-2S] centers in ferrochelatases are labile and rapidly degrade in the presence of dithionite.

Chapter 3 reports the analytical and spectroscopic characterization of [2Fe-2S] cluster from *A. thaliana* SirB ferrochelatase (AtSirB Fc), as well as the *in vitro* CD studies of cluster transfer between [2Fe-2S] cluster-loaded *A. thaliana* monothiol GrxS14 and cluster-depleted form of AtSirB Fc. Analytical gel filtration studies on AtSirB Fc indicate either dimeric or tetrameric organization of the protein as a function of pH, result which is also reflected in the UV-visible absorption, CD, and resonance Raman spectroscopic properties of [2Fe-2S] cluster from AtSirB Fc at different pHs. EPR studies of the dithionite-reduced AtSirB Fc indicate a $[2Fe\text{-}2S]^{2+}$ center more susceptible to reduction at pH > 8.0. Additionally, *in vitro* kinetic studies monitored by CD spectroscopy indicate that [2Fe–2S] clusters *A. thaliana* monothiol GrxS14 is rapidly and quantitatively transferred to apo chloroplast AtSirB Fc.

Chapter 4 reports the effect of the nitric oxide donor DEAE NONOate on the [2Fe-2S] clusters from the microbial *M. xanthus* and *C. crescentus* ferrochelatases, the yeast *S. pombe* ferrochelatase, the vertebrate *Zebrafish* ferrochelatase, and the mammalian human

ferrochelatase. Parallel studies using UV-visible absorption and EPR spectroscopy indicate that the [2Fe-2S] clusters from all ferrochelatases investigated are degraded in the presence of the NO donor DEAE NONOate, concomitant with the formation of monomeric dinitrosyl iron complex (DNIC) species. Taken together with the results indicating that the rates for the [2Fe-2S] cluster degradation/DNIC formation do not differ significantly among the five ferrochelatases studied, we hypothesize that the cluster might be degraded by NO and or reactive oxygen species in response to certain cellular conditions.

Abbreviations: ferrochelatase, Fc; erythropoietic protoporphyria, EPP; sideroblastic anemia, SA; 5-aminolevulinic acid, (ALA); 5-aminolevulinate synthase, ALAS2; *Homo sapiens, H. sapiens, Hs; Myxoccocus xanthus, M. xanthus; Streptomyces coelicolor, S. coelicolor; Propionibacter freudenreichii, P. freudenreichii; Arabidopsis thaliana, A. thaliana*; *N*-methylmesoporphyrin IX, *N*-MeMP; sirohydrochlorin, SirB; glutaredoxin, grx/glrx; iron responsive protein, IRP; iron responsive element, IRE; untranslated region, UTR; glutathione, GSH; cysteine, Cys; lysine, Lys; dinitrosyl iron complex, DNIC; circular dichroism, CD; variable temperature magnetic circular dichroism, VTMCD; electron paramagnetic resonance, EPR; nitric oxide, NO; dinitrosyl iron complex, DNIC; fumarate nitrate reductase, FNR;

References

1. Lill, R. and Muhlenhoff, U. (2008) *Annu. Rev. Biochem. 77*, 669-700.
2. Tripathy, B. C., Sherameti, I., and Oelmuller, R. (2010) *Plant Signaling & Behaviour 5*, 14-20.
3. Hou, S., Reynolds, M. F., Horrigan, F. T., Heinemann, S. H., and Hoshi, T. (2006) *Acc. Chem Res. 39*, 918-924.
4. Mense, S. M. and Zhang, L. (2006) *Cell Res. 16*, 681-692.
5. Gilles-Gozales, M. A. (200) *IUBMB Life 51*, 165-173.
6. Dioum, E. M., Rutter, J., Tuckerman, J. R., Gonzalez, G., Gilles-Gonzalez, M. A., and McKnight, S. L. (2002) *Science 298*, 2385-2387.
7. Tsiftsoglou, A. S., Tsamadou, A. I., and Papadopoulou, L. C. (2006) *Pharmacol. Ther. 111*, 327-345.
8. Faller, M., Matsunaga, M., Yin, S., Loo, J. A., and Guo, F. (2007) *Nat. Struct. Mol. Biol 14*, 23-29.
9. Khan, A. A. and Quingley, J. G. (2011) *Biochim. Biophys. Acta in press*.
10. Dailey, H. A. (1997) *J Biol Inorg Chem 2*, 411-417.
11. Kappas, A., Sassa, S., Galbraith, R. A., and Nordmann, Y. (1995) in *The metabolic and molecular basis of inherited disease* (Scriver, C. R., Beaudet, A. L., Sly, W. S., and Valle, D., Eds.) pp 2103-2159, McGraw-Hill, New York.
12. Kauppinen, R. (2005) *Lancet 365*, 241-252.
13. Rao, A. U., Carta, L. K., Lesuisse, E., and Hamza, I. (2005) *Proc. Natl. Acad. Sci. U. S. A 102*, 4270-4275.
14. Dunn, L. L., Rahmanto, Y. S., and Richardson, D. R. (2007) *Trends Cell Biol 17*, 93-100.
15. Poss, K. D. and Tonegawa, S. (1991) *Proc. Natl. Acad. Sci. U. S. A.* 10919-10924.

16. Nordmann, Y. and Deybach, J. M. (1990) in *Biosynthesis of heme and chlorophylls* (Dailey, H. A., Ed.) pp 491-542, McGraw-Hill, New York.
17. Meissner, P. N., Meissner, D. M., Sturrock, E. D., Davidson, B., and Kirsch, R. E. (1987) *S. Afr. Med. J 72*, 755-761.
18. Dailey, H. A. (2002) *Biochem. Soc. Trans. 30*, 590-595.
19. Dailey, H. A. and Dailey, T. A. (2003) in *The Porphyrin Handbook* (Kadish, K. M., Smith, R., and Guilard, R., Eds.) pp 93-121, Academic Press, New York.
20. Medlock, A. E. and Dailey, H. A. (2007) in *Tetrapyrroles* (Warren, M. J. and Smith, A. G., Eds.) pp 116-127, Landes Bioscience and Springer Science + Business Media, Austin.
21. Napier, I., Ponka, P., and Richardson, D. R. (2005) *Blood 105*, 1867-1874.
22. Goldberg, A., Ashenbruker, M., Cartwright, G. E., and Wintrobe, M. M. (1956) *Blood 11*, 821-833.
23. Yoneyama, A., OHYAMA, H., SUGITA, Y., and Yoshikawa, H. (1962) *Biochim. Biophys. Acta 62*, 261-268.
24. Yoneyama, A., Tamai, A., Yasuda, T., and Yoshikawa, H. (1965) *Biochim. Biophys. Acta 105*, 100-105.
25. Yoneyama, A., OHYAMA, H., SUGITA, Y., and YOSHIKAWA, H. (1962) *Biochim. Biophys. Acta 62*, 261-268.
26. Neuberger, A. and Tait, G. H. (1964) *Biochem. J 90*, 607-616.
27. JOHNSON, A. and JONES, O. G. (1964) *Biochim. Biophys. Acta 93*, 171-173.
28. Porra, R. J. and Lascelles, J. (1968) *Biochem. J 108*, 343-348.
29. Porra, R. J. and Lascelles, J. (1965) *Biochem. J 94*, 120-126.

30. Jones, M. S. and Jones, O. T. G. (1970) *Biochem. J. 119*, 453-462.

31. Jones, M. S. and Jones, O. T. G. (1969) *Biochem. J. 113*, 507-514.

32. Jones.O.T.G. (1968) *Biochem. J. 107*, 113-119.

33. Jones, T., Spencer, R., and Walsh, C. (1978) *Biochemistry 17*, 4011-4017.

34. Tokunaga, R. and Sano, S. (1972) *Biochim. Biophys. Acta 264*, 263-271.

35. Kassner, R. J. and Walchak, H. (1973) *Biochim. Biophys. Acta 304*, 294-303.

36. Dailey, H. A., Jr. and Lascelles, J. (1974) *Arch. Biochem. Biophys. 160*, 523-529.

37. Taketani, S. and Tokunaga, R. (1981) *J. Biol. Chem. 256*, 12748-12753.

38. Dailey, H. A. and Fleming, J. E. (1983) *J. Biol. Chem. 258*, 11453-11459.

39. Taketani, S. and Tokunaga, R. (1982) *Eur. J. Biochem. 127*, 443-447.

40. Hanson, J. W. and Dailey, H. A. (1984) *Biochem. J. 222*, 695-700.

41. Camadro, J. M. and Labbe, P. (1988) *J. Biol. Chem. 263*, 11675-11682.

42. Labbe-Bois, R. (1990) *J Biol Chem 265*, 7278-7283.

43. Taketani, S., Inazawa, J., Nakahashi, Y., Abe, T., and Tokunaga, R. (1992) *Eur. J Biochem. 205*, 217-222.

44. Taketani, S., Nakahashi, Y., Osumi, T., and Tokunaga, R. (1990) *J Biol Chem 265*, 19377-19380.

45. Brenner, D. A. and Frasier, F. (1991) *Proc. Natl. Acad. Sci. U. S. A 88*, 849-853.

46. Eldridge, M. G. and Dailey, H. A. (1992) *Protein Sci. 1*, 271-277.

47. Brenner, D. A., Didier, J. M., Frasier, F., Christensen, S. R., Evans, G. A., and Dailey, H. A. (1992) *Am. J. Hum. Genet. 50*, 1203-1210.

48. Dailey, H. A., Sellers, V. M., and Dailey, T. A. (1994) *J. Biol. Chem. 269*, 390-395.

49. Day, A. L., Parsons, B. M., and Dailey, H. A. (1998) *Arch. Biochem. Biophys. 359*, 160-169.

50. Sellers, V. M., Wang, K. F., Johnson, M. K., and Dailey, H. A. (1998) *J. Biol. Chem. 273*, 22311-22316.

51. Hansson, M. and Hederstedt, L. (1994) *Eur. J Biochem. 220*, 201-208.

52. Shepherd, M., Dailey, T. A., and Dailey, H. A. (2006) *Biochem. J. 397*, 47-52.

53. Dailey, T. A. and Dailey, H. A. (2002) *J. Bacteriol. 184*, 2460-2464.

54. Gokhman, I. and Zamir, A. (1990) *Nucleic Acids Res. 18*, 6130.

55. Magnus, I. A., Jarrett, A., Prankerd, T. A. J., and Rimington, C. (1961) *Lancet* 448-451.

56. Lecha, M., Puy, H., and Deybach, J. C. (2009) *Orphanet Journal of Rare Diseases* 4-19.

57. Dailey, H. A., Dailey, T. A., Wu, C.-K., Medlock, A. E., Wang, K.-F., Rose, J. P., and Wang, B.-C. (2000) *Cell. Mol. Life Sci. 57*, 1909-1926.

58. Lim, H. W. (1989) *Semin. Hematol. 26*, 114-119.

59. Bloomer, J., Bruzzone, C., Zhu, L., Scarlett, Y., Magness, S., and Brenner, D. (1998) *J. Clin. Invest.* 107-114.

60. Magness, S. T. and Brenner, D. A. (1999) *Biochim. Biophys. Acta* 161-174.

61. Magness, S. T., Tugores, A., and Brenner, D. A. (2000) *Blood* 3568-3577.

62. Jenkins, M. M., LeBoeuf, R. D., Ruth, G. R., and Bloomer, J. R. (1998) *Biochim. Biophys. Acta 1408*, 18-24.

63. Tutois, S., Montagutelli, X., Da, S., V, Jouault, H., Rouyer-Fessard, P., Leroy-Viard, K., Guenet, J. L., Nordmann, Y., Beuzard, Y., and Deybach, J. C. (1991) *J Clin. Invest 88*, 1730-1736.

64. Boulechfar, S., Lamoril, J., Montagutelli, X., Guenet, J. L., Deybach, J. C., Nordmann, Y., Dailey, H., Grandchamp, B., and de, V. H. (1993) *Genomics 16*, 645-648.

65. Frank, J., Nelson, J., Wang, X., Yang, L., Ahmad, W., Lam, H., Jugert, F. K., Kalka, K., Poh-Fitzpatrick, M. B., Goerz, G., Merk, H. F., and Christiano, A. M. (1999) *J. Investig. Med.* 278-284.

66. Rufenacht, U. B., Gouya, L., Schneider-Yin, X., Puy, H., Schafer, B. W., Aquaron, R., Nordmann, Y., Minder, E. I., and Deybach, J. C. (1998) *Am. J. Hum. Genet.* 1341-1352.

67. Schneider-Yin, X., Gouya, L., Dorsey, M., Rufenacht, U., Deybach, J. C., and Ferreira, G. C. (2000) *Blood* 1545-1549.

68. Sellers, V. M., Dailey, H. A., and Dailey, T. A. (1998) *Blood* 3980-3985.

69. Najahi-Missaoui, W. and Dailey, H. A. (2005) *Blood 106*, 1098-1104.

70. Whatley, S. D., Ducamp, S., Gouya, L., Grandchamp, B., Beaumont, C., Badminton, M. N., Elder, G. H., Holme, S. A., Anstey, A. V., Parker, M., Corrigall, A. V., Meissner, P. N., Hift, R. J., Marsden, J. T., Ma, Y., Mieli-Vergani, G., Deybach, J. C., and Puy, H. (2008) *Am. J Hum. Genet. 83*, 408-414.

71. Delaby, C., Lyoumi, S., Ducamp, S., Martin-Schmitt, C., Gouya, L., Deybach, J. C., Beaumont, C., and Puy, H. (2009) *Cell Mol. Biol (Noisy. -le-grand) 55*, 45-52.

72. Holme, S. A., Worwood, M., Anstey, A. V., Elder, G. H., and Badminton, M. N. (2007) *Blood 110*, 4108-4110.

73. Straka, J. C., Bloomer, J. R., and Kempner, E. S. (1991) *J. Biol. Chem. 266*, 24637-24641.

74. Burden, A. E., Wu, C., Dailey, T. A., Busch, J. L., Dhawan, I. K., Rose, J. P., Wang, B., and Dailey, H. A. (1999) *Biochim. Biophys. Acta 1435*, 191-197.

75. Al-Karadaghi, S., Hansson, M., Nikonov, S., Jonsson, B., and Hederstedt, L. (1997) *Structure 5*, 1501-1510.

76. Karr, S. R. and Dailey, H. A. (1988) *Biochem. J. 254*, 799-803.

77. Harbin, B. M. and Dailey, H. A. (1985) *Biochemistry 24*, 366-370.

78. Chow, K. S., Singh, D. P., Walker, A. R., and Smith, A. G. (1998) *Plant J 15*, 531-541.

79. Suzuki, T., Masuda, T., Inokuchi, H., Shimada, H., Ohta, H., and Takamiya, K. (2000) *Plant Cell Physiol 41*, 192-199.

80. Suzuki, T., Masuda, T., Singh, D. P., Tan, F. C., Tsuchiya, T., Shimada, H., Ohta, H., Smith, A. G., and Takamiya, K. (2002) *J Biol Chem 277*, 4731-4737.

81. Chenna, R., Sugawara, H., Koike, T., Lopez, R., Gibson, T. J., Higgins, D. G., and Thompson, J. D. (2003) *Nucleic Acids Res. 31*, 3497-3500.

82. Dailey, H. A., Finnegan, M. G., and Johnson, M. K. (1994) *Biochemistry 33*, 403-407.

83. Wu, C.-K., Dailey, H. A., Rose, J. P., Burden, A., Sellers, V. M., and Wang, B.-C. (2001) *Nat. Struct. Biol. 8*, 156-160.

84. Medlock, A. E. and Dailey, H. A. (2000) *Biochemistry 39*, 7461-7467.

85. Karlberg, T., Lecerof, D., Gora, M., Silvegren, G., Labbe-Bois, R., Hansson, M., and Al-Karadaghi, S. (2002) *Biochemistry 41*, 13499-13506.

86. Hansson, M. D., Karlberg, T., Rahardja, M. A., Al-Karadaghi, S., and Hansson, M. (2007) *Biochemistry 46*, 87-94.

87. Lecerof, D., Fodje, M. N., Alvarez, L. R., Olsson, U., Hansson, A., Sigfridsson, E., Ryde, U., Hansson, M., and Al-Karadaghi, S. (2003) *J Biol Inorg Chem 8*, 452-458.

88. Shipovskov, S., Karlberg, T., Fodje, M., Hansson, M. D., Ferreira, G. C., Hansson, M., Reimann, C. T., and Al-Karadaghi, S. (2005) *J Mol. Biol 352*, 1081-1090.

89. Lecerof, D., Fodje, M., Hansson, A., Hansson, M., and Al-Karadaghi, S. (2000) *J Mol. Biol 297*, 221-232.

90. Dailey, H. A., Wu, C. K., Horanyi, P., Medlock, A. E., Najahi-Missaoui, W., Burden, A. E., Dailey, T. A., and Rose, J. (2007) *Biochemistry 46*, 7973-7979.

91. Medlock, A., Swartz, L., Dailey, T. A., Dailey, H. A., and Lanzilotta, W. N. (2007) *Proc. Natl. Acad. Sci. U. S. A 104*, 1789-1793.

92. Medlock, A. E., Carter, M., Dailey, T. A., Dailey, H. A., and Lanzilotta, W. N. (2009) *J Mol. Biol 393*, 308-319.

93. Medlock, A. E., Dailey, T. A., Ross, T. A., Dailey, H. A., and Lanzilotta, W. N. (2007) *J Mol. Biol 373*, 1006-1016.

94. Franco, R., Pereira, A. S., Tavares, P., Mangravita, A., Barber, M. J., Moura, I., and Ferreira, G. C. (2001) *Biochem. J 356*, 217-222.

95. Franco, R., Ma, J. G., Lu, Y., Ferreira, G. C., and Shelnutt, J. A. (2000) *Biochemistry 39*, 2517-2529.

96. Sellers, V. M., Wu, C. K., Dailey, T. A., and Dailey, H. A. (2001) *Biochemistry 40*, 9821-9827.

97. Shi, Z. and Ferreira, G. C. (2004) *J Biol Chem 279*, 19977-19986.

98. Hansson, M. D., Lindstam, M., and Hansson, M. (2006) *J Biol Inorg Chem 11*, 325-333.

99. Spurlino, J. C., Lu, G. Y., and Quiocho, F. A. (1991) *J Biol Chem 266*, 5202-5219.

100. Dailey, H. A. (1985) *Biochemistry 24*, 1287-1291.

101. Gora, M., Rytka, J., and Labbe-Bois, R. (1999) *Arch. Biochem. Biophys. 361*, 231-240.

102. Hamza, I. and Gitlin, J. D. (2002) *J Bioenerg. Biomembr. 34*, 381-388.

103. Bandyopadhyay, S., Chandramouli, K., and Johnson, M. K. (2008) *Biochem. Soc. Trans. 36*, 1112-1119.

104. Johnson, D. C., Dean, D. R., Smith, A. D., and Johnson, M. K. (2005) *Annu. Rev. Biochem. 74*, 247-281.

105. Johnson, M. K. and Smith, A. D. (2005) in *Encyclopedia of Inorganic Chemistry, Second Edition* (King, R. B., Ed.) pp 2589-2619, John Wiley & Sons, Chichester.

106. KLEIN, J. R., KRUEGER, R. C., and MELNICK, I. (1956) *Arch. Biochem. Biophys. 64*, 302-310.

107. Al-Karadaghi, S., Franco, R., Hansson, M., Shelnutt, J. A., Isaya, G., and Ferreira, G. C. (2006) *Trends Biochem. Sci. 31*, 135-142.

108. Lanzilotta, W. N. and Dailey, H. A. (2007) in *Handbook of Metalloproteins* (Messerschmidt, A., Ed.) John Wiley & Sons, Ltd., UK.

109. Lavallee, D. K. (1988) in *Mechanistic Principles of Enzyme Activity* (Liebman, J. F. and Greenberg, A., Eds.) pp 279-317, VCH, New York.

110. Dailey, H. A. (1990) in *Biosynthesis of Hemes and Chlorophylls* (Dailey, H. A., Ed.) pp 123-155, McGraw-Hill, New York.

111. Dailey, H. A. (1996) in *Mechanisms of Metallocenter Assembly* (Hausinger, R. P., Eichorn, G. L., and Marzilli, L. G., Eds.) pp 77-98, VCH, New York.

112. Takeda, J., Ohya, T., and Sato, M. (1992) *Inorg. Chem. 31*, 2877-2880.

113. Cochran, A. G. and Schultz, P. G. (1990) *Science 249*, 781-783.

114. Li, Y. and Sen, D. (1997) *Biochemistry 36*, 5589-5599.

115. Morgan, M., Prudent, J. R., and Schultz, P. G. (1996) *J. Am. Chem. Soc. 118*, 7012-7013.

116. Blackwood, M. E., Jr., Rush, T. S. I., Romesberg, F., Schultz, P. G., and Spiro, T. G. (1998) *Biochemistry 37*, 779-782.

117. Blackwood, M. E., Jr., Rush, T. S. I., Medlock, A., Dailey, H. A., and Spiro, T. G. (1997) *J. Am. Chem. Soc. 119*, 12170-12174.

118. Fodje, M. N. and Al-Karadaghi, S. (2002) *Protein Eng 15*, 353-358.

119. Hoggins, M., Dailey, H. A., Hunter, C. N., and Reid, J. D. (2007) *Biochemistry 46*, 8121-8127.

120. Dailey, H. A. (1987) *Ann. N. Y. Acad. Sci. 514*, 81-86.

121. Price, M. J., Saiz, B. L., and Barton, L. L. (1989) *Biol. Met. 2*, 31-35.

122. Karlberg, T., Hansson, M. D., Yengo, R. K., Johansson, R., Thorvaldsen, H. O., Ferreira, G. C., Hansson, M., and Al-Karadaghi, S. (2008) *J Mol. Biol 378*, 1074-1083.

123. Hunter, G. A., Sampson, M. P., and Ferreira, G. C. (2008) *J Biol Chem 283*, 23685-23691.

124. Shen, Y. and Ryde, U. (2004) *J Inorg Biochem. 98*, 878-895.

125. Shen, Y. and Ryde, U. (2005) *Chemistry. 11*, 1549-1564.

126. Sigfridsson, E. and Ryde, U. (2003) *J Biol Inorg Chem 8*, 273-282.

127. Hansson, M. Structural and physicochemical studies on metal and porphyrin binding by the *Bacillus subtilis* ferrochelatase. 2009. Doctoral disertation, Lund University. Ref Type: Thesis/Dissertation

128. Shaw, G. C., Cope, J. J., Li, L., Corson, K., Hersey, C., Ackermann, G. E., Gwynn, B., Lambert, A. J., Wingert, R. A., Traver, D., Trede, N. S., Barut, B. A., Zhou, Y., Minet, E., Donovan, A., Brownlie, A., Balzan, R., Weiss, M. J., Peters, L. L., Kaplan, J., Zon, L. I., and Paw, B. H. (2006) *Nature 440*, 96-100.

129. Asuru, A. P. and Busenlehner, L. S. *International Journal of Mass Spectrometry In Press, Corrected Proof*.

130. Yoon, T. and Cowan, J. A. (2004) *J Biol Chem 279*, 25943-25946.

131. Bencze, K. Z., Yoon, T., Millan-Pacheco, C., Bradley, P. B., Pastor, N., Cowan, J. A., and Stemmler, T. L. (207) *Chem. Commun. (Camb.)* 1798-1800.

132. Pandolfo, M. and Pastore, A. (2009) *J Neurol. 256 Suppl 1*, 9-17.

133. Ferreira, G. C., Franco, R., Lloyd, S. G., Pereira, A. S., Moura, I., Moura, J. J., and Huynh, B. H. (1994) *J Biol Chem 269*, 7062-7065.

134. Link, T. A. (1999) *Adv. Inorg. Chem. 47*, 83-157.

135. Hagen, W. R., Silva, P. J., Amorim, M. A., Hagedoorn, P. L., Wassink, H., Haaker, H., and Robb, F. T. (2000) *J. Biol. Inorg. Chem. 5*, 527-534.

136. Yankovskaya, V., Horsefield, R., Törnroth, S., Luna-Chavez, C., Miyoshi, H., Léger, C., Byrne, B., Cecchini, G., and Iwata, S. (2003) *Science 299*, 700-704.

137. Berkovitch, F., Nicolet, Y., Wan, J. T., Jarrett, J. T., and Drennan, C. L. (2004) *Science 303*, 76-79.

138. Paddock, M. L., Wiley, S. E., Axelrod, H. L., Cohen, A. E., Roy, M., Abresch, E. C., Capraro, D., Murphy, A. N., Nechushtai, R., Dixon, J. E., and Jennings, P. A. (2007) *Proc. Natl. Acad. Sci. U. S. A 104*, 14342-14347.

139. Lin, J., Zhou, T., Ye, K., and Wang, J. (2007) *Proc. Natl. Acad. Sci. U. S. A 104*, 14640-14645.

140. Hou, X., Liu, R., Ross, S., Smart, E. J., Zhu, H., and Gong, W. (2007) *J Biol Chem 282*, 33242-33246.

141. Crouse, B. R., Sellers, V. M., Finnegan, M. G., Dailey, H. A., and Johnson, M. K. (1996) *Biochemistry 35*, 16222-16229.

142. Lloyd, S. G., Franco, R., Moura, J. J., Moura, I., Ferreira, G. C., and Huynh, B. H. (1996) *J. Am. Chem. Soc. 118*, 9892-9900.

143. Matsubara, H. and Saeki, K. (1992) *Adv. Inorg. Chem. 38*, 223-280.

144. Johnson, M. K. (1994) in *Encyclopedia of inorganic chemistry* (King, R. B., Ed.) pp 1896-1915, John Wiley & Sons, Chichester.

145. Raman, C. S., Li, H., Martasek, P., Kral, V., Masters, B. S., and Poulos, T. L. (1998) *Cell 95*, 939-950.

146. Raux-Deery, E., Leech, H. K., Nakrieko, K. A., McLean, K. J., Munro, A. W., Heathcote, P., Rigby, S. E. J., Smith, A. G., and Warren, M. J. (2005) *J. Biol. Chem. 280*, 4713-4721.

147. Crane, B. R. and Getzoff, E. D. (1996) *Curr. Opin. Chem. Biol. 6*, 744-756.

148. Crane, B. R., Siegel, L. M., and Getzoff, E. D. (1997) *Biochemistry 36*, 12101-12119.

149. Cornah, J. E., Terry, M. J., and Smith, A. G. (2003) *Trends Plant Sci. 8*, 224-230.

150. Phillips, J. D., Whitby, F. G., Kushner, J. P., and Hill, C. P. (2003) *EMBO J 22*, 6225-6233.

151. Warren, M. J., Stolowich, N. J., Santander, P. J., Roessner, C. A., Sowa, B. A., and Scott, A. I. (1990) *FEBS Lett. 261*, 76-80.

152. Leustek, T., Smith, M., Murillo, M., Singh, D. P., Smith, A. G., Woodcock, S. C., Awan, S. J., and Warren, M. J. (1997) *J Biol Chem 272*, 2744-2752.

153. Raux-Deery, E., Leech, H. K., Beck, R., Schubert, H. L., Santander, P. J., Roessner, C. A., Scott, A. I., Martens, J. H., Jahn, D., Thermes, C., Rambach, A., and Warren, M. J. (2003) *Biochem. J. 370*, 505-516.

154. Leech, H. K., Raux-Deery, E., Heathcote, P., and Warren, M. J. (2002) *Biochem. Soc. Trans. 30*, 610-613.

155. Schubert, H. L., Raux, E., Wilson, K. S., and Warren, M. J. (1999) *Biochemistry 38*, 10660-10669.

156. Leech, H. K., Raux, E., McLean, K. J., Munro, A. W., Robinson, N. J., Borrelly, G. P., Malten, M., Jahn, D., Rigby, S. E., Heathcote, P., and Warren, M. J. (2003) *J Biol Chem 278*, 41900-41907.

157. Brindley, A. A., Raux, E., Leech, H. K., Schubert, H. L., and Warren, M. J. (2003) *J Biol Chem 278*, 22388-22395.

158. Kiley, P. J. and Beinert, H. (2003) *Curr. Opin. Microbiol. 6*, 181-185.

159. Lill, R. (2009) *Nature 460*, 831-838.

160. Walden, W. E., Selezneva, A. I., Dupuy, J., Volbeda, A., Fontecilla-Camps, J. C., Theil, E. C., and Volz, K. (2006) *Science 314*, 1903-1908.

161. Wallander, M. L., Leibold, E. A., and Eisenstein, R. S. (2006) *Biochim. Biophys. Acta 1763*, 668-689.

162. Volz, K. (2008) *Curr. Opin. Struct. Biol 18*, 106-111.

163. Crack, J., Green, J., and Thomson, A. J. (2004) *J. Biol. Chem. 279*, 9278-8286.

164. Khoroshilova, N., Popescu, C., Münck, E., Beinert, H., and Kiley, P. J. (1997) *Proc. Natl. Acad. Sci. USA 94*, 6087-6092.

165. Lazazzera, B. A., Beinert, H., Khoroshilova, N., Kennedy, M. C., and Kiley, P. J. (1996) *J. Biol. Chem. 271*, 2762-2768.

166. Reinhart, F., Achebach, S., Koch, T., and Unden, G. (2008) *J Bacteriol. 190*, 879-886.

167. Dibden, D. P. and Green, J. (2005) *Microbiology 151*, 4063-4070.

168. Imlay, J. A. (2008) *Annu. Rev. Biochem. 77*, 755-776.

169. Watanabe, S., Kita, A., Kobayashi, K., and Miki, K. (2008) *Proc. Natl. Acad. Sci. U. S. A 105*, 4121-4126.

170. Demple, B., Ding, H., and Jorgensen, M. (2002) *Meth. Enzymol. 348*, 355-364.

171. Gaudu, P. and Weiss, B. (1996) *Proc. Natl. Acad. Sci. USA 93*, 10094-10098.

172. Grandoni, J. A., Switzer, R. L., Marakoff, C. A., and Zalkin, H. (1989) *J. Biol. Chem. 264*, 6058-6064.

173. Smith, J. L., Zaluzec, E. J., Wery, J.-P., Niu, L., Switzer, R. L., Zalkin, H., and Satow, Y. (1994) *Science 264*, 1427-1433.

174. Furukawa, T., Kohno, H., Tokunaga, R., and Taketani, S. (1995) *Biochem. J. 310 (Pt 2)*, 533-538.

175. Sellers, V. M., Johnson, M. K., and Dailey, H. A. (1996) *Biochemistry 35*, 2699-2704.

176. Bandyopadhyay, S., Gama, F., Molina-Navarro, M. M., Gualberto, J. M., Claxton, R., Naik, S. G., Huynh, B. H., Herrero, E., Jacquot, J.-P., Johnson, M. K., and Rouhier, N. (2008) *EMBO J. 27*, 1122-1133.

177. Fernandes, A. P. and Holmgren, A. (2004) *Antioxid. Redox. Signal. 6*, 63-74.

178. Herrero, E. and de la Torre-Ruiz, M. A. (2007) *Cell. Mol. Life Sci. 64*, 1518-1530.

179. Rodríguez-Manzaneque, M. T., Ros, J., Cabrito, I., Sorribas, A., and Herrero, E. (1999) *Mol. Cell. Biol. 19*, 8180-8190.

180. Rodríguez-Manzaneque, M. T., Tamarit, J., Bellí, G., Ros, J., and Herrero, E. (2002) *Mol. Biol. Cell 13*, 1109-1121.

181. Wheeler, G. L. and Grant, C. M. (2004) *Physiol Plant 120*, 12-20.

182. Bushweller, J. H., Aslund, F., Wuthrich, K., and Holmgren, A. (1992) *Biochemistry 31*, 9288-9293.

183. Rouhier, N., Couturier, J., and Jacquot, J. P. (2006) *J Exp. Bot. 57*, 1685-1696.

184. Couturier, J., Jacquot, J. P., and Rouhier, N. (2009) *Cell Mol. Life Sci. 66*, 2539-2557.

185. Rouhier, N., Couturier, J., Johnson, M. K., and Jacquot, J. P. (2010) *Trends Biochem. Sci. 35*, 43-52.

186. Mühlenhoff, U., Gerber, J., Richhardt, N., and Lill, R. (2003) *EMBO J. 22*, 4815-4825.

187. Lill, R. and Mühlenhoff, U. (2005) *Trends Biochem. Sci. 30*, 133-141.

188. Molina, M. M., Belli, G., de la Torre, M. A., Rodriguez-Manzaneque, M. T., and Herrero, E. (2004) *J Biol Chem 279*, 51923-51930.

189. Molina-Navarro, M. M., Casas, C., Piedrafita, L., Bellí, G., and Herrero, E. (2006) *FEBS Lett. 580*, 2273-2280.

190. Vilella, F., Alves, R., Rodriguez-Manzaneque, M. T., Belli, G., Swaminathan, S., Sunnerhagen, P., and Herrero, E. (2004) *Comp Funct. Genomics 5*, 328-341.

191. Kim, K. D., Chung, W. H., Kim, H. J., Lee, K. C., and Roe, J. H. (2010) *Biochem. Biophys. Res. Commun. 392*, 467-472.

192. Rouhier, N., Gelhaye, E., and Jacquot, J.-P. (2004) *Cell. Mol. Life Sci. 61*, 1266-1277.

193. Couturier, J., Stroher, E., Albetel, A. N., Roret, T., Muthuramalingam, M., Tarrago, L., Seidel, T., Tsan, P., Jacquot, J. P., Johnson, M. K., Dietz, K. J., Didierjean, C., and Rouhier, N. (2011) *J. Biol. Chem. 286*, 27515-27527.

194. Feng, Y., Zhong, N., Rouhier, N., Hase, T., Kusunoki, M., Jacquot, J. P., Jin, C., and Xia, B. (2006) *Biochemistry 45*, 7998-8008.

195. Rouhier, N., Unno, H., Bandyopadhyay, S., Masip, L., Kim, S. K., Hirasawa, M., Gualberto, J. M., Lattard, V., Kusunoki, M., Knaff, D. B., Georgiou, G., Hase, T., Johnson, M. K., and Jacquot, J. P. (2007) *Proc. Natl. Acad. Sci. U. S. A. 104*, 7379-7384.

196. Iwema, T., Picciocchi, A., Traore, D. A., Ferrer, J. L., Chauvat, F., and Jacquamet, L. (2009) *Biochemistry 48*, 6041-6043.

197. Johansson, C., Kavanagh, K. L., Gileadi, O., and Oppermann U. (2007) *J. Biol. Chem. 282*, 3077-3082.

198. Picciocchi, A., Saguez, C., Boussac, A., Cassier-Chauvat, C., and Chauvat, F. (2007) *Biochemistry 46*, 15018-15026.

199. Johansson, C., Roos, A. K., Montano, S. J., Sengupta, R., Filippakopoulos, P., Guo, K., von, D. F., Holmgren, A., Oppermann, U., and Kavanagh, K. L. (2010) *Biochem. J 433*, 303-311.

200. Rouault, T. A. and Tong, W.-H. (2005) *Nat. Rev. Mol. Cell. Biol. 6*, 345-Ir351.

201. Hentze, M. W., Muckenthaler, M. U., and Andrews, N. C. (2004) *Cell 117*, 285-297.

202. Rouault, T. A. (2006) *Nat. Chem Biol 2*, 406-414.

203. Tong, W. H. and Rouault, T. A. (2006) *Cell Metabolism 3*, 199-210.

204. Wingert, R. A., Galloway, J. L., Barut, B., Foott, H., Fraenkel, P., Axe, J. L., Weber, G. J., Dooley, K., Davidson, A. J., Schmidt, B., Paw, B. H., and Shaw, G. C. (2005) *Nature 436*, 1035-1039.

205. Camaschella, C., Campanelle, A. F. L., Boschetto, L., Merlini, R., Silvestri, L., Levi, S., and Iolascon, A. (2007) *Blood 110*, 1353-1358.

206. Crooks, D. R., Ghosh, M. C., Haller, R. G., Tong, W.-H., and Rouault, T. A. (2010) *Blood 115*, 860-869.

207. Agar, J. N., Dean, D. R., and Johnson, M. K. (2003) in *Biochemistry and Physiology of Anaerobic Bacteria* (Ljungdahl, L. G., Adams, M. W. W., Barton, L. L., Ferry, J. G., and Johnson, M. K., Eds.) pp 46-66, Springer-Verlag, New York.

208. Ye, H., Jeong, S. Y., Ghosh, M. C., Kovtunovych, G., Silvestri, L., Ortillo, D., Uchida, N., Tisdale, J., Camaschella, C., and Rouault, T. A. (2010) *J Clin. Invest 120*, 1749-1761.

209. DeLano, W. L. The PyMOL Molecular Graphics System. [1.2r3pre]. 2002. Palo Alto, CA, Schrödinger, LLC. Ref Type: Computer Program

210. Mapolelo, D. T. Characterization of the roles of A-type proteins and monothiol CGFS glutaredoxins in iron-sulfur cluster biogenesis. 2010. University of Georgia. Ref Type: Thesis/Dissertation

Table 1.1. Coordination motif for [2Fe-2S] clusters in different ferrochelatases. The amino acid residues involved in cluster ligation were identified via mutagenesis studies, except the ones from the human enzyme for which the cluster coordinating residues were determined by mutagenesis and crystallographic studies.

ORGANISM		COORDINATION MOTIF
EUKARYOTES		$C\text{-}X_{206}\text{-}C\text{-}X_{2}\text{-}C\text{-}X_{4}\text{-}C$
BACTERIA	*C. crescentus* *R. prowazekii*	$C\text{-}X_{173}\text{-}C\text{-}X_{6}\text{-}C\text{-}X\text{-}C$
	M. tuberculosis	$C\text{-}X_{?}\text{-}C\text{-}X_{8}\text{-}C\text{-}X_{4}\text{-}C$
	M. xanthus *A. vinelandii* *P. syringae* *Bd. bacteriovorus*	$C\text{-}X_{5}\text{-}C\text{-}C\text{-}X_{9}\text{-}C$
	P. freudenreichii *S. coelicolor*	$C\text{-}X_{?}\text{-}C\text{-}X_{3}\text{-}C\text{-}C$

Figure 1.1. The heme biosynthetic pathway in animal cells. The diagram shows the enzymes, their intracellular localization and the reaction they catalyze. Notations for porphyrin substituents: *M*, methyl side chain; *V*, vinyl side chain; *P*, propionate side chain; *A*, acetate side chain; Taken with permission from reference (*10*).

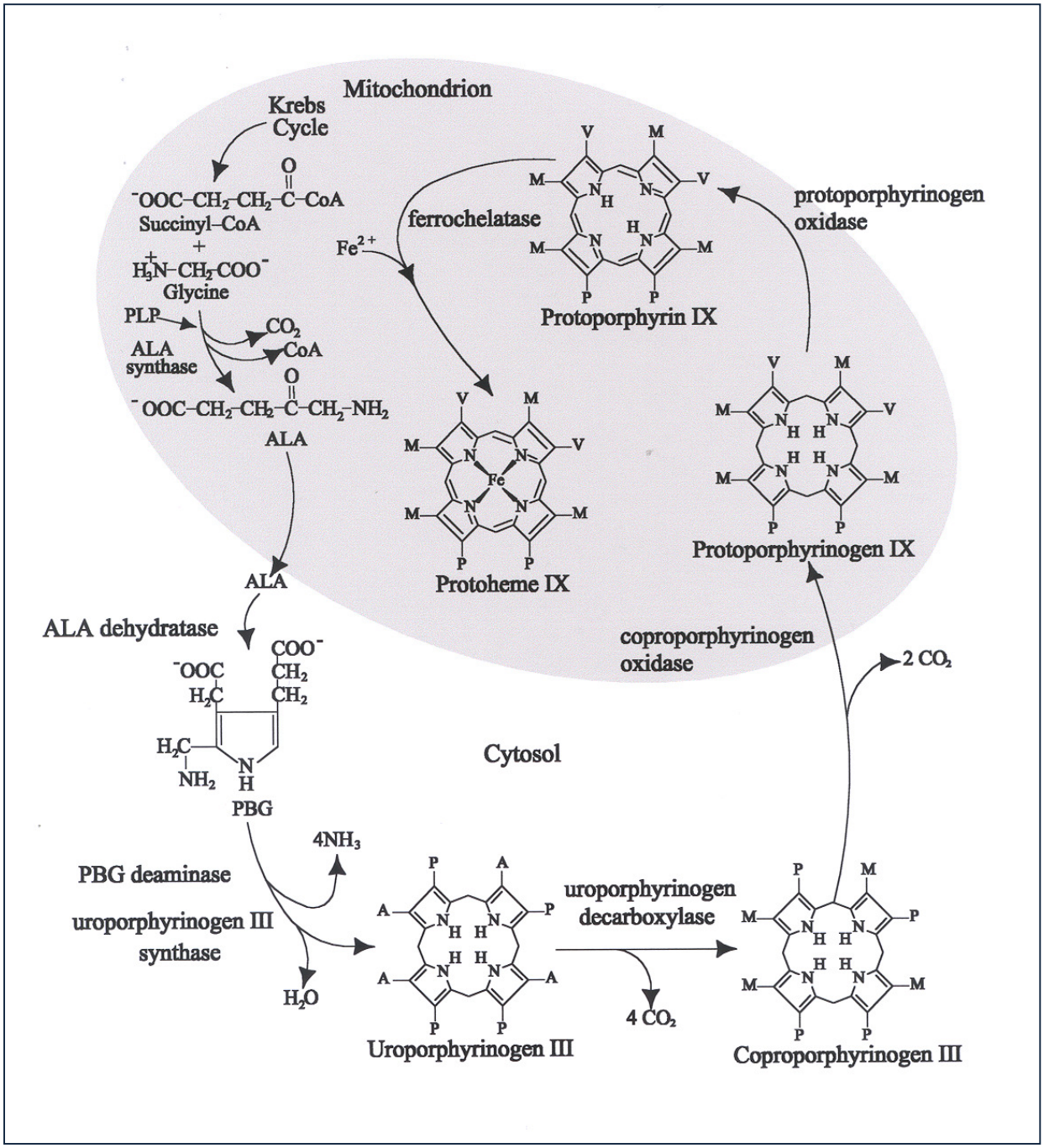
Mitochondrion
Krebs Cycle
Succinyl–CoA
Glycine
PLP
ALA synthase
CO2
CoA
ALA
ferrochelatase
Fe2+
Protoporphyrin IX
protoporphyrinogen oxidase
Protoheme IX
Protoporphyrinogen IX
ALA
ALA dehydratase
PBG
coproporphyrinogen oxidase
2 CO2
Cytosol
4NH3
PBG deaminase
uroporphyrinogen III synthase
H2O
uroporphyrinogen decarboxylase
4 CO2
Uroporphyrinogen III
Coproporphyrinogen III

Figure 1.2. Amino acid sequence comparison of selected ferrochelatases. Residues sharing 90% similarity are shaded magenta, while residues sharing 90% functional similarity are shaded in cyan. The potential conserved cysteine residues from some bacterial ferrochelatases found to possess the internal "cysteine-rich insertion" are boxed in black, whereas the cysteine ligands to the [2Fe-2S] cluster from different ferrochelatases that were identified via mutagenesis only and mutagenesis/structural studies are shaded in red. The putative The blue boxes indicate the regions of the human ferrochelatase that corresponds to the "cysteine-rich insertion" from some bacterial enzymes and indicate the region from Fig. 1.6 highlighted in blue. Sequence alignment was obtained using ClustalW program (*81*), accessible at www.expasy.org.

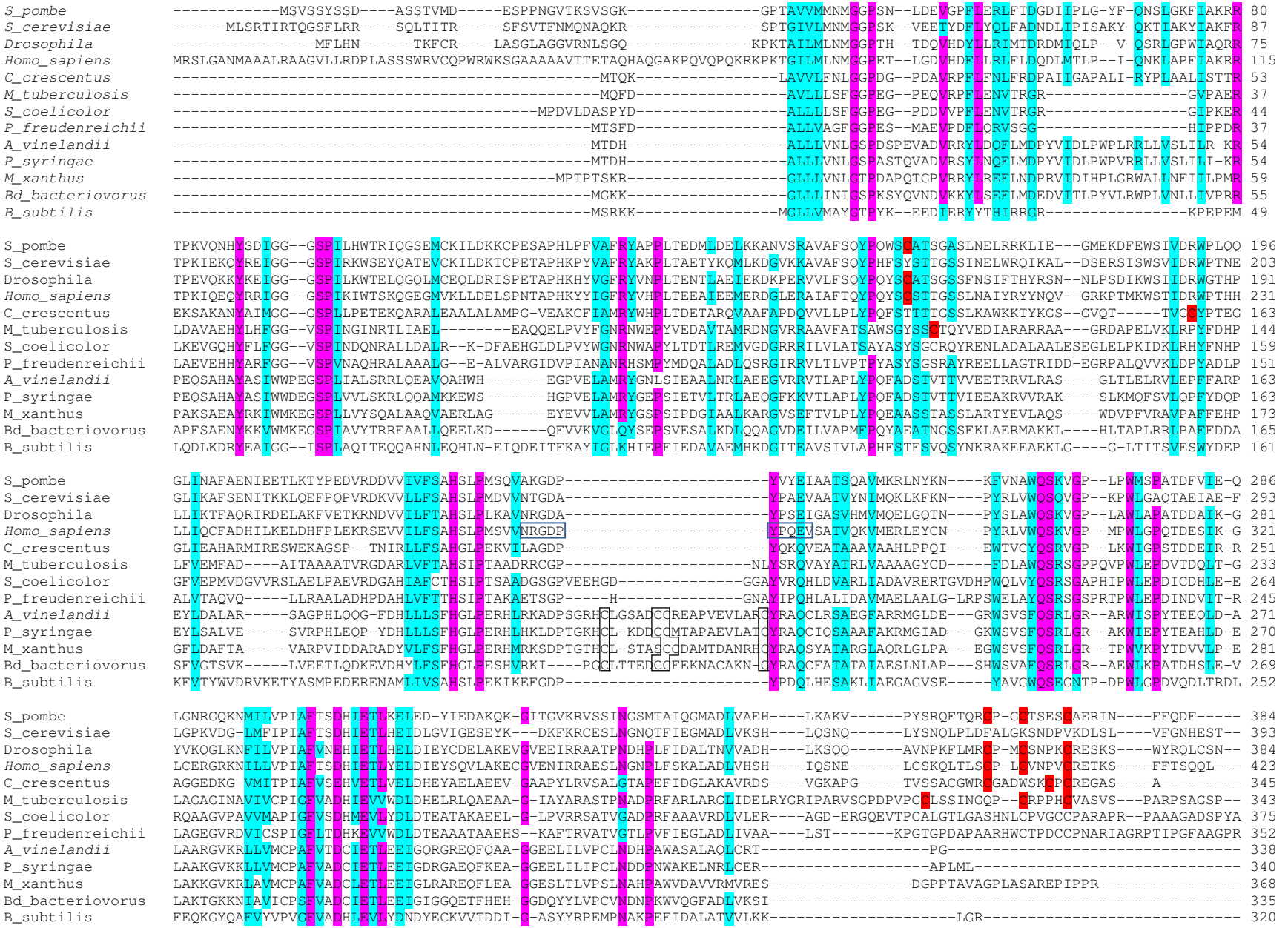
S_pombe
S_cerevisiae
Drosophila
Homo_sapiens
C_crescentus
M_tuberculosis
S_coelicolor
P_freudenreichii
A_vinelandii
P_syringae
M_xanthus
Bd_bacteriovorus
B_subtilis

Figure 1.3. Crystal structure of monomeric ferrochelatase from *B. subtilis* at 1.9 Å. Ribbon drawing of *B. subtilis* ferrochelatase monomer prepared with PYMOL program (*209*) showing its pseudo two-fold axis (Protein Data Bank 1AK1).

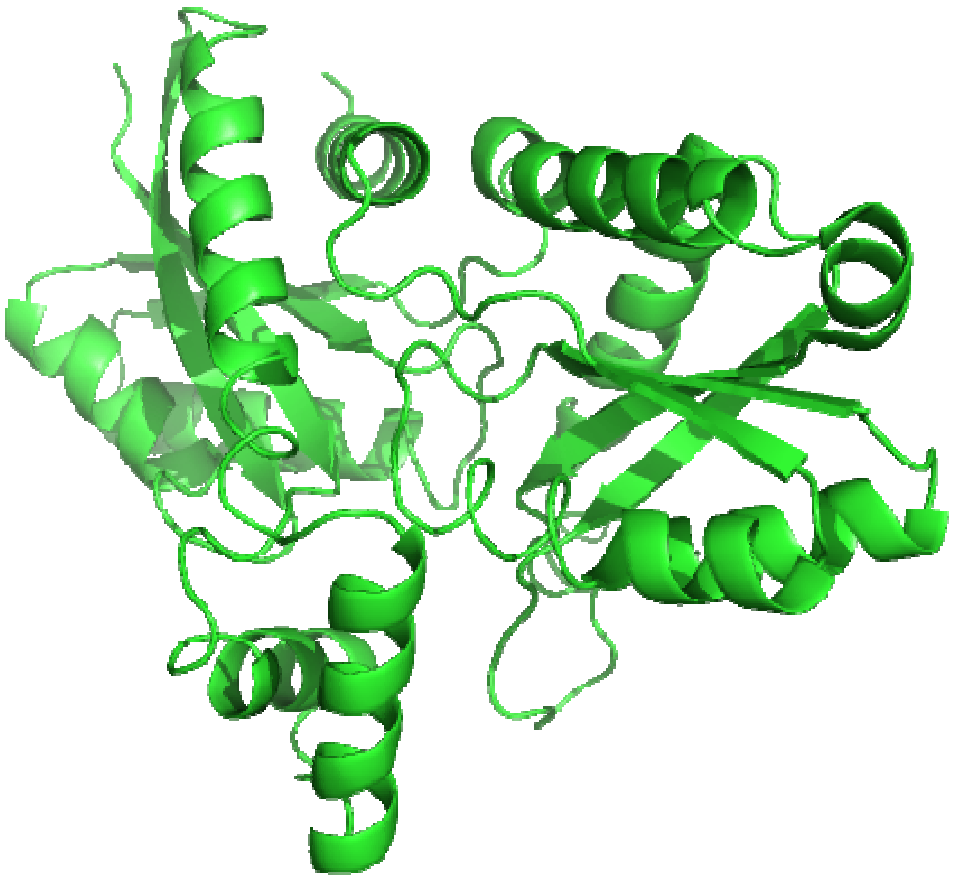

Figure 1.4. Crystal structure of homodimeric human ferrochelatase at 2.0 Å. Ribbon drawing of human ferrochelatase homodimer (Protein Data Bank 1HRK) prepared with PYMOL software (*209*). *Top*: view of the human ferrochelatase dimer showing the position of the two active sites, which can be determined by the presence of the cholate detergent molecules (orange sticks) associated with the crystallized protein. The arrows denote the four hydrophobic active-site lips, orientated downward. This region is suggested to associate with the matrix side of the inner mitochondrial membrane in vivo. *Bottom*: view of the human ferrochelatase dimer showing its pseudo two-fold axis. The carboxy terminal ends (purple regions) are present at the dimer interface. The region of human ferrochelatase corresponding to the cysteine-rich region in some bacterial ferrochelatases is colored blue (blue-line box in Figure 1.2). The [2Fe-2S] clusters are depicted as red and yellow balls and are located at the dimer interface.

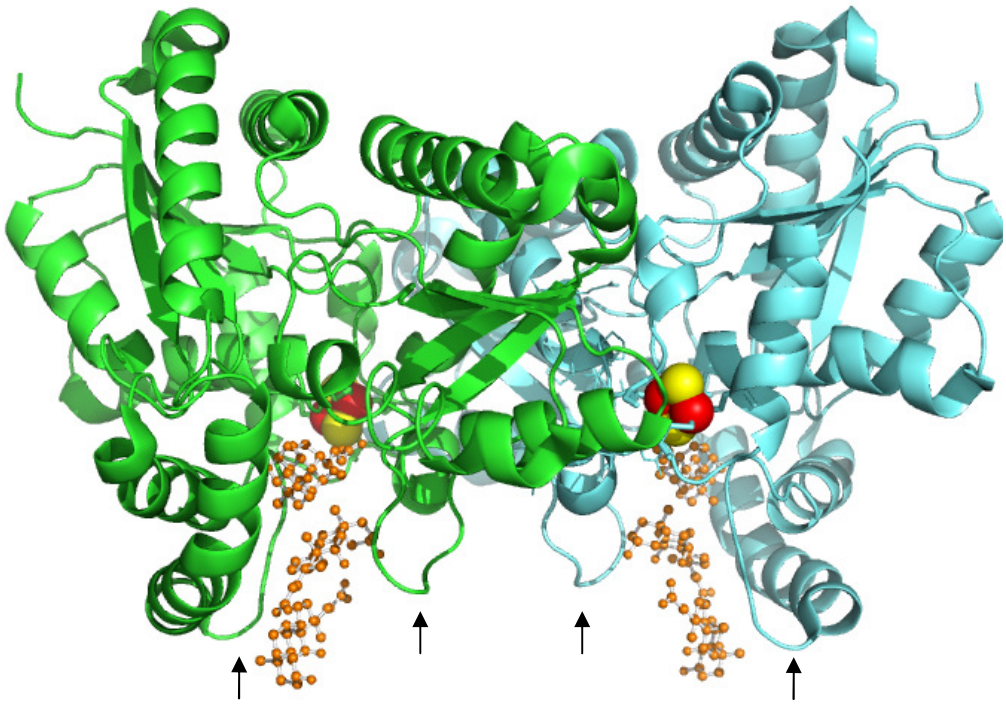

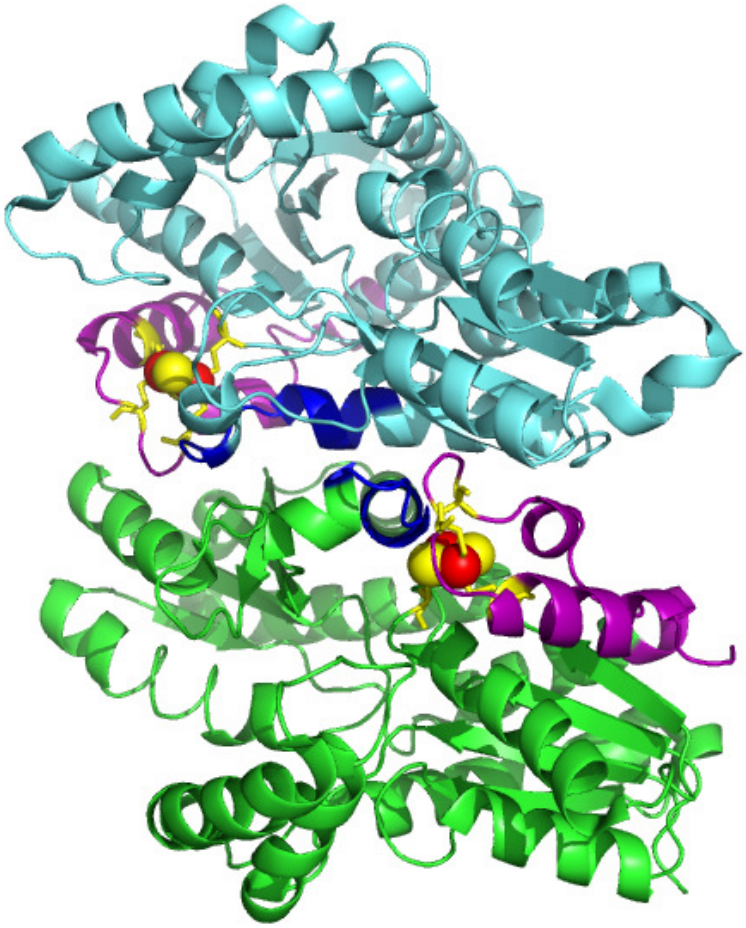

Figure 1.5. Structural alignment of the free, substrate-bound and product-bound forms of human ferrochelatase. (**a**) Contrasted super-positioning of the wild-type and substrate-free structures are shown in cream color. The upper lip of the active site that is altered in spatial orientation in the substrate-bound form relative to the wild-type enzyme structure is shown in green. The unwound π-helix segment of the product-bound form of human ferrochelatase is shown in red. Bound protoporphyrin IX is shown in brick and highlighted using dots to denote the electron density. The [2Fe-2S] cluster is shown as yellow and blue spheres. (**b**) Enlarged view of the bound protoporphyrin IX (brick) and bound heme (purple) in the same spatial orientation as shown in the cartoon model. The movement of the protoporphyrin/protoheme IX propionate 6, which is on the corner of the macrocycle in this orientation, is highlighted by the grey arrow. Taken with permission from reference (*93*).

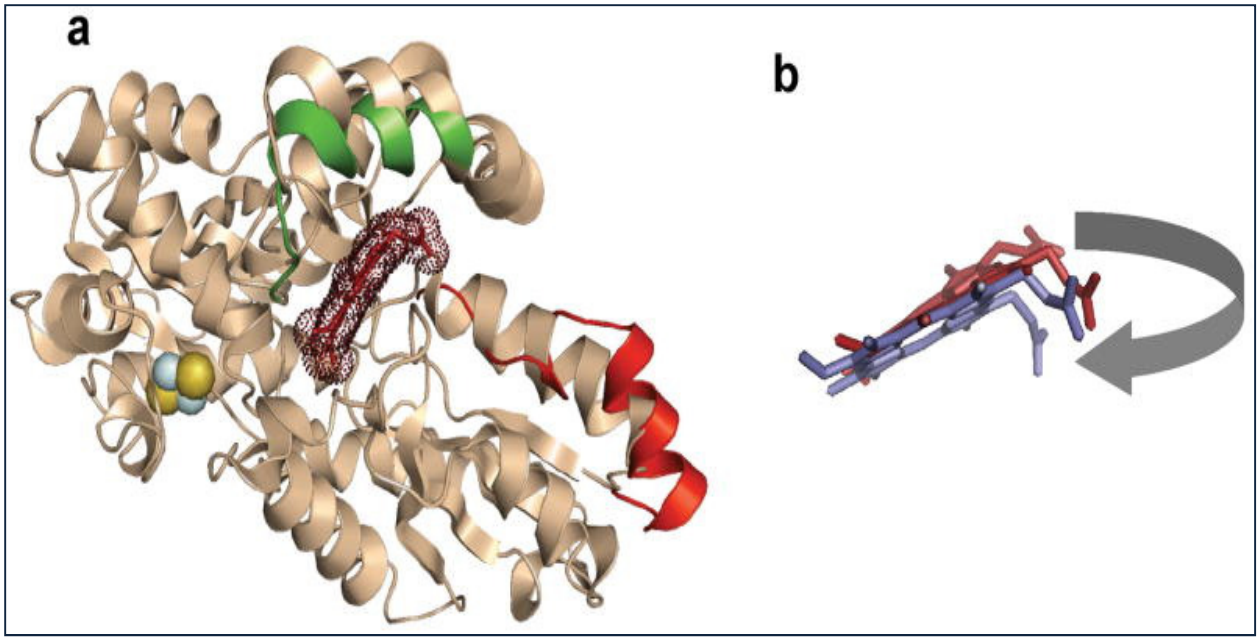
a
b

Figure 1.6. Crystal structure of [2Fe-2S] cluster-bound human ferrochelatase structure (Protein Data Bank 1HRK) showing the spatial orientation of the [2Fe-2S] center (red and yellow spheres, respectively) and the cysteine residues involved in its coordination (yellow sticks). The region depicted in purple indicates the C-terminal extension found in human, but not in most bacterial ferrochelatases. The blue color corresponds to the cysteine rich region of some bacterial ferrochelatase that can also coordinate a [2Fe-2S] cluster (blue-line box in fig. 1.2). The figure was prepared using Pymol program (*209*).

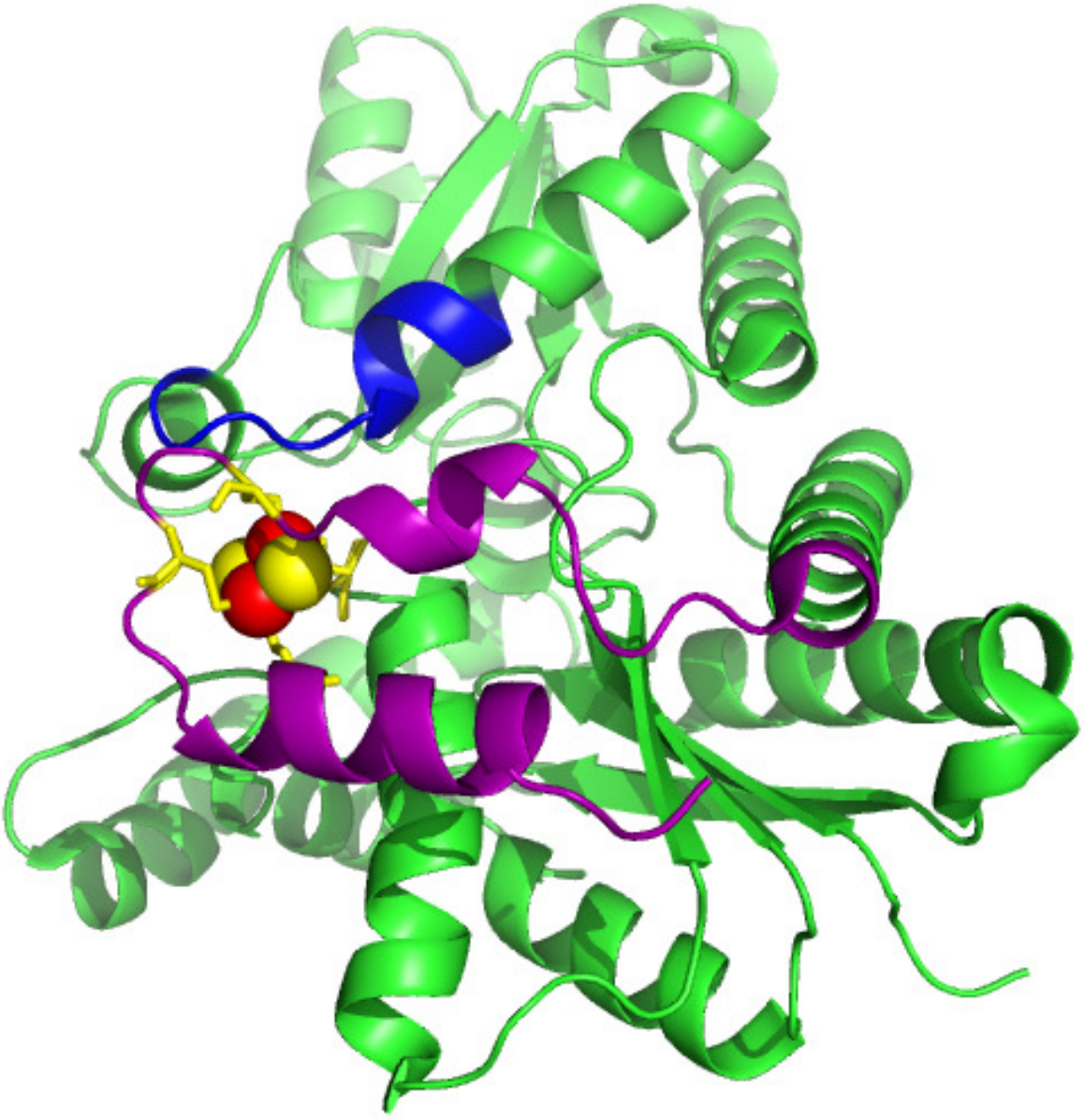

Figure 1.7. Heme and siroheme biosyntheses from uroporphyrinogen III. The figure outlines the different enzymes involved in the two biosynthetic pathways, the reactions catalyzed and the products. The role of iron in cellular metabolism is highlighted, including its role as substrate for heme/siroheme and Fe-S cluster biosyntheses. The relationship between siroheme role in Fe and S metabolism is also indicated. *P*, propionate side chain; *V*, vinyl side chain; *A*, acetate side chain; *UROD*, uroporphyrinogen III decarboxylase; *CPO*, coproporphyrinogen III oxidase; *PPO*, protoporphyrinogen oxidase; *Fc*, ferrochelatase; *UPM1*, uroporphyrinogen III methyltransferase; *SirC*, dihydrosirohydrochlorin dehydrogenase; *SirB Fc*, sirohydrochlorin ferrochelatase. Adapted from refrence (*146*).

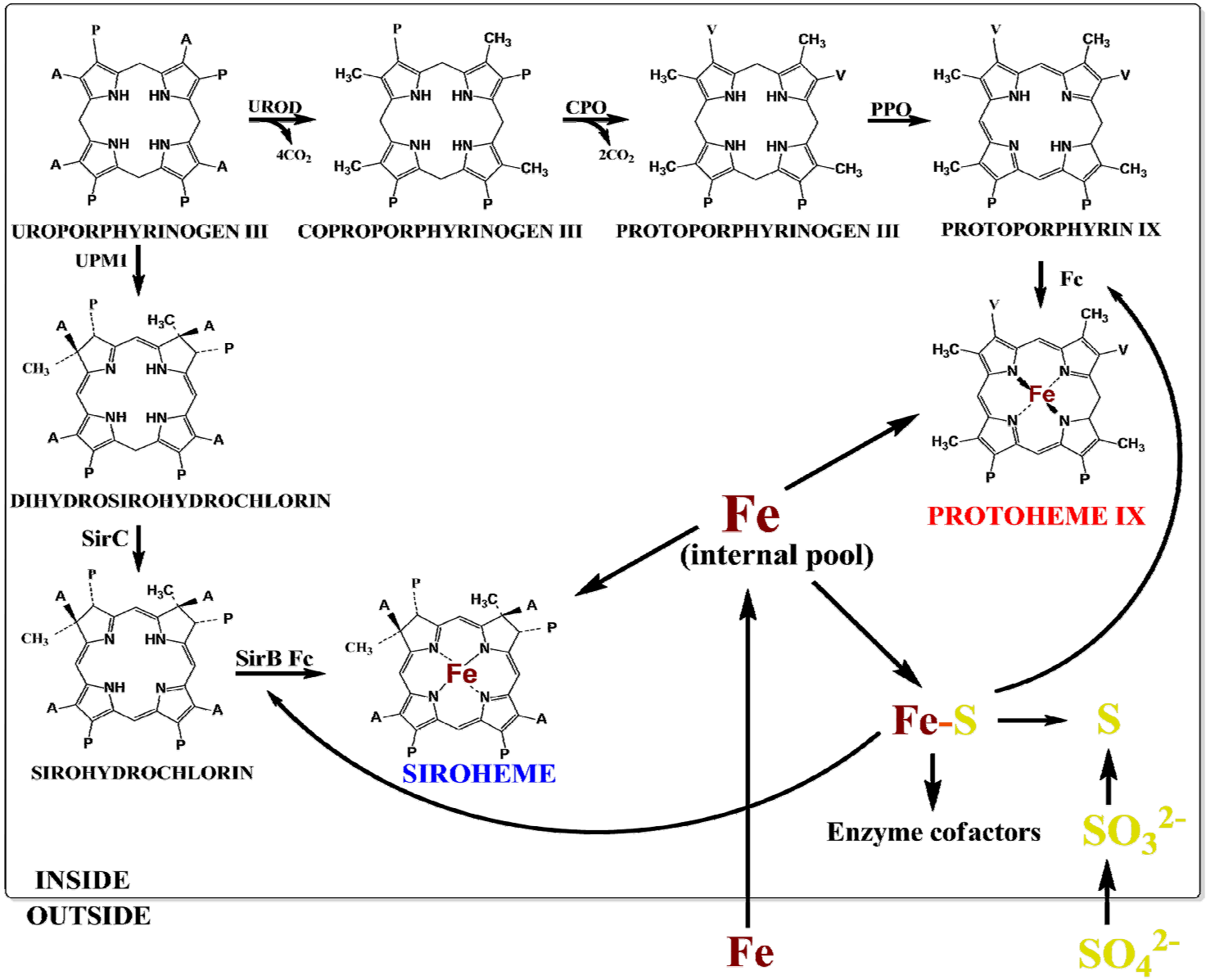
UROD
4CO2
CPO
2CO2
PPO
UROPORPHYRINOGEN III
COPROPORPHYRINOGEN III
PROTOPORPHYRINOGEN III
PROTOPORPHYRIN IX
UPM1
DIHYDROSIROHYDROCHLORIN
SirC
SirB Fc
SIROHYDROCHLORIN
SIROHEME
Fc
PROTOHEME IX
Fe
(internal pool)
Fe-S
S
Enzyme cofactors
SO3 2-
SO4 2-
Fe
INSIDE
OUTSIDE

Figure 1.8. Amino acid sequence comparison of *A. thaliana* and *B. megaterium* sirohydrochlorin ferrochelatases. Protein alignment of AtSirB Fc without the N-terminal targeting sequence and BmSirB Fc was obtained using ClustalW program (*81*), accessible at www.expasy.org. Residues sharing 90% similarity are shaded in magenta, while residues sharing 90% functional similarity are shaded in cyan. The cysteine resides thought to be involved in the [2Fe-2S] cluster ligation are shaded in red.

```
A_thaliana_SirBFc     ----------DADGIIIVDHGSRRRESNLMLEEFVKMFKEKTGYPIVEPAHMELAEPSIK  50
B_megaterium_SirBFc   MHKKLTKEVDYMDAVLYVCHGSRVKEGADQAVAFIERCKKNLDVPIQEVCFLELASPTIE  60

A_thaliana_SirBFc     DAFSLCVQQGAKRVVVSPFFLFPGRHWHTDIPSLTADAAKEFSGISYLITAPLGPHNLLL  110
B_megaterium_SirBFc   QGFEACIEQGATRIAIVPLLLLTAAHAKHDIPEEIQKVYERYPQVEVLYGEPFGVDERIV  120

A_thaliana_SirBFc     DVVNDRIQHCLSHVEGDADECLVCAGTN-----------------------KCKLYNS  145
B_megaterium_SirBFc   DILVERINETNVDKHEDSMVLLVGRGSSDPAVKRDLNEIAQLLKGKGAFKEVSTCYLAAA  180

A_thaliana_SirBFc     S-------------------------------------------------------- 146
B_megaterium_SirBFc   SPNLKEGLHLAKRTSYKQVFVLPYLLFTGILMNEIKEELEQLSTDAQQFILANYLGYHDG  240

A_thaliana_SirBFc     -------------------------
B_megaterium_SirBFc   LAHILSHQVKTLLSSKGNQYDVYRYA 260
```

Figure 1.9. Class I and II Grxs domain organization and classification. Domain organization of class I and class II Grxs from photosynthetic organisms such as cyanobacteria, algae and terrestrial plants, are shown as cyan and pink, respectively. The correspondence to class I and II in other model organisms such as *Sc, Saccharomyces cerevisiae; Hs, Homo sapiens; Ec, Escherichia coli* is also depicted. Blue, green, light brown, tan, and dark orange colored domains illustrate a domain of unknown function, a Trx-like domain, a HesB domain, a rhodanese domain, and a ferredoxin–thioredoxin reductase domain, respectively. Adapted from (*210*).

Class I

GrxC1 to C5, S12, *Hs* Grx1 and 2,

Ec Grx1 and 3, *Sc* Grx1, 2, 6 and 7

Class II

GrxS14/S15, *Sc* Grx5, *Hs* Grx5,

Ec Grx4, *Av* Grx-nif

GrxS16 (specific to plants)

GrxS17 (higher plants)

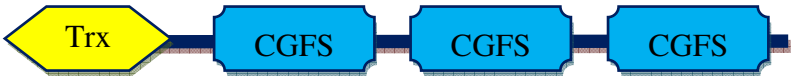

GrxS17 (lower plants, algae)

PICOT=*Hs* Grx3

Sc Grx3p, *Sc* Grx4p

Fusion proteins (*xanthomonadales-myxococcales*)

Desulfotalea psychrophila LSv54

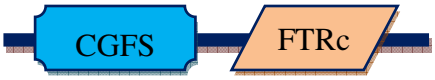

Figure 1.10. Crystal structures of monothiol *E. coli* Grx4 *versus* dithiol *H. sapiens* Grx2 active sites with bound [2Fe-2S] clusters. (**A**) Cartoon overlay of *E. coli* Grx4 monomer (orange) (PDB entry 1YKA) and cluster-bound homodimer (green) (PDB entry 2WCI) The GSH molecule present in the homodimer is shown as pale green sticks. (**B**) Cartoon overlay of monomer, GSH-bound monomer and cluster-bound homodimer structures of *H. sapiens* Grx2 (PDB entries 2CQ9, 2FLS, and 2HT9, respectively) shown in cyan, blue and purple, respectively. GSH molecule is represented as pale blue or pale pink sticks. The [2Fe-2S] clusters are depicted as gray, Fe and yellow, S spheres. For clarity, the second monomer of the homodimer structures and its related GSH molecule have been omitted. Major conformational changes between the monomer and dimer conformations in *E. coli* Grx4 structure is indicated by the black arrows. Taken with permission from reference (*196*).

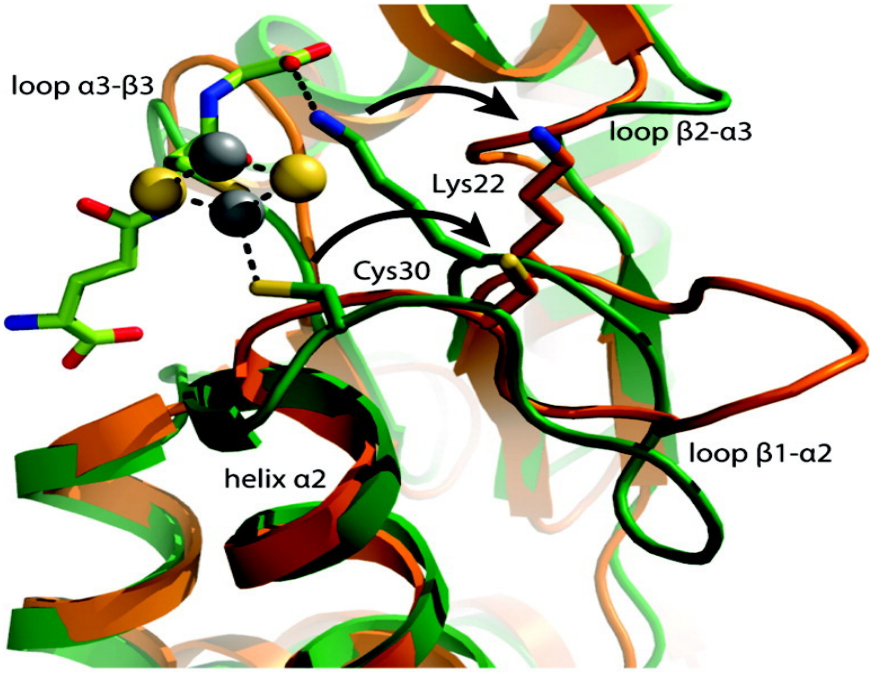
loop α3-β3
loop β2-α3
Lys22
Cys30
loop β1-α2
helix α2

A

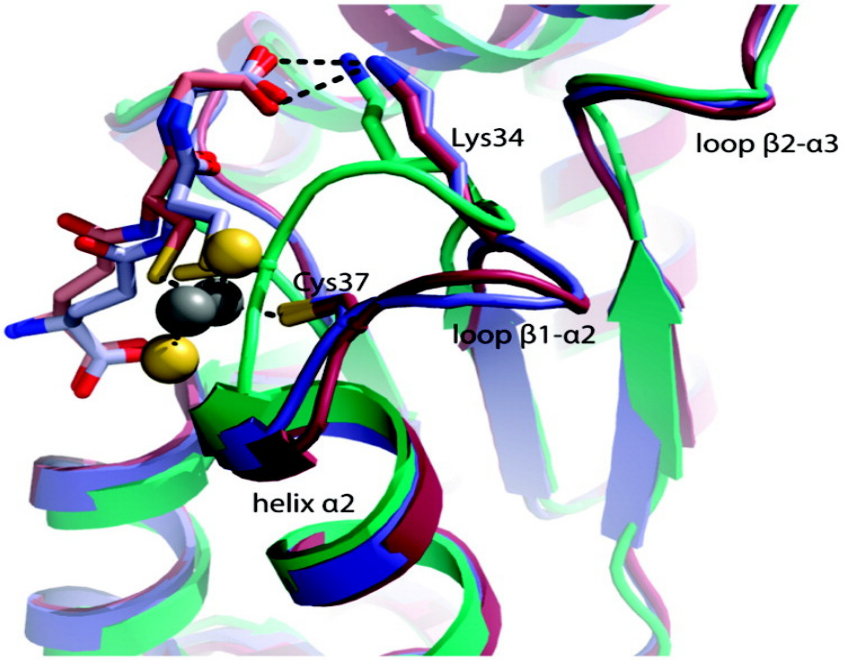
Lys34
loop β2-α3
Cys37
loop β1-α2
helix α2

B

Figure 1.11. Differences in the orientation of Grx monomers with respect to each other in *E. coli* monothiol Grx4 (A) and *H. sapiens* dithiol Grx2 (B). A continuous color spectrum ranging from blue, indicating the N-terminus, to red indicating, the C-terminus, was used to depict one monomer. Yellow and blue sticks represent the GSH moieties of *E. coli* Grx4 and human Grx2, respectively, whereas Fe-S clusters are shown as orange and yellow spheres, respectively. Taken with permission from reference (*196*).

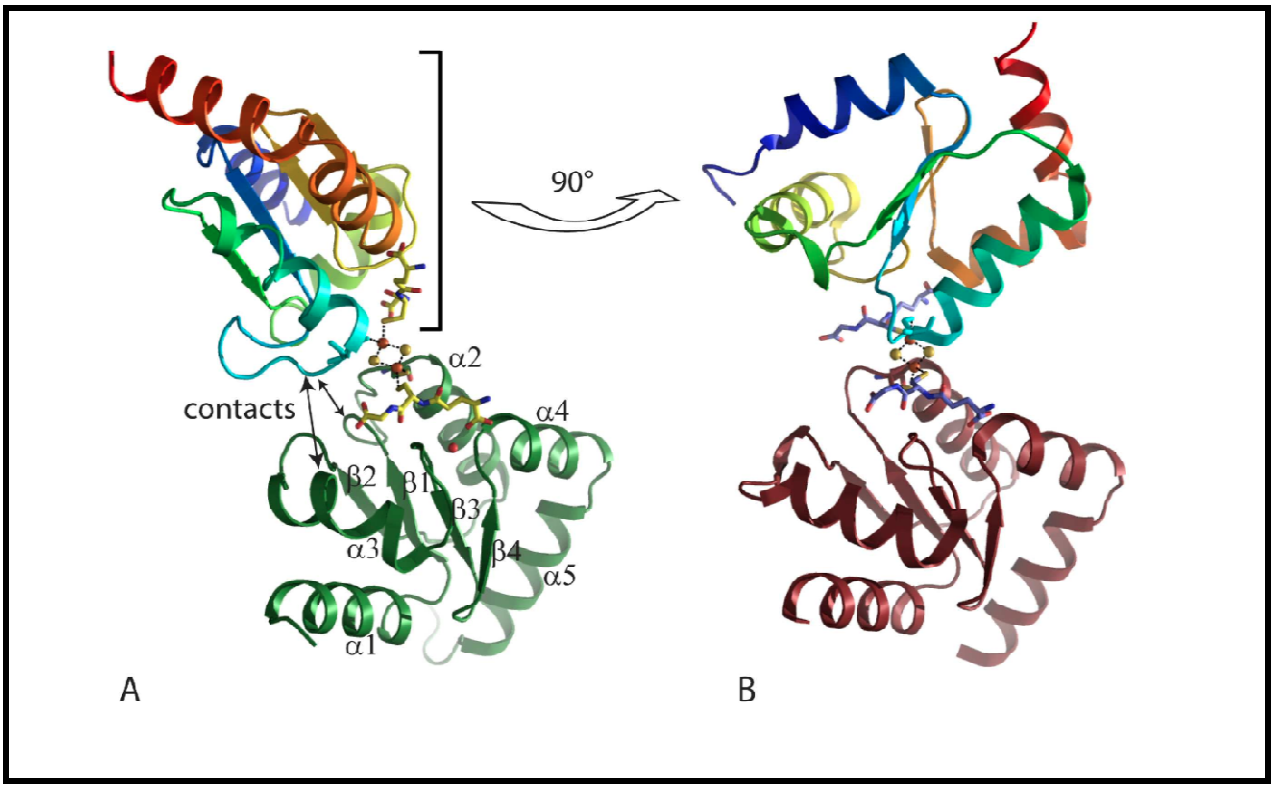
90°
α2
contacts
α4
β2
β1
β3
α3
β4
α5
α1
A
B

Figure 1.12. Model for heme regulation via Fe-S cluster biosynthesis in erythroid cells. Both heme and Fe–S cluster independent biosynthetic pathways require iron (red balls) which is imported into the mitochondrion. Under normal Fe–S clusters assembly conditions, dependent on Grx5, the bifunctional protein IRP1 acts as a cytoplasmic aconitase (c-aconitase), which requires a [4Fe-4S] cluster (shown as red and yellow balls) for catalytic function; as a result, translation of ALAS2 protein needed for the catalysis of the first step of heme biosynthesis proceeds normally. When the production of Fe–S clusters is impaired, IRP1 switches to IRE-binding activity, and binds the IRE present in the 50 UTR of ALAS2 mRNAs, preventing its synthesis and thereby blocking heme production. Adapted from reference (*204*).

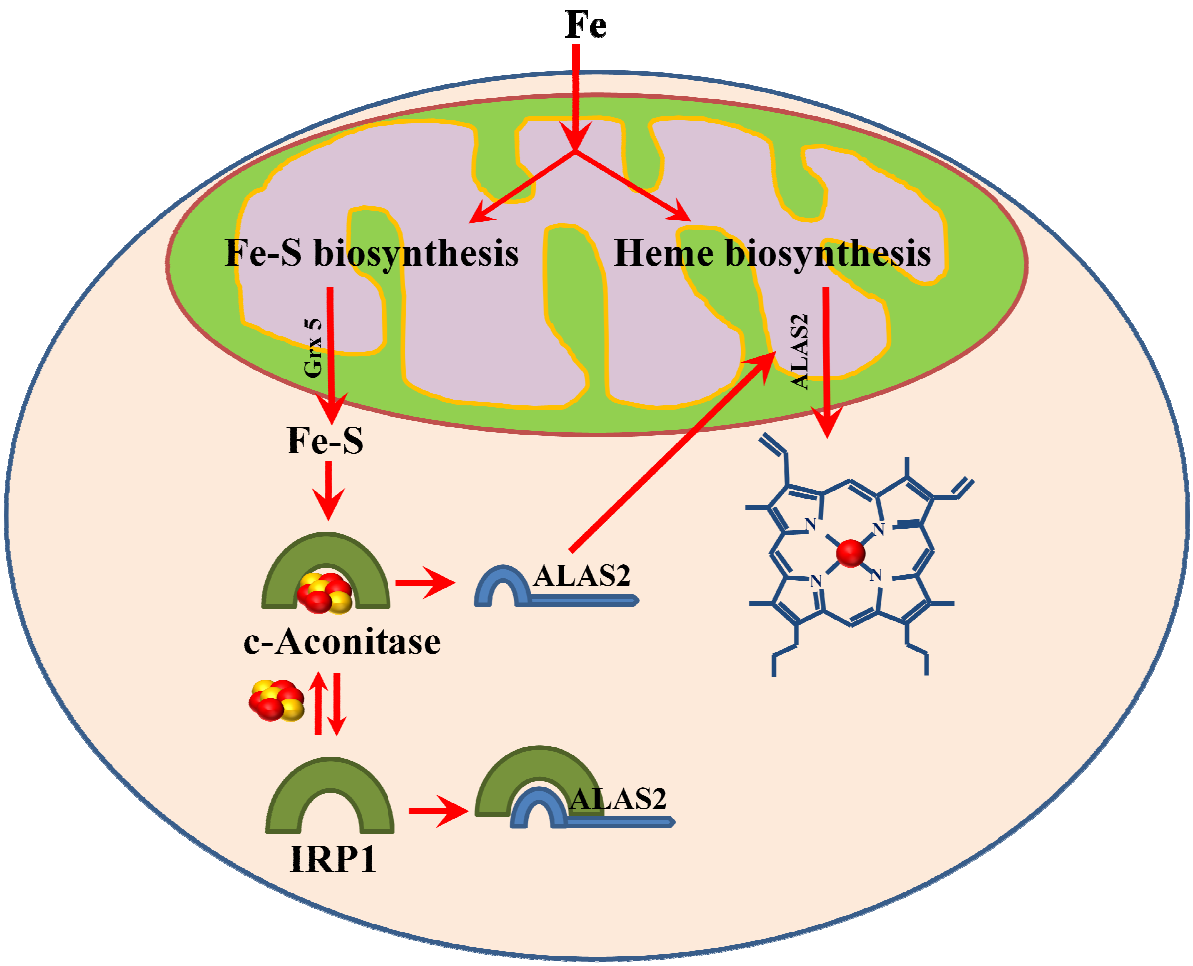
Fe
Fe-S biosynthesis
Heme biosynthesis
Grx 5
ALAS2
Fe-S
ALAS2
c-Aconitase
ALAS2
IRP1

CHAPTER 2

EFFECTS OF COORDINATION ENVIRONMENT AND SPATIAL ARRANGEMENT OF CYTEINE LIGANDS ON REDOX AND SPECTROSCOPIC PROPERTIES OF [2FE-2S] CENTERS FROM VARIOUS FERROCHELATASES

Angela-Nadia Albetel,[‡] Tamara A. Dailey,[§] Ish K. Dhawan,[‡] Harry A. Dailey,[§] and Michael K. Johnson[‡]

to be submitted to Journal of Biological Inorganic Chemistry

[‡]Department of Chemistry and Center for Metalloenzyme Studies, and [§]Biomedical and Health Sciences Institute, University of Georgia, Athens, Georgia, 30602, USA

Abbreviations: CD, circular dichroism; EPR, electron paramagnetic resonance; RR, resonance Raman; DT, sodium dithionite; CT, charge-transfer;

Abstract

Ferrochelatase (E.C. 4.99.1.1), the terminal enzyme of the heme biosynthetic pathway, catalyzes the insertion of ferrous iron into protoporphyrin IX with the formation of protoheme IX. Ferrochelatases from all metazoans, Actinobacteria and a handful of Gram negative bacteria contain a labile $[2Fe\text{-}2S]^{2+}$ center that is required for enzymatic activity. Crystallographic data on human ferrochelatase indicate that the cluster is coordinated by four cysteinyl residues with a unique spacing motif, which is reflected in the spectroscopic properties of the [2Fe-2S] center. The detailed redox and spectroscopic characterization of $[2Fe\text{-}2S]^{2+,+}$ cluster-containing ferrochelatases from human, *Schizosaccharomyces pombe, Caulobacter crescentus*, *Myxococcus xanthus*, *Mycobacterium tuberculosis*, *Streptomyces coelicolor*, and *Propionibacter freudenreichii* undertaken in this work indicates significant differences in the coordination environment and electronic properties of the $[2Fe\text{-}2S]^{2+,+}$ clusters that are ligated by distinct primary sequence arrangements of conserved cysteine residues in ferrochelatases. The marked differences in both the UV-visible/CD absorption and resonance Raman spectra are consistent with subtle structural and electronic effects rationalized as arising from variations in the spatial orientation of the amino acid residues surrounding the $[2Fe\text{-}2S]^{2+,+}$ centers and from differences in the Fe-S bond strengths and Fe-S_γ-C_β-C_α dihedral angles. EPR studies show distinctive ground and excited state properties for the paramagnetic $[2Fe\text{-}2S]^{+}$ clusters in each of the seven enzyme analyzed, with midpoint potentials (pH 8.0, 23°C) spanning from -385 mV to >-480 mV, depending on the organism the protein was isolated from. Except for the $[2Fe\text{-}2S]^{+}$ center in *S. pombe* enzyme which exhibits a unique spin-coupled EPR signal involving the $S = ½$ $[2Fe\text{-}2S]^{+}$ center and nearby organic radical, all other ferrochelatases investigated show rhombic or near-axial $S = ½$ EPR resonances with diverse *g*-value anisotropies. The differences in the redox,

structural, magnetic and vibrational properties of $[2Fe\text{-}2S]^{2+,+}$ centers in ferrochelatases are interpreted in terms of marked variations in the coordination environment of the $[2Fe\text{-}2S]^{2+,+}$ centers that result primarily from distinct primary sequence arrangements of conserved cysteine residues.

Introduction

Protoporphyrin IX ferrochelatases (E.C. 4.99.1.1) are a family of structurally diverse class II chelatases that are responsible for inserting ferrous iron into protoporphyrin IX, to yield protoheme IX and two protons, thus catalyzing the last step of the heme biosynthetic pathway (*1-3*). Interestingly, considerable structural diversity exists among ferrochelatases from different kingdoms of life. For instance, in organisms such as *Bacillus subtilis* and *Mycobacterium tuberculosis* ferrochelatases exist as monomers (*4;5*), whereas bovine and human enzymes have been shown to exist as homodimers (*1;6-8*). In addition, with the exception of Gram positive bacterial ferrochelatases, such as those from *B. subtilis* and *M. tuberculosis*, which are soluble proteins (*1;5;9;10*), the majority of prokaryotic and all eukaryotic ferrochelatases studied to date were found to be bound to cellular membranes (*1*).

Although comparison of all currently known ferrochelatases reveals less than 10% homology in their primary sequence, at the tertiary level the overall structure is highly conserved (*1*). A comparison of all currently known ferrochelatase sequences shows the presence of three distinct domains: the first domain (I) is an amino-terminal organelle-targeting motif and is present in all eukaryotes, being involved in targeting the enzyme to the mitochondrion and/or chloroplasts (*1;2;11*). The second domain (II) is present in all ferrochelatases and represents the core 330 amino acid residues. In addition, domain II contains all of the amino acids involved in catalysis. Finally, the third domain (domain III) present in all eukaryotes, a small number of recently identified prokaryotes including C*aulobacter crescentus, M. tuberculosis, Propionibacter freudenreichii*, and *Rickettsia prowazekii,* as well as plants, represents a carboxy-terminal extension that varies in length from 30 to 50 amino acids, with plants having the longest extensions (*2;5*). Domain III is involved in the dimerization motif for these enzymes and, with

the exception of yeast *Saccharomyces cerevisiae* and plant enzymes, it contains three of the four cysteinyl residues that ligate the [2Fe-2S] cluster, with the fourth cluster ligand residue being present in domain II (*8;12-15*). The [2Fe-2S] centers contained by all eukaryotic and prokaryotic ferrochelatases investigated thus far are labile, yet crucial for activity (*5;13;15;16*), although the specific role(s) of the [2Fe-2S] center have yet to be elucidated.

Despite an obvious diversity regarding the spatial arrangement of the cysteine residues coordinating the [2Fe-2S] cluster among ferrochelatases isolated from eukaryotic and prokaryotic organisms, it is now clear that all eukaryotic enzymes share the same [Cys-X_{206}-Cys-X_2-Cys-X_4-Cys] coordination motif, with three of the four cysteine residues involved in ligating the cluster being located in the C-terminal extension of the amino acid sequences of these ferrochelatases (*2*). In bacteria, three distinct primary sequence arrangements of conserved cysteine residues have been identified for the coordination of the [2Fe-2S] center: [C-X_{170}-C-X_6-C-X-C], found in *C. crescentus* and *R. prowazekii*, [C-X_{209}-C-X_3-C-C], present in *P. freudenreichii*, *Streptomyces coelicolor*, and [C-$X_?$-C-X_8-C-X_4-C], found in *M. tuberculosis* (*2;5*). Similarly to metozoan ferrochelatases, all of these bacterial enzymes contain three of the four cysteinyl ligands of the [2Fe-2S] clusters present in a C-terminal extension. Additionally, a separate class of bacterial ferrochelatases including those from *Myxococcus xanthus*, *Azotobacter vinelandii*, and *Bdellovibrio bacteriovorus* have been identified to contain a [2Fe-2S] cluster ligated by a set of four cysteinyl residues located in an internal amino acid insertion. The spatial arrangement between these conserved residues was determined to be [C-X_5-CC-X_9-C] via mutagenesis studies (*17*).

To date, X-ray crystal structures are available for ferrochelatases from *B. subtilis (4)*, *B. anthracis*, *S. cerevisiae (18)* and human (*8*). In addition to the crystallographic studies on the

human enzyme, spectroscopic studies have been carried out to investigate the structural, electronic, magnetic and vibrational properties of the $[2Fe\text{-}2S]^{2+,+}$ cluster present in this protein (*7;15*), with results indicating a number of interesting features exhibited by the [2Fe-2S] center. For instance, resonance Raman and variable-temperature magnetic dichroism measurements showed different dihedral angles, spatial orientation and surrounding environment for the cysteinyl residues coordinating the [2Fe-2S] cluster the human ferrochelatase in comparison to any other [2Fe-2S] clusters currently known and structurally characterized (*15*). As a result, it was initially suggested that one of the coordinating ligands of the [2Fe-2S] cluster might be oxygenic in nature (*15;19*). However, this initial hypothesis was ruled out once the crystal structure of human ferrochelatase revealed that two of the dihedral angles ($Fe\text{-}S_{\gamma}\text{-}C_{\beta}\text{-}C_{\alpha}$) for the cluster were close to 180°, therefore explaining the unusual resonance Raman and VTMCD data (*8*). Due to such a unique geometry, the peptide backbone is moved further away from the [2Fe-2S] cluster, resulting in a distinctly more "open" binding site. Crystallographic results also indicated that unlike most [2Fe-2S] cluster-containing proteins, the ligand geometry of the [2Fe-2S] cluster from human ferrochelatase minimizes any potential hydrogen bonding from the backbone imide protons. As a consequence, each cluster is only bonded by the ligating cysteine residues and has no additional hydrogen bonds.

In spite of the diversity demonstrated via site directed mutagenesis studies in the coordinating motifs for the [2Fe-2S] cluster present in different ferrochelatases, which is expected to be reflected in the structural, electronic or vibrational properties of the [2Fe-2S] centers, no detailed spectroscopic characterization has been reported to date for any other cluster-containing enzyme, except for that isolated from human. We report here a detailed comparison of the spectroscopic and redox properties of oxidized and reduced forms of wild type

ferrochelatases isolated from both prokaryotic (*M. tuberculosis*, *S. coelicolor*, *C. crescentus*, *M. xanthus*, *P. freudenreichii*) and eukaryotic (*S. pombe* and human) organisms using the combination of EPR, UV-visible absorption, CD absorption and resonance Raman spectroscopies. The seven different proteins employed in this study are representative examples of each of the different classes of ferrochelatases identified thus far in terms of oligomeric state and/or distinct primary sequence arrangements of conserved cysteine residues involved in ligating the [2Fe-2S] cluster. The implications of the results for the structural, magnetic, electronic and vibrational properties of the $[2Fe\text{-}2S]^{2+,+}$ clusters from ferrochelatases are discussed in relationship to their coordination environment.

Experimental Procedures

Materials. Materials used in this work were of reagent grade and were purchased from Fischer Scientific, Sigma-Aldrich Chemical Co, Invitrogen, or VWR International, unless otherwise stated.

Protein expression and purification. Recombinant proteins from *C. crescentus*, *M. xanthus*, *M. tuberculosis*, *S. coelicolor*, *P. freudenreichii*, *S. pombe* and human were produced and expressed in *Escherichia coli* and subsequently purified as previously described (*5*).

Chemical analysis. Protein concentrations were determined either by the DC protein assay (Bio-Rad) in conjunction with the microscale modified procedure of Brown et al (*20*), using bovine serum albumin as a standard (Roche), or estimated spectrophotometrically. The theoretical extinction coefficients at 280 nm used for spectroscopic quantitation of *M tuberculosis, S. coelicolor*, *C. crescentus, M. xanthus, P. freudenreichii, S. pombe* and human ferrochelatases were: $\varepsilon = 49{,}710\ M^{-1}\ cm^{-1}$,$\varepsilon = 40{,}255\ M^{-1}\ cm^{-1}$, $\varepsilon = 52{,}840\ M^{-1}\ cm^{-1}$, $\varepsilon = 49{,}765\ M^{-1}\ cm^{-1}$, $\varepsilon = 34{,}170\ M^{-1}\ cm^{-1}$,$\varepsilon = 47{,}300\ M^{-1}\ cm^{-1}$, $\varepsilon = 46{,}640\ M^{-1}\ cm^{-1}$, respectively. Protein

concentrations are based on protein monomer unless otherwise stated. Iron concentrations were determined after $KMnO_4$/HCl protein digestion as described by Fish (*21*), using a 1000 ppm atomic absorption iron standard to prepare standard solutions of known Fe concentration (Fluka).

Spectroscopic methods. Spectroscopic studies were carried out on ferrochelatase samples in 50 mM Tris-MOPS buffer, pH 8.0, containing 0.1 mM KCl, 1% (w/v) sodium cholate, unless otherwise specified. UV-visible absorption and CD spectra were recorded in 1 mm quartz cuvettes at room temperature, using a Shimadzu UV-3101PC spectrophotometer and Jasco J-715 spectropolarimeter, respectively. X-band (~9.6 GHz) EPR spectroscopy was performed on dithionite-reduced samples prepared under anaerobic conditions, using a Bruker ESP-300E spectrometer (Billerica, MA) equipped with an ER-4116 dual-mode cavity and an Oxford Instruments ESR-9 flow cryostat (Concord, MA) (4.2-300 K). Methyl viologen was added in the reduction mixture of *C. crescentus*, *M. tuberculosis*, and *P. freudenreichii* ferrochelatases in order to reach a lower reductive potential. Spin quantitations were carried out under non-saturating conditions by double integration, and calibrated using a 1 mM Cu-EDTA standard. Resonance Raman spectra were recorded at 20 K with a 457.9 nm excitation from Coherent Innova 10 W (Santa Clara, CA) argon ion laser incident on 17 µl frozen droplets of concentrated samples (1.3–5.3 mM) mounted on the cold finger of an Air Products Displex Model CSA-202E closed cycle refrigerator (Air Products, Allentown, PA). Spectra were recorded digitally using photon counting electronics of an Instruments SA Ramanor U1000 spectrometer (Instruments SA, Edison, NJ). Multiple scans (~ 80) were collected and averaged in order to increase the signal-to-noise ratio.

Redox potentiometry. Dye-mediated redox titration of *S. coelicolor* ferrochelatase was carried out in an anaerobic glovebox (O_2 < 2 ppm) at 23°C. The titration mixture contained a 2.8

ml solution of 50 μM *S. coelicolor* ferrochelatase in 50 mM Tris-MOPS, pH 8.0, 0.1 M KCl, 1.0% (w/v) sodium cholate. Eight redox dye mediators (methyl viologen (- 453 mV), benzyl viologen (- 350 mV), neutral red (- 325 mV), safranin O (- 289 mV), phenosafranin (- 252 mV), anthraquinone-1,5-disulphonate (- 170 mV), 2-hydroxy-1,4-naphthoquinone (- 145 mV), indigo-disulphonate (- 125 mV)) were added at final concentration of 50 μM each, in order to enhance the electronic contact between the protein molecules and the electrode. The reductant and oxidant used were sodium dithionite (20 mg/ml) and potassium ferricyanide (50 mg/ml) respectively. Titration points were taken from potentials ranging from -550 to -250 mV by adding small amounts of reductant to the fully oxidized *S. coelicolor* ferrochelatase. After each addition of reductant, the sample was stirred and allowed to come to a stable potential, then 250 μl of sample was transferred to an anaerobic EPR tube and frozen in liquid nitrogen. Potentials were measured using a Ag/AgCl electrode (+197 mV versus normal hydrogen electrode (NHE)) as the reference electrode. All EPR samples were measured at 35K, and the intensity of the [2Fe-2S]$^{1+}$ g = 1.94 was quantified using double integration, plotted against the potential and fitted to a Nernst equation curve (n = 1).

Results and Discussion

As purified recombinant ferrochelatases from human, yeast *S. pombe*, and bacterial *S. coelicolor, C. crescentus, P. freudenreichii, M. tuberculosis* and *M. xanthus* were purified, assayed, and analyzed for Fe content. The results are illustrated in Table 2.1. and indicate that, except for *S. coelicolor* and *P. freudenreichii* enzymes which contain somewhat lower levels of Fe/molecule (~1.5 Fe/molecule), all other five samples contain approximately 1.75-1.98 Fe/molecule, suggesting the presence of one [2Fe-2S] cluster per protein monomer.

UV-visible spectroscopy. The UV-visible absorption spectra of [2Fe-2S] complexes are broad and contain many overlapping bands due to charge-transfer (CT) transitions from both bridging S^{2-} and terminal $CysS^{-}$ ligands, which have not been specifically assigned (*22*). All five (half-filled) Fe^{3+} d orbitals are available as terminal orbitals for the CT transitions, and are expected to fall into two groups, d_σ and d_π with a separation, 10 *Dq*, estimated to be ~ 10000 cm^{-1} for tetrahedral Fe^{3+} in a sulfur environment. Each S^{2-} has four filled valence orbitals (*s*, p_x, p_y, p_z) available for CT transitions, while RS^{-} has three, the energies of these orbitals depending on the bonding interactions in the complex.

As expected for oxidized $[2Fe\text{-}2S]^{2+}$ cluster-containing proteins, the seven ferrochelatases investigated absorb light strongly and show overlapping absorption bands through the visible region and near-UV, which reflects $S \rightarrow Fe^{3+}$ charge-transfer electronic transitions. As a result, aerobically purified samples of each of the seven proteins exhibit a distinct brown-red color, and the UV-visible absorption spectra illustrated and compared in Figure 2.1. are similar to those of other proteins which contain $[2Fe\text{-}2S]^{2+}$ clusters, *e.g.,* ferredoxins (*23*), Rieske proteins (*24*), and spinach dihydroxy-acid dehydratase (*25*). In addition to the protein absorption bands at 280 nm, all UV-visible spectra exhibit bands in the 326-337 nm visible region, with two or more peaks and/or shoulders in the 418-460 nm and 511-570 nm regions, with varying relative intensities and extinction coefficients depending on the organism the ferrochelatase was isolated from (See Table 2.1). The differences in the absorption features and relative intensities of some bands can be interpreted in terms of subtle structural and electronic effects arising from variations in the intensity of numerous overlapping ligand-to-metal charge transfer electronic transitions that might have either more or less pronounced d_π- or d_σ - character. The absorption spectra of *C. crescentus, M. xanthus* and human proteins show an additional band at about 420 nm that was

attributed in part to a minor component of low-spin Fe(III) associated with ferrochelatase, that varied in intensity for different preparations.

Biological $[2Fe\text{-}2S]^{2+}$ clusters typically have visible absorption bands centered around 330 nm (ε in the range of 11 000-16 000 $M^{-1}cm^{-1}$), 420 nm (ε in the range of 8000-11 000 $M^{-1}cm^{-1}$), and 460 nm (ε in the range of 6000-10 000 $M^{-1}cm^{-1}$), with a broad shoulder centered around 550 nm (ε in the range of 3000-6 000 $M^{-1}cm^{-1}$) (*23;24;26;27*). On the basis of the theoretical and experimental ε_{280} values (ε ≈ 40.255mM^{-1} cm^{-1}, ε ≈52.840 mM^{-1} cm^{-1}, ε ≈49.765 mM^{-1} cm^{-1}, ε ≈ 34.170 mM^{-1} cm^{-1} , ε ≈49.710 mM^{-1} cm^{-1}, ε ≈ 47,300 M^{-1} cm^{-1},and ε ≈ 46.640 mM^{-1} cm^{-1} for *S. coelicolor*, *C. crescentus, M. xanthus, P. freudenreichii, M tuberculosis, S. pombe* and human ferrochelatases, respectively), the $\varepsilon_{326\text{-}337}$, $\varepsilon_{418\text{-}460}$, and $\varepsilon_{511\text{-}570}$ values for the $[2Fe\text{-}2S]^{2+}$ center in the seven ferrochelatases investigated are estimated to range between 9700-17 100 M^{-1} cm^{-1}, 6000-9500 M^{-1} cm^{-1}, and 2400-6100 M^{-1} cm^{-1}, respectively, if we consider only samples that contain >1.7 Fe/molecule (see Table 2.1). Although the extinction coefficients for ferrochelatases appear to be somewhat lower than those observed for other biological $[2Fe\text{-}2S]^{2+}$ clusters, the results are consistent with the presence of approximately one [2Fe-2S] cluster per protein monomer (see Table 2.1).

CD spectroscopy. The CD spectra of [2Fe-2S] cluster-containing metalloenzymes are extremely sensitive to the environment of the chromophore, and, as a consequence, circular dichroism absorption spectroscopy has emerged as a sensitive tool that provides diagnostic fingerprints for identifying and distinguishing between different biological $[2Fe\text{-}2S]^{2+,+}$ clusters. In addition, generally, $[2Fe\text{-}2S]^{2+,+}$ clusters exhibit visible CD spectra that are an order of magnitude more intense than those of biological [4Fe-4S] centers, making them suitable candidates for structural investigations using CD absorption spectroscopy. The room temperature

CD spectra of the as prepared recombinant ferrochelatases from human, *S. coelicolor*, *C. crescentus, M. xanthus, P. freudenreichii, M tuberculosis,* and *S. pombe* in the visible region are shown in Figure 2.2. and indicate significant differences in the relative positions and intensities of various bands, consistent with substantial changes in the cluster environments for the seven $[2Fe\text{-}2S]^{2+}$ centers investigated. Considering the low amino acid sequence homology and structural diversity among ferrochelatases (*1;2*), the uniqueness of each of the seven CD spectra presented in Figure 2.2. is most likely associated with variations in the protein conformation in the vicinity of the cluster and/or spatial arrangement and orientation of the $[2Fe\text{-}2S]^{2+}$ cluster-coordinating cysteine residues. Perhaps there are subtle variations in the polarity of the cluster binding pocket as defined by local residues as well as Langevin dipoles from backbone amides that are also relevant to the unusually low midpoint redox potentials observed for the $[2Fe\text{-}2S]^{2+,+}$ clusters from some of the bacterial ferrochelatases (see below) (*28*).

EPR spectroscopy. X-band EPR spectra in the $S = ½$ region of dithionite-reduced ferrochelatases from human, *S. coelicolor*, *M. xanthus, P. freudenreichii,* and *S. pombe* are shown and compared in Figure 2.3 and were obtained with samples frozen within 30 s of dithionite reduction, since all samples started to precipitate on prolonged exposure to excess dithionite. Dithionite reduction resulted in bleaching of the visible absorption and the appearance of a broad band centered at 550 nm (data not shown). This feature is characteristic of $[2Fe\text{-}2S]^{+}$ clusters and has been attributed to a Fe(II)/Fe(III) intervalence band (*29*). With the exception of *S. pombe* ferrochelatase, all samples investigated display either rhombic or near axial $S = ½$ EPR resonances, with the $[2Fe\text{-}2S]^{+}$ cluster from *M. xanthus* ferrochelatase exhibiting the greatest *g*-value anisotropy (g = 2.054, 1.930, 1.888), and the $[2Fe\text{-}2S]^{+}$ center from *S. coelicolor* enzyme presenting the smallest *g*-value anisotropy (g = 1.989, 1.970, 1.906). *P. freudenreichii*

ferrochelatase exhibits an EPR signal that is best simulated with g = 2.052, 1.958, 1.892 (see Figure 2.3). As expected, the [2Fe-2S]$^{+}$ cluster in human ferrochelatase displays an EPR signal identical to that observed in previously published reports (*15*), with g = 2.002, 1.936, 1.912. Considering the similarity in the spatial arrangement of the cysteine residues ligating the [2Fe-2S]$^{2+,+}$ clusters in human and yeast *S. pombe* ferrochelatases, and the previously reported marked similarities of the EPR spectra and g values obtained for various [2Fe-2S]$^{2+,+}$ cluster-containing ferrochelatases that share the same C-X_{206}-C-X_2-C-X_4-C coordination motif (*13-15*), a similar EPR spectrum was expected to be observed for the [2Fe-2S]$^{+}$ cluster from *S. pombe* ferrochelatase. Surprisingly though, the EPR spectrum of *S. pombe* ferrochelatase exhibits a more complex signal in the S = ½ region with components at g = 2.015, 1.998, 1.96, 1.914, 1.882 that suggests a complex signal resulting from weak spin coupling with a nearby S = ½ radical species. This is confirmed by the broad half-field g = 4.18 feature corresponding to $\Delta m_s = \pm 2$ transition that is characteristic of weakly spin coupled systems (*30;31*). Comparison of the amino acid residues located <10 Å of the [2Fe-2S]$^{+}$ center in various ferrochelatases sharing the C-X_{206}-C-X_2-C-X_4-C coordination motif (see Figure 2.4), reveals that Tyr194 (human enzyme numbering), which is located only about 5.9 Å away from the [2Fe-2S] center (see Figure 2.5), is replaced by Trp159 in the *S. pombe* homologue. Thus a tryptophan radical is the most likely candidate for the S = ½ radical species that is coupled to the S = ½ [2Fe-2S]$^{+}$ center in *S. pombe* ferrochelatase. As shown in Figure 2.4. all other eukaryotic ferrochelatases contain a Tyr at this position, similar to human enzyme, thus explaining the similarity in their EPR spectra.

Unfortunately, the [2Fe-2S]$^{2+}$ clusters from the bacterial *M. tuberculosis* and *C. crescentus* could not be reduced even upon prolonged incubation times (up to 10 minute) with sodium dithionite and/or addition of methyl viologen to the protein solution (added in an attempt

to lower the redox potential and increase cluster susceptibility to reduction), but protein precipitation was observed. In all samples for which the reduction of the $[2Fe\text{-}2S]^{2+}$ center was possible, the resonances undergo power saturation with microwave powers >0.25 mW at 15 K and are observed without significant broadening up to 100 K. These slow-relaxing properties are consistent with the presence of $[2Fe\text{-}2S]^{+}$ clusters in all ferrochelatases investigated.

Where spin quantitation was possible, for freshly prepared samples that were reduced under anaerobic conditions, the resonance accounted for approximately 0.85-1.0 spin/molecule (see Table 2.1), consistent with one $[2Fe\text{-}2S]^{+}$ cluster per monomer. The lower value (0.4 spin/molecule) obtained in the case of the $[2Fe\text{-}2S]^{+}$ cluster from *M. xanthus* ferrochelatase can be rationalized in terms of increased protein instability in the reduced form. Indeed, some protein precipitation was observed upon incubation with dithionite even for samples handled under strict anaerobic conditions, suggesting enhanced lability of the reduced cluster compared to the oxidized cluster. In addition, in the case of the bacterial *P. freudenreichii* ferrochelatase, only partial reduction of the $[2Fe\text{-}2S]^{2+}$ center was observed, and this was made possible only after addition of methyl viologen to the protein solution. As a consequence though, spin quantitation analysis was impossible in this case due to major contributions arising from the EPR signal corresponding to the methyl viologen radical species centered around g = 2.00 overlapping the EPR signal of the $[2Fe\text{-}2S]^{+}$ cluster.

The midpoint redox potential of the $[2Fe\text{-}2S]^{2+,+}$ cluster in *S. coelicolor* ferrochelatase was determined at pH 8.0 and 23°C by EPR measurements of the intensity of the g = 1.97 signal originating from the $[2Fe\text{-}2S]^{+}$ species. This signal diminishes upon raising the potential of the solution as the EPR silent $[2Fe\text{-}2S]^{2+}$ species is produced and reappears when the protein solution is subsequently reduced with dithionite. The intensity of the g = 1.97 signal of the [2Fe-

$2S]^{1+}$ cluster plotted against the poised potential and fitted to a Nernst equation curve (n = 1) (see Figure 2.6.) yielded a midpoint redox potential of -385 ± 10 mV upon averaging of the oxidative and reductive data sets. The midpoint redox potential of the $[2Fe\text{-}2S]^{2+,+}$ cluster in *S. coelicolor* ferrochelatase appears to be about 70 mV higher than the potential reported for the cluster of R115L human ferrochelatase (-453 mV) (*7*), and about 20 mV higher than the redox potential reported for the $[2Fe\text{-}2S]^{2+,+}$ cluster of mouse liver ferrochelatase (-405 mV) (*32*). Overall, the midpoint redox potential for the $[2Fe\text{-}2S]^{2+,+}$ centers in ferrochelatases is comparable to that of plant-type ferredoxins, for which the redox potential ranges from -325 mV to -425 mV, rather than that of vertebrate-type ferredoxins, which have generally higher redox potential, falling in the range from -235 mV to 275 mV (*33*). Unfortunately, the EPR measurements of the midpoint redox potentials of the $[2Fe\text{-}2S]^{2+,+}$ clusters in *M. xanthus* ferrochelatase was impractical due to marked protein instability in the reduced form. In addition, since the $[2Fe\text{-}2S]^{2+}$ clusters from *C. crescentus* and *M. tuberculosis* ferrochelatases are not reducible using dithionite, even in the presence of methyl viologen (see above), we estimate that the midpoint redox potential of this clusters at pH 8.0 and 23°C is < -480 mV. As stated above, the $[2Fe\text{-}2S]^{2+,+}$ centers in *P. freudenreichii* was only partially reduced upon addition of methyl viologen (see Figure 2.3.), and although its midpoint redox potential could not be determined accurately at room temperature and pH 8.0, it can be reasonably estimated to be lower than that of the human ferrochelatase (<-450 mV) (see Table 2.1.). For *S. pombe* ferrochelatase the midpoint redox potential of the $[2Fe\text{-}2S]^{2+,+}$ cluster is also expected to be similar to that of its human homolog or lower, yet it could not be determined also due to protein instability in the reduced form.

Taken together, the distinctive ground and excited state properties of the paramagnetic $[2Fe\text{-}2S]^{+}$ centers from all of the seven ferrochelatases investigated as resulted from the above

presented EPR study are best interpreted as effects of the differences in the cluster coordination motifs encountered in each of these individual proteins, therefore supporting the conclusion drawn from the UV-visible and CD absorption spectroscopic studies, as well as resonance Raman results (see below).

RR spectroscopy. Resonance Raman has emerged as a sensitive structural probe for oxidized $[2Fe\text{-}2S]^{2+}$ clusters in metalloenzymes, and reliable vibrational assignments based on extensive IR and Raman studies on isotopically labeled synthetic analog complexes, *e.g.* $[Fe_2S_2(SR)_4]^{2-}$, are available (*34-36*). Based on the arrangement of conserved cysteines, three distinct classes have been proposed for the [2Fe-2S] cluster-containing proteins with complete cysteinyl coordination (*37;38*): plant-type ferredoxins (typified by *Spinacia oleracea* ferredoxin), hydroxylase or Isc-type proteins (typified by adrenodoxin), and bacterial [2Fe-2S] ferredoxins or thioredoxin-type proteins (typified by *Clostridium pasteurianum* ferredoxins). Surprisingly, the most extensively investigated ferrochelatase, namely that isolated from human, does not fall in any of these three categories. Furthermore, the structural, electronic and vibrational properties of the [2Fe-2S] center in human ferrochelatase are significantly different from those of other structurally and spectroscopically characterized [2Fe-2S]-containing proteins with full cysteinyl ligation (*8;15*). These differences are explained by the unusual spatial orientation of the cysteine side chains in the human enzyme as illustrated in Figure 2.7. Superpositioning of crystal structure of human ferrochelatase with nine other various structurally characterized [2Fe-2S] cluster-containing proteins clearly depicts the substantial differences in the three dimensional orientation of the $[2Fe\text{-}2S]^{2+}$ cluster cysteine ligands (see Figure 2.7.). In addition, measurement of the Fe-S_γ-C_β-C_α dihedral angles for each of the ten proteins illustrated in Figure 2.7. indicates that only in human ferrochelatase two of the Fe-S_γ-C_β-C_α dihedral angles are close to 180°,

whereas no significant differences are observed in the respective dihedral angles of the remaining proteins (see Table 2.2.). Coupling of the Fe-S_γ stretching frequencies with the S_γ-C_β-C_α bending modes of the thiolate ligands that occurs near 300 cm^{-1} is one of the most important factors known to cause Raman shifts (*39*). This coupling is maximal when the Fe-S_γ-C_β-C_α dihedral angle is 180° because of the motion alignment of the Fe-S_γ and S_γ-C_β-C_α. As previously reported, the presence of such unusual dihedral angles in human ferrochelatase appear to account for the approximately 10 cm^{-1} up-shift of the predominantly Fe-S(Cys) vibrational mode centered around 295 cm^{-1} in this enzyme (*8*).

The vibrational properties of the $[2Fe\text{-}2S]^{2+}$ clusters in *S. pombe*, *P. freudenreichii, M. xanthus, C. crescentus, S. coelicolor*, and *M tuberculosis* ferrochelatases were characterized by resonance Raman and compared to the RR spectrum of the human enzyme. The low temperature (20 K) resonance Raman spectra of the oxidized $[2Fe\text{-}2S]^{2+}$ clusters from these seven proteins in the Fe-S stretching region (240-450 cm^{-1}), obtained with the visible 457.9-nm laser excitation are shown and compared in Figure 2.8. Although the Fe-S stretching frequencies are most similar to those of $[2Fe\text{-}2S]^{2+}$ clusters with complete cysteinyl ligation (*29;36*), distinctive features are observed in the Fe-S stretching frequencies and band intensities when compared to each other, to other structurally characterized [2Fe-2S] cluster-containing proteins (*29;36*) or to model compounds such as the $[Fe_2S_2(S_2\text{-}o\text{-xyl})^{2-}$ synthetic analog (*35*) (see Table 2.2). The Fe–S stretching modes for the $[2Fe–2S]^{2+}$ centers in the seven ferrochelatases investigated are readily assigned by direct analogy with the assignments established via $^{32/34}S^{b}$ and $^{54/56}Fe$ isotope shifts and normal mode calculations for the three representatives classes of the all cysteine-ligated $[2Fe–2S]^{2+}$ clusters mentioned above and the $[Fe_2S_2(S_2\text{-}o\text{-xyl})^{2-}$synthetic analogue (see Table 2.3) (*29;35*). The differences in the Fe-S frequencies observed in the RR spectra of the [2Fe-

$2S]^{2+}$ clusters in the seven ferrochelatases analyzed can be rationalized in terms of minor variations in the Fe-S bond strengths and differences in the Fe-S_γ-C_β-C_α dihedral angles which govern the extent of mixing between cysteinyl S_γ-C_β-C_α bending modes and the Fe-S_γ stretching modes. In addition, since band intensities in RR spectra depend critically on the symmetry and structural distortion in the electronic excited states, the differences observed in the relative band intensities in the RR spectra of the seven ferrochelatases analyzed can be interpreted in terms of changes in the energies of the numerous S→Fe(III) charge transfer excited states rather than significant structural differences. These observations are not surprising, if one considers the differences in the primary sequence arrangements of conserved cysteine residues coordinating the [2Fe-2S] centers in each of the ferrochelatases investigated here ([C-X_{206}-C-X_2-C-X_4-C] for human and *S. pombe* ferrochelatases; [C-X_{170}-C-X_6-C-X-C] for *C. crescentus* ferrochelatase; [C-X_{209}-C-X_3-C-C] for *P. freudenreichii* and *S. coelicolor* enzymes; [C-X_5-C-C-X_9-C] in *M. xanthus* ferrochelatase; and [C-$X_?$-C-X_8-C-X_4-C] in *M. tuberculosis* enzyme (*5;14;17;19*)), and the marked differences in the midpoint redox potentials (ranging from -385 mV for the $[2Fe\text{-}2S]^{2+,+}$ cluster in *S. coelicolor* ferrochelatase to -453 mV or less for human, *S. pombe*, and *P. freudenreichii* enzymes, to <-480mV in *M. tuberculosis* and *C. crescentus* proteins) and their EPR properties (see Table 2.1. and Figure 2.3).

Conclusions

The spectroscopic results presented herein provide supporting evidence for the assembly of $[2Fe\text{-}2S]^{2+,+}$ clusters with full cysteinyl ligation in all seven ferrochelatases investigated. Moreover, we conclude that the combination of UV-visible and CD absorption, resonance Raman and EPR spectroscopies which indicate distinctive redox, structural, electronic and vibrational properties for the $[2Fe\text{-}2S]^{2+,+}$ centers present in these enzymes that are most likely

due to marked differences in the coordination environment around the cluster as well as spatial arrangement and orientation of coordinating cysteine residues. The low redox potentials for the $[2Fe\text{-}2S]^{2+,+}$ redox couple, taken together with the instability of the reduced clusters, also indicates that the reduced state is unlikely to be utilized under physiological conditions. Nevertheless, crystallographic data will be required for a more complete understanding of the variations in the redox and spectroscopic properties of these $[2Fe\text{-}2S]^{2+}$ centers.

Acknowledgements

This work was supported by grant GM62524 (M.K.J.) from the National Institute of Health, and grant DK32303 (H.A.D.).

References

1. Dailey, H. A. and Dailey, T. A. (2003) in *The Porphyrin Handbook* (Kadish, K. M., Smith, R., and Guilard, R., Eds.) pp 93-121, Academic Press, New York.
2. Dailey, H. A., Dailey, T. A., Wu, C.-K., Medlock, A. E., Wang, K.-F., Rose, J. P., and Wang, B.-C. (2000) *Cell. Mol. Life Sci. 57*, 1909-1926.
3. Dailey, H. A. (1996) in *Mechanisms of Metallocenter Assembly* (Hausinger, R. P., Eichorn, G. L., and Marzilli, L. G., Eds.) pp 77-98, VCH, New York.
4. Al-Karadaghi, S., Hansson, M., Nikonov, S., Jonsson, B., and Hederstedt, L. (1997) *Structure 5*, 1501-1510.
5. Dailey, T. A. and Dailey, H. A. (2002) *J. Bacteriol. 184*, 2460-2464.
6. Straka, J. C., Bloomer, J. R., and Kempner, E. S. (1991) *J. Biol. Chem. 266*, 24637-24641.
7. Burden, A. E., Wu, C., Dailey, T. A., Busch, J. L., Dhawan, I. K., Rose, J. P., Wang, B., and Dailey, H. A. (1999) *Biochim. Biophys. Acta 1435*, 191-197.
8. Wu, C.-K., Dailey, H. A., Rose, J. P., Burden, A., Sellers, V. M., and Wang, B.-C. (2001) *Nat. Struct. Biol. 8*, 156-160.
9. Dailey, H. A. (2002) *Biochem. Soc. Trans. 30*, 590-595.
10. Hansson, M. and Hederstedt, L. (1994) *Eur. J Biochem. 220*, 201-208.
11. Karr, S. R. and Dailey, H. A. (1988) *Biochem. J. 254*, 799-803.
12. Dailey, H. A., Sellers, V. M., and Dailey, T. A. (1994) *J. Biol. Chem. 269*, 390-395.
13. Day, A. L., Parsons, B. M., and Dailey, H. A. (1998) *Arch. Biochem. Biophys. 359*, 160-169.
14. Sellers, V. M., Wang, K. F., Johnson, M. K., and Dailey, H. A. (1998) *J. Biol. Chem. 273*, 22311-22316.
15. Dailey, H. A., Finnegan, M. G., and Johnson, M. K. (1994) *Biochemistry 33*, 403-407.

16. Medlock, A. E. and Dailey, H. A. (2000) *Biochemistry 39*, 7461-7467.

17. Shepherd, M., Dailey, T. A., and Dailey, H. A. (2006) *Biochem. J. 397*, 47-52.

18. Karlberg, T., Lecerof, D., Gora, M., Silvegren, G., Labbe-Bois, R., Hansson, M., and Al-Karadaghi, S. (2002) *Biochemistry 41*, 13499-13506.

19. Crouse, B. R., Sellers, V. M., Finnegan, M. G., Dailey, H. A., and Johnson, M. K. (1996) *Biochemistry 35*, 16222-16229.

20. Brown, R. E., Jarvis, K. L., and Hyland, K. J. (1989) *Anal. Biochem. 180*, 136-139.

21. Fish, W. W. (1988) *Meth. Enzymol. 158*, 357-364.

22. Noodleman, L., Case, D. A., and Aizman, A. (1988) *J. Am. Chem. Soc. 110*, 1001-1005.

23. Palmer, G. (1973) in *Iron-Sulfur Proteins* (Lovenberg, W., Ed.) pp 285-325, Academic Press, Orlando, FL.

24. Fee, J. A., Findling, K. L., Yoshida, T., Hille, R., Tarr, G. E., Hearshen, D. O., Dunham, W. R., Day, E. P., Kent, T. A., and Münck, E. (1984) *J. Biol. Chem. 259*, 124-133.

25. Flint, D. H. and Emptage, M. H. (1988) *J. Biol. Chem. 263*, 3558-3564.

26. Stephens, P. J., Thomson, A. J., Dunn, J. B. R., Keiderling, T. A., Rawlings, J., Rao, K. K., and Hall, D. O. (1978) *Biochemistry 17*, 4770-4778.

27. Ta, D. T. and Vickery, L. E. (1992) *J. Biol. Chem. 267*, 11120-11125.

28. Soriano, A., Li, D., Bian, S., Agarwal, A., and Cowan, J. A. (1996) *Biochemistry 35*, 12479-12486.

29. Fu, W., Drozdzewski, P. M., Davies, M. D., Sligar, S. G., and Johnson, M. K. (1992) *J. Biol. Chem. 267*, 15502-15510.

30. Mathews, R., Charlton, S., Sands, R. H., and Palmer, G. (1974) *J. Biol. Chem. 249*, 4326-4328.

31. Steenkamp, D. J. and Singer, T. P. (1978) *Biochem. J. 169*, 361-369.

32. Lloyd, S. G., Franco, R., Moura, J. J., Moura, I., Ferreira, G. C., and Huynh, B. H. (1996) *J. Am. Chem. Soc. 118*, 9892-9900.

33. Hurley, J. K., Weber-Main, A. M., Hodges, A. E., Stankovich, M. T., Benning, M. M., Holden, H. M., Cheng, H., Xia, B., Markley, J. L., Genzor, C., Gomez-Moreno, C., Hafezi, R., and Tollin, G. (1997) *Biochemistry 36*, 15109-15117.

34. Spiro, T. G., Czernuszewicz, R. S., and Han, S. (1988) in *Resonance Raman spectra of heme and metalloproteins* (Spiro, T. G., Ed.) pp 523-554, John Wiley & Sons, New York.

35. Han, S., Czernuszewicz, R. S., and Spiro, T. G. (1989) *J. Am. Chem. Soc. 111*, 3496-3504.

36. Han, S., Czernuszewicz, R. S., Kimura, T., Adams, M. W. W., and Spiro, T. G. (1989) *J. Am. Chem. Soc. 111*, 3505-3511.

37. Meyer, J., Moulis, J.-M., and Lutz, M. (1986) *Biochim. Biophys. Acta 873*, 108-118.

38. Meyer, J., Bruschi, M. H., Bonicel, J. J., and Bovier-Lapierre, G. E. (1986) *Biochemistry 25*, 6054-6061.

39. Yachandra, V. K., Hare, J., Moura, I., and Spiro, T. G. (1983) *J. Am. Chem. Soc. 105*, 6455-6461.

40. DeLano, W. L. The PyMOL Molecular Graphics System. [1.2r3pre]. 2002. Palo Alto, CA, Schrödinger, LLC. Ref Type: Computer Program

41. Chenna, R., Sugawara, H., Koike, T., Lopez, R., Gibson, T. J., Higgins, D. G., and Thompson, J. D. (2003) *Nucleic Acids Res. 31*, 3497-3500.

Table. 2.1. UV-visible absorption band wavelengths and molar extinction coefficients for the ferrochelatases investigated in this work. The Fe/monomer values as determined from analytical assays, the spin/monomer values corresponding to the $[2Fe\text{-}2S]^{+}$ cluster concentration as determined by EPR spin quantifications, and the midpoint redox potentials obtained from dye-mediated redox titration and fitting of the data to the Nernst equation are also listed. Abbreviations used: *Mtb*, *Mycobacterium tuberculosis*; *Sc*, *Streptomyces coelicolor*; *Cc*, *Caulobacter crescentus*; *Mx*, *Myxococcus xanthus*; *Pf*, *Propionibacter freudenreichii*; *Sp*, *Schizosaccharomyces pombe*; Fc, ferrochelatase;

	Band (nm)	Shoulder (nm)	Shoulder (nm)	Shoulder (nm)	Fe / monomer	Spin / monomer	E (mV)
	ε ($M^{-1}cm^{-1}$)	ε ($M^{-1}cm^{-1}$)	ε ($M^{-1}cm^{-1}$)	ε ($M^{-1}cm^{-1}$)			
***Mtb* Fc**	326	426	467	-	1.70	-[a]	< - 480[a]
	9,762	7,282	6,077	-			
***Sc* Fc**	337	433	528	575	1.52	0.85	-385
	8,331	4,654	2,672	1,822			
***Cc* Fc**	332	420	459	557	1.98	-[a]	< -480[a]
	11,193	8,736	7,042	3,038			
***Mx* Fc**	322	418	455	570	1.8	0.4[b]	-[b]
	12,480	9,435	6,713	2,430			
***Pf* Fc**	337	420	461	568	1.46	-[c]	< -450[c]
	6,651	4,572	4,028	1,805			
***Sp* Fc**	327	450	520	582	1.86	1.00±0.15	< -450[b]
	15,770	8,180	6,100	3,790			
Human Fc	330	460	550	-	1.9	0.75 ± 0.25 (*15*)	-453 (*7*)
	17,090	8,410	5,900				

[a] The $[2Fe\text{-}2S]^{2+}$ could not be reduced even when methyl viologen was added as a mediator to decrease the redox potential of dithionite; [b] The midpoint redox potential could not be determined due to protein instability in the reduced form; [c] The midpoint redox potential could not be determined due to the significant contribution to the EPR signal arising from the radical species formed upon addition of methyl viologen.

Table 2.2. Arrangement of coordination residues and dihedral angles for the Fe-S_γ-C_β-C_α bonds among structurally characterized [2Fe-2S] cluster-containing proteins with full cysteine ligation. Dihedral angles were measured using the PyMOL software (*40*) starting from the lowest numbered residue (C196 in human ferrochelatase, bottom right corner in Figure 2.8.) and proceeding in a counterclockwise fashion following the diagram presented in Figure 2.8.

Protein	Coordination motif	Cys1	Cys2	Cys3	Cys4
Human Ferrochelatase (1HRK)	N-C-X_{206}-C-X_2-C-X_4-C-COO	160	103	109	179
Human Ferredoxin (3P1M)	N-C-X_4-C-X_2-C-X_{29}-C-COO	81	45	128	117
Spinach Ferredoxins (1A70)	N-C-X_4-C-X_2-C-X_{29}-C-COO	60	61	122	116
***C. pasteurianum* Fe-only Hydrogenase (1C4C)**	N-C-X_{11}-C-X_2-C-X_{29}-C-COO	66	65	124	118
Phthalate Dioxygenase Reductase (2PIA)	N-C-X_4-C-X_2-C-X_{27}-C-COO	61	67	113	128
Bovine Adrenodoxin (1AYF)	N-C-X_5-C-X_2-C-X_{36}-C-COO	66	59	138	115
CO Dehydrogenase (1FFV)	N-C-X_4-C-X_2-C-X_{11}-C-COO	56	53	129	125
Fumarate Reductase (1QLB)	N-C-X_4-C-X_2-C-X_{11}-C-COO	53	60	101	111
Aldehyde Dehydrogenase (3L4P) – first cluster	N-C-X_4-C-X_2-C-X_{11}-C-COO	59	67	118	118

Table 2.3. $[2Fe\text{-}2S]^{2+}$ Resonance Raman frequencies in *M tuberculosis, S. coelicolor*, *C. crescentus, M. xanthus, P. freudenreichii,* human, and *S. pombe* ferrochelatases by comparison to the $[Fe_2S_2(S_2\text{-}o\text{-}xyl)_2]^{2-a}$ synthetic model compound, and representative examples of the three major classes of all cysteinyl-ligated $[2Fe\text{-}2S]^{2+}$ cluster-containing proteins.

Mode[c]	*Mtb* Fc	*Sc* Fc	*Cc* Fc	*Mx* Fc	*Pf* Fc	Human Fc	*Sp* Fc	S_2-*o*-xyl[a]	*So* Fd[d]	*Cp* Fd[d]	Ado[d]
$\mathbf{B_{2u}}^{b}$	-	412	408	419	416	420	417	415	427	404	421
$\mathbf{A_g}^{b}$	389	386	386	391	392	398	390	391	395	387	393
$\mathbf{B_{3u}}^{b}$	361	356	353	352	352	365	360	342	367	366	349
$\mathbf{B_{1u}}^{t}$, $\mathbf{B_{2g}}^{t}$	350	351	330	336	330	350	346	327, 324[b]	357	353	341
$\mathbf{A_g}^{t}$	328	326	320	323	322	341	341	323	338	335	329
$\mathbf{B_{1g}}^{b}$	315	316	313	286	316	320	315	313	329	313	317
$\mathbf{B_{3u}}^{t}$	385	290	285	270	284	295	295	276	283	290	291

[a] *o*-Xylene-α,α-dithiolate analogue; assignments taken from ref. (*35*). [b] values calculated with 0 cm^{-1} $^{34}S^{b}$. [c] Symmetry labels for Fe-S stretching modes assuming an idealized $Fe_2S_2{}^{b}S_4{}^{t}$ core; *b*, bridging or inorganic S; *t*, terminal or cysteinyl S. [d] Assignments taken from ref.(*29*). *Mtb*, *Mycobacterium tuberculosis*; *Sc*, *Streptomyces coelicolor*; *Cc*, *Caulobacter crescentus*; *Mx*, *Myxococcus xanthus*; *Pf*, *Propionibacter freudenreichii*; *Sp*, *Schizosaccharomyces pombe*; *So*, *Spinacea oleracea*; *Cp*, *Clostridium pasteurianum*; Fc, ferrochelatase; Fd, ferredoxins; Ado, adrenodoxin.

Figure 2.1. Room temperature absorption spectra of various recombinant ferrochelatases. Recombinant ferrochelatases from *M. tuberculosis*, *S. coelicolor*, *C. crescentus*, *M. xanthus*, *P. freudenreichii*, *S. pombe*, and human were in 50 mM Tris-MOPS buffer, pH 8.0, with 0.1 M KCl, and 1% (w/v) sodium cholate. Spectra were recorded in 1 mm cuvettes and extinction coefficient (ε) values are based on protein monomers. The small amounts of Fe(III) low spin heme contained by *C. crescentus*, *M. xanthus*, and human enzymes are indicated by an asterisk.

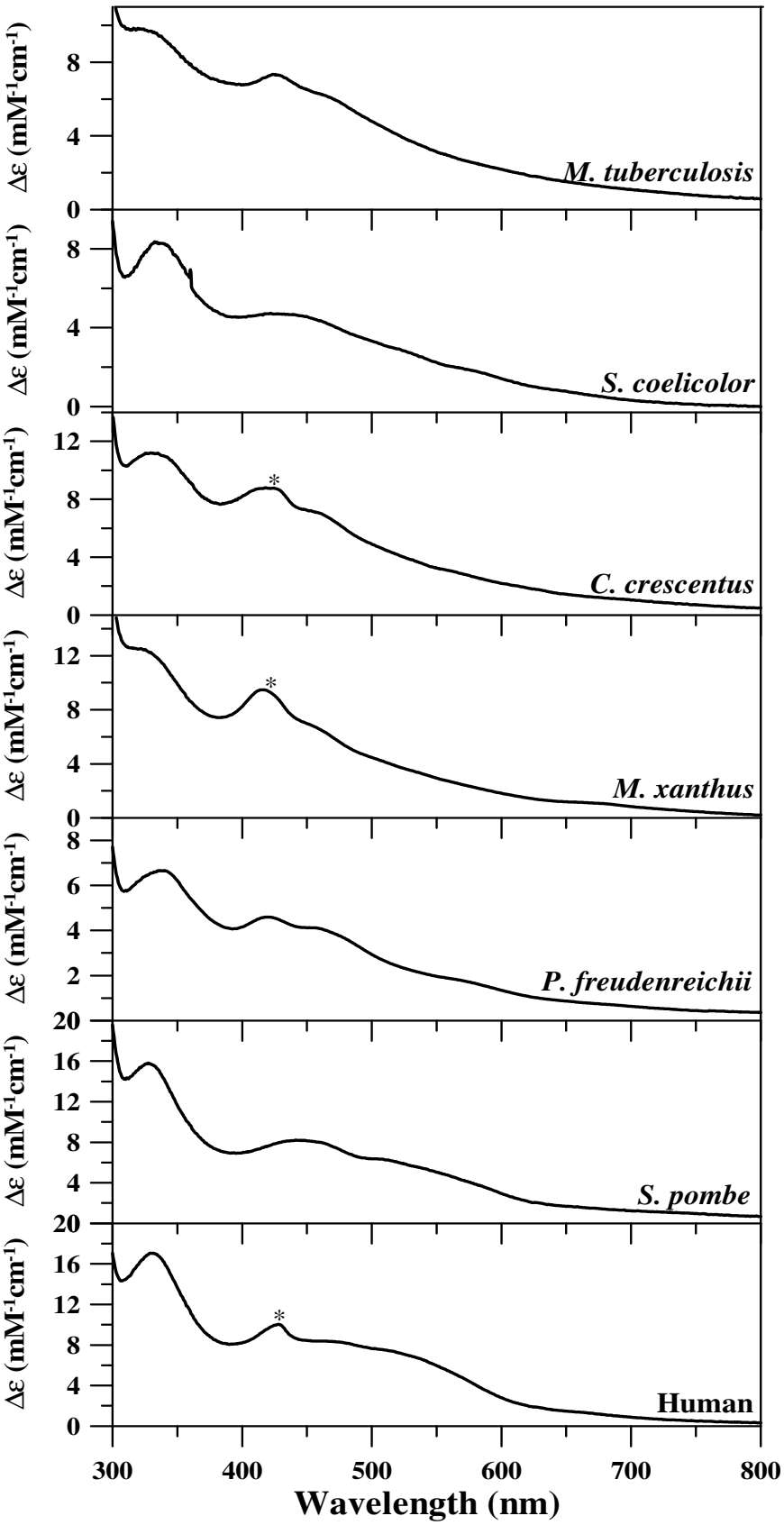
Δε (mM-1cm-1)
M. tuberculosis
S. coelicolor
C. crescentus
M. xanthus
P. freudenreichii
S. pombe
Human
*
Wavelength (nm)
300
400
500
600
700
800

Figure 2.2. Comparison of room temperature CD spectra of various ferrochelatases. Recombinant ferrochelatases from human, *S. coelicolor*, *C. crescentus, M. xanthus, P. freudenreichii, M tuberculosis,* and *S. pombe* ferrochelatases were in 50 mM Tris-MOPS buffer, pH 8.0, with 0.1 M KCl, and 1% (w/v) sodium cholate. Spectra were recorded in 1 mm cuvettes and $\Delta\varepsilon$ values are based on protein monomer concentration.

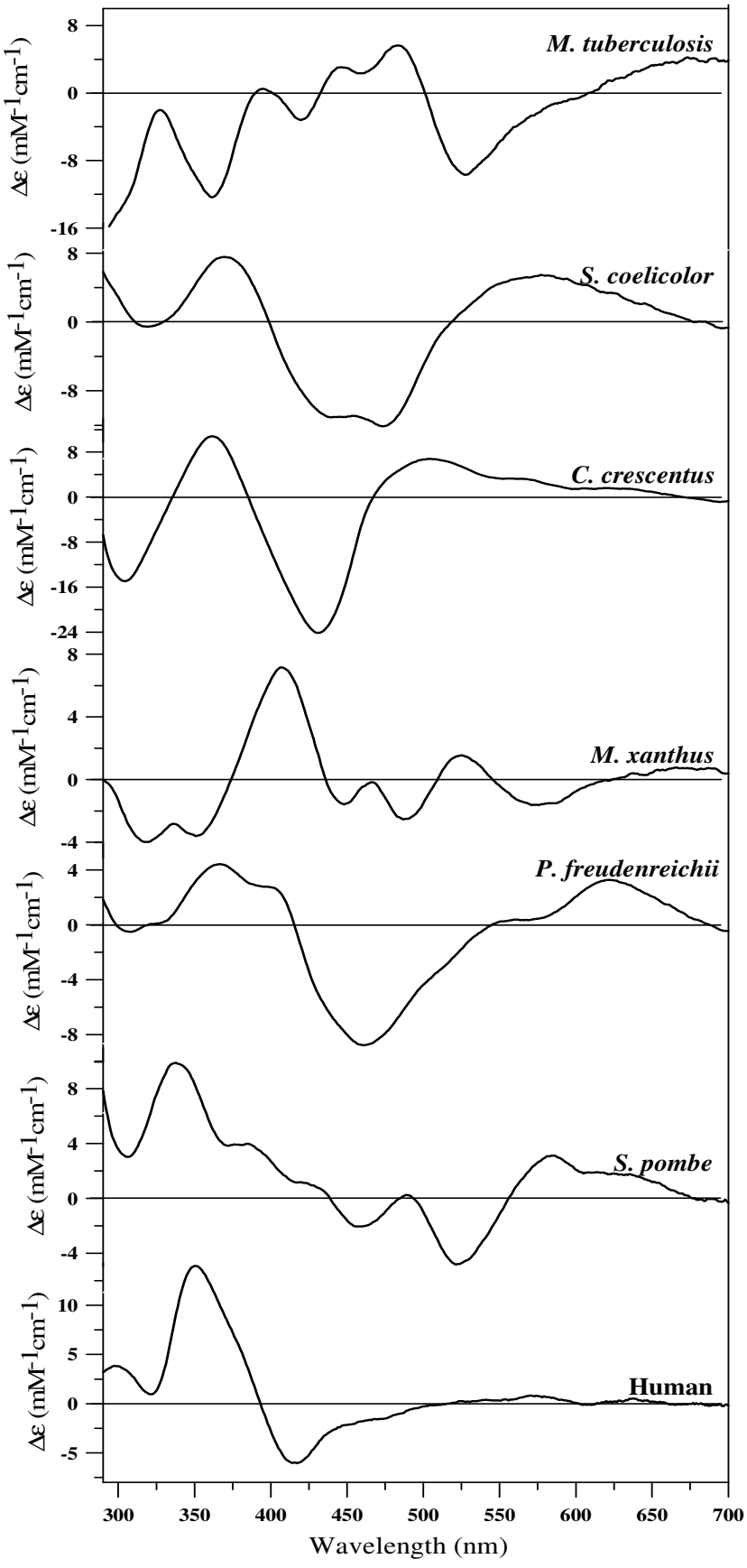
M. tuberculosis
S. coelicolor
C. crescentus
M. xanthus
P. freudenreichii
S. pombe
Human
Δε (mM-1cm-1)
Wavelength (nm)
300
350
400
450
500
550
600
650
700

Figure 2.3. Perpendicular-mode X-band EPR spectra of [2Fe-2S]$^{+}$ centers in dithionite-reduced ferrochelatases from *S. pombe*, *M. xanthus*, *S. coelicolor*, *P. freudenreichii*, and human in the *S* = 1/2 region. The inset shows the low-field EPR spectrum of the dithionite-reduced [2Fe-2S]$^{+}$ cluster in *S. pombe* ferrochelatase showing the half-field signal of the presence of a spin-coupled signal. All samples were in 50 mM Tris-MOPS buffer, pH 8.0, with 0.1 M KCl, and 1% (w/v) sodium cholate, and samples were reduced by anaerobic addition of approximately 10-fold excess sodium dithionite, except *P. freudenreichii* ferrochelatase which also required addition of methyl viologen for reduction. Spectra were recorded at 35 K under the following measurement conditions: microwave power, 5 mW; microwave frequency, 9.6 GHz; and modulation amplitude, 0.64 mT. The EPR spectrum of *P. freudenreichii* ferrochelatase shows an intense signal centered on g = 2.00 rising from the radical species formed upon addition of methyl viologen and marked with an asterisk.

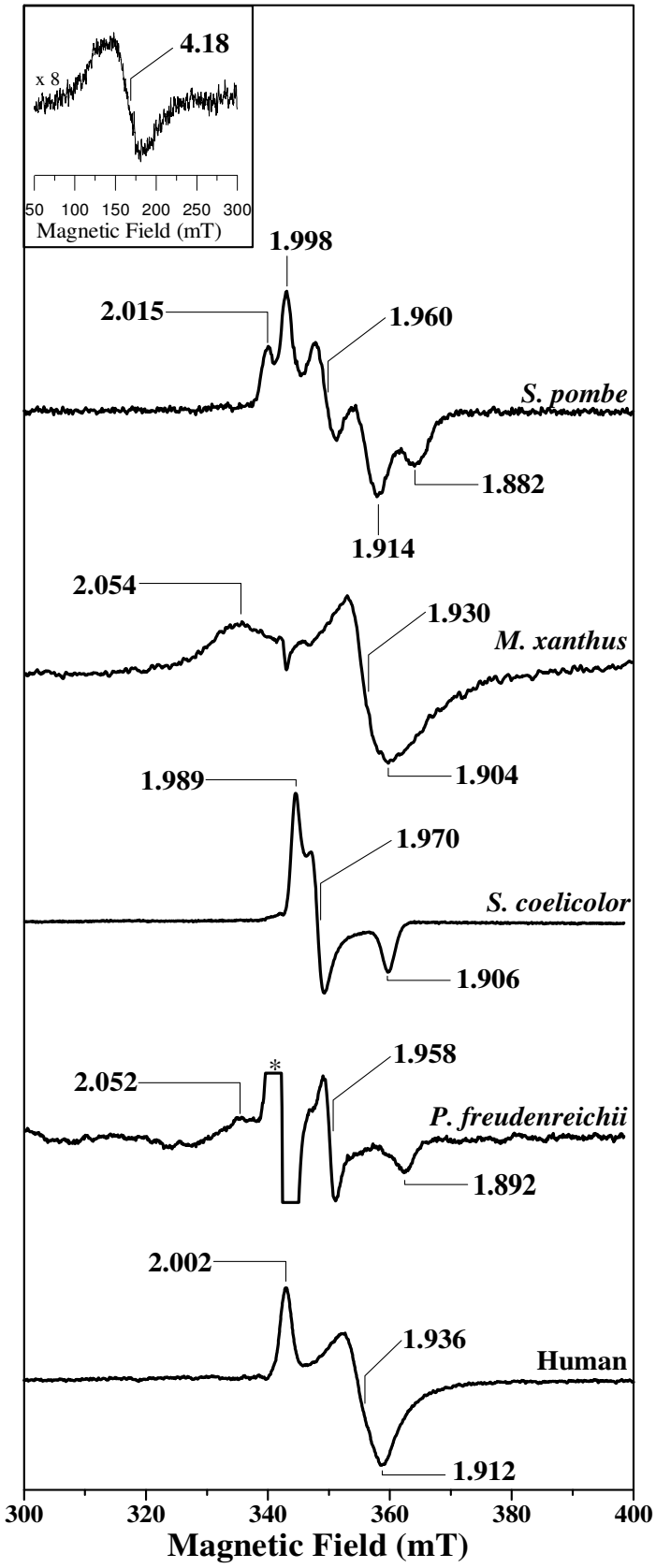
4.18
x 8
50 100 150 200 250 300
Magnetic Field (mT)
1.998
2.015
1.960
S. pombe
1.882
1.914
2.054
1.930
M. xanthus
1.904
1.989
1.970
S. coelicolor
1.906
1.958
2.052
*
P. freudenreichii
1.892
2.002
1.936
Human
1.912
300 320 340 360 380 400
Magnetic Field (mT)

Figure 2.4. **Amino acid sequence comparison of various ferrochelatases sharing the C-X_{206}-C-X_2-C-X_4-C.** Residues located within 10 Å from the $[2Fe\text{-}2S]^{2+,+}$ cluster are highlighted in green, and the conserved cysteine residues ligating the cluster are shaded in cyan. The amino acid residue believed to be involved in spin-spin coupling with the $[2Fe\text{-}2S]^{+}$ cluster in *S. pombe* ferrochelatase is highlighted in red. Sequence alignment was obtained using ClustalW program (*41*), accessible at www.expasy.org.

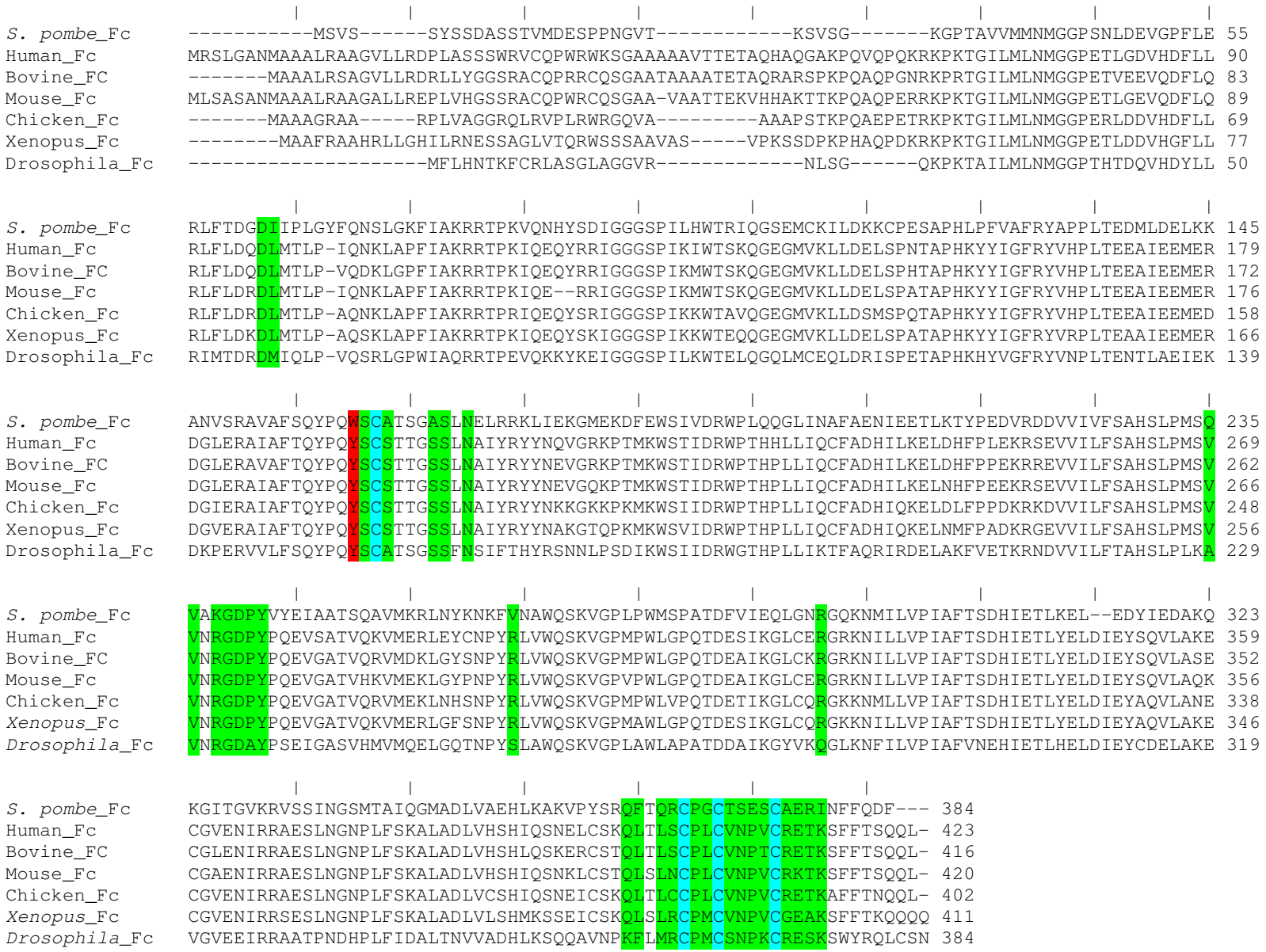
S. pombe_Fc
Human_Fc
Bovine_FC
Mouse_Fc
Chicken_Fc
Xenopus_Fc
Drosophila_Fc

Figure 2.5. The active site environment of the $[2Fe{-}2S]^{2+}$ cluster of human ferrochelatase. Tyr194 (green sticks) is located 5.9 Å away from one of the Fe atoms of the [2Fe-2S] cluster (Fe, brown balls; S, tan balls), and is replaced by Trp159 in the *S. pombe* enzyme. Cysteine residues ligating the cluster are shown as cyan sticks. The figure was generated from the PDB file 1HRK using the program PyMOL (*40*).

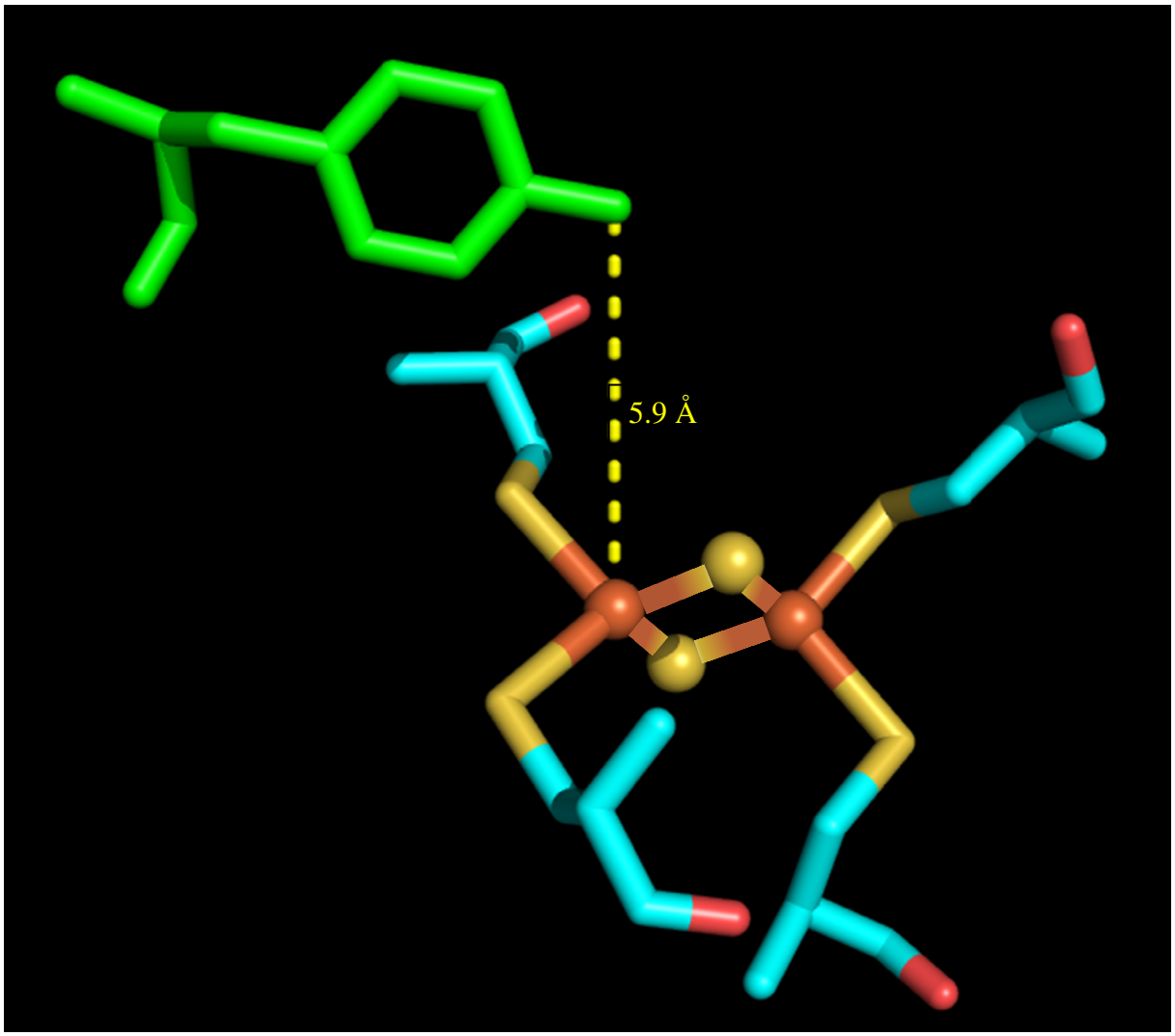
5.9 Å

Figure 2.6. EPR redox titration of the [2Fe-2S] cluster of recombinant *S. coelicolor* ferrochelatase. The plot shows the intensity of the g = 1.94 EPR signal as a function of the reduction potential during reductive titration. Data fitted to the Nernst equation yield a midpoint redox potential of -385 mV.

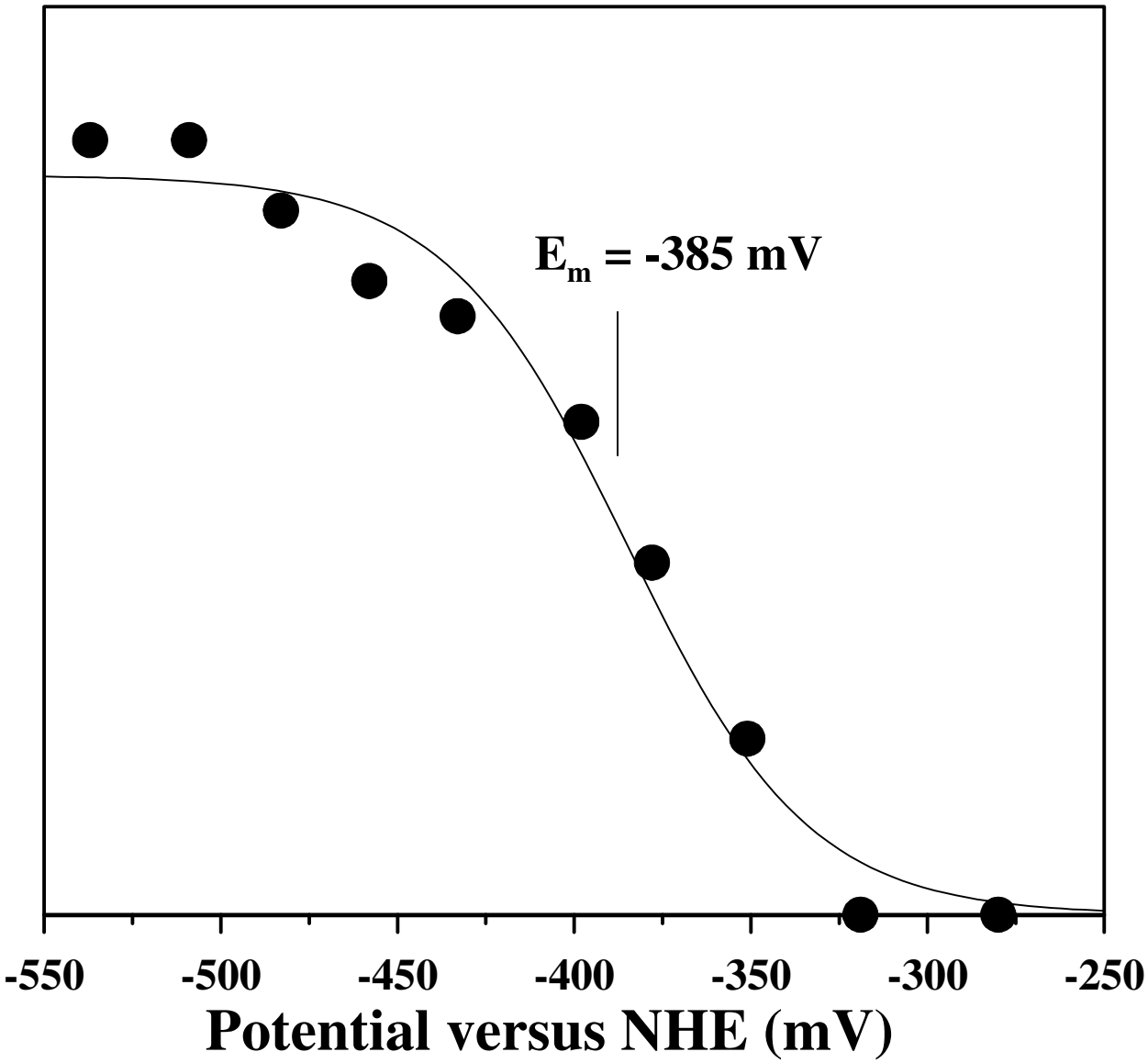
E_m = -385 mV
-550
-500
-450
-400
-350
-300
-250
Potential versus NHE (mV)

Figure 2.7. Structural alignment indicating the spatial orientation of coordinating cysteine residues for the [2Fe-2S] cluster of human ferrochelatase in comparison to various other proteins. Iron and sulfur atoms are depicted as spheres, whereas the ligands to the clusters are shown as sticks. Color coding: red, human ferrochelatase (1HRK); grey, human ferredoxins (3P1M); green, spinach ferredoxins (1A70); blue, bovine adrenodoxin (1AYF); yellow, Fe-only hydrogenase (1FEH); magenta, CO dehydrogenase (1FFV); cyan, fumarate reductase (1QLB); orange, phthalate dioxygenase reductase (2PIA); chocolate, aldehyde dehydrogenase (3L4P) – first cluster. The figure was prepared using PyMOL software (*40*).

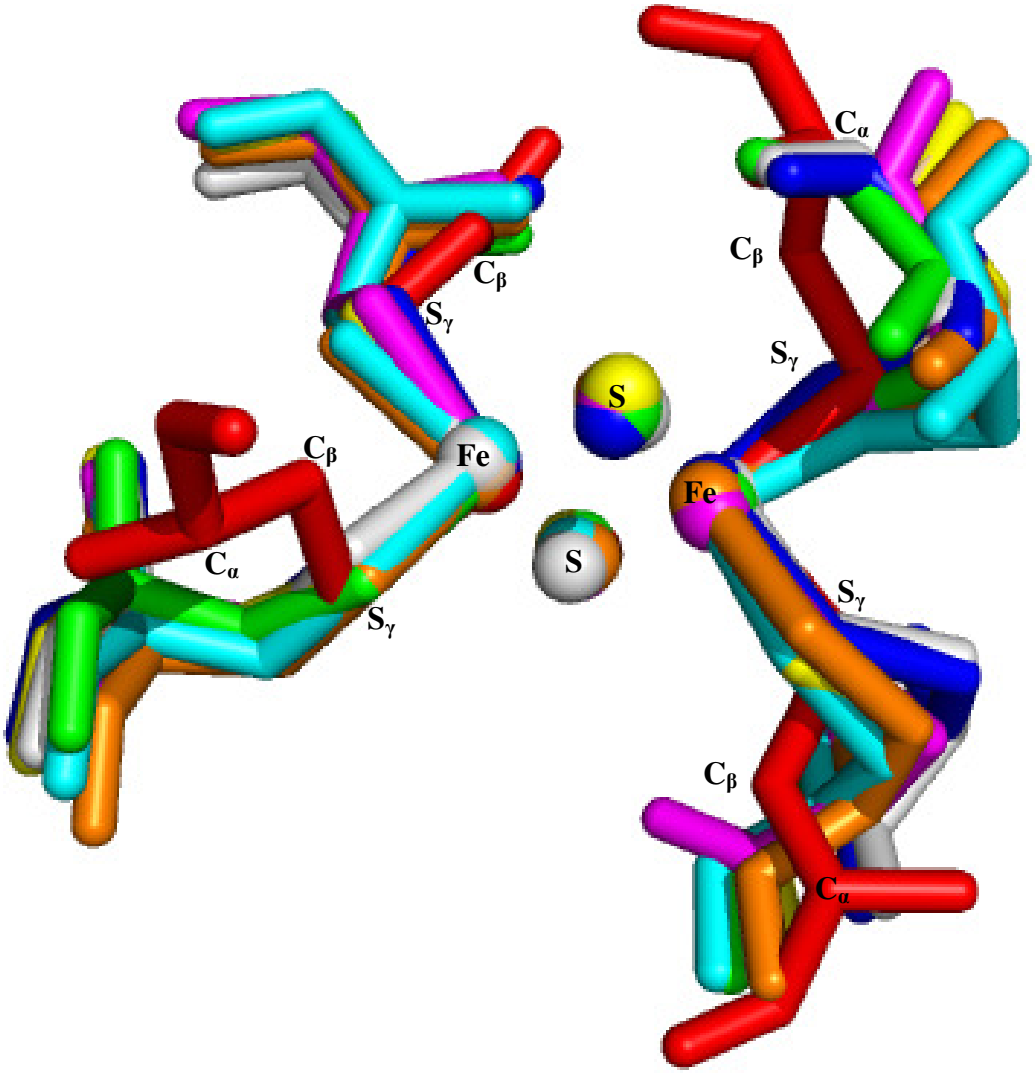
Cα
Cβ
Sγ
S
Fe
Cβ
Fe
Cα
S
Sγ
Sγ
Cβ
Cα

Figure 2.8. Comparison of the resonance Raman spectra of oxidized [2Fe-2S] centers from different ferrochelatases. Human (~3 mM), *S. coelicolor* (~3 mM), *C. crescentus* (5.3 mM), *M. xanthus* (2.4 mM), *P. freudenreichii* (~3 mM), *M tuberculosis* (1.3 mM), and *S. pombe* ferrochelatases (2.3 mM) ferrochelatases having cluster concentrations between 1.3-5.3 mM were in 50 mM Tris-MOPS buffer, pH 8.0, with 0.1 M KCl, and 1% (w/v) sodium cholate. The spectra were recorded at 20 K using a 457.9 nm excitation. Each scan involved advancing of the spectrometer in 0.5 cm^{-1} increments and photon counting for 1s/point with 6-cm^{-1} spectral resolution. Vibrational bands originating from the frozen buffer solution have been subtracted for each of the seven spectra after normalizing the intensities of the "ice-band" at 231 cm^{-1}, and a polynomial ramp fluorescence background has also been subtracted.

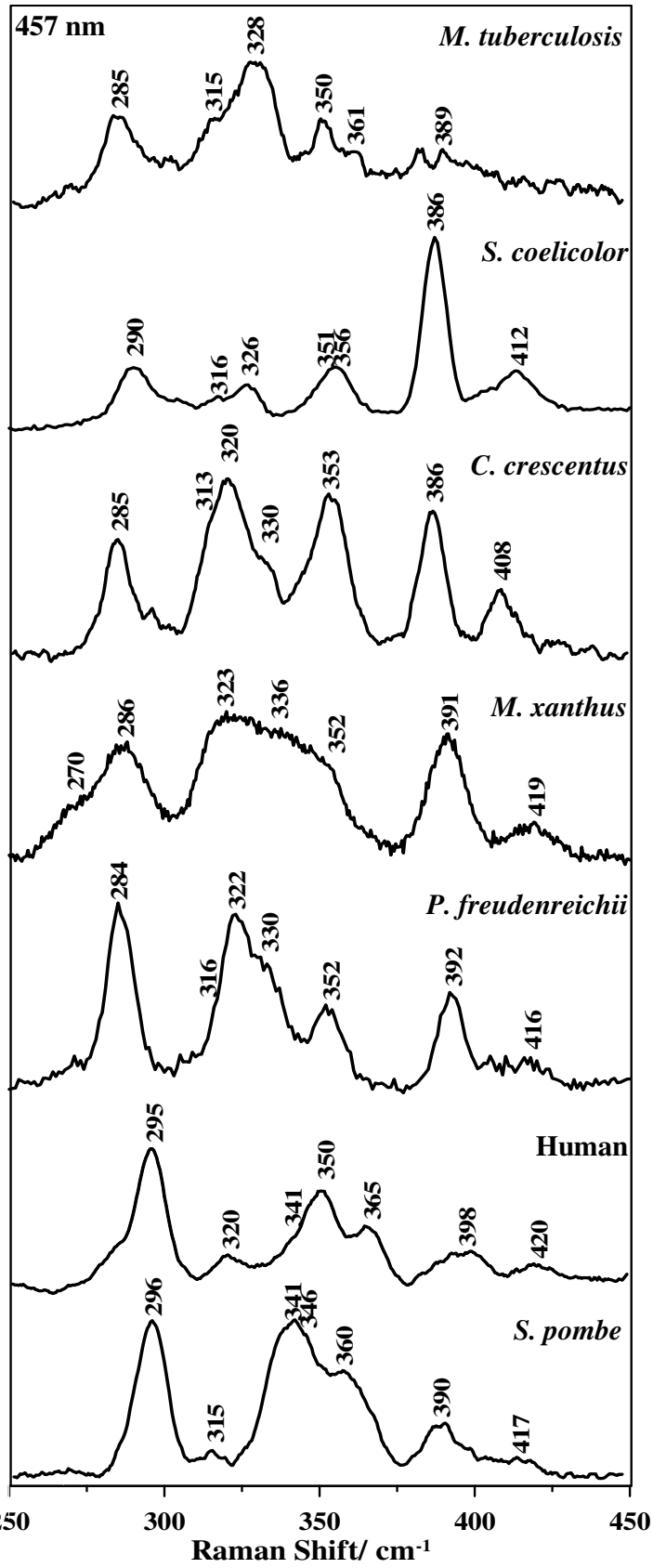
457 nm
M. tuberculosis
285
315
328
350
361
389
S. coelicolor
290
316
326
351
356
386
412
C. crescentus
285
313
320
330
353
386
408
M. xanthus
270
286
323
336
352
391
419
P. freudenreichii
284
316
322
330
352
392
416
Human
295
320
341
350
365
398
420
S. pombe
296
315
341
346
360
390
417
250
300
350
400
450
Raman Shift/ cm-1

CHAPTER 3

THE [2FE-2S] CLUSTER IN *A. THALIANA* SIROHYDROCHLORIN FERROCHELATASE: CHARACTERIZATION AND ROLE AS A SENSOR OF CELLULAR IRON-SULFUR CLUSTER STATUS

Angela-Nadia Albetel[‡], Jérémy Couturier, [§†] Nicolas Rouhier, [§] and Michael K. Johnson[‡]

to be submitted to the Journal of Biological Chemistry

[‡]Department of Chemistry and Center for Metalloenzyme Studies, University of Georgia, Athens, Georgia, 30602, USA.

[§]Unité Mixte de Recherches 1136 INRA-Nancy Université, Interactions Arbres Microorganismes, IFR 110, EFABA 54506 Vandoeuvre-lès-Nancy Cedex, France.

[†]Faculty of Biology – W5-134 University of Bielefeld D-33501 Bielefeld Germany.

Abbreviations: AtSirB Fc, *A. thaliana* sirohydrochlorin ferrochelatase; Grx, glutaredoxin; CGFS Grx, monothiol glutaredoxin with CGFS active site; Fe-S , iron-sulfur; EPR, electron paramagnetic resonance; CD, circular dichroism; DTT, dithiothreitol; GSH, glutathione; MOPS, morpholinepropanesulfonic acid; MES, 2-(*N*-morpholino)ethanesulfonic acid; CAPS, *N*-cyclohexyl-3-aminopropanesulfonic acid; CHES, *N*-Cyclohexyl-2-aminoethanesulfonic acid;

Abstract

Iron, an essential metal for the organism, is used in the cell mostly for heme/siroheme and iron-sulfur clusters biosyntheses. Fe-S clusters and heme are cofactors that play essential roles in many biological processes including but not limited to respiration, electron transport, regulation of gene transcription, as well as sensing of environmental or intracellular conditions, hence regulating gene expression at the translational or transcriptional level. Siroheme plays an essential role for sulfur and nitrogen metabolism in all living organisms. The mechanism that allows a cell to direct iron into either one of these biosynthetic pathways is unknown, but recently reported data shows that the maturation of apo-ferrochelatase, the enzyme involved in catalyzing the last step of heme biosynthesis, depends on the availability of newly formed Fe-S clusters and functional Fe-S cluster assembly machinery. In metazoans, Actinobacterial and a few Gram negative bacterial ferrochelatases, as well as plant sirohydrochlorin ferrochelatase, the enzymes that catalyze the last step siroheme biosynthesis, contain a [2Fe-2S] center, but its role has yet to be determined. In this work, cluster transfer from *A. thaliana* monothiol [2Fe-2S]-GrxS14 to apo *A. thaliana* sirohydrochlorin ferrochelatase in the presence of DTT was monitored by CD spectroscopy. Monothiol glutaredoxins (Grxs) have been shown to play a crucial role in both Fe-S cluster and heme biosynthesis. Our results indicate rapid and effective [2Fe-2S] cluster transfer with a second-order rate constant of 6000 $M^{-1}min^{-1}$ and >62% completion within 5 min. In addition, we show that *A. thaliana* sirohydrochlorin ferrochelatase is extremely sensitive to pH, being able to switch between two different oligomeric conformations with different [2Fe-2S] cluster environments, and that the cluster can only be inserted in the "high pH" form. Our results demonstrate that Grxs play a vital role in regulating siroheme biosynthesis in plants by functioning as the [2Fe-2S] cluster donor for the maturation and stabilization of *A. thaliana*

sirohydrochlorin ferrochelatase. Thus, for the first time we present direct evidence for the intimate connection between Fe-S clusters biogenesis and siroheme biosynthesis, and propose that the [2Fe-2S] cluster-binding site in ferrochelatases functions in sensing the cellular Fe-S cluster status via the extent of cluster loading of the monothiol Grx [2Fe-2S] cluster donor.

Introduction

Most iron acquired by eukaryotic cells is used for biosynthesis of iron-sulfur (Fe-S) clusters and heme, processes that occur in the mitochondrion and require the energy-dependent transport of reduced iron across the inner membrane of the organelle (*1*). Fe-S clusters comprise a structurally and functionally diverse class of biological prosthetic groups that constitute one of the most ancient and ubiquitous cofactors (*2;3*). Although the initial role attributed to Fe-S clusters was believed to be solely in electron transport (*4*), recent advances demonstrate new functions for Fe-S clusters, including substrate binding and activation (*5-8*), regulation of enzyme activity (*9*), sensing of external stimuli and gene regulation (*10-16*), locating/repairing damaged DNA (*17;18*), iron and electron storage/buffering (*19-21*), disulfide reduction (*22;23*), and as a sulfur donor (*24;25*). Heme, on the other hand, a complex of iron with protoporphyrin IX, is a cofactor found in essentially all aerobic organisms as well as a majority of anaerobes and facultative organisms. As the prosthetic group of many proteins, heme is involved in oxygen transport and storage, electron transport, regulation of gene transcription (*26;27*), as a gas sensor (*28*), in the regulation of circadian rhythm (*29*), during development (*30*) and in RNAi processing (*31*). In plants, in addition to Fe-S clusters and heme biosyntheses, iron is also used in the chloroplast for siroheme biosynthesis. As a prosthetic group in just two enzymes, sulfite and nitrite reductases, siroheme is an ancient tetrapyrrole cofactor that plays a crucial role in the assimilation of all inorganic S and the majority of N in the biosphere via involvement in the six electron reduction of sulfite and nitrite, respectively, Therefore, without siroheme, there would be no reduced S for the synthesis of the amino acids cysteine and methionine, and for the biogenesis of Fe-S centers (*32*).

In spite of a vast amount of information regarding the mechanisms of Fe-S clusters and heme/siroheme biosyntheses, the mechanism used by the cell for directing iron into either one of these biosynthetic processes has largely remained unknown. However, advances in understanding the mechanism of Fe–S cluster biosynthesis has recently led to the discovery of monothiol glutaredoxin proteins with CGFS active site (CGFS Grxs) as components of the Fe-S cluster assembly and delivery system (*33;34*). These are small molecular mass proteins widely spread throughout all kingdoms of life, and constitute class II of the six classes of glutaredoxins (*35;36*). Unlike dithiol glutaredoxins which play an important role in cellular regulatory/protective mechanisms via reduction of protein disulfides or glutathionylated proteins (*34;36;37*), *in vivo* data has recently shown that monothiol Grxs play a critical role in both the biogenesis of iron-sulfur clusters and cellular Fe homeostasis (*35*).

Most of the evidence concerning the role of Grxs in Fe-S cluster biogenesis has come from studies on the monothiol CGFS Grx, Grx5, from *Saccharomyces cerevisiae*, in which deletion of *grx5* gene induces higher susceptibility to oxidative stress and results in impaired respiratory growth due to the accumulation of free iron and deficient Fe-S cluster biogenesis (*38;39*). Complementation studies demonstrated that both prokaryotic and eukaryotic monothiol glutaredoxins were able to rescue the yeast *grx5* deletion strain, suggesting that their function has been conserved during evolution (*33;40*). In addition to the gene knock out studies, Grx5 was shown to impede the transfer of Fe-S clusters preassembled on the U-type Fe-S cluster scaffold protein, Isu1p, to acceptor proteins, according to ^{55}Fe immunoprecipitation studies in yeast (*41*). Moreover, monothiol Grxs have been shown to interact *in vivo* with A-type proteins such as yeast Isa1p (*42*), and *in vitro* cluster transfer reactions monitored by UV-visible and CD spectroscopies demonstrate that monothiol Grxs effectively transfer $[2Fe\text{-}2S]^{2+}$ clusters to A-type

proteins (*43*). Taken together with the recent studies indicating that IscU, the protein that functions as the primary scaffold for the assembly of Fe-S clusters and subsequent delivery to acceptor proteins (*4;44-46*), rapidly and effectively transfers its preassembled [2Fe-2S] cluster to apo-Grx5 in the presence of HscA/HscB chaperones in an ATP-dependent reaction (*47*), and that monothiol Grxs are able to insert $[2Fe\text{-}2S]^{2+}$ clusters in acceptor proteins (*33*). These data demonstrate that monothiol Grxs participate in the Fe-S cluster assembly machinery by functioning as carriers or storage proteins for preassembled clusters.

In vitro experiments using a wide variety of recombinant monothiol CGFS Grxs have recently shown that the as purified proteins contain a [2Fe-2S] center bound between two monomers. Under anaerobic conditions and in the presence of glutathione (GSH), the apo forms of monothiol Grxs have been shown to readily incorporate a labile $[2Fe\text{-}2S]^{2+}$ cluster during cysteine desulfurase-mediated cluster assembly, thus providing additional support for a role in Fe-S cluster biogenesis for monothiol CGFS Grxs.

Interestingly, the Fe-S cluster bound form of the mitochondrial monothiol Grx5 was shown to be essential for vertebrate heme synthesis and regulation of bone apoptosis (*48;49*). Deletion of the gene encoding for Grx5 in *shiraz* zebrafish resulted in low expression of ALAS2, the mitochondrial-located erythroid-specific δ-aminolevulinate synthase that catalyzes the first committed step of heme biosynthesis, leading to low heme levels and, consequently, causing severe hypochromic anemia (*49*). It was reasoned that the deficiency of Grx5 in zebrafish, resulted in the loss of the Fe-S cluster in IRP1, the iron regulatory protein responsible for posttranscriptional regulation of iron homeostasis (*50;51*), which was activated to an IRE-binding protein, thus decreasing the translation of ALAS2 that contains IRE in its 5' – UTR (*49*). These studies suggested for the first time that the Fe-S cluster biogenesis and heme biosynthesis

are closely connected and interrelated in the erythroid system via the regulation of ALAS2 translation by IRP1, and that the Fe-S cluster component Grx5 has a direct impact on iron and heme regulation in zebrafish (*49*). Although it has not been characterized thus far, the hypothesis suggesting a molecular relationship between anemia and the status of Fe-S cluster assembly is further supported by a study indicating that in humans, the Glrx5 mutation results in microcytic sideroblastic anemia, a disease observed in a male patient in Italy that manifests via iron overload in mitochondria and formation of ring sideroblasts (*52*). Moreover, recent *in vivo* studies indicate impaired Fe-S cluster biogenesis and mitochondrial iron overload in skeletal muscles under depletion of the scaffold protein IscU (*53*). Under such conditions of insufficient availability for Fe-S clusters, substantial instability and degradation was observed in ferrochelatase (*53*). In metazoans, Gram positive and a few Gram negative bacteria ferrochelatase has been shown to accommodate a [2Fe-2S] cluster that is vital for enzymatic activity (*54-56*). Taken together with the data indicating increased expression of ALAS2 and ferrochelatase during hemoglobinization for erythropoiesis which appears to depend on normal Glrx5 activity (*57*), the rapid degradation of ferrochelatase in the absence of its Fe-S cluster (*53*), and the lower levels of ferrochelatase protein observed in Glrx5 deficient patient lymphoblasts (*57*), it seems reasonable to propose that Glrx5 may deliver the preassembled [2Fe-2S] cluster for the maturation of ferrochelatase.

In this study, we attempted to establish a direct connection between Fe-S cluster and heme/siroheme biosynthetic pathways by investigating the ability of the CGFS monothiol glutaredoxin GrxS14 from plant *A. thaliana*, to transfer a [2Fe-2S] cluster to *A. thaliana* sirohydrochlorin ferrochelatase (referred to as AtSirB Fc hereafter). AtSirB Fc catalyzes the last step of siroheme biosynthesis by inserting ferrous iron into the tetrapyrrole ring of

sirohydrochlorin (*58*). In addition, the structural, electronic, vibrational and redox properties of the as purified [2Fe-2S] cluster-containing AtSirB Fc were investigated using the combination of analytical methods and UV−visible absorption, CD, EPR, and resonance Raman spectroscopies. The results indicate marked conformational changes in AtSirB Fc as a function of pH that affects not only the oligomeric status of the protein, but the environment of the protein in the vicinity of the [2Fe-2S] center.

Experimental Procedures

Chemicals and reagents. Materials used in this work were purchased from Fischer Scientific, Sigma-Aldrich Chemical Co, Invitrogen, or VWR International, unless otherwise stated, and were of reagent grade.

Cloning and construction of genes. A. thaliana monothiol CGFS glutaredoxin S14 (GrxS14) was cloned, expressed and purified according to the published procedure (*33*). The open reading frame sequence encoding AtSirB Fc (At1g50170) was amplified from leaf cDNA using AtSirB forward and reverse primers containing the *Nde*I and *Bam*HI restriction sites respectively (see Table 3.1.). Using the two complementary mutagenic primers, AtSirB H41H forward and reverse listed in Table 3.1, the internal *Nde*I restriction site was modified by introducing a silent mutation in the His41 codon. The final amplified sequence encodes the mature form of the protein, deprived of the first 79 amino acids corresponding to the putative organelle targeting sequence. To improve expression, a methionine followed by an alanine residue were added as initiators during cloning. Thus, the protein starts with the N-terminal sequence ^{1}MADADGII^{8} and ends with ^{144}LYNSS^{148} at the C-terminus. The amplified sequence was then cloned into pET15b (Novagen, Madison, WI) enabling overproduction of the protein as

an N-terminal His-tagged fusion protein, and subsequently expressed in *Escherichia coli* BL21(DE3) strain.

Protein expression and purification. For expression of the recombinant AtSirB Fc, LB cultures of 1L containing 100 μg of ampicillin/ml (final concentration) were inoculated with *E. coli* BL21(DE3) containing the AtSirB Fc plasmid and grown at 37°C with shaking. At cellular exponential phase (OD ~ 0.6-0.8 at 600 nm), 0.5% (v/v) ethanol was added to improve protein solubility, and the cultures were further incubated with shaking at 4°C for two hours. The cells were then induced by adding 100 μM IPTG (isopropyl-β-D-thiogalactopyranside), and allowed to grow at 20 °C for 16-20 additional hours. The bacteria were pelleted by centrifugation at 5000 *g* for 15 min and frozen at -80 °C overnight. The frozen pellet was resuspended in 50 mM Tris-morpholinepropanesulfonic acid [Tris-MOPS] pH 8.0, 100 mM KCl, 1% (w/v) sodium cholate, 2 mM dithiothreitol (DTT), 20 mM imidazole, 5% glycerol (buffer A), to which 1 mL Triton × 100 and 10 μg of phenylmethylsulphonyl fluoride/ml were added before lysing the cells by sonication four times (30 s each time) on ice, and centrifugation at 39,700 × *g* for 1 h at 4°C. The reddish-brown cell-free extract was loaded onto a column containing 3 ml of a 50% slurry of Talon matrix (Clontech) previously equilibrated with buffer A. The column was washed with 50 ml of buffer A, and the His-tagged protein was eluted from the column matrix in buffer A containing 300 mM imidazole. After the metal chelate column, the brown-colored fractions were concentrated to 0.5 ml final volume, transferred to an anaerobic glove box (Vacuum Atmosphere), and applied to a 25 ml Superdex G-75 10/300 gel filtration column (Pharmacia Biotech) equilibrated with either 50 mM sodium phosphate pH 7.4, 300 mM NaCl, 20 mM imidazole, 2 mM DTT buffer (buffer B), or 50 mM Tris-HCl pH 8.7, 300 mM NaCl, 1% Na cholate, 2 mM DTT (buffer C). The protein was eluted off the column using a flow rate of 0.4

mL/min, and the brown-colored fractions were analyzed via SDS-PAGE gel electrophoresis. The fractions containing the pure AtSirB Fc were pooled and concentrated together and further used for biochemical, analytical and spectroscopic analyses.

The cluster-depleted form of AtSirB Fc (called *apo* AtSirB Fc from this point forward) was obtained by storing as purified enzyme sample at 4°C for prolonged periods of time (until protein solution lost most of the brown color), followed by repurification at pH 8.0 in the presence of 2 mM DTT, using only a metal chelate column.

Preparation of samples for EPR. EPR samples at pH 7.4 and 8.7 were purified and prepared anaerobically (<4 ppm O_2) under argon atmosphere as described above, followed by reduction with 2-fold excess sodium dithionite, rapid transfer to EPR tubes and freezing in liquid nitrogen. All buffer solutions were degassed under vacuum with argon. X-band EPR spectra were recorded on a ESP 300E spectrometer (Bruker Instruments, Billerica, MA) equipped with an ER-4116 dual mode cavity and an ESR 900 flow cryostat (Oxford Instruments, Concord, MA) (4.2–300 K). Where possible, spectra were quantified under non-saturating conditions by double integration against a 1 mM Cu-EDTA standard.

Biochemical analyses. AtSirB Fc protein concentrations were determined by using bovine serum albumin as a standard (Roche) with Bio-Rad D_c protein assay in conjunction with the microscale modified procedure of Brown et al (*59*). Protein concentrations and molar extinction coefficients are based on protein monomer unless otherwise stated. Iron concentrations for AtSirB Fc were determined colorimetrically using bathophenanthroline under reducing conditions after digestion of the protein in 0.8% $KMnO_4$/ 0.2M HCl as described by Fish (*60*). A calibration curve was prepared using standard solutions of known Fe concentration, prepared from a 1000 ppm atomic absorption iron standard (Fluka). Analytical quantitation of

the [2Fe-2S] cluster concentration in *A. thaliana* GrxS14 was determined spectrophotometrically using the experimentally-determined extinction coefficient $\varepsilon_{411} \approx 8.8\ mM^{-1}cm^{-1}$ (*33*).

Determination of the oligomeric state of the "as purified" AtSirB Fc at pH 7.4 and 8.7. The oligomeric state of the as purified AtSirB Fc at pH 7.4 and 8.7 were assessed by gel-filtration chromatography using a 25 mL Superdex G-75 10/300 column (Pharmacia Biotech), equilibrated with either buffer A at pH 8.7 or buffer B at pH 7.4, and elution profiles were recorded at 280 nm with a flow rate of 0.4 mL/min. The molecular weight standards used were blue dextran (M_r 2,000,000), amylase (M_r 200,000), alcohol dehydrogenase (M_r 150,000), albumin (M_r 66,000), carbonic anhydrase (M_r 29,000) cytochrome c (M_r 12,400), and aprotinin (M_r 6,500) (Sigma-Aldrich).

Spectroscopic methods. UV-visible absorption and CD spectra were recorded in 1 mm quartz cuvettes (sealed to maintain anaerobicity where indicated) at room temperature, using a Shimadzu UV-3101 PC scanning spectrophotometer and Jasco J-715 spectropolarimeter, respectively. Resonance Raman spectra were recorded using an Ramanor U1000 spectrometer (Instruments SA, Edison, NJ) fitted with a cooled RCA 31034 photomultiplier tube with a 90° scattering geometry. Spectra were recorded digitally using photon counting electronics, and improvements in signal-to-noise were achieved by signal-averaging multiple scans. Band positions were calibrated using the excitation frequency and are accurate to $\pm$ 1 cm^{-1}. Lines from a Coherent Sabre (Santa Clara, CA) 10-W argon ion laser and plasma lines were removed using a Pellin Broca prism premonochromator. With the use of a custom-designed sample cell (*61*), samples at pH 7.4 or 8.7 with Fe-S cluster concentrations of 7.2 mM and 0.6 mM, respectively, were placed on the end of a cold finger of an Air Products Displex model CSA-202E closed cycle refrigerator (Air products, Allentown, PA). This enables the samples to be cooled to 20 K,

facilitating improved spectral resolution and preventing laser-induced sample degradation. Scattering was collected from the surface of frozen 17 µL droplets.

pK_a determination. Investigation of the pH effect on the CD spectra of AtSirB Fc and determination of pK_a were carried out aerobically on samples purified on the metal affinity column equilibrated with a mixed buffer system (100 mM 2-(*N*-morpholino)ethanesulfonic acid (MES), 100 mM MOPS, 100 mM Tris, 100 mM *N*-Cyclohexyl-2-aminoethanesulfonic acid (CHES), and 100 mM *N*-cyclohexyl-3-aminopropanesulfonic acid (CAPS)) pH 6.9 with 0.3 M NaCl, 5% glycerol and 20 mM imidazole. After loading the cell free extract, the column was washed with 50 ml of the mixed buffer system, followed by washing of the column with 50 ml of the same buffer containing 80 mM imidazole. The protein was eluted off the column using the mixed buffer system containing 500 mM imidazole, and the brown-colored fractions were pulled and concentrated together. 50 µl of AtSirB Fc samples, final concentration 60 µM, were incubated and stirred occasionally in separate test tubes with the mixed buffer system having the pH adjusted to 6.9, 7.1, 7.4, 7.7, 7.9, 8.1, 8.3, 8.5, 8.7 or 8.9. The protein was allowed to reach a conformational equilibrium for 20 minutes with occasional stirring at room temperature, and then analyzed in 1 cm semi-micro cuvettes using CD spectroscopy. The difference in the CD values at ~ 370 nm and 362 nm plotted against pH was used to determine the pK_a value and the number of protons involved in the conversion between the "low pH" and "high pH" forms of AtSirB Fc. The data was fit to an ideal titration curve obtained using Equation 3.1 from the Hill model, a traditional model used to measure cooperativity in protein-ligand interactions. For one pK_a value and Hill coefficient (*n*), the observed CD intensity ($\Delta\varepsilon_{obs}$) was simulated by the pK_a and the CD intensity of the protonated ($\Delta\varepsilon_P$) and unprotonated ($\Delta\varepsilon_D$) forms of AtSirB Fc.

$$\Delta\varepsilon_{obs} = \Delta\varepsilon_D + (\Delta\varepsilon_P - \Delta\varepsilon_D)\left[\frac{(10^{pH})^{\mathrm{n}}}{(10^{pH})^{\mathrm{n}} + (10^{pka})^{\mathrm{n}}}\right] \qquad \text{Equation 3.1.}$$

In this equation, Hill coefficient (n) represents the number of cooperative binding sites. When $n = 1$, the equation is a standard Henderson-Hasselbach protonation function.

In vitro Fe-S cluster transfer experiments from A. thaliana monothiol CGFS glutaredoxin S14 to apo AtSirB Fc. The time course of the cluster transfer from *A. thaliana* GrxS14 to *apo* AtSirB Fc was monitored at room temperature in 1 cm semi-micro cuvettes using CD spectroscopy. Cluster transfer experiments were carried out under anaerobic conditions in either 50 mM Tris-MOPS pH 8.0, 100 mM KCl, 0.1% [w/v] sodium cholate, 2 mM DTT, and the final concentrations of *apo* AtSirB Fc and GrxS14 in the reaction mixture were 39 μM and 31 μM, respectively. The reactions were initiated by addition of the [2Fe-2S] cluster-loaded GrxS14, and the cluster transfer was monitored until no evident change in CD was observed. Control experiments using similar reaction mixtures lacking AtSirB Fc were carried out to ensure that the disappearance of CD bands corresponding to GrxS14 were not due to protein instability in the presence of DTT. The change in the difference between the CD intensities at 469 nm and 406 nm with time was used to fit the data to second-order kinetics, and the initial rate constant for the [2Fe-2S] cluster transfer reaction was determined using the Chemical Kinetics Simulator program (IBM).

Results

The nature of the Fe-S cluster in the recombinant AtSirB Fc purified at pH 7.4 and pH 8.7 was assessed by using a combination of analytical and spectroscopic techniques.

Oligomeric state of AtSirB Fc depends on pH. To characterize the oligomeric state of AtSirB Fc, the protein was expressed and purified separately at pH 7.4 and 8.7, and the identity of the protein was confirmed by MALDI-TOF mass spectrometry (data not shown). Based on electron spray ionization mass spectrometry (ESI-MS), the protein was determined to have a

molecular mass of 18.5 kDa (data not shown), in excellent agreement with the predicted mass of the apo protein and SDS-PAGE analysis (see Figure 3.1, Panel A). Comparison of gel filtration elution profiles (Figure 3.1, Panel B) of AtSirB Fc at pH 7.4 and 8.7, hereafter termed the "low pH" and "high pH" forms, respectively, with those of proteins of known molecular mass, indicate molecular masses of 40 kDa and 68 kDa for the sample at low and high pH, respectively. These results are best interpreted in terms of a dimeric protein at low pH (predicted M_r = 37 kDa) and a tetrameric conformation at high pH (predicted M_r = 74 kDa).

UV-visible absorption and CD spectroscopy. Iron and protein analyses of samples purified at low and high pH to homogeneity contained 1.8 ± 0.1 (A_{415}/A_{279} = 0.41 ± 0.02) and 1.6 ± 0.2 (A_{415}/A_{279} = 0.46 ± 0.02) moles of Fe per mol of protein, respectively, consistent with the presence of one $[2Fe\text{-}2S]^{2+}$ cluster per monomer. The recombinant mature AtSirB Fc aerobically purified at pH 7.4 or 8.7 exhibits a brown color, indicative of the presence of a Fe-S center, and UV-visible absorption spectra shown in Figure 3.2. are very similar the previously reported data (*58*). In addition to the protein bands, the absorption spectrum of AtSirB Fc at low pH exhibits bands at 339 nm (ε ≈ 11.9 $M^{-1}cm^{-1}$), 416 nm (ε ≈ 7.9 $M^{-1}cm^{-1}$), and 451 nm (ε ≈ 7.3 $M^{-1}cm^{-1}$), whereas prominent bands at 319 nm (ε ≈ 11.9 $M^{-1}cm^{-1}$), 414 nm (ε ≈ 9.4 $M^{-1}cm^{-1}$), as well as a shoulder at approximately 462 nm (ε ≈ 6.3 $M^{-1}cm^{-1}$) are observed in the absorption spectrum of the protein at high pH. Therefore, both spectra indicate the presence of a $[2Fe\text{-}2S]^{2+}$ center. Based on the published extinction coefficients for biological $[2Fe\text{-}2S]^{2+}$ centers (*54*), these extinction coefficients are also indicative of the presence of approximately one cluster per protein monomer, hence supporting the results obtained from Fe analytical data. Interestingly, the absorption spectrum of AtSirB Fc at high pH resembles that of monothiol glutaredoxins which also have spectra dominated by a single band centered near 430 nm (*33;62;63*), whereas

the visible spectrum of the protein at low pH is rather similar to those of other biological [2Fe-2S]$^{2+}$ centers that generally exhibit two resolved bands centered around 420 and 460 nm (*64-68*).

The differences observed in the UV-visible absorption spectra for the low- and high pH forms of AtSirB Fc are reflected in marked differences in intensity and wavelengths of the visible CD bands. Thus, at pH 7.4, the CD spectrum of the protein is characterized by the presence of a positive band at 309, an intense band at 458 nm, a broad positive band centered around 609 nm, an intense negative band at 370 nm, and a broad negative band centered around 555 nm (see Figure 3.2 and Figure 3.7). At pH 8.7, the CD spectrum of AtSirB Fc is dominated by an intense positive band at 468 nm, two less-intense positive bands between 297-374 nm, a shoulder around 530 nm, an intense negative band at 407 nm, and a broad negative band centered around 604 nm (Figure 3.2 and Figure 3.7).

While the significant differences observed in the UV-visible and CD spectra of AtSirB Fc at low pH and high pH indicate changes in the excited state electronic structure of the [2Fe-2S]$^{2+}$ center, which are difficult to explain structurally, they do indicate differences in the cluster ligation and/or the chirality of the cluster environment.

EPR spectroscopy. Purified sample of recombinant AtSirB Fc do not exhibit an observable EPR signal, in agreement with the anticipated diamagnetic $S = 0$ ground state resulting from antiferromagnetic coupling of two high-spin ($S = 5/2$) Fe(III) centers. Attempts to reduce the [2Fe-2S]$^{2+}$ cluster in the low pH form of AtSirB Fc under anaerobic conditions in the presence of either excess or stoichiometric amounts of sodium dithionite were not successful due to protein instability in the reduced form and possibly to a higher redox potential for dithionite at low pH that makes it a less potent reductant. In contrast, as shown in Figure 3.3, freshly prepared dithionite-reduced samples of AtSirB Fc purified under anaerobic conditions at pH 8.7 exhibit a

rhombic $S = 1/2$ resonance which is well simulated with $g = 1.99$, 1.96, and 1.91 that account for approximately 0.4 ± 0.15 spin/molecule. The resonance undergoes power saturation with microwave powers > 10 mM at 35 K and is observed without significant broadening up to 100 K; relaxation behavior typical of a $S = ½$ $[2Fe\text{-}2S]^{+}$ center (see Figure 3.3). Some difficulties were experienced during preparation of AtSirB Fc at pH 8.7 due to [2Fe-2S] cluster instability at pH > 8.5, especially during the concentration of the sample, and this may explain the low spin/molecule value. Alternatively the low spin quantification may be a consequence of a redox potential <-460 mV

Resonance Raman spectroscopy. Resonance Raman spectroscopy was used to confirm the presence and provide a more direct assessment of the ligation and vibrational properties of the $[2Fe\text{-}2S]^{2+}$ center in AtSirB Fc. The low temperature (20 K) resonance Raman spectra of oxidized $[2Fe\text{-}2S]^{2+}$ AtSirB Fc at recorded at pH 7.4 (7.2 mM) and 8.7 (0.6 mM) in the Fe-S stretching region (240-450 cm^{-1}) using 457.9-, 487.9- and 514.5-nm excitation are compared in Figure 3.4 and show significant differences as a function of pH. At high pH, the Fe-S stretching frequencies of the $[2Fe\text{-}2S]^{2+}$ cluster is very similar to those of other structurally characterized $[2Fe\text{-}2S]^{2+}$ cluster-containing proteins with complete cysteinyl ligation, and can readily be assigned by direct analogy with the published data (*65;69*). Interestingly though, in addition to Raman bands corresponding to Fe-S stretching and vibrational modes, the resonance Raman spectrum of the $[2Fe\text{-}2S]^{2+}$ AtSirB Fc at low pH exhibits a band centered around 251 cm^{-1} that is best interpreted as an indication of the presence of a histidine ligand based on the published data for structurally characterized Rieske-type proteins (two histidine ligands at a unique Fe site) (*70-73*), His-to-Cys variants of Rieske-type proteins (one histidine ligand) (*70*) and the structurally characterized outer mitochondrial membrane protein mitoNEET (one histidine ligand) (*74*).

Partial histidine ligation is evident by the presence of two bands in the 250–320 cm^{-1} region of the resonance Raman spectrum, one between 250–275 cm^{-1} and one between 285–310 cm^{-1} (*70-74*), in place of one broad band between 282–302 cm^{-1} that is attributed primarily to the out-of-phase symmetric FeS_4 breathing mode in $[2Fe\text{-}2S]^{2+}$ centers with complete cysteine ligation or with one serine, aspartate, or arginine in place of a cysteine ligand (*25;65;69;75;76*). The observation of a low energy vibration mode near 251 cm^{-1} in the low pH form of [2Fe-2S] AtSirB Fc raises the possibility of partial histidyl ligation based the available pH-dependence and N-isotope shift data for the Rieske-type and mitoNEET proteins. The distribution of Fe-N(His) stretching over the low energy Fe-S stretching modes and internal modes of coordinated cysteine ligands and enhancement via the visible S-to-Fe charge transfer transitions argues against assignment of the band in the 250-275 cm^{-1} region to a relatively pure Fe-N(His) stretching mode (*70;72-74*). However, interpretation of the resonance Raman spectrum of the low pH $[2Fe\text{-}2S]^{2+}$ center in terms of a single His ligand should be viewed as tentative at present and requires confirmation using other techniques such as ^{14}N ENDOR.

The differences in the relative intensities of corresponding Raman bands reflect changes in the excitation profiles resulting from perturbation of the excited-state electronic structure. The Fe-S stretching modes in [2Fe-2S] AtSirB Fc at low pH are generally similar to those in the high pH form of the protein, except for 3 cm^{-1} downshifts in the 313-320 bands, and 3-8 cm^{-1} upshift in the 330-340 cm^{-1} bands. This suggests weaker bonding in the Fe_2S_2 core and stronger Fe-S(Cys) bonds for the [2Fe-2S] center in AtSirB Fc at low pH compared to the high pH form, which may explain the greater stability of the $[2Fe\text{-}2S]^{2+}$ center in the low pH form of the protein.

Measurement of pK_a value. To determine the pK_a value and the number of protons involved in the conversion between the "low pH" and "high pH" forms, the changes in AtSirB

Fc spectroscopic features as a function of pH was monitored via CD spectroscopy. As shown in Figure 3.5, superposition of CD spectra recorded in solutions with pH ranging between 6.9 and 8.9 reveals the presence of four isosbestic points at 309 nm, 396 nm, 461 nm, and 574 nm, and a sharp transition profile that occurs in the range of pH 6.7 and 8.7 (inset in Figure 3.5).

In the inset of Figure 3.5 we have plotted the pH transition profile of AtSirB Fc and have compared the titration curves predicted by cooperative and noncooperative Hill equations. The transition between the "low pH" and "high pH" signals follows a cooperative one-proton curve centered around pH 7.95, with approximately two protonation sites (n = 2.1). The results are supported by both analytical and spectroscopic data which suggest that AtSirB Fc undergoes significant conformational changes involving both a change in the oligomeric status of the protein and significant spatial rearrangement of residues around the [2Fe-2S] center, possibly including an exchange of residues coordinating the cluster.

In vitro cluster transfer from [2Fe-2S] GrxS14 to apo AtSirB Fc. The available data suggests that CGFS monothiol Grxs function as cluster carrier/storage proteins of preassembled Fe-S clusters for the subsequent delivery to acceptor proteins (*33;47*). We have therefore investigated whether the chloroplastic monothiol GrxS14 is the physiologically relevant [2Fe-2S] cluster donor for the maturation of the chloroplastic AtSirB Fc.

Direct evidence for rapid and quantitative cluster transfer from $[2Fe\text{-}2S]^{2+}$ GrxS14 to apo AtSirB Fc carried out at pH 8.0 under anaerobic conditions was provided by CD studies as a function of time using a reaction mixture involving 1:1.2 stoichiometry of [2Fe-2S] GrxS14 and apo AtSirB Fc (see Figure 3.6). CD has been proven to be a very sensitive and useful tool for distinguishing between biological [2Fe-2S] clusters due to marked differences in the chirality and protein environment surrounding these metal centers which are reflected in their CD spectra.

Assessment of the extent of intact cluster transfer was followed via concomitant decrease and increase of the CD spectra of the GrxS14 cluster donor and AtSirB Fc acceptor, respectively. Simulated cluster transfer CD spectra corresponding to 0-100% cluster transfer in 10% increments were calculated from a weighted average of the spectra corresponding to $[2Fe\text{-}2S]^{2+}$ cluster-bound GrxS14 and $[2Fe\text{-}2S]^{2+}$ cluster-bound AtSirB Fc. Comparison of the time course of CD changes in the reaction mixture (Figure 3.6A) with simulated data (Figure 3.6B) indicates quantitative cluster transfer from [2Fe–2S] GrxS14 to apo AtSirB Fc that is 62% complete after 5 min and 100% complete after approximately 45 min.

Kinetic analysis of cluster transfer from $[2Fe\text{-}2S]^{2+}$ cluster-loaded GrxS14 to apo AtSirB Fc was performed by monitoring the difference in the UV-visible CD intensity at 469 and 406 nm as a function of time, followed by conversion to percent [2Fe-2S] cluster reconstituted on AtSirB Fc calculated from simulated data. The CD intensity at 469 and 406 nm were chosen for the quantitative determination of the rates of the cluster transfer, in order to maximize the difference in CD intensity for the donor and acceptor protein. On the basis of the initial concentrations of GrxS14 [2Fe-2S] clusters and apo AtSirB Fc, the data is well fit by second-order kinetics with a rate constant of 6,000 M^{-1} min^{-1}.

The agreement between the observed and simulated data and the rapid rate of AtSirB Fc reconstitution suggests effective and intact cluster transfer from [2Fe–2S] cluster-loaded GrxS14 to apo AtSirB Fc. Additional CD studies of the reaction mixture in the absence of the apo AtSirB Fc indicated up to 10% degradation of the [2Fe–2S] cluster on GrxS14 after 130 min (data not shown), therefore arguing strongly against cluster degradation and subsequent reassembly of apo AtSirB Fc.

Surprisingly, attempts to reconstitute AtSirB at pH 7.3 results in the appearance of CD spectra with time that resemble the high pH form of the protein, rather than the low pH form

(data not shown), perhaps indicating that the [2Fe-2S] cluster can only be inserted in the high pH form in AtSirB Fc. In addition, kinetic analysis of the rate of [2Fe-2S] cluster transfer at low pH was determined to be about 5-fold lower compared to the rate constant at pH 8.0.

Discussion

A previous study indicated that recombinant AtSirB Fc contains a [2Fe-2S] center as evidenced by UV-visible absorption and EPR spectroscopy (*58*). The [2Fe-2S] cluster was shown to be irreversibly reduced by sodium dithionite, and the redox potential was determined to be -372 ± 4 mV (*58*). By comparison to metazoan ferrochelatases involved with heme biosynthesis, the [2Fe-2S] center in AtSirB Fc was suggested to be ligated by a set of four conserved cysteine residues located at the C-terminus of the amino acid sequence (*58*).

In this study the nature and properties of the [2Fe-2S] center present in the recombinant AtSirB have been investigated via means of spectroscopic and analytical techniques. As indicated by the analytical and spectroscopic results described above, AtSirB Fc undergoes a conformational transition from a dimeric to a tetrameric state that is accompanied by marked changes in the protein environment in the vicinity of the [2Fe-2S] center, as a function of pH. Although, no such conformational transitions have been reported for other ferrochelatases, the presence of one [2Fe-2S] cluster per AtSirB Fc monomer as evidenced by protein and iron analyses, and supported by EPR results, is in agreement with the available data indicating that eukaryotic and prokaryotic ferrochelatases accommodate one [2Fe-2S] cluster per protomer (*15*).

The lack of sharp isosbestic points in the CD spectra run at various pH values (Figure 3.5) and the apparent cooperativity in proton dissociation (inset in Figure 3.5) observed for the transition of AtSirB Fc from pH 6.9 to pH 8.9 are probably related phenomena. They can be attributed to conformational changes that may involve interconversion from a dimeric to a

tetrameric state, and proton dissociation at an amino acid residue that either directly coordinates or is located sufficiently close to the [2Fe-2S] center. Both processes would induce significant changes in the protein environment surrounding the cluster, thus explaining the marked differences observed in the spectroscopic properties of the "low pH" and "high pH" forms of the as isolated AtSirB Fc. In fact, considering the above resonance Raman results suggesting that upon transitioning from high pH to low pH, one cysteine residue coordinating the $[2Fe\text{-}2S]^{2+}$ cluster is replaced by a histidine ligand, it is reasonable to suggest that perhaps protonation of a nitrogen atom of the histidine imidazole ring triggers rapid conformational rearrangement of the protein in the form of dimer/tetramer interconversion.

The role of [2Fe-2S] clusters in ferrochelatases has not been elucidated to date, and all hypotheses that have been considered thus far, have eventually been ruled out. For instance, direct involvement of the cluster in catalysis can be readily dismissed since plants, yeast *Saccharomyces cerevisiae* and most prokaryotes have ferrochelatases that lack this cofactor, yet retain enzymatic activity (*56;77-79*). Likewise, the discovery that the as isolated monomeric ferrochelatase from *Mycobacterium tuberculosis* contains a [2Fe-2S] cluster diminished the support for a role of the cluster in the dimerization motif (*78*). Similarly to its counterparts in other ferrochelatases, the inability to reduce the cluster on AtSirB Fc to a stable $[2Fe\text{-}2S]^{+}$ state argues against a redox role for these centers (*58*) (see Chapter 2 and references therein). Based on *in vivo* and *in vitro* studies demonstrating inactivation of the mammalian ferrochelatase by nitric oxide via destruction of the [2Fe-2S] center, it was hypothesized that in mammals the cluster may play a role in cellular defense against pathogens (*12*). Although the finding of [2Fe-2S] clusters in *Drosophila* (*80*), the yeast *S. pombe* (*78*), and bacterial ferrochelatases (*78;79*) seemed to diminish the support for this hypothesis, it cannot eliminate it completely. The recent

major advances in understanding the extensive [2Fe-2S] cluster trafficking in both eukaryotes and prokaryotes raises the possibility that the [2Fe-2S] cluster-binding site in ferrochelatases may play a role in sensing the cellular [2Fe-2S] cluster concentrations for subsequent regulation of Fe utilization and direction towards heme/siroheme or Fe-S cluster biogenesis.

Several lines of evidence argue for a role of the [2Fe-2S] cluster-binding site in ferrochelatases in sensing Fe levels based on the levels of [2Fe-2S] cluster-bound monothiol Grxs. Human *in vivo* studies indicate that decreased availability for newly formed Fe-S clusters due to either iron-depletion of the cell or impairment of the Fe-S cluster assembly machinery results in impaired maturation of apo-ferrochelatase and subsequent rapid degradation by unknown proteases (*53*). *In vivo* data also indicate that monothiol Glrx5 is required for normal expression of ALAS2 and ferrochelatase (*57*). The *in vitro* results presented in this study clearly demonstrate that monothiol glutaredoxins with CGFS active sites are the excellent candidates for the physiological [2Fe-2S] cluster donors for posttranslational maturation and stabilization of sirohydrochlorin ferrochelatase in plants, and, by extrapolation, all other [2Fe-2S] cluster-containing ferrochelatases. Thus, for the first time, this work provides direct evidence that the [2Fe-2S] cluster-binding site in ferrochelatases and plant sirohydrochlorin ferrochelatases act as sensors of Fe-S cluster status in the cell via the extent of cluster loading of monothiol glutaredoxins which function as Fe-S cluster carrier/storage proteins. Furthermore, the data presented in this study demonstrate that heme/siroheme biosynthesis is regulated by the cellular Fe-S cluster status.

Acknowledgements

This work was supported by grants from the National Institute of Health (GM62524 to MKJ) and from the ANR programs (GNP05010G and JC07_204825 to NR). We would like to thank Prof. Harry A. Dailey for helpful scientific suggestions and discussions. We also thank Dennis R. Phillips for help with mass spectrometry at University of Georgia Proteomics and Mass Spectrometry (PAMS) Core Facility.

References

1. Lill, R. and Muhlenhoff, U. (2008) *Annu. Rev. Biochem. 77*, 669-700.
2. Beinert, H. (2000) *JBIC,J. Biol. Inorg. Chem. 5*, 2-15.
3. Beinert, H. (2000) *Eur. J. Biochem. 267*, 5657-5664.
4. Johnson, M. K. and Smith, A. D. (2005) in *Encyclopedia of Inorganic Chemistry, Second Edition* (King, R. B., Ed.) pp 2589-2619, John Wiley & Sons, Chichester.
5. Yeh, A. P., Hu, Y., Jenney, F. E., Adams, M. W. W., and Rees, D. C. (2000) *Biochemistry 39*, 2499-2508.
6. Sofia, H. J., Chen, G., Hetzler, B. G., Reyes-Spindola, J. F., and Miller, N. E. (2001) *Nucleic Acids Res. 29*, 1097-1106.
7. Darnault, C., Volbeda, A., Kim, E. J., Legrand, P., Vernède, X., Lindahl, P. A., and Fontecilla-Camps, J. C. (2003) *Nat. Struct. Biol. 10*, 271-279.
8. Jarrett, J. T. (2003) *Curr. Opin. Chem. Biol. 7*, 174-182.
9. Grandoni, J. A., Switzer, R. L., Marakoff, C. A., and Zalkin, H. (1989) *J. Biol. Chem. 264*, 6058-6064.
10. Demple, B., Ding, H., and Jorgensen, M. (2002) *Meth. Enzymol. 348*, 355-364.
11. Gaudu, P. and Weiss, B. (1996) *Proc. Natl. Acad. Sci. USA 93*, 10094-10098.
12. Sellers, V. M., Johnson, M. K., and Dailey, H. A. (1996) *Biochemistry 35*, 2699-2704.
13. Alen, C. and Sonenshein, A. L. (1999) *Proc. Natl. Acad. Sci. USA 96*, 10412-10417.
14. Tang, Y. and Guest, J. R. (1999) *Microbiology 145*, 3069-3079.
15. Wu, C.-K., Dailey, H. A., Rose, J. P., Burden, A., Sellers, V. M., and Wang, B.-C. (2001) *Nat. Struct. Biol. 8*, 156-160.
16. Kiley, P. J. and Beinert, H. (2003) *Curr. Opin. Microbiol. 6*, 181-185.

17. Boal, A. K., Yavin, E., Lukianova, O. A., O'Shea, V. L., David, S. S., and Barton, J. K. (2005) *Biochemistry 44*, 8397-8407.

18. Boal, A. K., Genereux, J. C., Sontz, P. A., Gralnick, J. A., Newman, D. K., and Barton, J. K. (2009) *Proc. Natl. Acad. Sci. U. S. A 106*, 15237-15242.

19. Thauer, R. K. and Schönheit, P. (1982) in *Iron-Sulfur Proteins* (Spiro, T. G., Ed.) pp 329-341, Wiley, New York.

20. Reeve, J. N., Beckler, G. S., Cram, D. S., Hamilton, P. T., Brown, J. W., Krzycki, J. A., Kolodziej, A. F., Alex, L. A., Orme-Johnson, W. H., and Walsh, C. T. (1989) *Proc. Natl. Acad. Sci. USA 86*, 3031-3035.

21. Hedderich, R., Albracht, S. P. J., Linder, D., Koch, J., and Thauer, R. K. (1992) *FEBS Lett. 298*, 65-68.

22. Dai, S., Schwendtmayer, C., Johansson, K., Ramaswamy, S., Schürmann, P., and Eklund, H. (2000) *Quart. Rev. Biophys. 33*, 67-108.

23. Walters, E. M. and Johnson, M. K. (2004) *Photosynth. Res. 79*, 249-264.

24. Jameson, G. N. L., Cosper, M. M., Hernández, H. L., Johnson, M. K., and Huynh, B. H. (2004) *Biochemistry 43*, 2022-2031.

25. Cosper, M. M., Krebs, B., Hernandez, H., Jameson, G., Eidsness, M. K., Huynh, B. H., and Johnson, M. K. (2004) *Biochemistry 43*, 2007-2021.

26. Mense, S. M. and Zhang, L. (2006) *Cell Res. 16*, 681-692.

27. Hou, S., Reynolds, M. F., Horrigan, F. T., Heinemann, S. H., and Hoshi, T. (2006) *Acc. Chem Res. 39*, 918-924.

28. Gilles-Gozales, M. A. (200) *IUBMB Life 51*, 165-173.

29. Dioum, E. M., Rutter, J., Tuckerman, J. R., Gonzalez, G., Gilles-Gonzalez, M. A., and McKnight, S. L. (2002) *Science 298*, 2385-2387.

30. Tsiftsoglou, A. S., Tsamadou, A. I., and Papadopoulou, L. C. (2006) *Pharmacol. Ther. 111*, 327-345.

31. Faller, M., Matsunaga, M., Yin, S., Loo, J. A., and Guo, F. (2007) *Nat. Struct. Mol. Biol 14*, 23-29.

32. Crane, B. R. and Getzoff, E. D. (1996) *Curr. Opin. Chem. Biol. 6*, 744-756.

33. Bandyopadhyay, S., Gama, F., Molina-Navarro, M. M., Gualberto, J. M., Claxton, R., Naik, S. G., Huynh, B. H., Herrero, E., Jacquot, J.-P., Johnson, M. K., and Rouhier, N. (2008) *EMBO J. 27*, 1122-1133.

34. Rouhier, N., Gelhaye, E., and Jacquot, J.-P. (2004) *Cell. Mol. Life Sci. 61*, 1266-1277.

35. Rouhier, N., Couturier, J., Johnson, M. K., and Jacquot, J. P. (2010) *Trends Biochem. Sci. 35*, 43-52.

36. Herrero, E. and de la Torre-Ruiz, M. A. (2007) *Cell. Mol. Life Sci. 64*, 1518-1530.

37. Lillig, C. H., Berndt, C., and Holmgren, A. (2008) *Biochim. Biophys. Acta 1780*, 1304-1317.

38. Rodríguez-Manzaneque, M. T., Ros, J., Cabrito, I., Sorribas, A., and Herrero, E. (1999) *Mol. Cell. Biol. 19*, 8180-8190.

39. Rodríguez-Manzaneque, M. T., Tamarit, J., Bellí, G., Ros, J., and Herrero, E. (2002) *Mol. Biol. Cell 13*, 1109-1121.

40. Molina, M. M., Belli, G., de la Torre, M. A., Rodriguez-Manzaneque, M. T., and Herrero, E. (2004) *J Biol Chem 279*, 51923-51930.

41. Mühlenhoff, U., Gerber, J., Richhardt, N., and Lill, R. (2003) *EMBO J. 22*, 4815-4825.

42. Vilella, F., Alves, R., Rodriguez-Manzaneque, M. T., Belli, G., Swaminathan, S., Sunnerhagen, P., and Herrero, E. (2004) *Comp Funct. Genomics 5*, 328-341.

43. Mapolelo, D. T. Characterization of the roles of A-type proteins and monothiol CGFS glutaredoxins in iron-sulfur cluster biogenesis. 2010. University of Georgia. Ref Type: Thesis/Dissertation

44. Bandyopadhyay, S., Chandramouli, K., and Johnson, M. K. (2008) *Biochem. Soc. Trans. 36*, 1112-1119.

45. Johnson, D. C., Dean, D. R., Smith, A. D., and Johnson, M. K. (2005) *Annu. Rev. Biochem. 74*, 247-281.

46. Agar, J. N., Dean, D. R., and Johnson, M. K. (2003) in *Biochemistry and Physiology of Anaerobic Bacteria* (Ljungdahl, L. G., Adams, M. W. W., Barton, L. L., Ferry, J. G., and Johnson, M. K., Eds.) pp 46-66, Springer-Verlag, New York.

47. Shakamuri, P. The role of molecular chaperones in mediating cluster transfer from [2Fe-2S] cluster-bound IscU. 2011. University of Georgia. Ref Type: Thesis/Dissertation

48. Linares, G. R., Xing, W., Govoni, K. E., Chen, S. T., and Mohan, S. (2009) *Bone 44*, 795-804.

49. Wingert, R. A., Galloway, J. L., Barut, B., Foott, H., Fraenkel, P., Axe, J. L., Weber, G. J., Dooley, K., Davidson, A. J., Schmidt, B., Paw, B. H., and Shaw, G. C. (2005) *Nature 436*, 1035-1039.

50. Walden, W. E., Selezneva, A. I., Dupuy, J., Volbeda, A., Fontecilla-Camps, J. C., Theil, E. C., and Volz, K. (2006) *Science 314*, 1903-1908.

51. Hentze, M. W., Muckenthaler, M. U., and Andrews, N. C. (2004) *Cell 117*, 285-297.

52. Camaschella, C., Campanelle, A. F. L., Boschetto, L., Merlini, R., Silvestri, L., Levi, S., and Iolascon, A. (2007) *Blood 110*, 1353-1358.

53. Crooks, D. R., Ghosh, M. C., Haller, R. G., Tong, W.-H., and Rouault, T. A. (2010) *Blood 115*, 860-869.

54. Dailey, H. A., Finnegan, M. G., and Johnson, M. K. (1994) *Biochemistry 33*, 403-407.

55. Dailey, H. A., Dailey, T. A., Wu, C.-K., Medlock, A. E., Wang, K.-F., Rose, J. P., and Wang, B.-C. (2000) *Cell. Mol. Life Sci. 57*, 1909-1926.

56. Dailey, H. A. and Dailey, T. A. (2003) in *The Porphyrin Handbook* (Kadish, K. M., Smith, R., and Guilard, R., Eds.) pp 93-121, Academic Press, New York.

57. Ye, H., Jeong, S. Y., Ghosh, M. C., Kovtunovych, G., Silvestri, L., Ortillo, D., Uchida, N., Tisdale, J., Camaschella, C., and Rouault, T. A. (2010) *J Clin. Invest 120*, 1749-1761.

58. Raux-Deery, E., Leech, H. K., Nakrieko, K. A., McLean, K. J., Munro, A. W., Heathcote, P., Rigby, S. E. J., Smith, A. G., and Warren, M. J. (2005) *J. Biol. Chem. 280*, 4713-4721.

59. Brown, R. E., Jarvis, K. L., and Hyland, K. J. (1989) *Anal. Biochem. 180*, 136-139.

60. Fish, W. W. (1988) *Meth. Enzymol. 158*, 357-364.

61. Drozdzewski, P. M. and Johnson, M. K. (1988) *Appl. Spectrosc. 42*, 1575-1577.

62. Rouhier, N., Unno, H., Bandyopadhyay, S., Masip, L., Kim, S. K., Hirasawa, M., Gualberto, J. M., Lattard, V., Kusunoki, M., Knaff, D. B., Georgiou, G., Hase, T., Johnson, M. K., and Jacquot, J. P. (2007) *Proc. Natl. Acad. Sci. U. S. A. 104*, 7379-7384.

63. Couturier, J., Stroher, E., Albetel, A. N., Roret, T., Muthuramalingam, M., Tarrago, L., Seidel, T., Tsan, P., Jacquot, J. P., Johnson, M. K., Dietz, K. J., Didierjean, C., and Rouhier, N. (2011) *J. Biol. Chem. 286*, 27515-27527.

64. Stephens, P. J., Thomson, A. J., Dunn, J. B. R., Keiderling, T. A., Rawlings, J., Rao, K. K., and Hall, D. O. (1978) *Biochemistry 17*, 4770-4778.

65. Han, S., Czernuszewicz, R. S., Kimura, T., Adams, M. W. W., and Spiro, T. G. (1989) *J. Am. Chem. Soc. 111*, 3505-3511.

66. Link, T. A. (1999) *Adv. Inorg. Chem. 47*, 83-157.

67. Jung, Y.-S., Gao-Sheridan, H. S., Christiansen, J., Dean, D. R., and Burgess, B. K. (1999) *J. Biol. Chem. 274*, 32402-32410.

68. Agar, J. N., Krebs, B., Frazzon, J., Huynh, B. H., Dean, D. R., and Johnson, M. K. (2000) *Biochemistry 39*, 7856-7862.

69. Fu, W., Drozdzewski, P. M., Davies, M. D., Sligar, S. G., and Johnson, M. K. (1992) *J. Biol. Chem. 267*, 15502-15510.

70. Kounosu, A., Li, Z., Shokes, J. E., Scott, R. A., Imai, T., Urushiyama, A., and Iwasaki, T. (2004) *J. Biol. Chem. 279*, 12519-12528.

71. Kuila, D., Schoonover, J. R., Dyer, R. B., Batie, C. J., Ballou, D. P., Fee, J. A., and Woodruff, W. H. (1992) *Biochim. Biophys. Acta 1140*, 175-183.

72. Rotsaert, F. A., Pikus, J. D., Fox, B. G., Markley, J. L., and Sanders-Loehr, J. (2003) *J. Biol. Inorg. Chem. 8*, 318-326.

73. Iwasaki, T., Kounosu, A., Kolling, D. R. J., Crofts, A. R., Dikanov, S. A., Jin, A., Imai, T., and Urushiyama, A. (2004) *J. Am. Chem. Soc. 126*, 4788-4789.

74. Tirrell, T. F., Paddock, M. L., Conlan, A. R., Smoll, E. J., Nechushtai, R., Jennings, P. A., and Kim, J. E. (2009) *Biochemistry 48*, 4747-4752.

75. Meyer, J., Fujinaga, J., Gaillard, J., and Lutz, M. (1994) *Biochemistry 33*, 13642-13650.

76. Moulis, J.-M., Davasse, V., Golinelli, M.-P., Meyer, J., and Quinkal, I. (1996) *JBIC,J. Biol. Inorg. Chem. 1*, 2-14.

77. Medlock, A. E. and Dailey, H. A. (2000) *Biochemistry 39*, 7461-7467.

78. Dailey, T. A. and Dailey, H. A. (2002) *J. Bacteriol. 184*, 2460-2464.

79. Shepherd, M., Dailey, T. A., and Dailey, H. A. (2006) *Biochem. J. 397*, 47-52.

80. Sellers, V. M., Wang, K. F., Johnson, M. K., and Dailey, H. A. (1998) *J. Biol. Chem. 273*, 22311-22316.

Table 3.1. Primers used in this study for cloning and construction of AtSirB Fc. The *Nde*I and *Bam*HI cloning restriction sites are underlined in the primers. The mutagenic codons are in bold.

AtSirB forward	5’CCCCCCCCCATATGGCTGATGCTGATGGGATTATA
AtSirB reverse	5’CCCCGGATCCCTAAGAACTATTGTAGAGCTT
AtSirB H41H forward	5’GTAGAGCCTGCT**CAC**ATGGAATTGGCTGAG
AtSirB H41H reverse	5’CTCAGCCAATTCCATGT**GAG**CAGGCTCTAC

Figure 3.1. Analytical characterization of AtSirB Fc at pH 7.4 and 8.7. (A) SDS-PAGE analysis of as purified AtSirB Fc at pH 7.4 (*left panel*) and pH 8.7 (*right panel*) as eluted off the S75 column. (B) Gel filtration chromatograms of [2Fe-2S] cluster-bound AtSirB Fc purified in 50 mM sodium phosphate, 0.3 M NaCl, 2 mM DTT, pH 7.4 (*black line*), and 50 mM Tris-HCl, 0.3 M NaCl, 1% (w/v) sodium cholate, 2 mM DTT, pH 8.7 (*red line*).

(A)

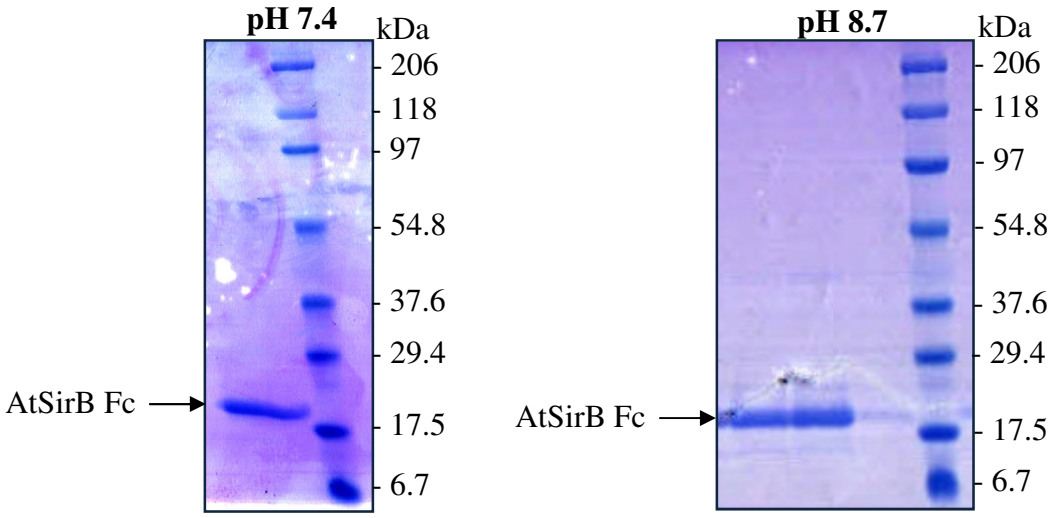
pH 7.4
kDa
206
118
97
54.8
37.6
29.4
17.5
6.7
AtSirB Fc
pH 8.7
kDa
206
118
97
54.8
37.6
29.4
17.5
6.7
AtSirB Fc

(B)

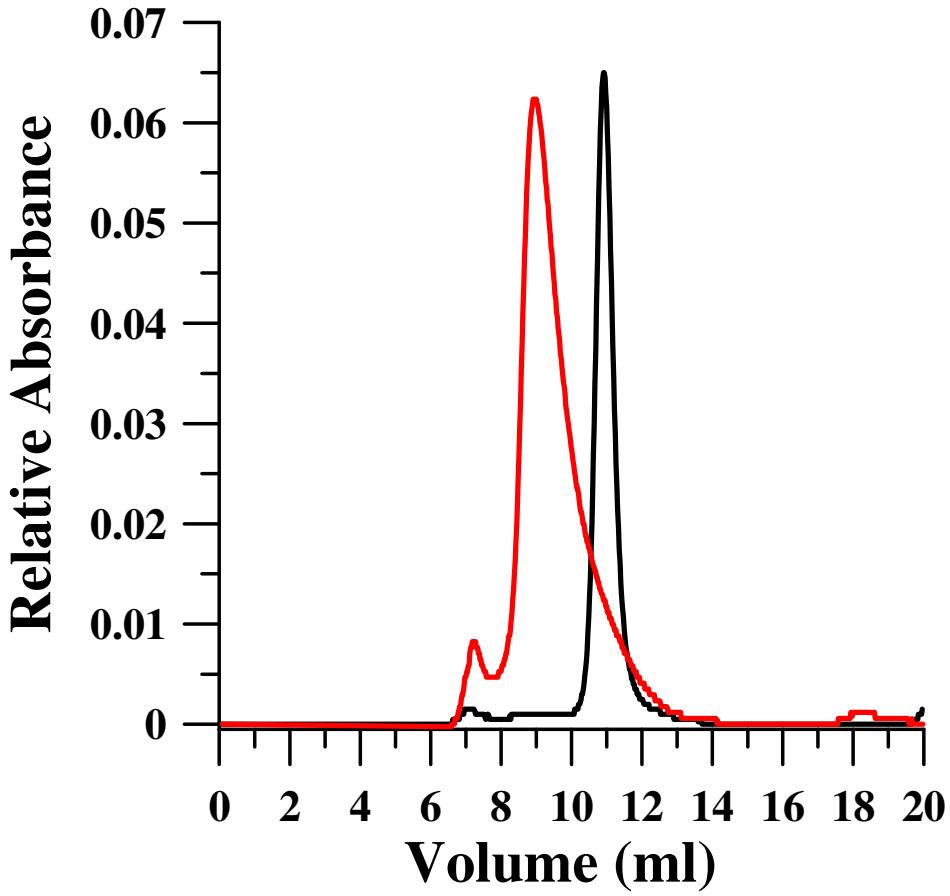
Relative Absorbance
0.07
0.06
0.05
0.04
0.03
0.02
0.01
0
0 2 4 6 8 10 12 14 16 18 20
Volume (ml)

Figure 3.2. Comparison of the UV-visible absorption spectrum (*Upper*) and CD spectrum (*Lower*) of $[2Fe\text{-}2S]^{2+}$ cluster-bound AtSirB Fc at pH 7.4 (*black line*) and 8.7 (*red line*). $\Delta\varepsilon$ values are expressed as a function of protein monomer concentration. Spectra were recorded in 1 cm cuvettes.

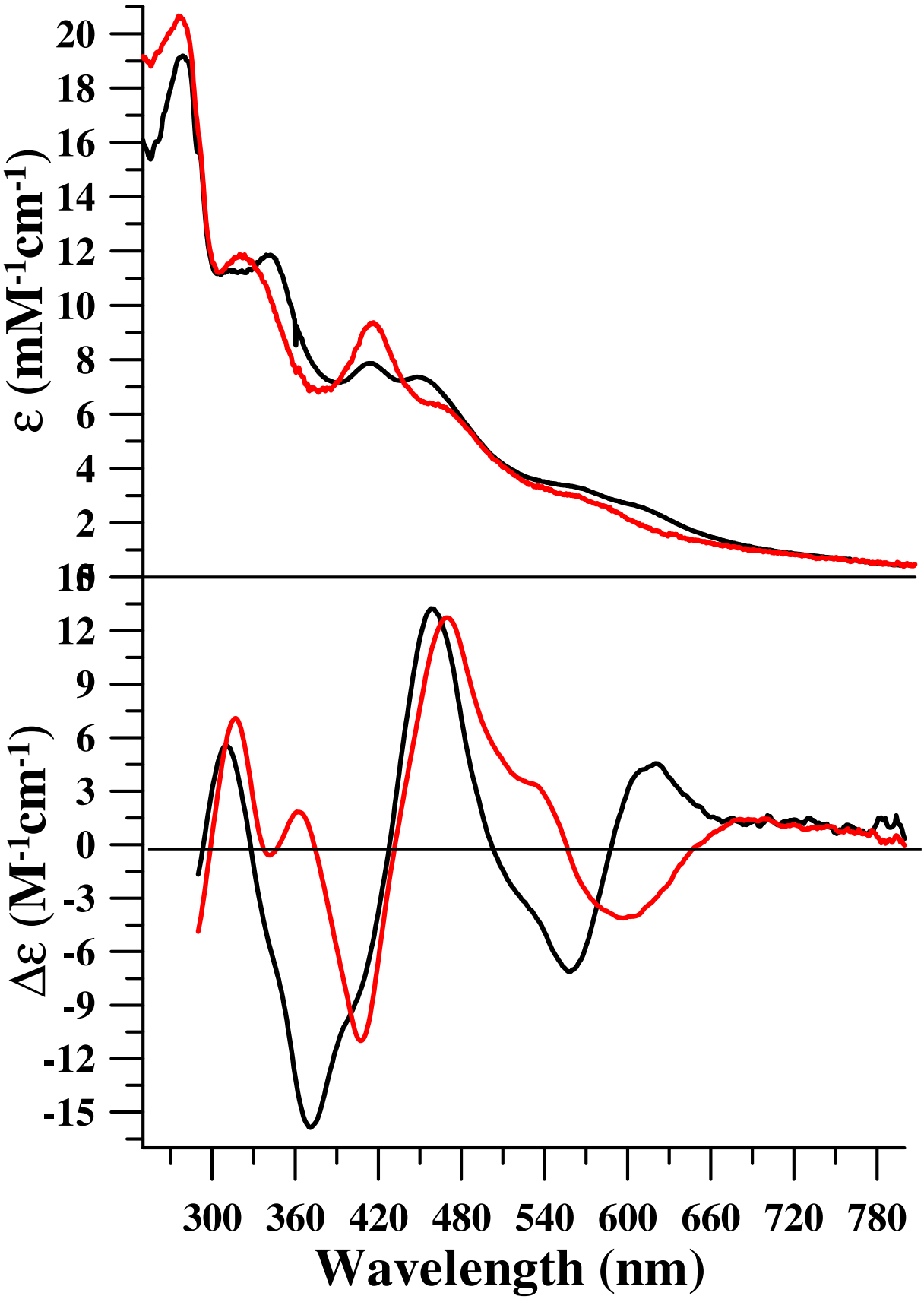
ε (mM-1cm-1)
20
18
16
14
12
10
8
6
4
2
Δε (M-1cm-1)
12
9
6
3
0
-3
-6
-9
-12
-15
300
360
420
480
540
600
660
720
780
Wavelength (nm)

Figure 3.3. Perpendicular-mode X-band EPR spectra of [2Fe-2S]$^{+}$ center in dithionite-reduced AtSirB Fc. As purified recombinant AtSirB Fc (124 μM) was in 50 mM Tris-HCl, 0.3 M NaCl, 1% (w/v) sodium cholate, 2 mM DTT, pH 8.7 recorded at 4.6 K, 10 K, 35 K, 68 K, 100 K in the S = ½ region. Samples were reduced by anaerobic addition of approximately 2-fold excess sodium dithionite. Spectra were recorded under the following measurement conditions: microwave power, 5 mW; microwave frequency, 9.6 GHz; and modulation amplitude, 0.64 mT.

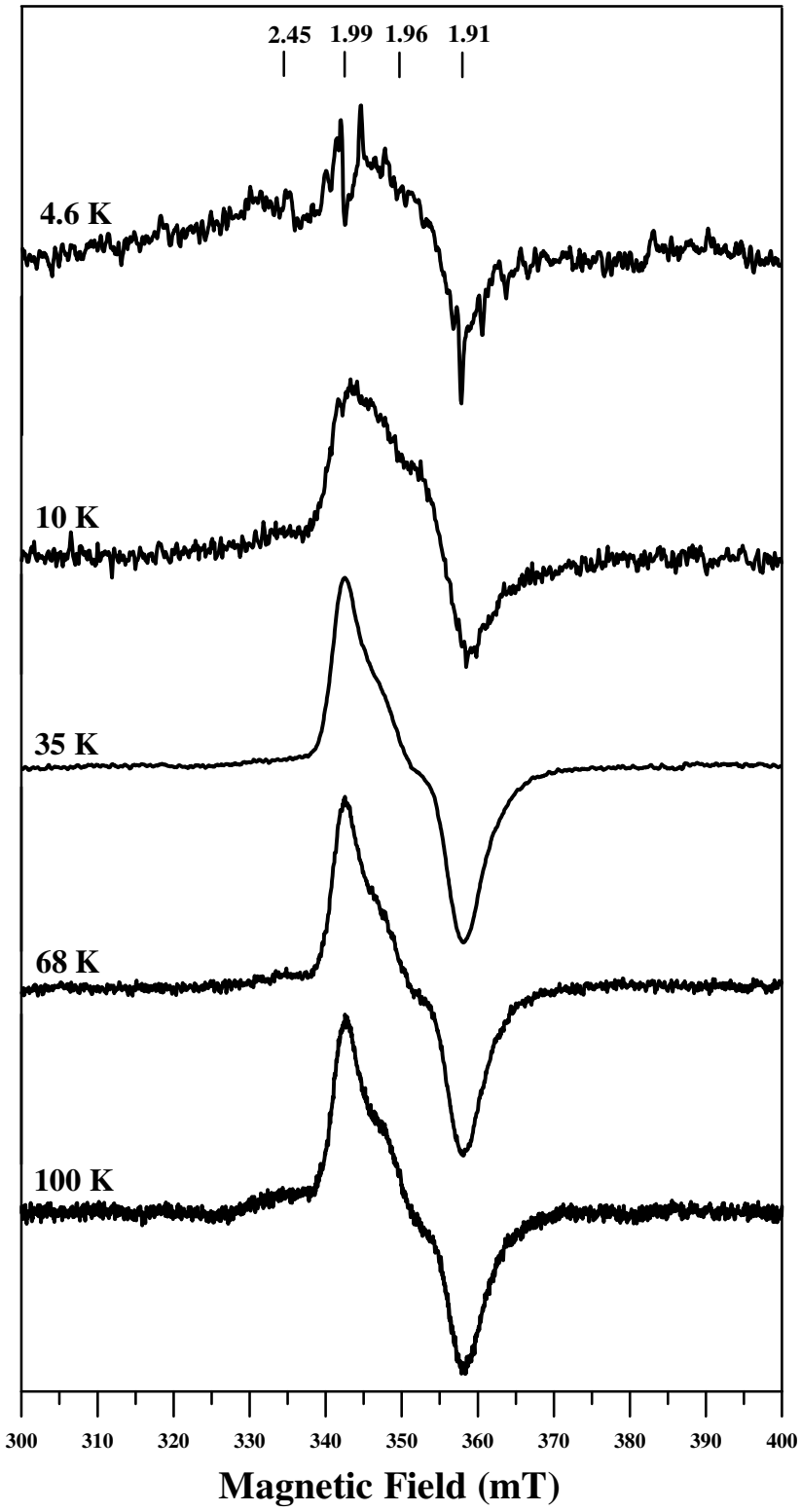
2.45
1.99
1.96
1.91
4.6 K
10 K
35 K
68 K
100 K
300
310
320
330
340
350
360
370
380
390
400
Magnetic Field (mT)

Figure 3.4. Comparison of the resonance Raman spectra of the oxidized [2Fe-2S] cluster-bound forms of AtSirB Fc. Aerobically purified samples of recombinant At-SirB Fc were in 50 mM sodium phosphate, 0.3 M NaCl, 2 mM DTT, pH 7.4 (*black line*), and 50 mM Tris-HCl, 0.3 M NaCl, 1% (w/v) sodium cholate, 2 mM DTT, pH 8.7 (*red line*). Samples were ~ 7.2 mM at pH 7.4 and 0.6 mM at pH 8.7 in [2Fe-2S] cluster, and were in the form of frozen droplets at 20 K. Spectra are sums of 100 scans, with each scan involving the photon counting for 1 s each 0.5 cm^{-1} with a spectral bandwidth of 7 cm^{-1}. Lattice modes of ice have been substracted.

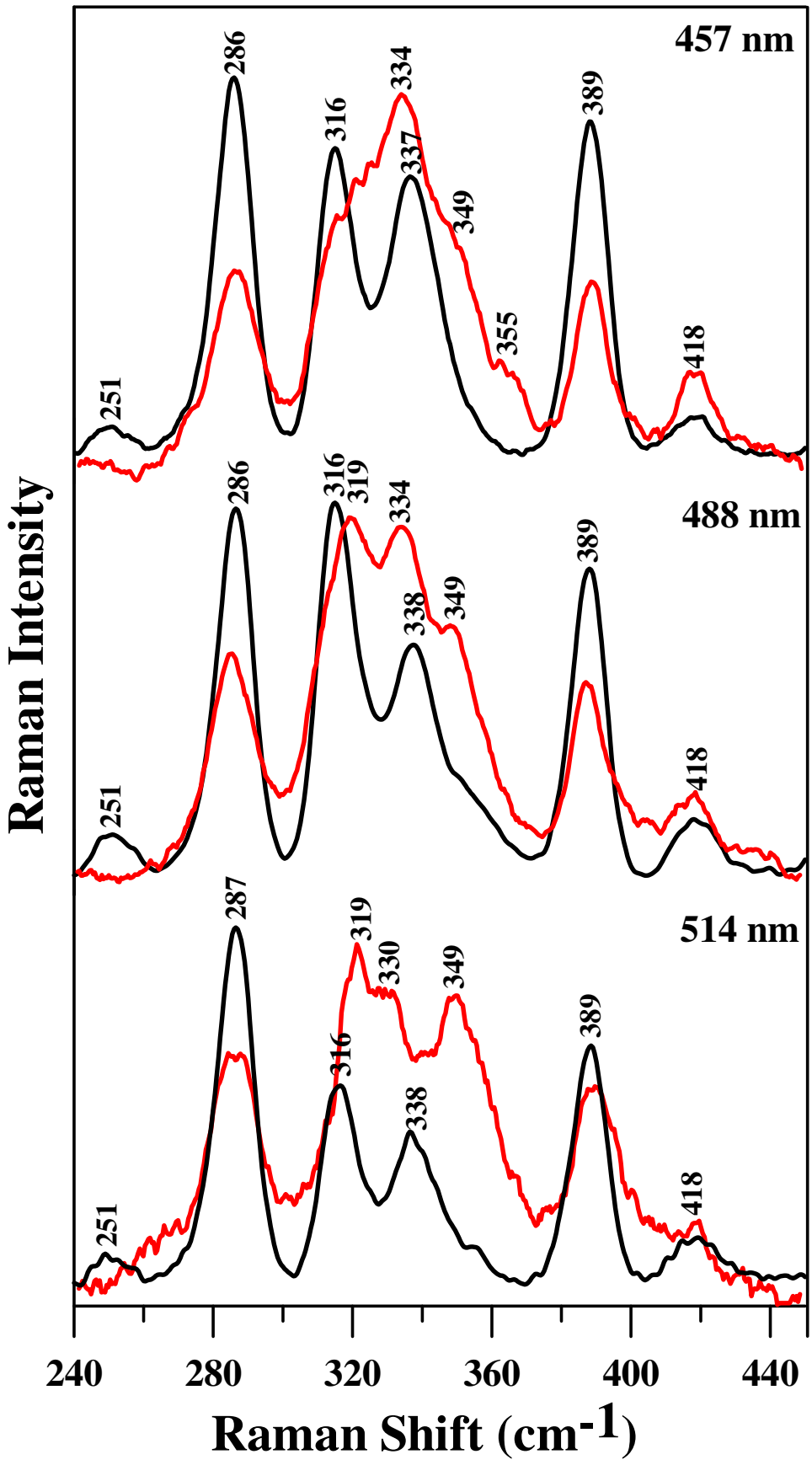
457 nm
286
316
334
337
349
355
389
418
251
488 nm
286
316
319
334
338
349
389
418
251
514 nm
287
319
330
349
316
338
389
418
251
Raman Intensity
240
280
320
360
400
440
Raman Shift (cm-1)

Figure 3.5. Dependence of CD spectrum of AtSirB Fc on pH. Spectra were recorded in 1 cm semi-micro cuvettes after incubation of the protein (60 μM) with a mixed buffer system with pH ranging from 6.9 (*black line*) to 8.9 (*red line*). Spectra corresponding to samples having pH 7.1, 7.4, 7.7, 7.9, 8.1, 8.3, 8.5, 8.7 are shown as grey lines, and the black arrows indicate the direction of the change in CD intensity as a function of pH. (*Inset*) Titration curves fitted using the Hill equation for AtSirB Fc. The data points correspond to the extent of changes in the CD intensities determined by the difference in the UV-visible CD intensity at 370 and 362 nm, as a function of pH. The solid curve is calculated using line using Hill equation (n = 2.1) and pK_a 7.95, while the broken line shows a non-linear regression fit to a one proton dissociation process (Hill coefficient n = 1).

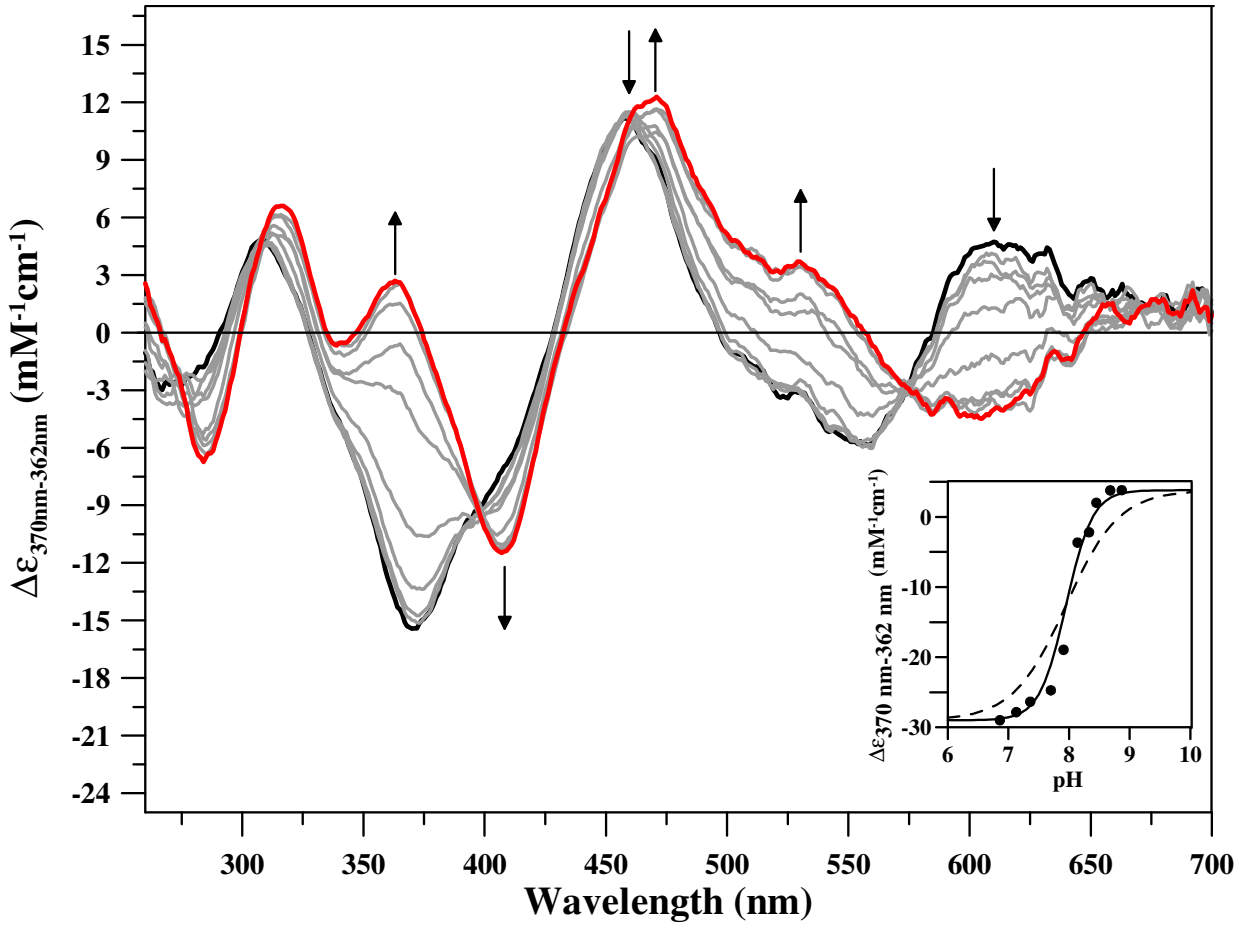
15
12
9
6
3
0
-3
-6
-9
-12
-15
-18
-21
-24
$\Delta\varepsilon_{370nm-362nm}$ (mM^{-1}cm^{-1})
300
350
400
450
500
550
600
650
700
Wavelength (nm)
0
-10
-20
-30
$\Delta\varepsilon$370 nm-362 nm (mM^{-1}cm^{-1})
6
7
8
9
10
pH

Figure 3.6. Time course of cluster transfer from [2Fe-2S] cluster-loaded *A. thaliana* monothiol GrxS14 (*broken line*) to apo AtSirB Fc monitored by UV-visible CD spectroscopy. (**A**) CD spectra were recorded at 1, 3, 6, 9, 12, 15, 30, 45, and 60 min after addition of GrxS14 (31 μM) to a solution containing apo AtSirB Fc (39 μM) incubated with 2 mM DTT in 50 mM Tris-MOPS pH 8.0, 100 mM KCl, and 0.1% [w/v] sodium cholate. The spectrum at zero time (*thick line*) corresponds to AtSirB Fc showing the presence of less than 20% residual [2Fe-2S] cluster. The arrows indicate the change in the CD intensity with time at selected wavelengths. (**B**) Simulated CD spectra corresponding to quantitative cluster transfer from the $[2Fe\text{-}2S]^{2+}$ cluster-loaded GrxS14 to apo AtSirB Fc in 10% increments of cluster formation of holo AtSirB Fc for the reaction mixture shown in (A). Δε values are based on the $[2Fe\text{-}2S]^{2+}$ cluster concentration for GrxS14. Spectra were recorded at room temperature in a 1-cm semi-micro cuvette.

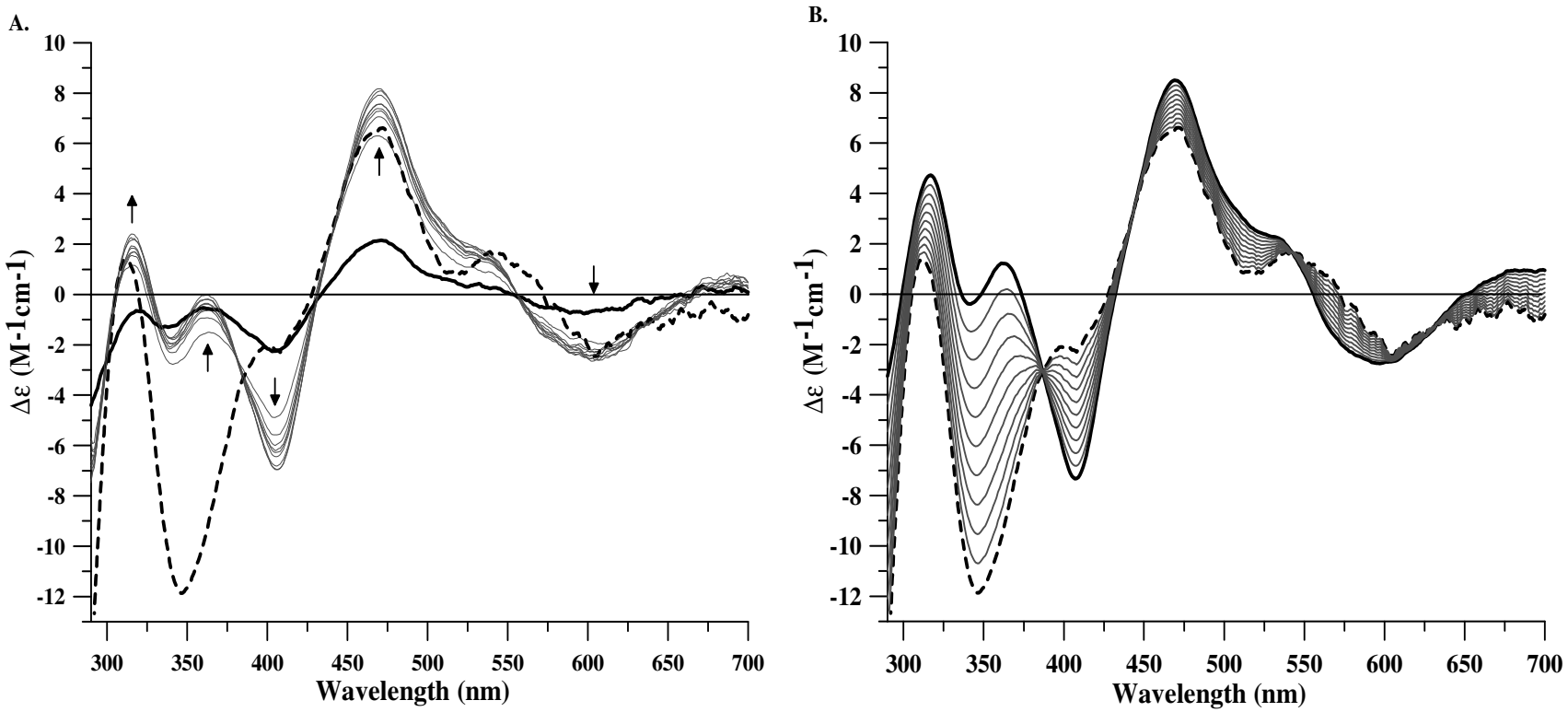
A.
B.
Δε (M-1cm-1)
Wavelength (nm)
10
8
6
4
2
0
-2
-4
-6
-8
-10
-12
300
350
400
450
500
550
600
650
700

Figure 3.7. Kinetic analysis of cluster transfer from *A. thaliana* monothiol GrxS14 to apo AtSirB Fc. The reaction was monitored by CD at room temperature as a function of the stoichiometry of GrxS14 [2Fe-2S] to apo AtSirB Fc. The experimental conditions are as described in Figure 3.6, and the data points correspond to the extent of [2Fe-2S] AtSirB Fc formation as a function of time, as determined by the difference in the UV-visible CD intensity at 469 and 406 nm, followed by conversion to percent [2Fe-2S] cluster reconstituted on AtSirB Fc based on simulated data (as illustrated in Figure 3.6 for similar reaction stoichiometry as in the cluster transfer experiment). The solid line corresponds to the best fit to second-order kinetics with k = 6 000 $M^{-1}min^{-1}$ based on the initial [2Fe-2S] cluster concentration on GrxS14 (0.031 mM) and the initial concentration of apo-AtSirB Fc (0.039 mM).

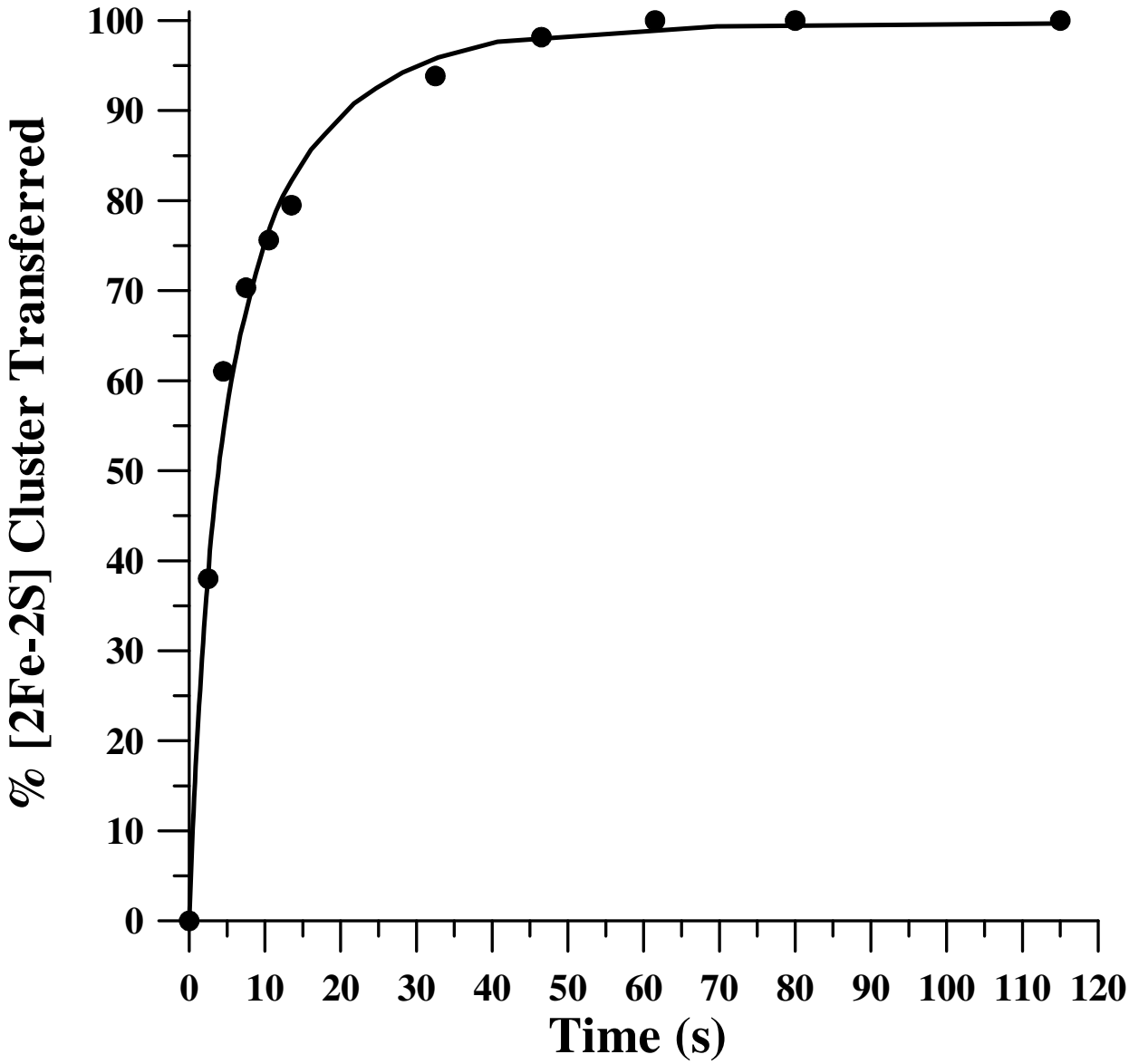
% [2Fe-2S] Cluster Transferred
100
90
80
70
60
50
40
30
20
10
0
0
10
20
30
40
50
60
70
80
90
100
110
120
Time (s)

CHAPTER 4

NITRIC OXIDE INTERACTION WITH THE [2FE-2S] CENTER IN FERROCHELATASES: A POSSIBLE REGULATORY ROLE WITH IMPACT ON THE CATALYTIC ACTIVITY

Angela-Nadia Albetel,[‡] Tamara A. Dailey,[§] Harry A. Dailey,[§] and Michael K. Johnson[‡]

to be submitted to J. Biol. Chem.

[‡]Department of Chemistry and Center for Metalloenzyme Studies, and [§]Biomedical and Health Sciences Institute,University of Georgia, Athens, Georgia, 30602, USA

Abbreviations: EPR, electron paramagnetic resonance; DTT, dithiothreitol; NO, nitric oxide; DEA/NO, Diethylamine NONOate; SNAP, *S*-nitroso-*N*-acetylpenicillamine; DNIC, dinitrosyl-iron-cysteine complex; ROS, reactive oxygen species; Fe-S cluster, iron-sulfur cluster; IRP, Iron Responsive Protein; IRE, Iron Responsive Element; UTR, untranslated region; ALA, 5-aminolevulinic acid synthetase; TfR, transferrin receptor; SoxR, Superoxide Reductase; FNR, fumarate and nitrate reductase;

Abstract

The effect of the nitric oxide donor, diethylamine NONOate (DEA/NO) on [2Fe-2S] clusters from human, zebrafish, *Schizosaccharomyces pombe, Caulobacter crescentus,* and *Myxococcus xanthus* ferrochelatases has been investigated to assess the role of these centers as nitric oxide sensors and involvement in antibacterial host defense in eukaryotes. UV-visible absorption spectroscopy indicates rapid loss of [2Fe-2S] clusters from all ferrochelatases examined upon incubation with the NO-generating compound, DEA/NO, concomitant with the formation of a dinitrosyl-iron-cysteine (DNIC) complex. EPR studies of the product formed upon [2Fe-2S] cluster degradation in the presence of the NO-donor DEA/NO reveal the presence of axial $S = ½$ resonances, $g_{\perp} = 2.033$, and $g_{\parallel} = 2.017$, confirming the formation of cysteinyl-coordinated monomeric iron-dinitrosyl species. Moreover, the second order rate constants for both the [2Fe-2S] cluster disassembly and the DNIC complex production reactions are comparable for all ferrochelatases investigated, suggesting that the enzymes from prokaryotic organism behave similarly to eukaryotic ferrochelatases in the presence of NO. In addition, activity assays on *wild type* and C219S variant of bacterial *M. xanthus* ferrochelatase indicate that the [2Fe-2S] cluster is required for enzymatic activity in prokaryotic as well as in eukaryotic ferrochelatases. We hypothesize that the degradation of the [2Fe-2S] center in ferrochelatases under nitrosative and/or oxidative stress conditions might be part of a more complex mechanism used by the cell to regulate Fe utilization toward heme or Fe-S cluster biosynthesis.

Introduction

Protoporphyrin IX ferrochelatases (E.C. 4.99.1.1) are a family of class II chelatases that catalyze the last step of the heme biosynthetic pathway, by inserting ferrous iron into protoporphyrin IX, to yield protoheme IX and two protons (*1-3*). All metazoan, Gram positive and a handful of Gram negative bacterial ferrochelatases contain a labile [2Fe-2S] cluster that is crucial for activity, but its role has yet to be elucidated. Since the initial discovery of the [2Fe-2S] cluster in human ferrochelatase (*4;5*) a variety of hypotheses have been forwarded for its potential role, but no compelling data exists to support any of them. For instance, it is obvious that the cluster does not play a direct role in catalysis, since many organisms possess a ferrochelatase that lacks this metal center. Also, no redox role can be assigned to the [2Fe-2S] center from ferrochelatases since enzymatic activity assays are always carried out in the presence of the ferrous iron substrate, and therefore no redox reaction is required for catalysis. In addition, the sensitivity of the [2Fe-2S] clusters from ferrochelatases to reductive agents (see Chapter 2) suggests that it cannot be involved in electron transfer. A role in the structural stabilization of the protein was considered, but the subsequent structure determination of human ferrochelatase (*6*) demonstrates that the cluster plays only a minor role in the dimerization process, and that it has no contribution to the maintenance of the active site conformation.

Based on two lines of evidence, a possible role for the [2Fe-2S] cluster from ferrochelatases as a nitric oxide sensor in relation to host defense mechanisms of eukaryotes has been proposed (*7*). First, in cultured rat hepatocytes (*8*) and murine erythroleukemia cells (*7*) treated with the NO-donor, *S*-nitroso-*N*-acetylpenicillamine (SNAP), ferrochelatase activity was shown to be decreased. An identical effect was also observed in a cultured macrophage cell line that had NO production stimulated by cytokine (lipopolysaccharide and interferon-γ) (*9*).

Secondly, incubation of the purified recombinant human and murine ferrochelatases with NO or the NO-generating compounds SNAP or 3-morpholinosydnonimine, resulted in rapid degradation of the [2Fe-2S] cluster and concomitant loss of enzymatic activity (*7;9*).

Nitric oxide had been used in a variety of research studies, particularly in the area of transition metal chemistry, in which the addition of NO, with its unpaired electron, often resulted in products that were suitable to study by EPR. Vanin and Commoner (*10-14*) and their co-workers had described the so-called "g = 2.03" signal observed for complexes generated synthetically by reaction of NO with iron and cysteine or found in cells treated with exogenous NO. This signal was attributed to a dinitrosyl-iron-dithiol complex with thiol groups provided by either low molecular weight compounds or by protein. In addition, it had been demonstrated by others that a g = 2.03 signal can be observed when NO is added to purified Fe-S proteins (*15-24*). In more recent cellular experiments, where cells have been induced to produce NO, it has been shown that the activities of some Fe- or Fe-S-containing proteins are often decreased and moreover that these cells, when examined by EPR, display the typical $g \approx 2.03$ signal (*25;26*). Similar EPR signals concerted with decreased enzymatic activity had also been observed when human and murine ferrochelatases were treated with NO or the NO generating compound SNAP, hence leading to the suggestion that the [2Fe-2S] center might act as a sensor of NO produced by macrophages as a response to bacterial infections (*7;9*). However, the typical DNIC $g \approx 2.03$ EPR signal was also observed upon incubation of the *Drosophila melanogaster (27)*, chicken (*28*) and *Xenopus* (*28*) [2Fe-2S] cluster-containing ferrochelatases with SNAP, and taken together with the subsequent finding of [2Fe-2S] clusters in yeast *Schizosaccharomyces pombe* ferrochelatase *(29)*, and some bacterial enzymes (*29;30*), these data seemed to diminish the support for a role of the [2Fe-2S] cluster from ferrochelatases in a local immune response. Yet,

although nonmammalian [2Fe-2S] cluster-containing ferrochelatases from *D. melanogaster (27)*, chicken (*28*) and frog *Xenopus* (*28*) appear to behave in a similar fashion to the murine and human homologs in the presence of the NO-donor, SNAP, the effect of nitric oxide on [2Fe-2S] clusters from bacterial ferrochelatases or yeast *S. pombe* has not been investigated thus far, therefore limiting the available information required for a general conclusion regarding the role of the [2Fe-2S] center.

We report here results of our *in vitro* studies on the reaction of the NO-donor, diethylamine NONOate (DEA/NO), with purified ferrochelatases from mammalian (human), vertebrate zebrafish, yeast *S. pombe*, and bacterial *Caulobacter crescentus* and *Myxococcus xanthus* monitored via UV-visible absorption and EPR spectroscopy. We present data indicative of rapid disassembly of the [2Fe-2S] cluster, concerted with the formation of dinitrosyl-iron-cysteine complexes for all enzymes examined. Furthermore, the effect of hydrogen peroxide on the [2Fe-2S] cluster from human ferrochelatase was also investigated in order to address the possibility that the [2Fe-2S] center from ferrochelatases may play a role in both the cellular response to nitrosative and oxidative stress. In addition, we investigated the effect of removal of the [2Fe-2S] cluster from bacterial *M. xanthus* ferrochelatase on its enzymatic activity in order to assess the requirement for the presence of the [2Fe-2S] center for catalytic activity.

Experimental Procedures

Materials. Materials used in this work were of reagent grade and were purchased from Fischer Scientific, Sigma-Aldrich Chemical Co, Cayman Chemicals, Invitrogen, or VWR International, unless otherwise stated.

Protein expression and purification. Recombinant ferrochelatases from *C. crescentus, S. pombe,* wild type and C219S *M. xanthus,* zebrafish and human were produced and expressed in *Escherichia coli* and subsequently purified as previously described (*29*).

Chemical analysis. Protein concentrations were estimated spectrophotometrically based on their theoretical extinction coefficients at 278 nm: $\varepsilon \approx 46{,}640\ M^{-1}\ cm^{-1}$, $\varepsilon \approx 44{,}640\ M^{-1}\ cm^{-1}$, $\varepsilon \approx 47{,}300\ M^{-1}\ cm^{-1}$ $\varepsilon \approx 52{,}840\ M^{-1}\ cm^{-1}$, and $\varepsilon \approx 49{,}765\ M^{-1}\ cm^{-1}$, for human, zebrafish, *S. pombe, C. crescentus,* and *M. xanthus* ferrochelatase, respectively.

UV-visible absorption and circular dichroism spectroscopy. Spectroscopic studies were carried out on ferrochelatase samples in solubilization buffer (50 mM Tris-MOPS buffer, pH 8.0, containing 0.1 mM KCl, 1% sodium cholate), unless otherwise specified. UV-visible absorption and CD spectra were recorded in either 1 mm or 1 cm quartz cuvettes at room temperature, using a Shimadzu UV-3101PC spectrophotometer and Jasco J-715 spectropolarimeter, respectively.

Enzyme activity. In vitro activity of wild type and C219S mutant of *M. xanthus* proteins was assayed aerobically at room temperature according to the published procedure (*31*). Freshly prepared ferrous ammonium sulfate and mesoporphyrin IX (Porphyrin Products, Logan, UT) were used as substrates. Substrates preparation was conducted according to the published procedure (*31*). One mL of ferrochelatase assay mixture contained 100 μM ferrous ammonium sulfate, 100 μM mesoporphyrin IX, and 10 mM β-mercaptoethanol (added to provide a reducing environment) in 50 mM Tris-MOPS, pH 8.0, 0.1 M KCl, 1% [wt/vol] sodium cholate buffer. Ferrochelatase (1 nmol/mL) was added last to start the reaction. The specific ferrochelatase activity for wild-type and C219S mutant proteins is expressed as nanomoles of heme per milligrams of ferrochelatase per minute.

NO assays. NO assay experiments were performed under anaerobic conditions (<4 ppm oxygen) at 13-15°C using diethylamine NONOate (DEA/NO) (Cayman Chemical) as the NO-donor. Following an initial scan, DEA/NO (in 10 mM NaOH, final concentration 2mM) was added to recombinant ferrochelatases from human (33 μM), zebrafish (26 μM), *S. pombe* (34 μM), *C. crescentus* (34 μM), and *M. xanthus* (38μM) in 1.5 mL solubilization buffer containing 10 μg phenylmethylsulfonyl fluoride/mL and 2 mM DTT, and to the reference cuvette, and to the reference cuvette. To quantitate the loss of the [2Fe-2S] cluster following addition of the NO donor, DEA/NO, repetitive UV-visible absorption scans were recorded (800-250 nm) at 5 minutes interval using a Shimadzu 3100PC dual-beam spectrophotometer. The temperature was maintained at 13°C throughout the experiments using a Peltier-type temperature controller.

EPR spectroscopy. EPR samples of DEA/NO-treated *C. crescentus* and *M. xanthus*, *S. pombe*, zebrafish, and human ferrochelatases were prepared under anaerobic conditions using identical assay cocktails as for the UV-VIS absorption studies. EPR tubes were transferred at 5 minutes interval from an anaerobic chamber and immediately frozen in liquid nitrogen. The assay mixtures were kept at 13-15°C at all times during the experiment using an ice bath. X-band EPR spectra were recorded using a Bruker Instruments ESP-300S spectrometer (Billerica, MA) equipped with an ER-4116 dual mode cavity and an Oxford Instruments ESR 900 flow cryostat (Concord, MA) (4.2-300 K). Spectra were quantified by double integration against a 1 mM Cu-EDTA standard, under non-saturating conditions.

Data analysis. The initial rate constants for the [2Fe-2S] cluster degradation, and the rate constants for product formation were determined using Chemical Kinetics Simulator software package (IBM) by fitting the rate of [2Fe-2S] cluster degraded based on the decrease in the

absorption values at 510 nm with time, and the rate of DNIC produced based on the increase in the DNIC EPR signal with time, to second-order kinetics.

Results

Recombinant ferrochelatases from human, zebrafish, *S. pombe*, *C. crescentus*, and *M. xanthus* were purified and treated with the NO-donor, DEA/NO, under anaerobic conditions (<4 ppm O_2). In all experiments care was taken to maintain the temperature between 13-15°C to avoid protein degradation.

Enzyme assays. Previous studies indicate that eukaryotic ferrochelatases require the presence of a [2Fe-2S] cluster for enzymatic activity (*2;4;7;27;28;32-34*). In bacterial *C. crescentus* ferrochelatase mutation of any of the cysteine residues involved in ligating the [2Fe-2S] cluster to serine causes an approximately 95% reduction in the catalytic rate. Additionally, no enzymatic activity could be detected by in vitro assays for *C. crescentus* ferrochelatase when the carboxyl-terminus domain containing three of the cysteine residues ligating the [2Fe-2S] center was truncated (*29*). The spectroscopic studies carried out in this work indicate that, in contrast to the wild type form, the purified recombinant C219S *M. xanthus* ferrochelatase was colorless, and UV-visible absorption and CD spectra did not exhibit any of the characteristic bands indicative of the presence of a [2Fe-2S] cluster (Figure 4.1). In vitro ferrochelatase assays on expressed wild type and C219S variant of *M. xanthus* ferrochelatase show the formation of 37.1 nanomoles of heme / mg of enzyme / min and 1.92 nanomoles of heme / mg of enzyme / min, respectively, indicating an approximately 19.5-fold or 95% decrease in the specific activity of the enzyme when the [2Fe-2S] cluster is not present (Figure 4.2). Taken together, these results indicate that ferrochelatase activity largely depends on the presence of an intact [2Fe-2S] cluster in both eukaryotic and prokaryotic enzymes.

NO Assays. The effect of DEA/NO on the UV-visible absorption spectra of human, zebrafish, *S. pombe*, *C. crescentus*, and *M. xanthus* ferrochelatases in the 300-600 nm region is shown in Figure 4.1. The UV-visible absorption spectra of the as purified enzymes in this region consist of bands at 330 nm, 460 nm and 550 nm arising exclusively from the $[2Fe\text{-}2S]^{2+}$ centers, thus providing a convenient and direct tool for monitoring the effect of DEA/NO on the cluster. However, except for the absorption spectrum of *S. pombe* ferrochelatase, the visible spectra corresponding to all other proteins employed in this study show an additional band at 420 nm that varied in intensity for different preparations and was attributed in part to a minor component of ferrochelatase-associated low-spin Fe(III) heme. The decrease in the absorbance bands at 330 nm, 460 nm and 550 nm observed in Figure 4.3 indicate that the $[2Fe\text{-}2S]^{2+}$ clusters from human (33 μM), zebrafish (26 μM), *S. pombe* (34 μM), *C. crescentus* (34 μM), and *M. xanthus* (38μM) ferrochelatases are degraded over a period of 50 min, 35 min, 120 min, 275 min, and 240 min, respectively, when the enzymes were exposed to 2 mM DEA/NO. Furthermore, upon addition of the fast NO-releasing compound, DEA/NO, the absorbance bands at 330 nm, 460 nm and 550 nm were progressively replaced by a broad band at 395 nm in the human, zebrafish, and *M. xanthus* ferrochelatases absorption spectra, and a prominent shoulder at 386 nm in *S. pombe* and *C. crescentus* enzymes. As depicted in Figure 4.3, two isosbestic points are observed near 365 nm and 404 nm, and the final spectrum was attributed to monomeric dinitrosyl-iron-cysteine (DNIC) complexes (*19*). Some difficulty was experienced with slow protein precipitation especially in the case of human and zebrafish ferrochelatases.

EPR spectroscopy. EPR studies were used for the identification and detection of species formed upon reaction of DEA/NO with ferrochelatases from human, zebrafish, *S. pombe*, *C. crescentus,* and *M. xanthus*. No EPR signals are observed for any of the as purified

ferrochelatases in accord with the presence of a $S = 0$ $[2Fe\text{-}2S]^{2+}$ cluster. The main species detected at 35 K upon anaerobic addition of 2 mM DEA/NO to human (33 μM), zebrafish (26 μM), *S. pombe* (34 μM), *C. crescentus* (34 μM), and *M. xanthus* (38μM) exhibited an axial S = ½ EPR signal, $g_{\perp} = 2.033$ and $g_{\parallel} = 2.017$, that was again indicative of the generation of a monomeric DNIC, ($\{Fe(NO)_2\}^9$ in the notation introduced by Enemark and Feltham (*35*)) (see Figure 4.4) (*13;14;22*). Identical resonances have been observed for other NO-treated iron–sulfur proteins where the product of the NO-induced cluster degradation appears to be a monomeric DNIC species (*19-23;36*). Control experiments under identical conditions using 50 mM Tris-MOPS pH=8.0 solubilization buffer in the presence of 2 mM DEA/NO show very weak EPR signals (data not shown), indicating that the EPR spectrum observed upon incubating each of the five ferrochelatases with DEA/NO can be associated with the formation of the DNIC species, and not a free nitrosyl-radical species in solution.

Determination of rates of [2Fe-2S] cluster degradation and DNIC formation. Plots of % [2Fe-2S] cluster degradation calculated from ΔA_{510} versus time, and % DNIC formation determined from Δspin/molecule values versus time were used to quantitatively assess the rates of the [2Fe-2S] cluster degradation and DNIC formation, respectively. As shown in Figure 4.5, and Table 4.1, the data can be fit to a good approximation by second order kinetics with 12 $M^{-1}min^{-1}$, 17 $M^{-1}min^{-1}$, 15 $M^{-1}min^{-1}$, 8.5 $M^{-1}min^{-1}$, 10 $M^{-1}min^{-1}$ rate constants for the [2Fe-2S] cluster disassembly, and 21 $M^{-1}min^{-1}$, 20 $M^{-1}min^{-1}$, 15 $M^{-1}min^{-1}$, 16 $M^{-1}min^{-1}$, 14 $M^{-1}min^{-1}$ rate constants for the DNIC formation, corresponding to human, zebrafish, *S. pombe*, *C. crescentus,* and *M. xanthus* ferrochelatase, respectively. The good agreement between the second order rate constant values for the [2Fe-2S] cluster disassembly and the DNIC formation obtained for each particular enzyme investigated provides no evidence for a well-defined intermediate species and

indicates that NO-induced cluster degradation is the rate limiting step in the formation of the DNIC product. It should be noted that, although the observed EPR signal results from $\{Fe(NO)_2\}^9$ electronic structure of the DNIC species, the Fe in the complex may also exist in the $\{Fe(NO)_2\}^{10}$ EPR-silent state (*22*). Additionally, in one experimental trial, UV-visible absorption data indicated the possible formation of a dimeric DNIC species (data not shown), which is also diamagnetic, and hence EPR-silent. The quantitation of these species by EPR is not possible and will require more discriminating techniques such as Mössbauer spectroscopy. As shown in Table 4.1, as a result of these experimental complications, the maximum spin/molecule values obtained for the quantitation of the EPR signals did not exceed 0.86 spin/molecule. In addition, since both the [2Fe-2S] clusters and the DNIC species exhibit overlapping spectral features in the visible region of the absorption spectrum (see Figure 4.1.), some difficulties were encountered when fitting the data for the % [2Fe-2S] cluster disassembly determined from the decrease in the absorption values. Therefore, the readings reflecting the loss of the [2Fe-2S] cluster may be slightly overestimated especially in the second half of the reaction incubation time due to the positive contributions arising from the increasing in the DNIC absorption features. However, immediately after addition of DEA/NO, these contributions are expected to be minor, hence the quantitative determination of the rate constants corresponding to the degradation of the [2Fe-2S] clusters were obtained best by fitting only the initial decrease in A_{510} to second order kinetics. Of no surprise was the discovery that the [2Fe-2S] cluster on human ferrochelatase is destroyed with comparable rate constant not only by NO, but also by hydrogen peroxide (unpublished data).

Discussion

Over the past two decades it has become clear that NO is a vital physiological signaling and effector molecule that plays a wide arrays of biological functions not only in animals and

humans, but also in plants and bacteria (*37;38*). In eukaryotic systems, NO was shown to be involved in a tremendous number of processes including control of vascular tone and blood pressure, protection against pathogens and cancer, hormone regulation, nerve cell transmission, and angiogenesis (*39-47*). In prokaryotes NO was initially believed to be mainly involved in the denitrification process as part of the nitrogen cycle (*38;48;49*). However, recent studies have demonstrated new roles for this small molecule in bacterial cellular processes such as biosynthetic nitration reactions responsible for toxin production, bacterial protection against oxidative stress, and implication as a signaling molecule in the regulation of growth responses (*49-54*). As an effector molecule, whose reactive form depends on the local environment (the presence of reactive oxygen species, redox potential, etc.), NO can attack metalloproteins, inducing quick cellular adjustments to a sudden change in their environment. Of particular importance is the data indicating that NO regulates iron storage, transport, and utilization by targeting specific metalloproteins (*55;56*).

In eukaryotic systems, NO is endogenously produced by four known nitric oxide synthase (NOS) proteins, namely NOS-1-3 and the recently discovered mitochondrial NOS (mtNOS) (*44;45;57*). The NOS-1 and NOS-3 isoforms, also known as neuronal NOS (nNOS) and endothelial NOS (eNOS), respectively, are constitutively active regulatory proteins, being involved in the regulation of biological processes via production of small amounts of NO. In contrast, as its name implies, the NOS-2 isoform or the so called inducible NOS (iNOS) is inducible by lipopolysaccharides (LPS) and cytokines [i.e. interferon-γ (IFN-γ)] (*58;59*) and produces relatively large amounts of NO that is responsible for the cytotoxic effect against parasites and tumor cells (*60-62*). Bound to the matrix face of the mitochondrial inner membrane, the mtNOS isoform has been shown to resemble nNOS, being constitutively active

and functionally up-regulated by hypoxia (*63;64*). Although a definitive role(s) of mtNOS has yet to be elucidated, the general consensus is that this novel mitochondrial enzyme functions as a crucial biochemical regulator of mitochondrial bioenergetics (*64-66*).

Over the past ten years prokaryotic NOSs homologous to animal NOSs have been identified and characterized, and despite some interesting differences in cofactor utilization and redox partners, the bacterial enzymes are in many ways alike their mammalian counterparts (*48;49*).

The presence of a NOS in the mitochondrion could have important implications for Fe metabolism, as the mitochondrion is the only site for heme biosynthesis and a major generator of iron-sulfur clusters within the cell (*67-69*). Considering the tremendous rate of Fe uptake by the mitochondrion in erythroid cells (*67*), in addition to the data demonstrating that NO binds Fe and can affect intracellular Fe trafficking, NO can also attack [Fe-S] clusters within proteins and change their activity with immediate effect on Fe homeostasis. One of the most important examples that illustrate the implication of NO in Fe metabolism is the effect of NO on the iron-regulatory protein 1 (IRP1), a bifunctional metalloprotein that exhibits two mutually exclusive activities, either as aconitase or mRNA-binding protein, depending on the integrity of a versatile [4Fe-4S] cluster (*22;70*). As a mRNA-binding protein, IRP1 functions as a *trans*-regulator that posttranscriptionally controls the expression of a variety of molecules that play essential functions in Fe homeostasis (*71-77*). Thus, IRP1 binds to hairpin-loop structures called iron-responsive elements (IREs), located in the 5'- or 3'-untranslated regions (UTRs) of several mRNAs, including those encoding ferritin, cytosolic and mitochondrial aconitase, 5-aminolevulinic acid synthetase (ALAS) and the highly specific transferrin receptor (TfR), subsequently regulating their translation into the respective proteins. As aconitase, the protein is loaded with a fully assembled [4Fe-4S] cluster, which is part of the active site, being directly

involved in the conversion of *cis*-aconitate to isocitrate (*78*). The mechanism by which IRP1 switches between the two different functions directly depends on the amount of Fe present in the cell. As a consequence, high Fe levels within cells promote the assembly of a [4Fe-4S] cluster in IRP1, with loss of IRE-binding activity. Conversely, in cells depleted of Fe, the [4Fe-4S] cluster is not present, and, under these conditions, IRP1 can bind to the IREs and inhibit/enhance translation of specific mRNAs (*71;77*). Apart from iron, several signals and effectors such as nitric oxide, oxygen tension (*79-81*), phosphorylation (*82;83*) and oxygen stress (*71;84-87*) are also able to modulate IRP1 activities. In particular, NO has been demonstrated to activate the RNA-binding activity of IRP1 via a mechanism that involves both depletion of the intracellular Fe and complete disruption of its [4Fe-4S] cluster (*55;70;72-76;88-90*). In addition, it has been demonstrated that low cellular Fe levels induce the transcription of the inducible NOS, suggesting a regulatory loop between iron metabolism and the NO/NOS pathway (*91*). Thus, IRP1 has been proposed to be the dominant sensor and transducer of NO for posttranscriptional regulation of iron metabolism and participation in Fe-S cluster repair after exposure to NO.

Similar examples of Fe-S cluster containing proteins that act as either dedicated or secondary NO sensors have also been described in bacteria. However, unlike in eukaryotic systems, in prokaryotes NO-induced activation of such transcriptional regulators seems to regulate expression of genes involved in protection of the organism against nitrosative and/or oxidative stress. For instance, SoxR and FNR (fumarate and nitrate reductase regulatory protein) are iron-sulfur proteins that primarily mediate responses to superoxide and oxygen, respectively (*92;93*), and yet, both of these regulatory proteins have also been shown to respond to NO *in vivo* and *in vitro* via direct nitrosylation of their Fe-S centers (*19;24;94*). Interestingly, the SoxRS regulon, which protects *E. coli* against macrophage killing and is expressed upon

activation of SoxR protein, has been suggested to be induced by NO (rather than superoxide) in murine macrophages (*95*), supporting the hypothesis that SoxR is also sensing NO in addition to superoxide, thus enabling researchers to view it a secondary NO sensor. Another example of a secondary NO sensor is the [2Fe-2S] cluster-containing IscR repressor responsible for the transcriptional regulation of the *isc* operon, which encodes proteins that are required for the Fe-S cluster biogenesis pathway (*96*). It is presumed that the major physiological role of IscR is to modulate *isc* expression according to the cell's requirement for clusters. The homoeostatic mechanism is not well understood, although it probably involves reversible assembly and disassembly of the cluster, according to the availability of iron and/or sulfur (*96*). There is evidence that IscR also mediates responses to oxygen (*97*), NO (*94;98*), and hydrogen peroxide (*99*), and that the apo form of IscR can apparently function as an activator of transcription (*100*). On the other hand, the IscR homologue NsrR has been shown to act as a dedicated NO sensor by regulating gene expression in response to NO in several species (*101-106*). IscR and NsrR share three conserved cysteine residues, and preliminary evidence suggest that the *Bacillus subtilis*, *Streptomyces coelicolor* and *Neisseria gonorrhoeae* NsrR proteins accommodate a sensory iron-sulfur cluster that is required for DNA-binding activity (*104;107-109*). Interestingly, in *E. coli* NsrR appears to repress the *ytfE* gene, which is responsible for the transcription of YtfE, a di-iron protein proposed to be involved in the biosynthesis of iron-sulfur clusters, which is particularly important in cells subjected to stress conditions. In fact, expression of *Escherichia coli ytfE* was found to be highly stimulated by oxidative and nitrosative stress, as well as under iron starvation conditions, leading to the suggestion that YtfE might actually be involved in the repair of stress-damaged iron-sulfur clusters (*110-113*). The observation that the expression of YtfE is stimulated under low cellular iron levels is, in fact, of no surprise considering the

observation that NsrR-regulated genes can be derepressed by iron starvation, which is consistent with an iron requirement for NsrR activity (*102*).

In the context of a seemingly tight relationship between iron metabolism and oxidative and nitrosative stress conditions (*89*), the finding that both eukaryotic and prokaryotic recombinant ferrochelatases are susceptible to inactivation by NO and furthermore, that the second order rate constants of the [2Fe-2S] cluster disassembly reactions are not significantly different may suggest that, similarly to the [4Fe-4S] cluster in aconitase, the [2Fe-2S] center in ferrochelatases may also be degraded by NO as a response to low levels of Fe/Fe-S cluster within the cell. Moreover, the degradation of the [2Fe-2S] center in human ferrochelatase by hydrogen peroxide may suggest that, as seen in other cases where Fe-S clusters act as sensors of both NO and reactive oxygen species (i.e. aconitase/IRP1 or IscR systems), the [2Fe-2S] center in ferrochelatases might also sense cellular oxidative stress conditions.

The fact that ferrochelatase, a protein responsible for heme biosynthesis, a major Fe consuming pathway, which in metazoans and in some prokaryotes contains and requires for proper function the presence of a [2Fe-2S] cluster, a cofactor that must be provided by the other major cellular iron consuming pathway, namely the Fe-S cluster assembly machinery, makes it a suitable candidate responsible for balancing the use of iron in the mitochondrion. In fact, the involvement of the [2Fe-2S] center from ferrochelatase in sensing the cellular iron-sulfur cluster status in eukaryotes is proposed in Chapter 3 of this thesis. However, the model we have proposed only discusses the mechanism of ferrochelatase activation under sufficient levels of iron-sulfur clusters within the cell via the extent of the [2Fe-2S] cluster-loaded form of monothiol glutaredoxins, which have been shown to act as iron-sulfur carriers or storage proteins (*114-118*), without explaining how ferrochelatase would be inactivated under conditions of low

cellular Fe-S cluster concentrations for subsequent intracellular Fe utilization for the *de novo* formation of Fe-S clusters. Taken together, the data indicating that ferrochelatase activity depends on the presence of an intact [2Fe-2S] cluster not only in eukaryotes (*2;7;27-29;119*), but in prokaryotic enzymes as well (see our in vitro activity assays described above and reference (*29*)), and the results demonstrating that the [2Fe-2S] center in ferrochelatase is damaged by both NO and hydrogen peroxide, it is tempting to speculate that perhaps under oxidative stress conditions leading to low cellular Fe-S clusters levels, endogenous NO production by NOS leads to rapid and efficient degradation of the [2Fe-2S] cluster from ferrochelatase. This would result in the inactivation of the enzyme, therefore, decreasing heme production. Consequently Fe can be channeled towards the *de novo* biosynthesis of Fe-S clusters, while the cluster-depleted ferrochelatase would be most likely degraded via specific proteases as previously observed (*120*). This hypothesis is also supported by the observation that Fe-S clusters appear to be the primary targets of NO and ROS (*18-20;24;36;81;84;89;99;121-123*). In addition, NO production enhances the IRE-activity of the IRP1 protein, resulting in binding of IRP1 to the 5' IRE of *ALAS* mRNAs, blocking translation and thereby preventing the formation and accumulation of other nocive intermediates of heme biosynthesis, therefore ultimately avoiding cellular toxicity. Alternatively, high levels of Fe-S clusters result in building of these centers on storage or carrier proteins such as the monothiol glutaredoxins, which have been shown to play a crucial role in storage and transfer of [2Fe-2S] clusters in the cell (*114-118*). Consequently, monothiol glutaredoxins transfer their cluster to ferrochelatase for the maturation and activation of the enzyme, thus restoring heme production. Our studies on the NO-response of [2Fe-2S] clusters from both eukaryotic and prokaryotic ferrochelatases have therefore revealed not only a

crucial role for NO in both Fe-S cluster and heme homeostasis, but also a possible mechanism for the inactivation of ferrochelatase as a response to levels of Fe-S clusters in the cell.

The results of this study cannot answer questions concerning the mechanism by which heme and Fe-S cluster biosynthesis are interrelated in organism in which ferrochelatase lacks a [2Fe-2S] cluster, nor do they explain how Fe/Fe-S cluster deplete cellular conditions could trigger NO/ROS production for the inactivation of ferrochelatase. However, considering that in higher organisms heme is solely produced in the mitochondrion, the presence of a mitochondrial NOS that is also attached to the inner membrane and is induced by hypoxia at least explains NO production in this compartment. In fact, some studies demonstrate that mtNOS activity is enhanced in lipopolysaccharide-treated rats (*124;125*), perhaps explaining the early observation regarding the inactivation of ferrochelatase in a cultured macrophage cell line that had NO production stimulated by cytokine (lipopolysaccharide and interferon-γ) (*9*). Furthermore, the previous observation that iNOS activity and expression is controlled by intracellular iron levels, also adds support to the above described hypothesis.

Acknowledgements

This work was supported by grants from the National Institute of Health (GM62524 to M.K.J., and DK32303 to H.A.D.).

References

1. Dailey, H. A. and Dailey, T. A. (2003) in *The Porphyrin Handbook* (Kadish, K. M., Smith, R., and Guilard, R., Eds.) pp 93-121, Academic Press, New York.
2. Dailey, H. A., Dailey, T. A., Wu, C.-K., Medlock, A. E., Wang, K.-F., Rose, J. P., and Wang, B.-C. (2000) *Cell. Mol. Life Sci. 57*, 1909-1926.
3. Dailey, H. A. (1996) in *Mechanisms of Metallocenter Assembly* (Hausinger, R. P., Eichorn, G. L., and Marzilli, L. G., Eds.) pp 77-98, VCH, New York.
4. Dailey, H. A., Finnegan, M. G., and Johnson, M. K. (1994) *Biochemistry 33*, 403-407.
5. Dailey, H. A., Sellers, V. M., and Dailey, T. A. (1994) *J. Biol. Chem. 269*, 390-395.
6. Wu, C.-K., Dailey, H. A., Rose, J. P., Burden, A., Sellers, V. M., and Wang, B.-C. (2001) *Nat. Struct. Biol. 8*, 156-160.
7. Sellers, V. M., Johnson, M. K., and Dailey, H. A. (1996) *Biochemistry 35*, 2699-2704.
8. Kim, Y. M., Bergonia, H. A., Muller, C., Pitt, B. R., Watkins, W. D., and Lancaster, J. R., Jr. (1995) *J. Biol. Chem. 270*, 5710-5713.
9. Furukawa, T., Kohno, H., Tokunaga, R., and Taketani, S. (1995) *Biochem. J. 310 (Pt 2)*, 533-538.
10. Vanin, A. F. (1967) *Biokhimiya 32*, 228-232.
11. Vanin, A. F., Blyumenfel'd, A., and Chetverikov, A. G. (1967) *Biofizika 12*, 829-838.
12. Woolum, J. C., Tiezzi, E., and Commoner, B. (1968) *Biochim. Biophys. Acta 160*, 311-320.
13. Vanin, A. F., Serezhenkov, V. A., Mikoyan, V. D., and Genkin, M. V. (1998) *Nitric. Oxide. 2*, 224-234.
14. Vanin, A. F. (2009) *Nitric Oxide 21*, 1-13.

15. Foster, M. W. and Cowan, J. A. (1999) *J. Am. Chem. Soc. 121*, 4093-4100.

16. Salerno, J. C. (1985) *Biochem. Soc. Trans. 13*, 611-615.

17. Salerno, J. C. and Siedow, J. N. (1979) *Biochim. Biophys. Acta 579*, 246-251.

18. Reddy, D., Lancaster, J. R., Jr., and Cornforth, D. P. (1983) *Science 221*, 769-770.

19. Cruz-Ramos, H., Crack, J., Wu, G., Hughes, M. N., Scott, C., Thomson, A. J., Green, J., and Poole, R. K. (2002) *EMBO J. 21*, 3235-3244.

20. Drapier, J. C. (1997) *Methods: A Companion to Meth. Enzymol. 11*, 319-329.

21. Butler, A. R., Glidewell, C., and Li, M.-H. (1988) *Adv. Inorg. Chem. 32*, 335-393.

22. Kennedy, M. C., Antholine, W. E., and Beinert, H. (1997) *J. Biol. Chem. 272*, 20340-20347.

23. Lee, M., Arosio, P., Cozzi, A., and Chasteen, N. D. (1994) *Biochemistry 33*, 3679-3687.

24. Ding, H. and Demple, B. (2000) *Proc. Natl. Acad. Sci. USA 97*, 5146-5150.

25. Stadler, J., Bergonia, H. A., Di, S. M., Sweetland, M. A., Billiar, T. R., Simmons, R. L., and Lancaster, J. R., Jr. (1993) *Arch. Biochem. Biophys. 302*, 4-11.

26. Bastian, N. R., Yim, C. Y., Hibbs, J. B., Jr., and Samlowski, W. E. (1994) *J. Biol. Chem. 269*, 5127-5131.

27. Sellers, V. M., Wang, K. F., Johnson, M. K., and Dailey, H. A. (1998) *J. Biol. Chem. 273*, 22311-22316.

28. Day, A. L., Parsons, B. M., and Dailey, H. A. (1998) *Arch. Biochem. Biophys. 359*, 160-169.

29. Dailey, T. A. and Dailey, H. A. (2002) *J. Bacteriol. 184*, 2460-2464.

30. Shepherd, M., Dailey, T. A., and Dailey, H. A. (2006) *Biochem. J. 397*, 47-52.

31. Najahi-Missaoui, W. and Dailey, H. A. (2005) *Blood 106*, 1098-1104.

32. Medlock, A. E. and Dailey, H. A. (2000) *Biochemistry 39*, 7461-7467.

33. Dailey, T. A., Boynton, T. O., Albetel, A. N., Gerdes, S., Johnson, M. K., and Dailey, H. A. (2010) *J. Biol. Chem. 285*, 25978-25986.

34. Burden, A. E., Wu, C., Dailey, T. A., Busch, J. L., Dhawan, I. K., Rose, J. P., Wang, B., and Dailey, H. A. (1999) *Biochim. Biophys. Acta 1435*, 191-197.

35. Enemark, J. H. and Feltham, R. D. (1974) *Coord. Chem. Rev. 13*, 339-406.

36. Landry, A. P., Duan, X., and Ding, H. (2011) *Free Radic. Biol. Med. 50*, 1582-1590.

37. Nitric Oxide in Plant Growth, Development and Stress Physiology. Lamattina, L. and Polacco, J. C. 1[6]. 2007. Springer. Plant Cell Monographs. Ref Type: Serial (Book,Monograph)

38. Zumft, W. G. (1993) *Arch. Microbiol. 160*, 253-264.

39. Barbato, J. E. and Tzeng, E. (2004) *J. Vasc. Surg. 40*, 187-193.

40. Nott, A. and Riccio, A. (2009) *Cell Cycle 8*, 725-730.

41. Yun, H. Y., Dawson, V. L., and Dawson, T. M. (1996) *Crit Rev. Neurobiol. 10*, 291-316.

42. Yun, H. Y., Dawson, V. L., and Dawson, T. M. (1997) *Mol. Psychiatry 2*, 300-310.

43. Feldman, P. L., Griffith, O. W., and Stuehr, D. J. (1993) *Chem. Eng. News 71*, 26-38.

44. Griffith, O. W. and Stuehr, D. J. (1995) *Annu. Rev. Physiol 57*, 707-736.

45. Alderton, W. K., Cooper, C. E., and Knowles, R. G. (2001) *Biochem. J. 357*, 593-615.

46. Lipton, S. A. (2001) *Nature 413*, 118-9, 121.

47. Pfeiffer, S., Mayer, B., and Hemmens, B. (1999) *Angew. Chem. Int. Ed. 38*, 1149-1154.

48. Sudhamsu, J. and Crane, B. R. (2009) *Trends Microbiol. 17*, 212-218.

49. Crane, B. R., Sudhamsu, J., and Patel, B. A. (2010) *Annu. Rev. Biochem. 79*, 445-470.

50. Buddha, M. R., Keery, K. M., and Crane, B. R. (2004) *Proc. Natl. Acad. Sci. U. S. A 101*, 15881-15886.

51. Kers, J. A., Wach, M. J., Krasnoff, S. B., Widom, J., Cameron, K. D., Bukhalid, R. A., Gibson, D. M., Crane, B. R., and Loria, R. (2004) *Nature 429*, 79-82.

52. Wach, M. J., Kers, J. A., Krasnoff, S. B., Loria, R., and Gibson, D. M. (2005) *Nitric Oxide 12*, 46-53.

53. Gusarov, I. and Nudler, E. (2005) *Proc. Natl. Acad. Sci. U. S. A 102*, 13855-13860.

54. Shatalin, K., Gusarov, I., Avetissova, E., Shatalina, Y., McQuade, L. E., Lippard, S. J., and Nudler, E. (2008) *Proc. Natl. Acad. Sci. U. S. A 105*, 1009-1013.

55. Wardrop, S. L., Watts, R. N., and Richardson, D. R. (2000) *Biochemistry 39*, 2748-2758.

56. Watts, R. N., Ponka, P., and Richardson, D. R. (2003) *Biochem. J. 369*, 429-440.

57. Knowles, R. G. and Moncada, S. (1994) *Biochem. J. 298 (Pt 2)*, 249-258.

58. Nathan, C. F. and Hibbs, J. B., Jr. (1991) *Curr. Opin. Immunol. 3*, 65-70.

59. Moncada, S. and Higgs, A. (1993) *N. Engl. J. Med. 329*, 2002-2012.

60. Hibbs, J. B., Jr., Taintor, R. R., Vavrin, Z., and Rachlin, E. M. (1988) *Biochem. Biophys. Res. Commun. 157*, 87-94.

61. Hibbs, J. B., Jr., Taintor, R. R., and Vavrin, Z. (1984) *Biochem. Biophys. Res. Commun. 123*, 716-723.

62. Nath, D. A., Balla, G., Vercelotti, G. M., Balla, J., Jacob, H. S., Lewitt, M. D., and Rosenberg, M. E. (1992) *J. Clin. Invest. 90*, 267-270.

63. Lacza, Z., Paskar, M., Figueroa, V. P., Zhang, V., Rajapaske, N., and Busija, D. W. (2001) *Free Radic. Biol. Med. 31*, 1609-1615.

64. Ghafourifar, P. and Richter, C. (1997) *FEBS Lett. 418*, 291-296.

65. Ghafourifar, P. and Cadenas, E. (2005) *Trends Pharmacol. Sci. 26*, 190-195.

66. Kato, K. and Giulivi, C. (2006) *Front Biosci. 11*, 2725-2738.

67. Ponka, P. (2002) *Molecular and Cellular Fe Transport* Marcel Dekker Inc., New York.

68. Lill, R. and Kispal, G. (2000) *TIBS 25*, 352-356.

69. Lill, R. and Muhlenhoff, U. (2008) *Annu. Rev. Biochem. 77*, 669-700.

70. Stys, A., Galy, B., Starzynski, R. R., Smuda, E., Drapier, J. C., Lipinski, P., and Bouton, C. (2011) *J. Biol. Chem. 286*, 22846-22854.

71. Hentze, M. W. and Kuhn, L. C. (1996) *Proc. Natl. Acad. Sci. U. S. A 93*, 8175-8182.

72. Drapier, J. C., Hirling, H., Wietzerbin, J., Kaldy, P., and Kuhn, L. C. (1993) *EMBO J. 12*, 3643-3649.

73. Weiss, G., Goossen, B., Doppler, W., Fuchs, D., Pantopoulos, K., Werner-Felmayer, G., Wachter, H., and Hentze, M. W. (1993) *EMBO J. 12*, 3651-3657.

74. Oria, R., Sanchez, L., Houston, T., Hentze, M. W., Liew, F. Y., and Brock, J. H. (1995) *Blood 85*, 2962-2966.

75. Richardson, D. R., Neumannova, V., Nagy, E., and Ponka, P. (1995) *Blood 86*, 3211-3219.

76. Cairo, G. and Pietrangelo, A. (2000) *Biochem. J. 352 Pt 2*, 241-250.

77. Domachowske, J. B. (1997) *Biochem. Mol. Med. 60*, 1-7.

78. Beinert, H. and Kennedy, M. C. (1993) *FASEB J. 7*, 1442-1449.

79. Hanson, E. S. and Leibold, E. A. (1999) *Gene Expr. 7*, 367-376.

80. Hanson, E. S., Foot, L. M., and Leibold, E. A. (1999) *J. Biol. Chem. 274*, 5047-5052.

81. Hanson, E. S. and Leibold, E. A. (1998) *J. Biol. Chem. 273*, 7588-7593.

82. Brown, N. M., Anderson, S. A., Steffen, D. W., Carpenter, T. B., Kennedy, M. C., Walden, W. E., and Eisenstein, R. S. (1998) *Proc. Natl. Acad. Sci. U. S. A 95*, 15235-15240.

83. Fillebeen, C., Chahine, D., Caltagirone, A., Segal, P., and Pantopoulos, K. (2003) *Mol. Cell Biol. 23*, 6973-6981.

84. Pantopoulos, K. and Hentze, M. W. (1998) *Proc. Natl. Acad. Sci. U. S. A 95*, 10559-10563.

85. Gardner, P. R. and Fridovich, I. (1991) *J. Biol. Chem. 266*, 19328-19333.

86. Gardner, P. R. and Fridovich, I. (1992) *J. Biol. Chem. 267*, 8757-8763.

87. Gardner, P. R., Raineri, I., Epstein, L. B., and White, C. W. (1995) *J. Biol. Chem. 270*, 13399-13405.

88. Cairo, G., Ronchi, R., Recalcati, S., Campanella, A., and Minotti, G. (2002) *Biochemistry 41*, 7435-7442.

89. Pantopoulos, K., Weiss, G., and Hentze, M. W. (1996) *Mol. Cell Biol. 16*, 3781-3788.

90. Soum, E. and Drapier, J. C. (2003) *J. Biol. Inorg. Chem. 8*, 226-232.

91. Weiss, G., Werner-Felmayer, G., Werner, E. R., Grünewald, K., Watcher, H., and Hentze, M. W. (1994) *J. Exp. Med. 180*, 969-976.

92. Khoroshilova, N., Beinert, H., and Kiley, P. J. (1995) *Proc. Natl. Acad. Sci. USA 92*, 2499-2503.

93. Hidalgo, E. and Demple, B. (1994) *EMBO J. 13*, 138-146.

94. Pullan, S. T., Gidley, M. D., Jones, R. A., Barrett, J., Stevanin, T. M., Read, R. C., Green, J., and Poole, R. K. (2007) *J. Bacteriol. 189*, 1845-1855.

95. Nunoshiba, T., DeRojas-Walker, T., Tannenbaum, S. R., and Demple, B. (1995) *Infect. Immun. 63*, 794-798.

96. Schwartz, C. J., Giel, J. L., Patschkowski, T., Luther, C., Ruzicka, F. J., Beinert, H., and Kiley, P. J. (2001) *Proc. Natl. Acad. Sci. USA 98*, 14895-14900.

97. Giel, J. L., Rodionov, D., Liu, M., Blattner, F. R., and Kiley, P. J. (2006) *Mol. Microbiol. 60*, 1058-1075.

98. Hyduke, D. R., Jarboe, L. R., Tran, L. M., Chou, K. J., and Liao, J. C. (2007) *Proc. Natl. Acad. Sci. U. S. A 104*, 8484-8489.

99. Zheng, M., Wang, X., Templeton, L. J., Smulski, D. R., LaRossa, R. A., and Storz, G. (2001) *J. Bacteriol. 183*, 4562-4570.

100. Yeo, W.-S., Lee, J.-H., Lee, K.-C., and Roe, J.-H. (2006) *Mol. Microbiol. 61*, 206-218.

101. Heurlier, K., Thomson, M. J., Aziz, N., and Moir, J. W. (2008) *J. Bacteriol. 190*, 2488-2495.

102. Bodenmiller, D. M. and Spiro, S. (2006) *J. Bacteriol. 188*, 874-881.

103. Bang, I. S., Liu, L., Vazquez-Torres, A., Crouch, M. L., Stamler, J. S., and Fang, F. C. (2006) *J. Biol. Chem. 281*, 28039-28047.

104. Nakano, M. M., Geng, H., Nakano, S., and Kobayashi, K. (2006) *J. Bacteriol. 188*, 5878-5887.

105. Beaumont, H. J., Lens, S. I., Reijnders, W. N., Westerhoff, H. V., and van Spanning, R. J. (2004) *Mol. Microbiol. 54*, 148-158.

106. Overton, T. W., Whitehead, R., Li, Y., Snyder, L. A., Saunders, N. J., Smith, H., and Cole, J. A. (2006) *J. Biol. Chem. 281*, 33115-33126.

107. Tucker, N. P., Le Brun, N. E., Dixon, R., and Hutchings, M. I. (2010) *Trends Microbiol. 18*, 149-156.

108. Tucker, N. P., Hicks, M. G., Clarke, T. A., Crack, J. C., Chandra, G., Le Brun, N. E., Dixon, R., and Hutchings, M. I. (2008) *PLoS. One. 3*, e3623.

109. Isabella, V. M., Lapek, J. D., Jr., Kennedy, E. M., and Clark, V. L. (2009) *Mol. Microbiol. 71*, 227-239.

110. Todorovic, S., Justino, M. C., Wellenreuther, G., Hildebrandt, P., Murgida, D. H., Meyer-Klaucke, W., and Saraiva, L. M. (2008) *J. Biol. Inorg. Chem. 13*, 765-770.

111. Justino, M. C., Almeida, C. C., Teixeira, M., and Saraiva, L. M. (2007) *J. Biol. Chem. 282*, 10352-10359.

112. Justino, M. C., Almeida, C. C., Goncalves, V. L., Teixeira, M., and Saraiva, L. M. (2006) *FEMS Microbiol. Lett. 257*, 278-284.

113. Justino, M. C., Vicente, J. B., Teixeira, M., and Saraiva, L. M. (2005) *J. Biol. Chem. 280*, 2636-2643.

114. Rouhier, N., Unno, H., Bandyopadhyay, S., Masip, L., Kim, S. K., Hirasawa, M., Gualberto, J. M., Lattard, V., Kusunoki, M., Knaff, D. B., Georgiou, G., Hase, T., Johnson, M. K., and Jacquot, J. P. (2007) *Proc. Natl. Acad. Sci. U. S. A. 104*, 7379-7384.

115. Bandyopadhyay, S., Gama, F., Molina-Navarro, M. M., Gualberto, J. M., Claxton, R., Naik, S. G., Huynh, B. H., Herrero, E., Jacquot, J.-P., Johnson, M. K., and Rouhier, N. (2008) *EMBO J. 27*, 1122-1133.

116. Feng, Y., Zhong, N., Rouhier, N., Hase, T., Kusunoki, M., Jacquot, J. P., Jin, C., and Xia, B. (2006) *Biochemistry 45*, 7998-8008.

117. Johansson, C., Kavanagh, K. L., Gileadi, O., and Oppermann U. (2007) *J. Biol. Chem. 282*, 3077-3082.

118. Iwema, T., Picciocchi, A., Traore, D. A., Ferrer, J. L., Chauvat, F., and Jacquamet, L. (2009) *Biochemistry 48*, 6041-6043.

119. Wang, K. F., Wu, C. K., Sellers, V. M., Rose, J. P., Wang, B. C., and Dailey, H. A. (1999) *Acta Crystallogr. D. Biol Crystallogr. 55*, 1201-1203.

120. Crooks, D. R., Ghosh, M. C., Haller, R. G., Tong, W.-H., and Rouault, T. A. (2010) *Blood 115*, 860-869.

121. Flint, D. H., Smyk-Randall, E., Tuminello, J. F., Draczynska-Lusiak, B., and Brown, O. R. (1993) *J. Biol. Chem. 268*, 25547-25552.

122. Flint, D. H., Tuminello, J. F., and Emptage, M. H. (1993) *J. Biol. Chem. 268*, 22369-22376.

123. Pantopoulos, K. and Hentze, M. W. (1995) *Proc. Natl. Acad. Sci. U. S. A 92*, 1267-1271.

124. Boveris, A., Alvarez, S., and Navarro, A. (2002) *Free Radic. Biol. Med. 33*, 1186-1193.

125. Alvarez, S. and Boveris, A. (2004) *Free Radic. Biol. Med. 37*, 1472-1478.

Table 4.1. Second order rate constants for [2Fe-2S] cluster degradation ($k_{[2Fe-2S]}$) and DNIC formation (k_{DNIC}) for the reaction of [2Fe-2S] cluster-containing ferrochelatases from eukaryotic and prokaryotic organisms with the NO donor, DEA/NO. Maximum spin/molecule values obtained from quantitation of the DNIC EPR signals are also listed.

Organism	**Type**	**$Spin_{max}$/molecule**	**$k_{[2Fe-2S]}$**	**k_{DNIC}**
Human	mammalian	0.856	12 $M^{-1}min^{-1}$	21 $M^{-1}min^{-1}$
Zebrafish	vertebrate	0.851	17 $M^{-1}min^{-1}$	20 $M^{-1}min^{-1}$
S. pombe	yeast	0.716	15 $M^{-1}min^{-1}$	15 $M^{-1}min^{-1}$
C. crescentus	bacteria	0.543	8.5 $M^{-1}min^{-1}$	16 $M^{-1}min^{-1}$
M. xanthus	bacteria	0.768	10 $M^{-1}min^{-1}$	14 $M^{-1}min^{-1}$

Figure 4.1. UV-visible absorption (*top*) and CD (*bottom*) spectra of wild type (*solid line*) and C219S variant (*broken line*) of *M. xanthus* ferrochelatase showing the presence and absence of a [2Fe-2S] center, respectively. Spectra were recorded in a 1 mm quartz cuvette.

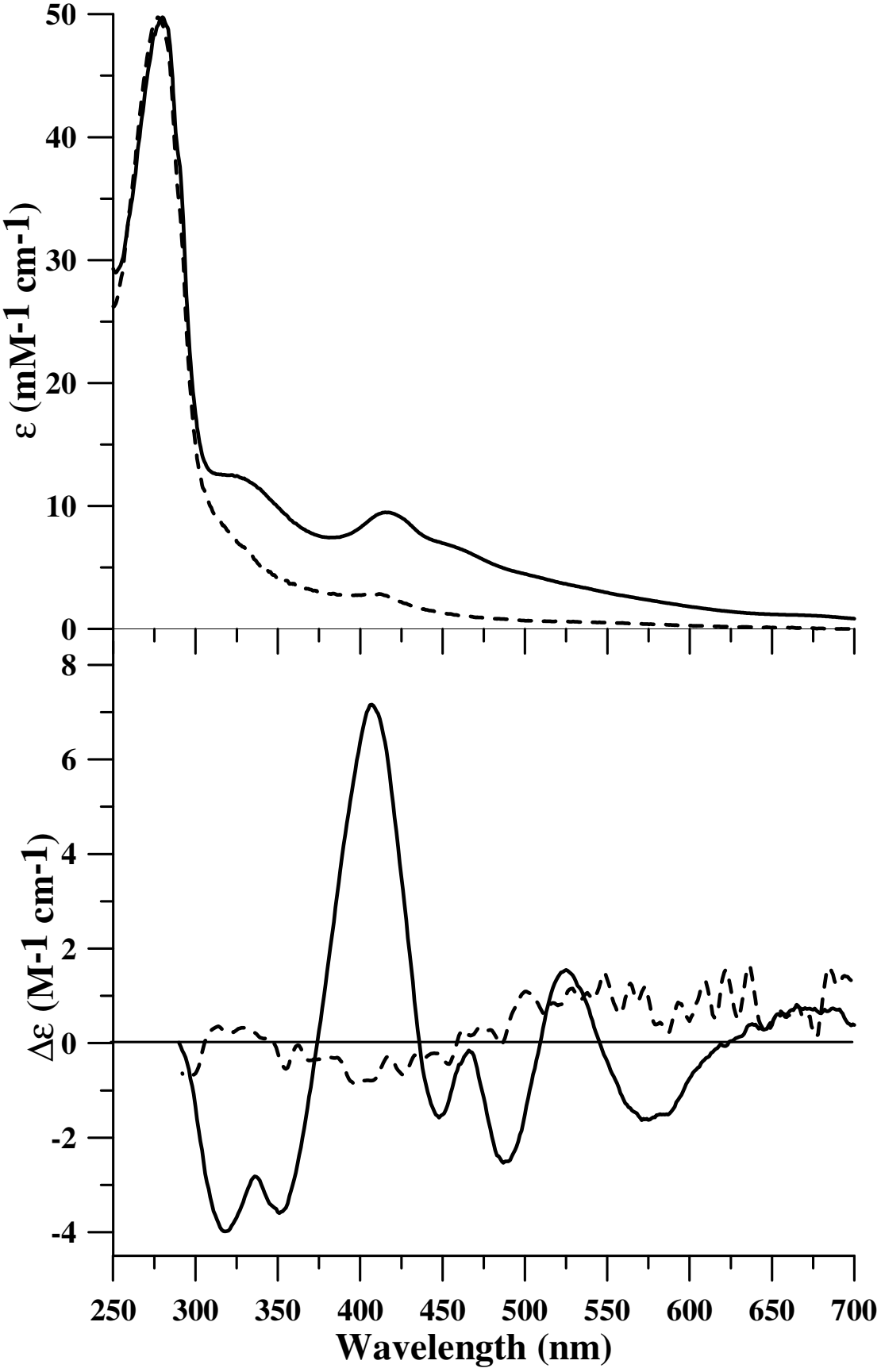
50
40
30
20
10
0
ε (mM-1 cm-1)
8
6
4
2
0
-2
-4
Δε (M-1 cm-1)
250
300
350
400
450
500
550
600
650
700
Wavelength (nm)

Figure 4.2. Enzymatic activity of wild type and C219S *M. xanthus* ferrochelatase. A 9.5-fold decrease in the measured ferrochelatase activity is observed in the case of the cluster-lacking C219S variant compared to the wild type enzyme, indicating that the presence of an intact [2Fe-2S] center is crucial for catalysis in prokaryotic organisms.

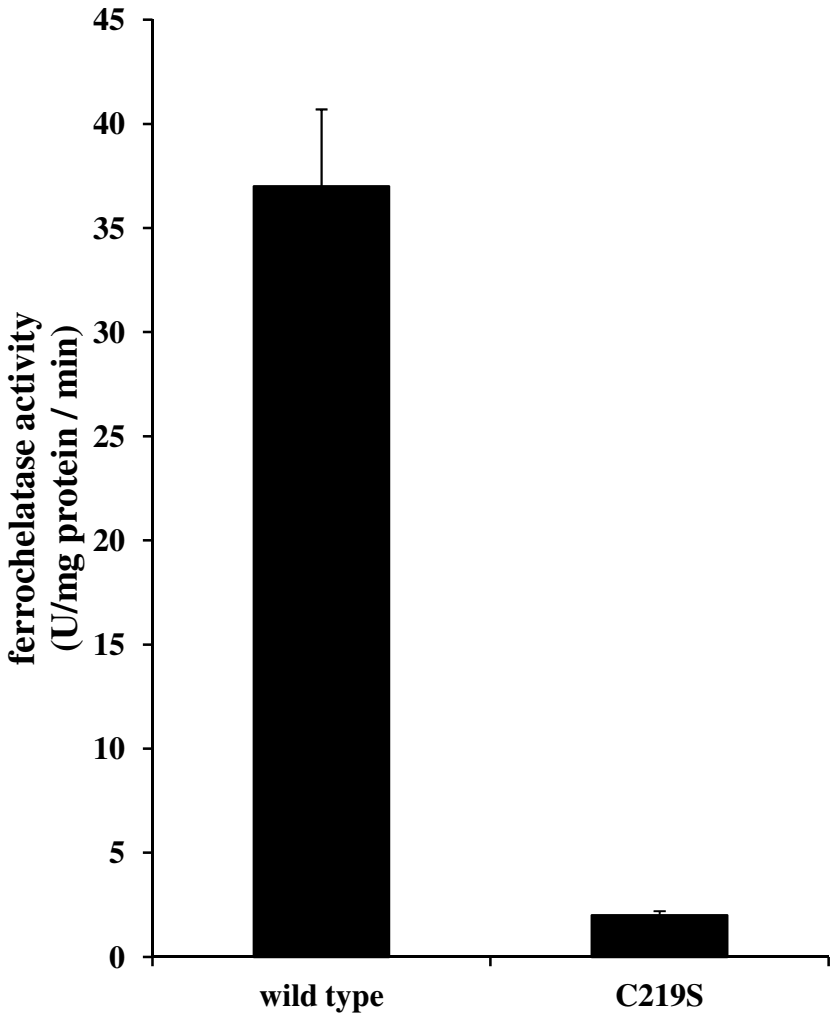
45
40
35
30
25
20
15
10
5
0
ferrochelatase activity
(U/mg protein / min)
wild type
C219S

Figure 4.3. Time course of the effect of DEA/NO on the UV-visible absorption spectra of various ferrochelatases. Recombinant proteins from *(a)* human, 33 µM, *(b)* zebrafish, 26 µM, *(c) S. pombe*, 34 µM, *(d) C. crescentus*, 34 µM, and *(e) M. xanthus*, 38 µM in 50 mM Tris-MOPS pH=8.0 solubilization buffer containing 10 µg/ml PMSF and 2 mM DTT. DEA/NO, final concentration 2 mM, was added anaerobically at 13°C to each enzyme investigated. Absorption at all wavelengths corresponding to the [2Fe-2S] clusters (black arrows) decreases with increased length of exposure to DEA/NO, whereas absorption at either 386 nm or 395 nm (red arrows) increases with increased length of exposure to NO-donor DEA/NO. The peaks labeled with a star correspond to various amounts of heme contamination. Spectra were recorded in a 1 cm quartz cuvette.

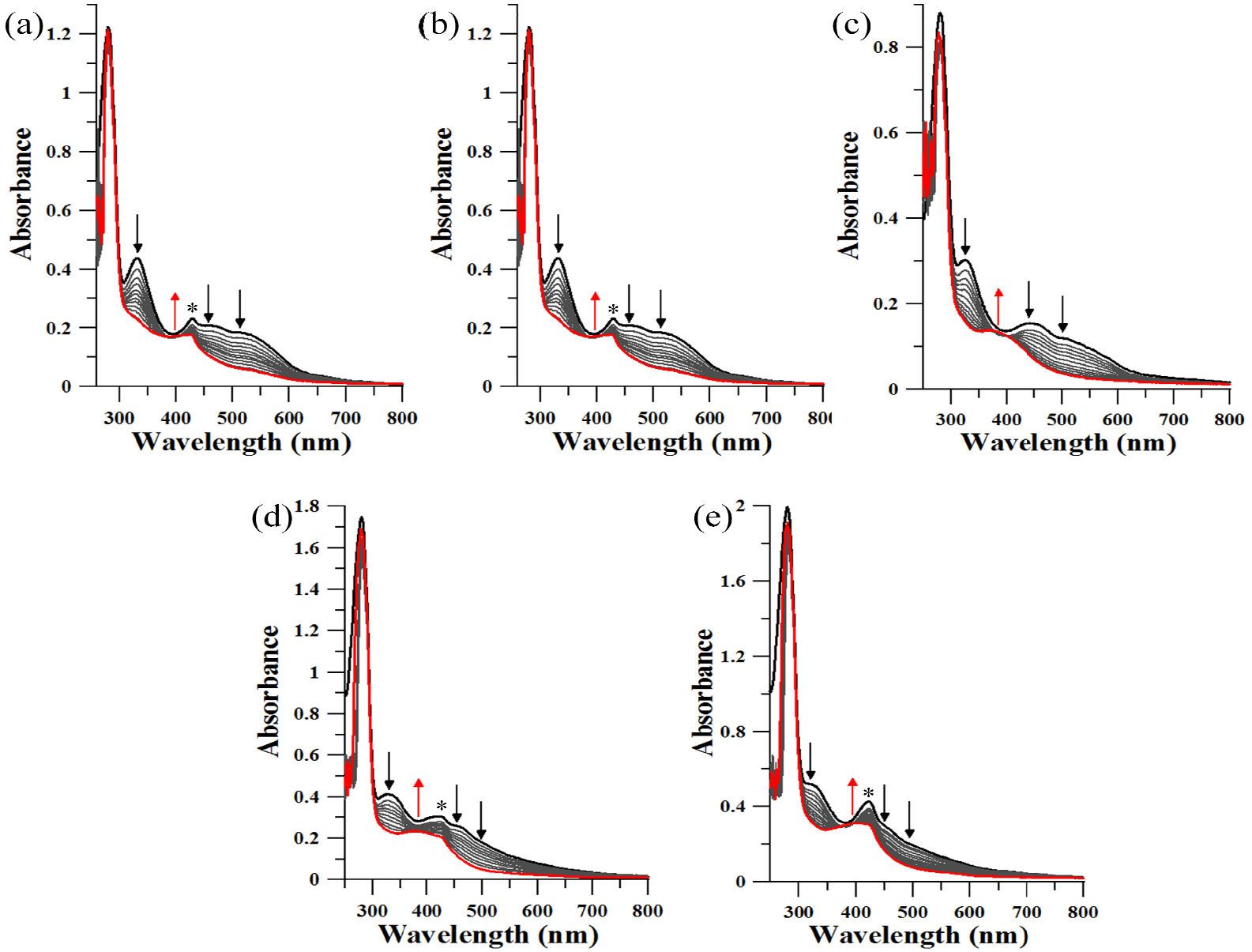
(a)
(b)
(c)
(d)
(e)
Absorbance
Wavelength (nm)
*

Figure 4.4. EPR spectra of NO-treated recombinant ferrochelatases. Treatment of human, 33 μM, zebrafish, 26 μM, *S. pombe*, 34 μM, *C. crescentus*, 34 μM, and *M. xanthus*, 38 μM, with DEA/NO results in the formation of a DNIC species upon degradation of the $[2Fe\text{-}2S]^{2+}$ cluster. EPR conditions: microwave frequency, 9.60GHz; modulation amplitude, 0.64 mT; microwave power, 1 mW; temperature, 35 K.

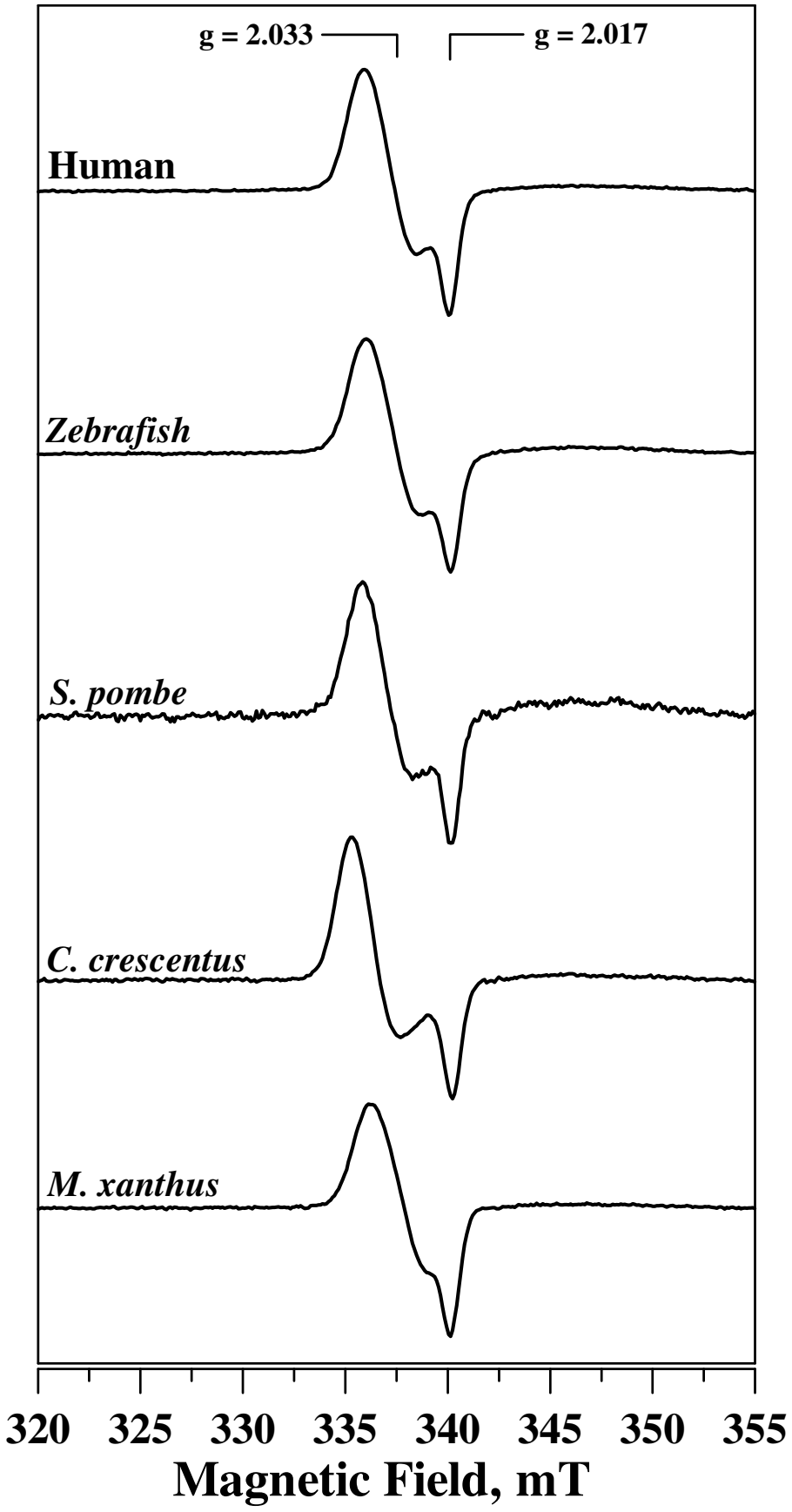
g = 2.033
g = 2.017
Human
Zebrafish
S. pombe
C. crescentus
M. xanthus
320
325
330
335
340
345
350
355
Magnetic Field, mT

Figure 4.5. Time-dependent formation of DNIC species (Δ) and degradation of the [2Fe-2S] clusters (○) from different ferrochelatases in the presence of NO. *(a)* Human, 33 μM, *(b)* zebrafish, 26 μM, *(c) S. pombe*, 34 μM, *(d) C. crescentus*, 34 μM, and *(e) M. xanthus*, 38 μM, ferrochelatases in the presence of 2 mM DEA/NO. The solid lines show a theoretical fitting of the data to second-order kinetics.

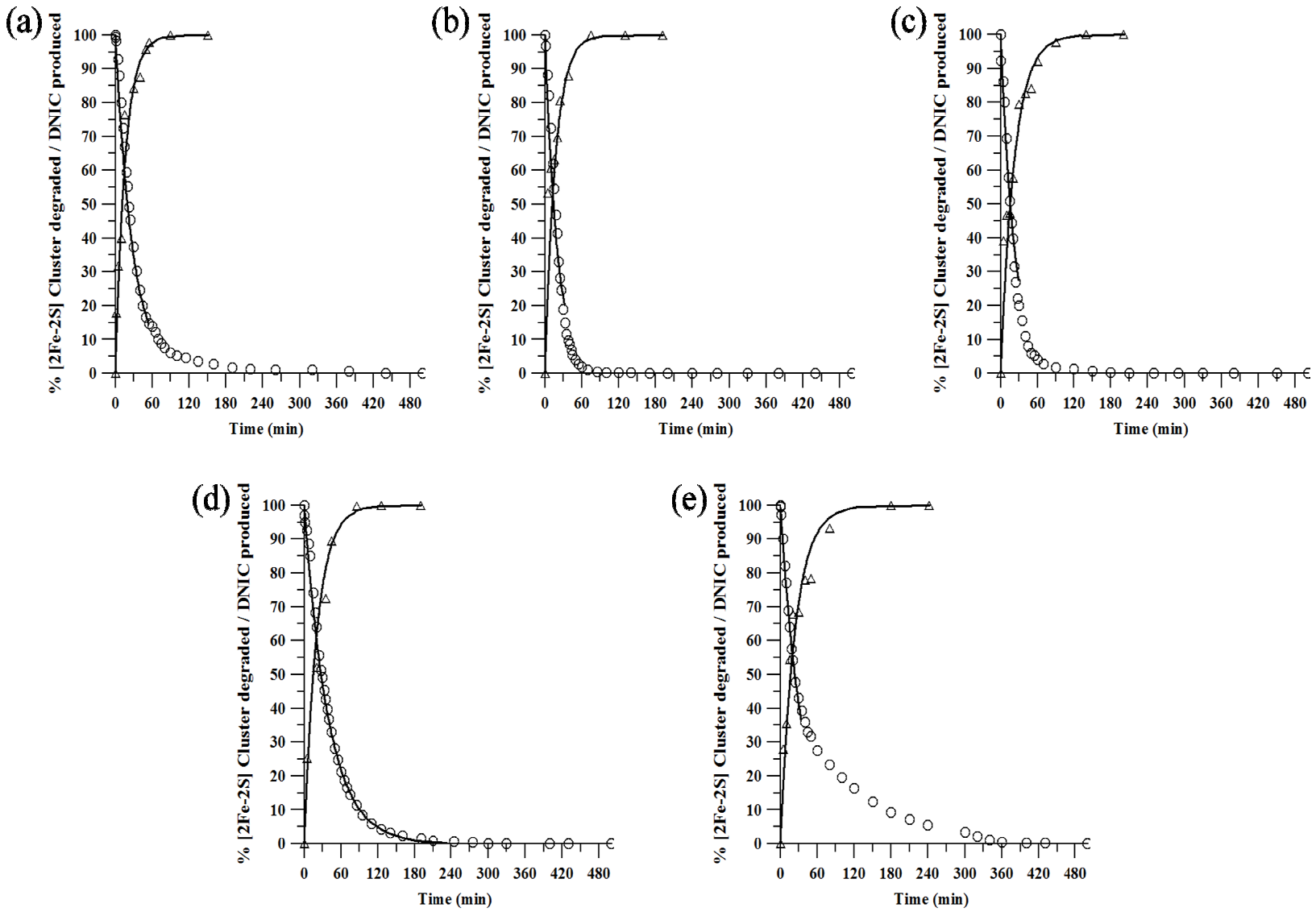
(a)
(b)
(c)
(d)
(e)
% [2Fe-2S] Cluster degraded / DNIC produced
Time (min)
0
10
20
30
40
50
60
70
80
90
100
0
60
120
180
240
300
360
420
480

CHAPTER 5

CONCLUSIONS AND FUTURE DIRECTIONS

The overall objectives of this research project were to investigate the nature, properties and role of [2Fe-2S] centers in ferrochelatases using a combination of biochemical and analytical techniques (protein and Fe assays, enzyme assays, gel electrophoresis, gel filtration chromatography), and biophysical techniques (UV-visible absorption, CD, EPR, resonance Raman spectroscopies). Experiments were carried out using ferrochelatases isolated from both eukaryotic and prokarytic organisms, as well as sirohydrochlorin ferrochelatase from plant *Arabidopsis thaliana* (*At*) in order to understand and characterize the nature and spectroscopic properties of the [2Fe-2S] centers in these enzymes. In addition, the putative role of the [2Fe-2S] center in ferrochelatases in regulating heme/siroheme biosynthesis in response to cellular Fe-S cluster levels was addressed by using UV-visible CD spectroscopy.

In spite of a wealth of information concerning the structural properties of [2Fe-2S] cluster in human ferrochelatase (*1;2*), the low degree of homology in amino acid sequences among currently known ferrochelatases, and the vast diversity in the primary sequence arrangement of coordinating ligands for the [2Fe-2S] clusters present in ferrochelatases from different organisms (*3-8*), the effect of such variations on the spectroscopic properties of these metal centers has not been investigated to date. Previous studies indicate full cysteinyl ligation for the [2Fe-2S] center in all eukaryotes, with three of the cysteine ligands located in a C-terminal extension of the protein, and the fourth cysteine coming from the core amino acid sequence (*1;6;9-11*). A handful of prokaryotes were also found to contain ferrochelatases that possess a [2Fe-2S] cluster that is

also ligated by a set of four cysteine residues. However, five distinct coordination motifs have been identified thus far for the ligation of [2Fe-2S] centers in bacterial ferrochelatases (*3;5;6*). In order to understand the electronic, magnetic, vibrational and redox properties of [2Fe-2S] clusters in ferrochelatase as a function of the coordination environment and variations in the distinct primary sequence arrangements of conserved cysteine residues, we isolated and analytically and spectroscopically characterized the [2Fe-2S] cluster-containing ferrochelatase from human, yeast *Schizosaccharomices pombe* (*S. pombe*), and bacteria *Mycobacterium tuberculosis* (*M. tuberculosis*), *Caulobacter crescentus* (*C. crescentus*), *Myxococcus xanthus* (*M. xanthus*), *Propionibacter freudenreichii* (*P. freudenreichii*), *Streptomyces coelicolor* (*S. coelicolor*), and this work is presented in Chapter 2. The seven ferrochelatases investigated exhibit distinct particularities in the UV-visible, CD, EPR and resonance Raman spectra and the results are consistent with significant differences in the electronic, magnetic and vibrational properties of [2Fe-2S] clusters ligated by different cysteine coordination motifs in each of these proteins. Although final determination of the exact orientation of cysteine residues ligating the [2Fe-2S] clusters in ferrochelatases will require crystallographic data, it is likely that the spatial position will not vary significantly, given the clear conservation of structure found between human (*1*), yeast (*12*), and bacterial (*13*) protoporphyrin (IX) ferrochelatases reported to date. In addition, considering the low redox potentials and the irreversible reduction of the [2Fe-2S] clusters in ferrochelatases, as well as the marked instability of the enzymes in the reduced form, it seems very unlikely that the cluster plays a redox role in the cell.

In fact, several hypotheses have been considered concerning the role of [2Fe-2S] centers in ferrochelatases, yet no precise role has been demonstrated to date (*4;6*). In an attempt to address a possible role for the [2Fe-2S] cluster binding site in ferrochelatases as sensor of the

cellular Fe-S cluster concentration, we have conducted cluster transfer experiments from the [2Fe-2S] cluster-loaded chloroplastic *A. thaliana* monothiol glutaredoxin S14 (GrxS14) to the cluster-depleted *A. thaliana* sirohydrochlorin ferrochelatase (AtSirB Fc). This work is presented in Chapter 3, together with the analytical and spectroscopic characterization of AtSirB Fc at different pHs. Monothiol glutaredoxins with CGFS active sites are ubiquitous in eukaryotes and prokaryotes and they have been proposed to function as Fe-S cluster carrier/storage proteins (*14-16*). Considering the intact and stoichiometric cluster transfer and the fast second order rate constant observed for the cluster transfer reaction, we propose that the [2Fe-2S] cluster binding-site in ferrochelatases functions in regulating heme/siroheme biosynthesis in response to cellular Fe-S cluster availability via the extent of the [2Fe-2S] cluster-loaded form of monothiol GrxS14. The analytical and spectroscopic characterization of AtSirB Fc indicates that the protein undergoes a dimer/tetramer interconversion as a function of pH, and these conformational changes triggers a change in the ligand coordination of the [2Fe-2S] center. Interestingly, the [2Fe-2S] cluster appears to only be inserted in the "high pH' form in AtSirB Fc when the protein is incubated with the cluster donor GrxS14. However, further studies at molecular level using monothiol glutaredoxins and protoporphyrin IX ferrochelatases are needed to confirm the involvement of the [2Fe-2S] cluster binding-site in regulating heme biosynthesis. Additional studies including biophysical and biochemical techniques are also needed to address unambiguously the nature of the ligands to the [2Fe-2S] cluster in AtSirB Fc

In order for it to be a sensor of the cellular Fe-S cluster status, a mechanism must exist for the inactivation of ferrochelatase via its [2Fe-2S] cluster binding site. Based on the previous *in vivo* and *in vitro* studies indicating that the human enzyme is inactivated by NO via destruction of the [2Fe-2S] cluster (*17*), we have investigated the possibility that NO and/or

reactive oxygen species (ROS) could be the potential stimuli used by the cell for the inactivation of ferrochelatase under low concentrations of cellular Fe-S cluster. NO has recently been shown to be involved in Fe homeostasis by targeting specific metalloproteins under cellular Fe depletion conditions (*18;19*). In particular, Fe-S clusters appear to be the primary targets of both NO and ROS, and the inactivation of several Fe-S cluster-containing proteins that function in sensing the cellular Fe/Fe-S cluster conditions has been shown to occur via destruction of their Fe-S centers (*20-35*). As shown in Chapter 4, [2Fe-2S] cluster-containing ferrochelatases from vertebrate human and *Zebrafish*, yeast *S. pombe*, and bacteria *C. crescentus* and *M. xanthus* are all inactivated by NO via degradation of their Fe-S centers with similar rate constants.

A suggested model for the posttranslational regulation of ferrochelatase function is presented in Figure 5.1. According to this model, [2Fe-2S] cluster-loaded monothiol Grx, which serves as the primary sensor of the cellular Fe-S cluster status (*36;37*) would rapidly and effectively transfer its cluster for the maturation and activation of ferrochelatase. Under such conditions, heme biosynthesis would proceed normally (Figure 5.1A). On the other hand, under conditions of low cellular Fe-S cluster levels as a result of oxidative stress leading to insufficient Fe and/or impaired Fe-S cluster biosynthesis, low levels of [2Fe-2S] clusters on monothiol Grxs would channel Fe into Fe-S cluster biosynthesis at the expense of heme biosynthesis (Figure 5.1B). Clearly more studies are needed to be conducted at both cellular and molecular levels in order to further investigate the involvement of NO/ROS in downregulating heme biosynthesis.

Abbreviations: AtSirB Fc, *Arabidopsis thaliana* sirohydrochlorin ferrochelatase; Grx, glutaredoxin; NO, nitric oxide; ROS, reactive oxygen species; *S. pombe*, *Schizosaccharomices pombe*; *M. tuberculosis*, *Mycobacterium tuberculosis*; *C. crescentus*, *Caulobacter crescentus*; *M.*

xanthus, *Myxococcus xanthus*; *P. freudenreichii*, *Propionibacter freudenreichii*; *S. coelicolor*, *Streptomyces coelicolor*;

References

1. Wu, C.-K., Dailey, H. A., Rose, J. P., Burden, A., Sellers, V. M., and Wang, B.-C. (2001) *Nat. Struct. Biol. 8*, 156-160.
2. Dailey, H. A., Finnegan, M. G., and Johnson, M. K. (1994) *Biochemistry 33*, 403-407.
3. Shepherd, M., Dailey, T. A., and Dailey, H. A. (2006) *Biochem. J. 397*, 47-52.
4. Dailey, H. A. and Dailey, T. A. (2003) in *The Porphyrin Handbook* (Kadish, K. M., Smith, R., and Guilard, R., Eds.) pp 93-121, Academic Press, New York.
5. Dailey, T. A. and Dailey, H. A. (2002) *J. Bacteriol. 184*, 2460-2464.
6. Dailey, H. A., Dailey, T. A., Wu, C.-K., Medlock, A. E., Wang, K.-F., Rose, J. P., and Wang, B.-C. (2000) *Cell. Mol. Life Sci. 57*, 1909-1926.
7. Sellers, V. M., Wang, K. F., Johnson, M. K., and Dailey, H. A. (1998) *J. Biol. Chem. 273*, 22311-22316.
8. Crouse, B. R., Sellers, V. M., Finnegan, M. G., Dailey, H. A., and Johnson, M. K. (1996) *Biochemistry 35*, 16222-16229.
9. Medlock, A. E. and Dailey, H. A. (2000) *Biochemistry 39*, 7461-7467.
10. Wang, K. F., Wu, C. K., Sellers, V. M., Rose, J. P., Wang, B. C., and Dailey, H. A. (1999) *Acta Crystallogr. D. Biol Crystallogr. 55*, 1201-1203.
11. Day, A. L., Parsons, B. M., and Dailey, H. A. (1998) *Arch. Biochem. Biophys. 359*, 160-169.
12. Karlberg, T., Lecerof, D., Gora, M., Silvegren, G., Labbe-Bois, R., Hansson, M., and Al-Karadaghi, S. (2002) *Biochemistry 41*, 13499-13506.
13. Al-Karadaghi, S., Hansson, M., Nikonov, S., Jonsson, B., and Hederstedt, L. (1997) *Structure 5*, 1501-1510.

14. Vilella, F., Alves, R., Rodriguez-Manzaneque, M. T., Belli, G., Swaminathan, S., Sunnerhagen, P., and Herrero, E. (2004) *Comp Funct. Genomics 5*, 328-341.

15. Bandyopadhyay, S., Gama, F., Molina-Navarro, M. M., Gualberto, J. M., Claxton, R., Naik, S. G., Huynh, B. H., Herrero, E., Jacquot, J.-P., Johnson, M. K., and Rouhier, N. (2008) *EMBO J. 27*, 1122-1133.

16. Shakamuri, P. The role of molecular chaperones in mediating cluster transfer from [2Fe-2S] cluster-bound IscU. 2011. University of Georgia. Ref Type: Thesis/Dissertation

17. Sellers, V. M., Johnson, M. K., and Dailey, H. A. (1996) *Biochemistry 35*, 2699-2704.

18. Watts, R. N., Ponka, P., and Richardson, D. R. (2003) *Biochem. J. 369*, 429-440.

19. Wardrop, S. L., Watts, R. N., and Richardson, D. R. (2000) *Biochemistry 39*, 2748-2758.

20. Reddy, S. G., Wong, K. K., Parast, C. V., Peisach, J., Magliozzo, R. S., and Kozarich, J. W. (1998) *Biochemistry 37*, 558-563.

21. Reddy, D., Lancaster, J. R., Jr., and Cornforth, D. P. (1983) *Science 221*, 769-770.

22. Cruz-Ramos, H., Crack, J., Wu, G., Hughes, M. N., Scott, C., Thomson, A. J., Green, J., and Poole, R. K. (2002) *EMBO J. 21*, 3235-3244.

23. Drapier, J. C. (1997) *Methods: A Companion to Meth. Enzymol. 11*, 319-329.

24. Stys, A., Galy, B., Starzynski, R. R., Smuda, E., Drapier, J. C., Lipinski, P., and Bouton, C. (2011) *J. Biol. Chem. 286*, 22846-22854.

25. Ding, H. and Demple, B. (2000) *Proc. Natl. Acad. Sci. USA 97*, 5146-5150.

26. Nitric Oxide in Plant Growth, Development and Stress Physiology. Lamattina, L. and Polacco, J. C. 1[6]. 2007. Springer. Plant Cell Monographs. Ref Type: Serial (Book,Monograph)

27. Hanson, E. S. and Leibold, E. A. (1999) *Gene Expr. 7*, 367-376.

28. Hanson, E. S. and Leibold, E. A. (1998) *J. Biol. Chem. 273*, 7588-7593.

29. Pantopoulos, K. and Hentze, M. W. (1998) *Proc. Natl. Acad. Sci. U. S. A 95*, 10559-10563.

30. Pantopoulos, K., Weiss, G., and Hentze, M. W. (1996) *Mol. Cell Biol. 16*, 3781-3788.

31. Weiss, G., Goossen, B., Doppler, W., Fuchs, D., Pantopoulos, K., Werner-Felmayer, G., Wachter, H., and Hentze, M. W. (1993) *EMBO J. 12*, 3651-3657.

32. Zheng, M., Wang, X., Templeton, L. J., Smulski, D. R., LaRossa, R. A., and Storz, G. (2001) *J. Bacteriol. 183*, 4562-4570.

33. Flint, D. H., Smyk-Randall, E., Tuminello, J. F., Draczynska-Lusiak, B., and Brown, O. R. (1993) *J. Biol. Chem. 268*, 25547-25552.

34. Flint, D. H., Tuminello, J. F., and Emptage, M. H. (1993) *J. Biol. Chem. 268*, 22369-22376.

35. Pantopoulos, K. and Hentze, M. W. (1995) *Proc. Natl. Acad. Sci. U. S. A 92*, 1267-1271.

36. Li, H., Mapolelo, D. T., Dingra, N. N., Naik, S. G., Lees, N. S., Hoffman, B. M., Riggs-Gelasco, P. J., Huynh, B. H., Johnson, M. K., and Outten, C. E. (2009) *Biochemistry 48*, 9569-9581.

37. Muhlenhoff, U., Molik, S., Godoy, J. R., Uzarska, M. A., Richter, N., Seubert, A., Zhang, Y., Stubbe, J., Pierrel, F., Herrero, E., Lillig, C. H., and Lill, R. (2010) *Cell Metab 12*, 373-385.

Figure 5.1. Suggested model for the activation/inactivation of ferrochelatase as a function of the cellular Fe-S cluster status. (A) Under normal cellular conditions of Fe-S cluster concentration, monothiol Grxs with CGFS active site functioning as cluster carrier/storage proteins, deliver an intact [2Fe-2S] cluster for the posttranslational maturation and stabilization of ferrochelatase/sirohydrochlorin ferrochelatase. In the cluster-loaded form, ferrochelatase/sirohydrochlorin ferrochelatase becomes catalytically active and heme/siroheme biosynthesis is accomplished. (B) Under conditions of low cellular Fe/Fe-S clusters levels or impaired Fe-S cluster biosynthetic pathway, ferrochelatase/sirohydrochlorin ferrochelatase is inactivated via destruction of its [2Fe-2S] cluster in by NO/NOS. Consequently, heme/siroheme biosynthesis is arrested temporarily.

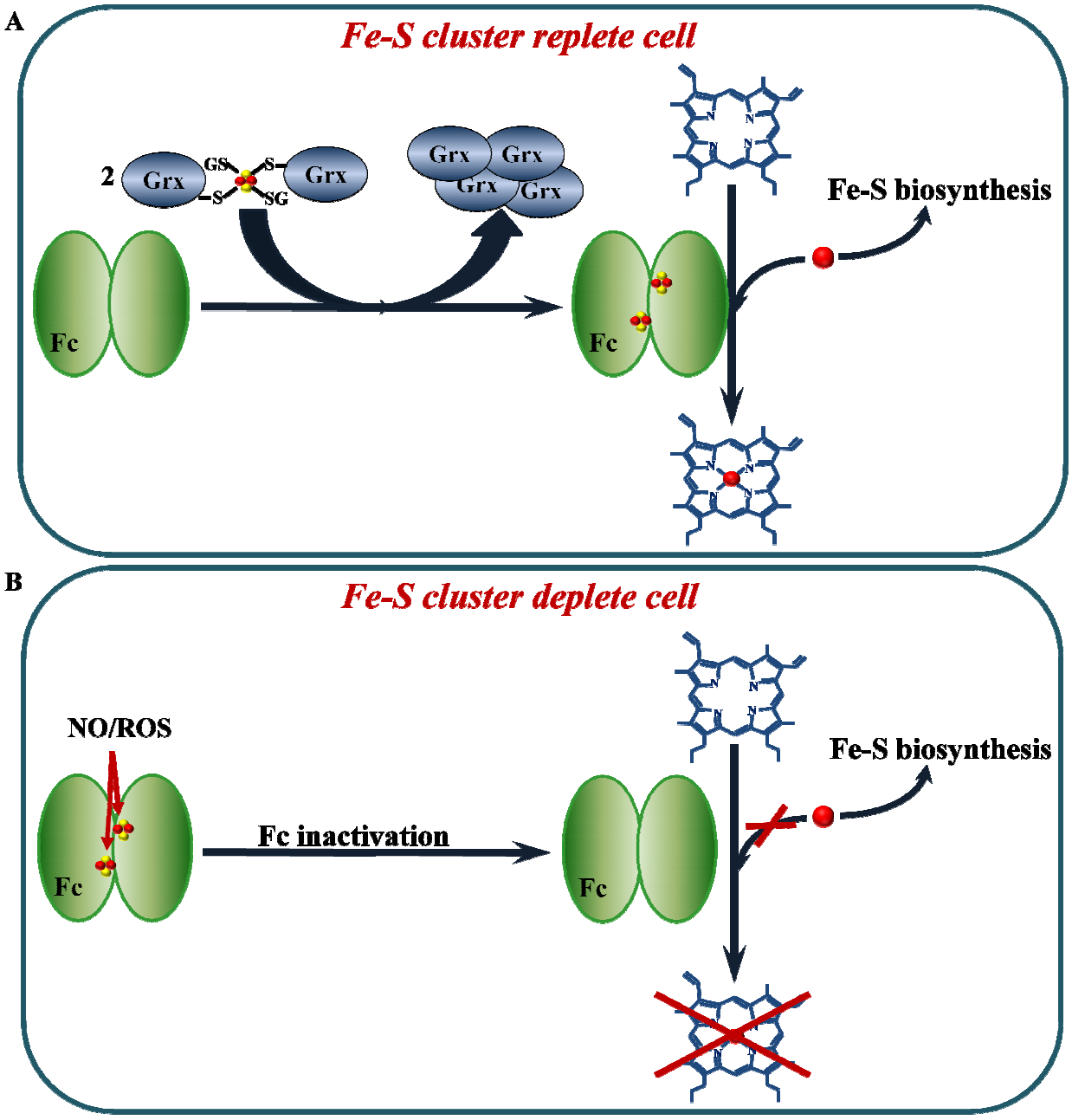
A
Fe-S cluster replete cell
2
Grx
GS
S
S
SG
Grx
Grx
Grx
Grx
Grx
Fe-S biosynthesis
Fc
Fc
B
Fe-S cluster deplete cell
NO/ROS
Fc inactivation
Fe-S biosynthesis
Fc
Fc